2020

DDI1/2 and RTF2-Dependent Regulation of RNASE H2 at the Replisome Ensures Genome Stability

Brooke A. Conti

DDI1/2 AND RTF2-DEPENDENT REGULATION OF RNASE H2 AT THE REPLISOME ENSURES GENOME STABILITY

A Thesis Presented to the
Faculty of The Rockefeller University
in Partial Fulfillment of the Requirements
for the degree of Doctor of Philosophy

by
Brooke A. Conti
June 2020

DDI-RTF2-DEPENDENT REGULATION OF RNASE H2 AT THE REPLISOME ENSURES GENOME STABILITY

Brooke A. Conti, Ph.D.
The Rockefeller University 2020

Proteasome shuttle proteins, DNA Damage Inducible 1 (DDI1) and DNA Damage Inducible 2 (DDI2), are active in the replication stress response (Kottemann et al., 2018). Under conditions of replication stress, DDI1/2 function to remove Replication Termination Factor 2 (RTF2) from the replisome. Persistence of RTF2 at the replisome compromises the replication stress response, resulting in accumulation of single-stranded DNA, inefficient replication fork restart, genome instability, and cell death. During unperturbed replication, RTF2 travels with the replication fork (Kottemann et al., 2018). Here we examine the function of RTF2 and address why RTF2's removal from the replisome is necessary for recovery from replication stress.

We find that loss of RTF2 results in murine embryonic lethality and that RTF2 is required for normal DNA replication elongation speeds. By isolation of proteins on nascent DNA (iPOND), replisomes deficient for RTF2 concurrently lack RNase H2, a heterotrimeric enzyme responsible for removing RNA in the context of RNA-DNA heteroduplexes. Like RTF2, RNase H2 is necessary for normal replication speed. RTF2-deficient cells exhibit phenotypes consistent with loss of RNase H2 and an increase in genome-embedded ribonucleotides, including the accumulation of DNA damage.

In the absence of DDI1/2, the persistence of RNase H2 at a stalled replication fork also compromises the replication stress response. We show that direct replication restart is dependent on PRIM1, the primase component of DNA polymerase α. The dependence on PRIM1 for replication restart is greater than its requirement during processive DNA replication. Our data suggest there might be a competition between PRIM1 and RNase H2, which regulates the synthesis and degradation of the RNA primer.

Our data support a model whereby the DDI-RTF2 axis regulates RNase H2 levels at the replisome during stress. RNase H2 travels with the replication fork to remove genome-embedded ribonucleotides resulting from random polymerase incorporation or inefficient Okazaki fragment maturation. However, upon DNA damage and replication stalling, RNase H2 must be removed from the replication fork to allow for proper restart using PRIM1-synthesized RNA primers. The work presented here provides a new perspective on the reorganization of the replisome that is required upon replication stress and addresses a fundamental need for regulation of replication-coupled ribonucleotide incorporation during DNA replication and repair.

Acknowledgements

I would not have been able to reach this point in my scientific career without the support of many others. I have had a fantastic opportunity to work with incredible scientists and staff at Rockefeller University and cannot imagine a better experience elsewhere.

I would first like to thank my advisor, Agata Smogorzewska, for the immense amount of time and energy she invested in providing mentorship. I feel extremely grateful not only your advice and support, but also for creating a work environment where I was able to take risks and learn from my mistakes. I am continually humbled by your intellectual curiosity, erudite comments, and dedication to scientific rigor.

I would also like to thank my thesis committee, Fred Cross and Titia de Lange, for their insights and expertise, always pushing me to think one step further and design clear experiments. Your remarks have been invaluable in the development of this project. Thank you to David Cortez for acting as my external examiner in the final stages of my graduate career and making the trip from Nashville for my defense.

I would like to thank the Dean's office, Andrea, Cris, Kristen, Marta, Stephanie, Emily, and Sid, for coordinating a wonderful graduate experience and always making sure everything is running smoothly.

I would like to thank all the Rockefeller Resource Centers that have been instrumental in completing this work, especially the Bioimaging Resource Center, the Proteomics Resource Center, the Flow Cytometry Resource Center, the Genomics Resource Center, the Bioinformatics Resource Center, the Cyro-EM Resource Center, the Transgenics Resource Center, the Precision Fabrication Facility, and the Center for Comparative Biosciences.

The Smogorzewska lab has been a wonderful place to work thanks to all past and current members who have helped with projects and have been generous with their ideas in lab meetings. I would especially like to thank Anderson Wang, Molly Kottemann, Kimberly Rickman, Ryan White, Sunandini Sridhar, Penelope Ruiz, Cayla Broton, and Nicolas Blobel who acted as mentors and friends with whom I could discuss scientific ideas and whom made every day enjoyable over many shared laughs, coffee breaks, and happy hours at Faculty Club, despite the scientific roller coaster. A big thank you to Ryan White, Penelope Ruiz and Kimberly Rickman for reading and providing feedback on portions of this thesis. A very special thank you to Francis Lach – your patience in processing requests, Metafer expertise, general care for the lab and mechanical tinkering (especially building our first combing machine and slide holders) are always immensely appreciated. Thank you also to Tom Wiley who was responsible for maintaining the RTF2 mouse colony.

I would like to thank my previous science mentors, Tommie Hata, Deirdre O'Mara, Zachary Schafer, Kelsey Weigel, Xiaokui Zhang, and Lin Kang, for introducing and fostering a love of science. Your mentorship, support, and friendship through the years has been irreplaceable.

I would also like to thank my friends and family who have supported me over these years and through my entire life. Thank you for asking questions about my research, listening to practice talks of my scientific presentations, despite having no background in the subject. You have cheered me every step of the way and I am eternally grateful. Patrick, you have been my rock. Thank you for always believing in me. Dad, you are always proud of me no matter what and that means the world. Thank you for instilling your values of hard work, grit, determination, and the sentiment of being the best you can be for the world. Mom, thank you for your constant nurture and care. You have an unique ability to provide a sense of comfort and calm, reminding me to stay balanced. Austin and Hunter, thank you for always taking pride and being continually interested in the work I do.

Table of Contents

List of Figures

List of Tables

List of Abbreviations

9-1-1	RAD9-RAD1-HUS1
AAA+	ATPase Associated with Diverse Cellular Activities
AA	Amino Acid
ACS	Autonomous Consensus Sequence
AEP	Archaeo-Eukaryotic Primase
ADAR	Adenosine Deaminase RNA Specific
ADP	Adenosine Diphosphate
AGS	Aicardi-Goutières Syndrome
AID	Auxin Inducible Degron
AND-1	Acidic Nucleoplasmic DNA-binding Protein
APC	Anaphase Promoting Complex
ARS	Autonomously Replicating Sequences
ATM	Ataxia Telangiectasia Mutated
ATP	Adenosine Triphosphate
ATR	Ataxia Telangiectasia Mutated and Rad3 Related
ATRIP	Ataxia Telangiectasia Mutated and Rad3 Related-interacting Protein
BER	Base Excision Repair
BIR	Break-induced Replication

BL6	C57 Black 6
BLM	Bloom Syndrome Protein
bp	Base Pair
BrdU	5’-bromo-2’-deoxyuridine
BSA	Bovine serum albumin
CDC6	Cell Division Cycle 6
CDC7	Cell Division Cycle 7
CDC25A	Cell Division Cycle 25 A
CDC45	Cell Division Cycle 45
CDT1	Chromatin Licensing and DNA Replication Factor 1
CDK	Cyclin-dependent Kinase
CDK2	Cyclin-dependent Kinase 2
cGAS	Cyclic GMP-AMP synthase
CHK1	Checkpoint Kinase 1
CldU	5’-Cholor-2’-deoxyuridine
CLSPN	Claspin
CMG	Cdc45-MCM2-7-GINS
Cre	Causes Recombination Recombinase
CRISPR	Clustered Regularly Interspaced Short Palindromic Repeats
CSF	Cerebrospinal Fluid
CTD	Carboxyl Terminal Domain

D-loop	Displacement Loop
DAPI	4,6-diamidino-2-phenylindole
DDI1	DNA Damage Inducible 1
DDI2	DNA Damage Inducible 2
DDK	Dbf4-dependent Kinase
DDR	DNA Damage Response
DNA	Deoxyribonucleic Acid
DNA2	DNA Replication Helicase/nuclease 2
DNA-PKcs	DNA-dependent Protein Kinase, catalytic subunit
dNTP	Deoxynucleoside Triphosphate
dpc	Days Post Coitum
DPC	DNA-protein Complex
DSB	Double-strand Break
dsDNA	Double-stranded DNA
DUE-B	DNA Unwinding Element Binding Protein
E2	Ubiquitin Conjugating Enzyme
E3	Ubiquitin Ligase
EdU	5’-ethynyl-2’-deoxyuridine
ETAA1	Ewing’s Tumor-associated Antigen 1
EV	Empty Vector
EXO1	Exonuclease 1

FBS	Fetal Bovine Serum
FEN1	Flap Endonuclease 1
Flp	Flippase Recombinase
FRT	FLP Target
G0	Gap Phase 0
G1	Gap Phase 1
G2	Gap Phase 2
GFP	Green Fluorescent Protein
GINS	*Go-Ichi-Ni-San*
H2AX	Histone H2A Family Member X
HLTF	Helicase-like Transcription Factor
HU	Hydroxyurea
ICL	Interstrand Crosslink
IdU	5'-iodo-2'-deoxyuridine
IF	Immunofluorescence
IFIH1	Interferon Induced With Helicase C Domain 1
INF	Interferon
IP	Immunoprecipitation
iPOND	Isolation of Proteins on Nascent DNA
kDa	Kilodalton
KO	Knockout
KOMP	Knockout Mouse Project

LacZ	Lac Operon Z
LC-MS	Liquid Chromatography-Mass Spectrometry
LIG1	DNA ligase 1
LoxP	Locus of X(cross)-over in P1
Luc	Luciferase
M	Mitosis
MCM	Minichromosome Maintenance
MEF	Mouse Embryonic Fibroblast
mESC	Mouse Embryonic Stem Cell
MMC	Mitomycin C
MMR	Mismatch Repair
MPS1	Mat1-Pausing Site
MRE11	Meiotic Recombination 11 Homolog, Double-strand Break Nuclease
MTBP	Mdm2-binding Protein
NeoR	Neomycin Resistance Gene
NER	Nucleotide Excision Repair
NLS	Nuclear Localization Signal
nPLA	Nascent Proximity Ligation Assay
NTD	Amino-terminal Domain
OF	Okazaki Fragment
pADPr	Poly [ADP-ribose]

ORC	Origin Recognition Complex
PARP1	Poly [ADP-ribose] polymerase 1
PBS	Phosphate Buffered Saline
PCNA	Proliferating Cell Nuclear Antigen
PCR	Polymerase Chain Reaction
PI3K	Phosphatidylinositol-4,5-bosphosphate 3-kinase
PIP	PCNA-interacting Protein
POL α	DNA Polymerase Alpha
POL δ	DNA Polymerase Delta
POL ε	DNA Polymerase Epsilon
POLA1	DNA Polymerase Alpha, Catalytic Subunit
POLA2	DNA Polymerase Alpha, Accessory Subunit
POLD3	DNA Polymerase Delta Subunit 3
pre-RC	Pre-replicative Complex
PRIM1	DNA Primase Subunit 1
PRIM2	DNA Primase Subunit 2
PRIMPOL	Primase and DNA Directed Polymerase
PSM	Peptide Spectral Match
PTM	Post Translational Modification
RECQ1	RecQ-like Helicase
RECQ4	RecQ-like Helicase 4

RED	Ribonucleotide Excision Repair Defective
RER	Ribonucleotide Excision Repair
RFC	Replication Factor C
RPC	Replication Progression Complex
RING	Really Interesting New Gene
RNA	Ribonucleic Acid
RNAi	Ribonucleic Acid Interference
RNase H1	Ribonuclease H1
RNase H2	Ribonuclease H2
RNASEH2A	Ribonuclease H2 Subunit A
RNASEH2B	Ribonuclease H2 Subunit B
RNASEH2C	Ribonuclease H2 Subunit C
rNTP	Ribonucleoside Triphosphate
RPA	Replication Protein A
RNA-seq	RNA Sequencing
RT-qPCR	Quantitative Reverse Transcription PCR
RTF2	Replication Termination Factor 2
RTS1	Replication Termination Site 1
RVP	Retroviral Protease Domain
S Phase	Synthesis Phase
SAMHD1	SAM and HD Domain Containing Deoxynculeoside Triphosphate Triphosphohydrolase

SAP	SAF-A/B, Acinus and PIAS
SCF	Skp, Cullin, F-box containing complex
SHPRH	SNF2 histone linker PHD RING helicase
SIM	SUMO Interacting Motif
siRNA	Short Interfering Ribonucleotide
SMARCAL1	SWI/SNF Related, Matrix Associated, Actin Dependent Regulator Of Chromatin, Subfamily A Like 1
SSB	Single-strand Break
ssDNA	Single-stranded DNA
STING	Stimulator of Interferon Genes
SUMO	Small Ubiquitin-Like Modifier
SV40	Simian Virus 40-large T Antigen
TIPIN	Timeless Interacting Protein
TIR1	Transport Inhibitor Response 1
TLS	Translesion Synthesis
TOP1	Topoisomerase 1
TOPBP1	DNA Topoisomerase 2-binding Protein 1
TREX1	Three-primer Repair Exonuclease 1
UBL	Ubiquitin-like Domain
UBA	Ubiquitin-associated Domain
ULP1	Ubiquitin-like-specific Protease 1
UTR	Untranslated Region

UV	Ultraviolet Radiation
VCP	Valosin-containing Protein
WRN	Werner Syndrome Helicase
XLPDR	X-linked Reticulate Pigmentary Disorder
ZRANB3	Zinc finger RANBP2-type containing 3

Chapter 1: Introduction

1.1 Eukaryotic cell cycle

The continuity of life depends on the accurate duplication of a cell's genetic information and the equal division of this genetic material between two daughter cells. This process is collectively called the cell cycle. The quest to understand how the genetic information is propagated from one generation to the next began with seminal work from Watson, Crick, Wilkins, and Franklin that presented a structure of deoxyribonucleic acid (DNA) which "immediately suggest[ed] a possible copying mechanism for the genetic material" (Watson and Crick, 1953). This copying mechanism, called DNA replication, is a complex process conserved from the smallest single-cell prokaryotes to multi-cellular eukaryotes including metazoans, even though the proteins involved evolved largely independently (reviewed in (Leipe et al., 1999)).

As organisms increase in complexity, genomes increase in size. For example, bacterial genomes are composed of approximately 5 million base pairs (bp) (reviewed in (Land et al., 2015)), whereas mammalian genomes are greater than 5 billion bps (reference genome is approximately 2.7 billion bps in mice (Church et al., 2009) and approximately 3.2 billion bps in human (U.S. Department of Energy Office of Science, 2016; Venter et al., 2001)). Larger genomes also have a different structural organization to package the genetic material inside a cell. For example, prokaryotes contain a single circular chromosome whereas most eukaryotes contain multiple linear chromosomes. Mammalian cells thus face additional challenges to the completion of DNA replication in an accurate and timely manner. To deal with these challenges, mammalian DNA replication has developed specific machinery, additional switches, and mechanisms of repair that may not be present in prokaryotes and lower eukaryotes.

In this introductory chapter, I will review the timing of DNA replication within the cell cycle, the process of DNA replication, and replication-coupled DNA repair. The final section of the chapter will discuss factors, DNA Damage Inducible 1 (DDI1), DNA Damage Inducible 2 (DDI2), and Replication Termination Factor 2 (RTF2), which recently have been identified as important for DNA replication and replication-coupled DNA repair.

1.1.1 The cell cycle and timing of mammalian DNA replication

Mammalian DNA replication is temporally organized within the cell cycle. Four discrete phases form a full cell cycle: Gap Phase 1 (G_1), Synthesis Phase (S), Gap Phase 2 (G_2), and Mitosis (M) (Figure 1.1) (reviewed in (Cooper, 2000)). In G_1, the cell is metabolically active while replication origin licensing occurs at specific sites. The transition from G_1 to S phase ensures that these origins are activated only once per cell cycle. Once origins fire in S phase, the replication machinery, termed the replisome, proceeds to unwind and replicate DNA. By G_2, DNA synthesis is largely complete and cell growth continues in preparation for M phase. During M phase, cells undergo cellular

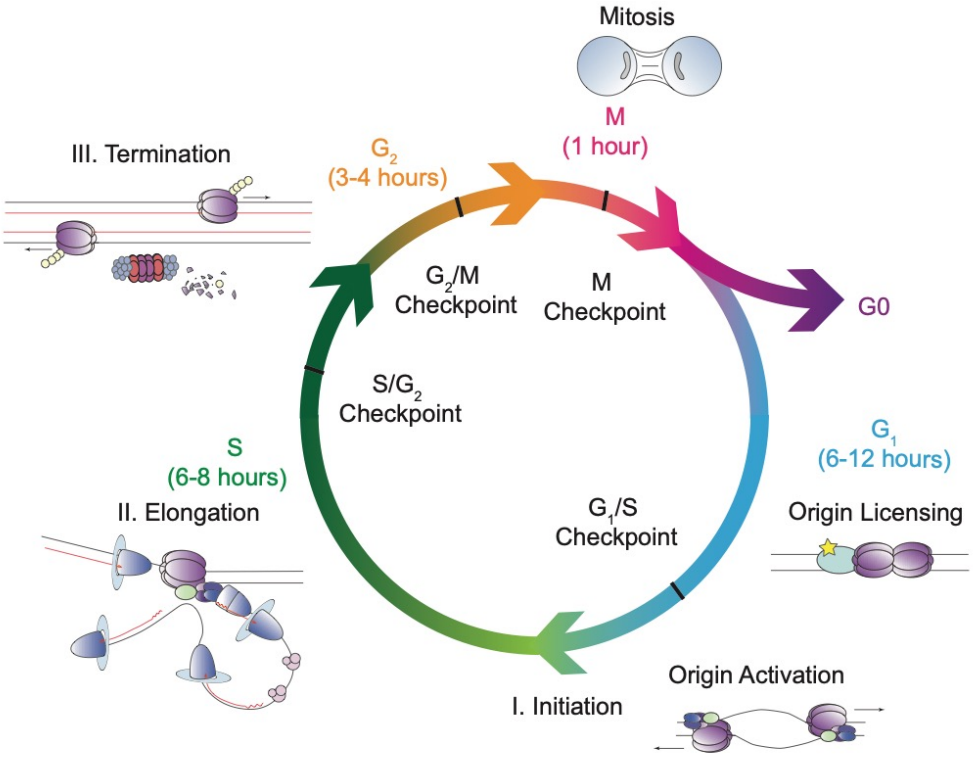

Figure 1.1. The mammalian cell cycle.
The cell cycle for most cultured mammalian cells occurs over the course of approximately 24 hours. Important events for DNA replication (initiation, elongation, and termination) are overlaid according to their timing in the cell cycle.

division where sister chromatids are aligned on the metaphase plate and are separated into two daughter cells.

There are several mechanisms in place to ensure that damaged or incompletely replicated chromosomes are not passed onto daughter cells. Checkpoints are biological chemical pathways that control transitions from one phase to the next (reviewed in (Elledge, 1996)). For example, the S-to-G_2 checkpoint, monitors the completion of DNA replication (Rao and Johnson, 1970). This checkpoint is dependent on Ewing's Tumor-associated Antigen 1 (ETAA1)-stimulated baseline Ataxia Telangiectasia Mutated and Rad3 related kinase (ATR) (Bass and Cortez, 2019; Saldivar et al., 2018).

1.2 Eukaryotic DNA replication

Much of our current understanding of eukaryotic DNA replication comes from experiments in *Saccharomyces cerevisiae.* While *S. cerevisiae* has been a fruitful model system, it does not fully address the complexity of mammalian DNA replication. This introduction will describe many of the discoveries made in budding yeast while highlighting key differences in metazoans. DNA replication can be divided into three phases: initiation, elongation, and termination. These phases will be discussed in turn.

1.2.1 Initiation of DNA replication

Origins of replication are the sites at which DNA replication is initiated. In *S. cerevisiae,* these sites are well-defined autonomously replicating sequences (ARS), containing a common sequence of 11 bps called the autonomous consensus sequence (ACS). In metazoans, origins of replication are less precisely defined than in yeast and thus it is more appropriate to refer to mammalian origins of replication as initiation sites. A stochastic model, in terms of both time and space, in which DNA initiation occurs at one of many potential sites that is randomly chosen depending on the chromatin context has been proposed (reviewed in (Leonard and Méchali, 2013)). In both yeast and metazoans, only a fraction of potential replication initiation sites are used in a given S phase (Cayrou et al., 2011; Linskens and Huberman, 1988). Initiation of replication occurs in two stages: the loading of the core helicase late in M and early in G_1 (origin licensing) and the activation of the helicase and replisome assembly at the onset of S phase (origin activation) (reviewed in (Bell and Dutta, 2002; Masai et al., 2010)).

In yeast, origin licensing requires the pre-replicative complex (pre-RC), which is composed of the origin recognition complex (ORC), Cell division cycle 6 (Cdc6), Chromatin licensing and DNA replication factor 1 (Cdt1) and the Minichromosome maintenance (Mcm) hexamer (composed of Mcm2-7), to assemble at the origins of replication. The ORC, composed of six subunits (Orc1-Orc6), five of which are related to ATPase Associated with Diverse Cellular Activities (AAA+) protein family of ATPases, binds to potential origin sequences and serves as a foundation (Bell and Stillman, 1992).

ORC recruits Cdc6, another AAA+ ATPase. Cdt1 and the mini Mcm2-7 then join the ORC-Cdc6 complex at the origin sequences. ORC-Cdc6-Cdt1 load Mcm2-7 onto the origin in a reaction requiring ATP hydrolysis (Bowers et al., 2004; Perkins and Diffley, 1998; Randell et al., 2006). ORC, CDC6, and CDT1 are also required for MCM2-7 loading in mammalian cells (Cook et al., 2002; Giordano-Coltart et al., 2005; Rialland et al., 2002; Takeda et al., 2005). The two hexametric rings of Mcm2-7 are loaded onto double-stranded DNA (dsDNA) in a head-to-head (amino-to-amino) configuration with the DNA duplex passing through the central channel of the hexamer (Evrin et al., 2009; Georgescu et al., 2017; Remus et al., 2009). Experiments in *Xenopus laevis* extracts suggest that once Mcm2-7 is loaded, subsequent steps for the initiation of DNA replication do not require ORC, Cdc6, and Cdt1 (Hua and Newport, 1998; Maiorano et al., 2000; Rowles et al., 1999) (reviewed in (Bell and Kaguni, 2013)) (Figure 1.2).

Origin activation, defined by the transformation of MCM2-7 into an active helicase, requires several additional factors. The MCM4-6-7 subcomplex purified from human cells contains ATP-dependent helicase activity *in vitro* (Ishimi, 1997; You et al., 1999), however, MCM2-7, does not have detectable helicase activity, suggesting additional proteins are required for helicase activation. The *Go-Ichi-Ni-San* ($GINS^{Sld5\text{-}Psf1\text{-}Psf2\text{-}Psf3}$) complex and Cell division cycle 45 (Cdc45) together with Mcm2-7 form the replicative helicase, collectively referred to as CMG (Cdc45-MCM-GINS) (Gambus et al., 2006; Moyer et al., 2006). Cdc45 and GINS allosterically remodel the core of the Mcm2-7 complex to allow for helical activity (Costa et al., 2014; Ilves et al., 2010; Moyer et al., 2006). The active CMG binds DNA and translocates in the 3'-5' direction on the leading-strand template by a pumpjack motion (Yuan et al., 2016).

The process of CMG assembly and activation is stimulated by two protein kinases, cyclin-dependent kinase (CDK; CDK2 in humans) and DBF4-dependent kinase (DDK; CDC7-DBF4 heterodimer in humans) and requires several additional regulatory factors. The regulatory components for CMG assembly in metazoans are divergent from those in yeast and there has been some debate regarding the functional homologs. The proteins most likely required for CDC45 loading are CDK2-phosophorylated TRESLIN (Boos et al., 2011), DBF4-phosophorylated DNA unwinding element binding protein (DUE-B) (Chowdhury et al., 2010), Mdm2-binding Protein (MTBP) (Boos et al., 2013), and Topoisomerase II binding protein I (TOPBP1) (Kumagai et al., 2011). By comparison, little is known about GINS loading. Factors that facilitate origin activation include MCM10, RecQ-like Helicase 4 (RECQ4) and Acidic Nucleoplasmic DNA-Binding Protein 1 (AND-1) (Im et al., 2009). The molecular mechanisms for recruitment of the polymerases in human cells are still not well understood (reviewed in (Moiseeva and Bakkenist, 2018; Tanaka and Araki, 2013)).

Several redundant mechanisms prevent the re-licensing of origins in S phase. This ensures that initiation only occurs once per cell cycle and prevents re-duplication of the

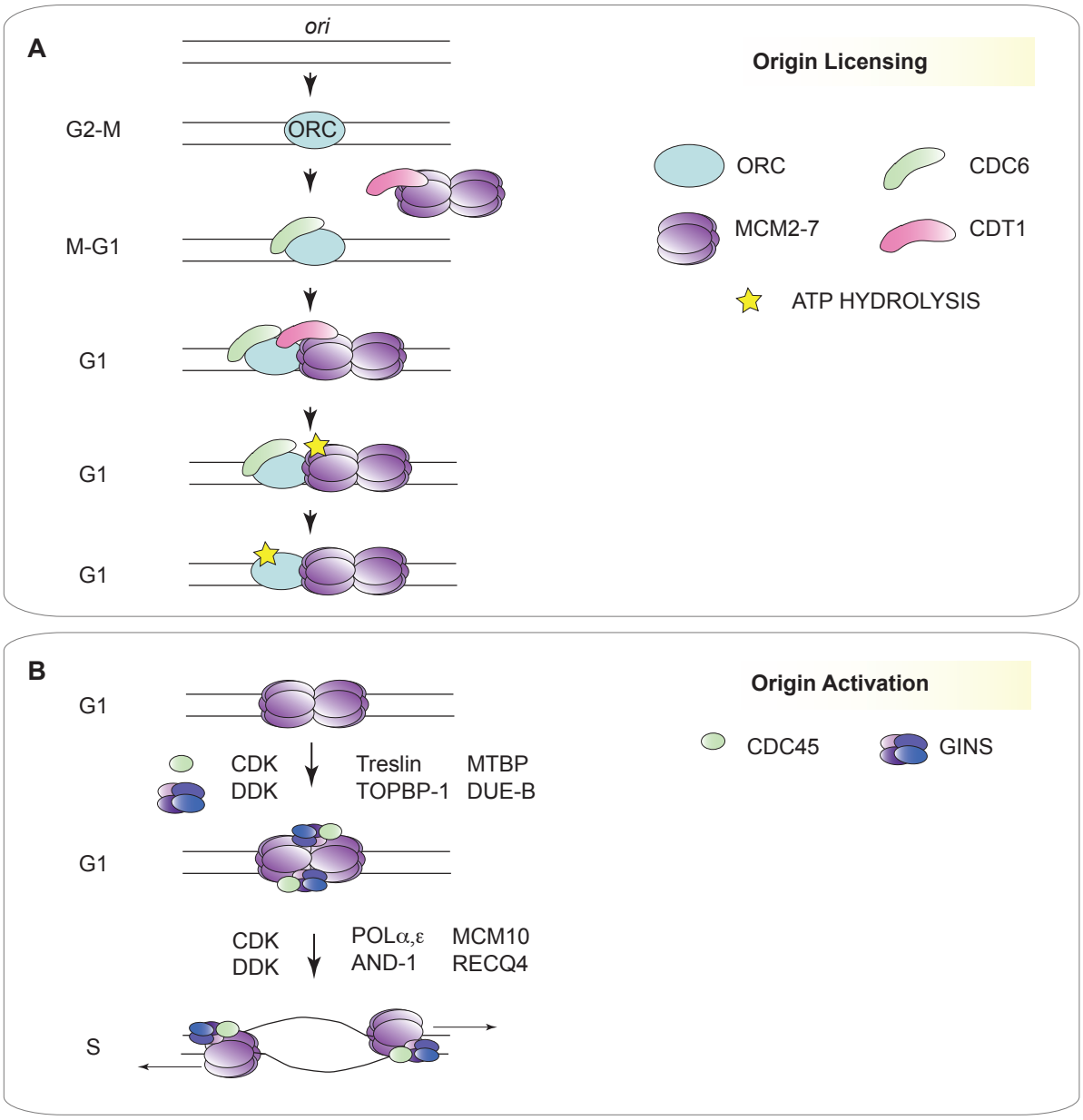

Figure 1.2. Mammalian DNA replication initiation.
(A) To begin origin licensing, ORC binds to potential origins sequences. Subsequently CDC6 associates with ORC. MCM2-7 in association with CDT1 join the ORC-CDC6 complex. In yeast, hydrolysis of ATP on Cdc6 leads to “loading” of the MCM complex and release of Cdt1. Dissociation of Cdc6 from the origin and hydrolysis of ATP associated with the ORC completes pre-RC assembly. (B) Once MCM2-7 is loaded onto the origin, conversion into an active CMG helicase requires CDC45 and GINS. CDK- and DDK-dependent signaling stimulate active replication. There are many additional layers of regulation to prevent re-duplication.

genome without an intervening mitosis. Since the mechanisms to prevent re-duplication in metazoans differ from those in yeast, I will focus solely on those relevant to metazoans.

Negative regulation can degrade or inhibit factors required for firing, such as ORC1, CDC6, and CDT1. ORC1, the required scaffold for licensing, is selectively degraded during S phase by both cyclin A-Cyclin Dependent Kinase 1 (CDK1)-dependent and CDK1-independent mechanisms and it is resynthesized solely during the M-to-G1phase transition to regulate assembly of the licensing complex (Kreitz et al., 2001; Li and DePamphilis, 2002; Li et al., 2004; Mendez et al., 2002; Natale et al., 2000; Ohta et al., 2003; Tatsumi et al., 2003). Regulating the availability of CDC6 also prevents re-licensing as CDC6 is required for helicase loading. CDC6 is degraded following ubiquitination by the anaphase promoting complex (APC)/C^{CDH1} ligase in G_1 (Mendez and Stillman, 2000; Petersen et al., 2000). In S and G_2, degradation of CDC6 is mediated by $CRL4^{CDT2}$ and $SCF^{Cyclin\ F}$, respectively (Clijsters and Wolthuis, 2014; Walter et al., 2016). In addition, CDK-dependent phosphorylation of CDC6 exposes a nuclear export signal promoting its export from the nucleus (Delmolino et al., 2001; Fujita et al., 1999; Jiang et al., 1999; Petersen et al., 2000; Saha et al., 1998). Regulatory mechanisms also limit the levels of CDT1. CDK-dependent phosphorylation of CDT1 promotes its ubiquitination by the SCF^{Skp2} and DDB1-CUL4 E3 ubiquitin ligase, which subsequently results in CDT degradation (Kondo et al., 2004; Li et al., 2003b; Liu et al., 2004; Nishitani et al., 2006; Sugimoto et al., 2004). GEMININ, a protein expressed only in S, G_2, and M, also binds and sequesters CDT1 in an inactive form to inhibit erroneous CDT1 function (Cook et al., 2004; Tada et al., 2001; Wohlschlegel et al., 2000; Wu et al., 2014; Yanagi et al., 2002).

Positive regulation of ORCs, CDT1, and CDC6, is also important to promote DNA replication initiation. A recent report shows that OBI1-dependent ubiquitination of ORC3 and ORC5 promotes origin firing (Coulombe et al., 2019). Despite GEMININ's role in negative regulation, GEMININ simultaneously stabilizes and accumulates CDT1 for firing (Ballabeni et al., 2004). USP37 deubiquitinates CDT1 to promote helicase loading (Hernandez-Perez et al., 2016). Cyclin E/CDK2 phosphorylation of CDC6 inhibits APC/C^{CDH1}-mediated proteolysis of CDC6 (Mailand and Diffley, 2005). It is clear that the layers of regulation are complex and all of these mechanisms ensure that re-replication does not occur without an intervening cell division.

DNA replication stress responses, discussed in detail later, inhibit DNA initiation to induce cell cycle arrest. For example, effectors of DNA replication stress response pathways promote degradation of Cell Division Cycle 25 A (CDC25A), a phosphatase crucial for CDK2 activation (Mailand et al., 2000; Sorensen et al., 2003). Active p53 also induces transcription of p21 which directly inhibits CDK2 activity (Harper et al., 1995). Valosin-containing protein (VCP)/p97 ubiquitinates and degrades CDT1 upon exposure to ultraviolet (UV) radiation to inhibit origin firing (Raman et al., 2011).

1.2.2 The replisome and DNA replication elongation

Once initiation has successfully been completed, replication elongation can proceed. DNA replication is performed by a multi-protein machine, termed the replisome, which replicates both parental DNA strands at the same time resulting in two semi-conservative daughter duplexes. All replisomes must contain the following core components: a DNA helicase, a single-stranded DNA (ssDNA) binding protein, a primase, DNA polymerases, a pentameric clamp loader, and ring-shaped sliding clamps (reviewed in (O'Donnell et al., 2013)) (Figure 1.3).

The initiation of synthesis begins when the CMG helicase encircles the leading-strand and acts to unwind DNA duplexes ahead of the replication fork. Unwinding requires Replication Protein A (RPA), a ssDNA binding protein, to stabilize ssDNA. RPA is a heterotrimeric protein complex, made of subunits referred to as RPA70 (70 kDA), RPA32 (32 kDa), and RPA14 (14 kDa), that contains six oligosaccharide/oligonucleotide binding (OB) folds responsible for sequential binding to the ssDNA in a 5' to 3' polarity (de Laat et al., 1998). RPA is essential for DNA replication initiation and elongation (Fairman and Stillman, 1988; Wobbe et al., 1987; Wold and Kelly, 1988); (reviewed in (Zou et al., 2006)).

The primosome, also known as Pol α-primase, is a four-subunit complex wherein two subunits are responsible for DNA priming activity (PRIM1, PRIM2) and two subunits are responsible for DNA polymerase α (Pol α) activity (POLA1, POLA2). DNA primase initiates ribonucleic acid (RNA) synthesis *de novo* and intramolecularly transfers the mature RNA primer to Pol α for subsequent extension with deoxynucleoside triphosphates (dNTPs). During the initiation step, DNA Primase Subunit 1 (PRIM1, also known as p49) binds to the DNA template and two cognate ribonucleotide triphosphates (rNTPS), one at the initiation site and the other at the elongation site, and catalyzes the formation of a dinucleotide (Baranovskiy et al., 2016a; Baranovskiy et al., 2016b; Copeland and Wang, 1993; Sheaff and Kuchta, 1993). Structural studies suggest DNA Primase Subunit 2 (PRIM2, also known as p58) binds and holds the RNA-DNA duplex, the 5' triphosphate of the RNA primer and 3' overhang of the DNA template (Baranovskiy et al., 2016b). While PRIM2 holds the RNA-DNA heteroduplex, PRIM1 catalyzes the attachment of rNTPs to the 3' end of the developing RNA primer.

Biochemical evidence suggests Pol α-primase does not dissociate from the primer during the transition from RNA to DNA synthesis and that there is an intramolecular mechanism of RNA primer transfer between the active sites of primase and Pol α within the primosome itself (Copeland and Wang, 1993; Kuchta et al., 1990; Sheaff et al., 1994). The Baranovskiy structure suggests that the nature of this transfer may be the result of a counting mechanism for determining an optimal RNA primer length. Due to the strength of the PRIM2 bond with the 5' RNA end, PRIM2's helical carboxyl terminal domain (CTD) spirals away from PRIM1. These studies propose that after synthesizing a 9 mer primer,

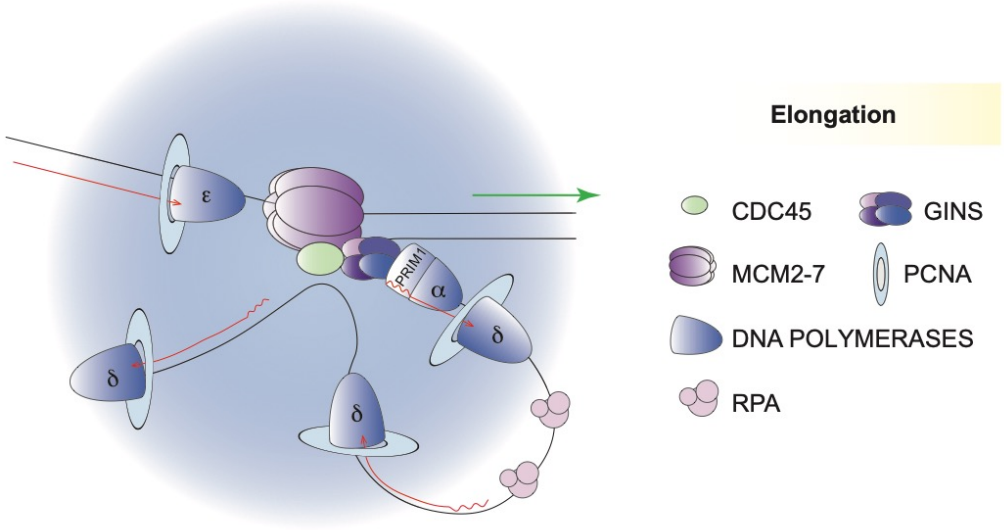

Figure 1.3. Mammalian DNA replication elongation.
During DNA replication elongation, CMG unwinds the DNA duplex creating ssDNA that is coated by RPA. Subsequently the primase makes and deposits an RNA primer to provide a 3'-hydroxyl group for the DNA polymerases to continue synthesis. PCNA increases the processivity of the DNA polymerases and provides a platform for the recruitment of other factors. The diffuse blue cloud represents over 500 proteins at the replisome, many which remain functionally undescribed.

steric hindrance between PRIM2's helical CTD with PRIM2's amino-terminal domain (NTD) forces the transfer of the RNA-DNA template to the polymerase subunits. This model of intramolecular transfer predicts that if the primase components do not successfully synthesize a 9 mer primer, there is no steric hindrance and the 3' end of the primer will not reach Pol α's active site (reviewed in (Baranovskiy and Tahirov, 2017)).

After the RNA primer is intramolecularly transferred, Pol α then extends up to an additional 20 nucleotides with dNTPs, yielding an approximately 30-nucleotide chimeric primer, called the α segment. After synthesis of the α segment, Pol α is replaced with DNA polymerase ε (Pol ε) or DNA polymerase δ (Pol δ). Pol α does not contain proofreading activity and thus polymerase switching occurs to maintain the fidelity of the genetic code. Single-molecule analysis using a mutant of Pol α-primase that is able to produce RNA primers but is unable to extend these primers with dNTPs shows that the DNA polymerase activity of Pol α-primase is not required for processive synthesis (Lewis et al., 2019).

The antiparallel structure of the DNA double helix and the 3'-5' direction of the DNA polymerases' catalytic activity confine the mechanism of replication, resulting in leading- and lagging-strand synthesis. The leading-strand is synthesized in the same direction as the movement of the replication fork while the lagging-strand is synthesized in the opposite direction. On the leading-strand, Pol ε replaces Pol α on the CTD-tier of CMG (Bai et al., 2017) and replication elongation proceeds continuously as the CMG helicase unwinds more DNA ahead of Pol ε (Clausen et al., 2015; Miyabe et al., 2011; Nick McElhinny et al., 2008; Pursell et al., 2007; Sun et al., 2015). On the lagging-strand, Pol δ replaces Pol α for continued synthesis (Bai et al., 2017). The lagging-strand must be continually primed to provide new 3' ends for extension as the CMG helicase unwinds DNA behind Pol δ. The lagging-strand is thus synthesized in short fragments, named Okazaki fragments (OF) (Okazaki et al., 1968; Sakabe and Okazaki, 1966).

The replicative polymerases have high polymerase fidelity due to their structure resembling a clasped right hand holding a string that creates a tight active site intolerant of misalignment between the template base and incoming nucleotide. Pol ε and Pol δ both contain exonucleolytic activity to further increase their fidelity (Byrnes et al., 1976);(reviewed in (Pursell and Kunkel, 2008)). However, given the sizes of OFs and chimeric primers, the Pol α-primase synthesizes up to twenty percent of the lagging-strand and, therefore, approximately ten percent of the genome is synthesized by a polymerase without exonucleolytic activity and subject to an increased nucleotide misincorporation rate. These misincorporated ribonucleotides can be removed by the mismatch repair (MMR) pathway.

The pentameric clamp loader, Replication Factor C (RFC), is responsible for loading the sliding clamp, Proliferating Cell Nuclear Antigen (PCNA), at the primer-template junction (reviewed in (Moldovan et al., 2007)). PCNA is a ring-shaped homotrimer that encircles DNA, tethering the polymerases to DNA and dramatically

increasing their processivity (the number of nucleotides a polymerase can synthesize before falling off) (Bravo et al., 1987; Prelich et al., 1987; Tan et al., 1986). PCNA also serves as a central hub for recruiting and regulating other factors at the replication fork for a variety of processes. Most interacting partners bind to PCNA via a PIP (PCNA-interacting peptide) box, generally containing a consensus PIP sequence (Jónsson et al., 1998; Prestel et al., 2019). The PIP-box sequence of PCNA interacting partners binds to the hydrophobic pocket on the front face of PCNA, which points in the direction of DNA synthesis (reviewed in (Boehm et al., 2016; Choe and Moldovan, 2017)).

A minimal set of factors purified from *S. cerevisiae* can recapitulate DNA synthesis *in vitro*, but many additional components are required for efficient replication. For example, Csm3 (human homolog Timeless-interacting protein (TIPIN)), Tof1 (human homolog TIMELESS), and Mrc1 (human homolog Claspin (CLSPN)), are a part of the replisome progression complex (RPC) and facilitate maximal replication speeds in yeast (Cho et al., 2013; Gambus et al., 2006; Lewis et al., 2017; Masai et al., 1999; Smith-Roe et al., 2013; Yeeles et al., 2017). Until recently, most biochemical replication experiments have been performed with naked DNA templates and thus it is important to remember that DNA replication in mammalian cells occurs in a more complex environment. *In vitro* experiments in *S. cerevisiae* have begun to address replication in the context of chromatinized DNA and have identified several chromatin remodeling proteins as essential for achieving maximal replication speeds. These factors include the FACT complex, Nhp6, INO80, ISW2A, pNuA4, and pSAGA (Kurat et al., 2017). There is a growing understanding of the complexity of DNA elongation in yeast, but still many of the proteins identified at the mammalian replisome have yet to be functionally defined. In human cells, there are over 500 proteins that travel with the replication fork (Alabert et al., 2014; Dungrawala et al., 2015; Sirbu et al., 2013; Wessel et al., 2019).

While it is easy to imagine DNA replication as a linear process, where two replication forks generated from the same origin move away from one another, it has been proposed that DNA replication occurs in specific nuclear structures, called replication factories. This model of DNA replication proposes that the molecular machinery for multiple replication forks are brought together at distinct loci (Hozák et al., 1993; Kitamura et al., 2006). In these replication factories, parental DNA is pulled through and nascent strands are extruded allowing for the two replication forks generated from the same origin to remain associated with one another.

1.2.3 Okazaki fragment maturation

Okazaki fragment (OF) maturation, the process by which lagging-strand fragments are joined together, involves the removal of the RNA primer, either by direct enzymatic processing or by strand displacement of the RNA primer resulting in a flap that must be enzymatically processed. To complete maturation, OFs are then ligated. The mechanisms of RNA primer removal are also relevant to the processing of the leading-strand primer, albeit at a much lower frequency. In eukaryotes, there are three models of

RNA primer removal to allow for OF maturation. The usage and interplay between these pathways are unknown (reviewed in (Balakrishnan and Bambara, 2013; Giannattasio and Branzei, 2019; Kao and Bambara, 2003)) (Figure 1.4).

In the first model, RNA-DNA primers are hydrolyzed directly by the ribonuclease H2 (RNase H2) complex (Qiu et al., 1999b) (Figure 1.4A). RNase H2 cleaves all ribonucleotides of the RNA primer except the last one (between the 3'-most rNTP and initial dNTP) which is removed by a 5' DNA exonuclease, either flap endonuclease 1 (FEN1) or exonuclease 1 (EXO1) (Liu et al., 2017). In yeast, RNase H2 can degrade the RNA primer (Murante et al., 1998; Turchi et al., 1994). However, deletion of RNase H2, RNase H1, or the combination of both, does not cause an obvious phenotype and thus the processing by RNase H2 is judged to be a backup pathway of OF processing in *S. cerevisiae* (Chen et al., 2000; Ohle et al., 2016; Qiu et al., 1999b). The contribution of RNase H2 to OF removal in the mammalian system has yet to be convincingly assessed.

In the other two models (Figure 1.4B,C), RNA-DNA primers are displaced by Pol δ, creating a single-strand DNA flap. These flaps, either short (2-10 nucleotides) or long (>20 nucleotides), are differentially processed based on their length. The short flap pathway is thought to be the predominant pathway of OF maturation. The short flap structure is cleaved by FEN1. It has been proposed that the interaction between Pol δ's 3' exonuclease and polymerase activities limits forward movement of 2-3 nucleotides and thus several cycles of Pol δ-driven removal and gap-filling coupled with Fen1-mediated flap cleavage occur until the α segment is completely removed (Garg et al., 2004; Jin et al., 2003; Jin et al., 2001; Maga et al., 2001).

In the event that strand displacement synthesis becomes uncoupled from flap cutting, an alternative model is proposed. This third model (Figure 1.4C), the long flap pathway, differs from the short flap pathway due to an increase of the flap size perhaps because of a missed cleavage opportunity (Zaher et al., 2018). These long flaps are recognized and bound with RPA, which inhibits the flap endonuclease activity of FEN1, but recruits DNA2 and stimulates DNA2 nuclease activity to cleave the flap to a shorter size (Ayyagari et al., 2003; Bae et al., 2001; Bae and Seo, 2000; Kao et al., 2004; Zaher et al., 2018). The now short flap is then processed using the short flap pathway. The long flap pathway's relevance to the mammalian system remains unclear as there is no strong evidence for a role of DNA2 in OF maturation analogous to its role in yeast. It is unknown at what rate long flaps are generated in the mammalian system, whether FEN1 and EXO1 alone can process them, or whether additional factors are needed for their resolution. Once the RNA primer is removed from the preceding OF and Pol δ has synthesized the intervening region with DNA, DNA ligase I (LIG1) functions to seal the nick between OFs.

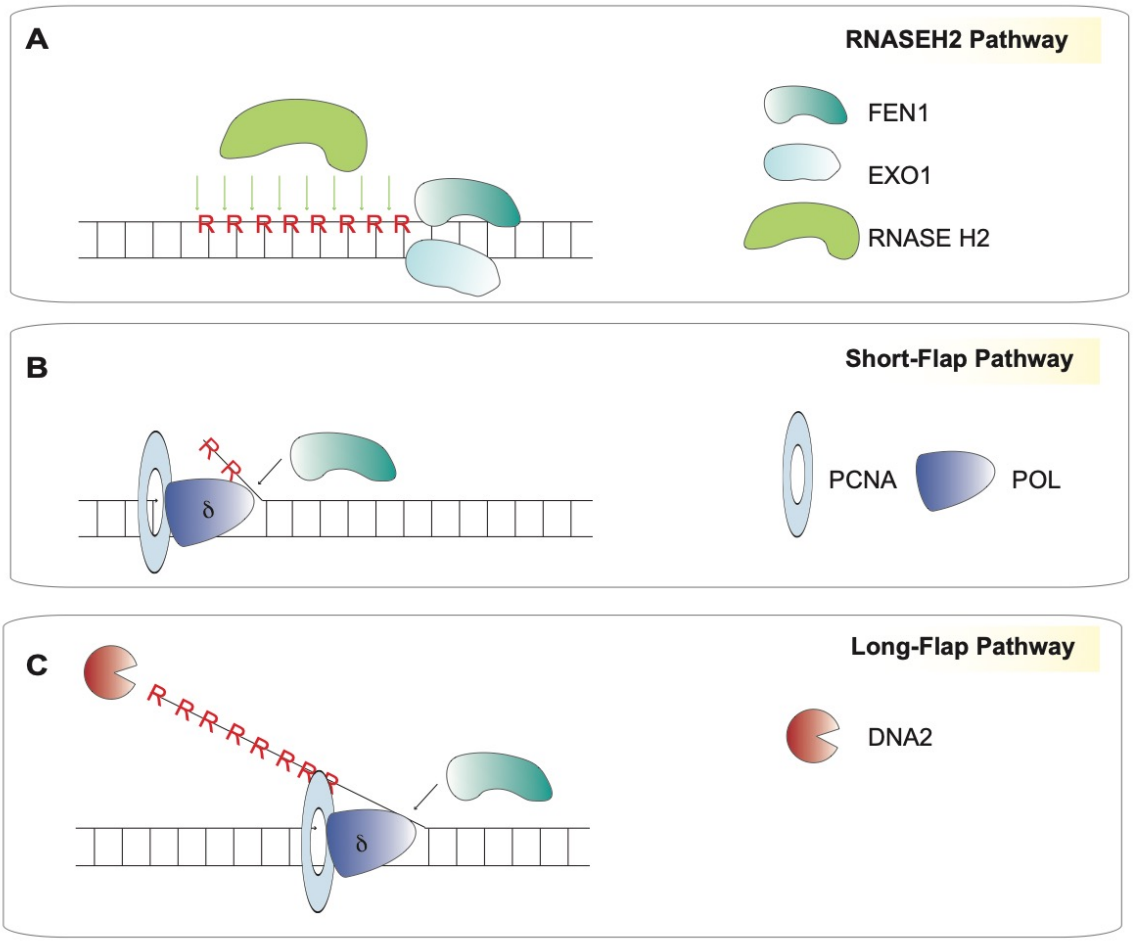

Figure 1.4. Models of RNA primer removal and Okazaki fragment maturation. RNA primers must be removed from newly synthesized daughter strands to allow for the OFs to be ligated together, producing a fully replicated lagging-strand. There are three models of RNA primer removal. (A) RNase H2 can cut 5' to any genome-embedded ribonucleotide. Since RNase H2 does not have activity on the 3' end, Fen1 or Exo1 function to fully remove the primer cutting the 3' end of the DNA-embedded ribonucleotide. (B,C) Both the short flap and long flap pathway rely on Pol δ–dependent displacement of the RNA primer on the preceding OF. The short flap undergoes nucleolytic processing by Fen1. The long flap must first be degraded from the 5' end by Dna2 until a short flap that can be processed by Fen1 is generated.

1.2.4 Termination of DNA replication

DNA replication termination occurs when two replication forks progressing bidirectionally encounter each other moving in opposite directions. Previously thought to be a passive process, recent characterization of termination suggests there is active disassembly of the replisome (reviewed in (Bailey et al., 2015; Dewar and Walter, 2017)).

Studies from *X. laevis* and *S. cerevisiae* suggest a mechanism of replisome disassembly. DNA replication termination does not occur until converging CMGs pass one another, providing a way to avoid premature replisome disassembly (Dewar et al., 2015). Disassembly of the replisome requires cullin ubiquitin ligase (E3)-dependent ubiquitination of MCM7 (K-48 chains) occurs. This ubiquitin chain is recognized by VCP/p97, resulting in the removal of MCM7 from chromatin (Dewar et al., 2017; Maric et al., 2014; Moreno et al., 2014) and the inactivation of the CMG helicase. This process emphasizes the importance of proteasome-mediated turnover of replication factors (Figure 1.5A).

Similar to initiation, termination is generally stochastic, however, there are examples of precise DNA termination sites. These sequences can be sequence-specific replication fork barriers, such as *Ter* sites in *S. cerevisiae* (Hidaka et al., 1989), the *Replication Termination Site 1* (*RTS1)* site in *Schizosaccharomyces pombe* (Dalgaard and Klar, 2001)*,* or rDNA loci in mammalian cells (Little et al., 1993). Polar termination of DNA replication occurring in the rDNA locus is dependent on the cis-acting factors, TTF1 (human homolog of *S. pombe* Rtf1), TIPIN, and TIMELESS (Gerber et al., 1997) (Figure 1.5B).

1.3 Replication-coupled DNA repair

DNA replication is a highly regulated process whereby the genetic information is duplicated. The replication machinery encounters many challenges that threaten the transmission of genetic information in an accurate and timely manner. The term “replication stress” encompasses the diverse ways that progression of the replisome may be hindered, slowed or completely stalled (reviewed in (Zeman and Cimprich, 2014). Since replication stress obstructs the completion of accurate and efficient replication, the cell has mechanisms to repair lesions that contribute to replication stress. While repair can occur outside of S phase, these lesions also need to be addressed promptly during DNA replication.

Replication-coupled DNA repair refers to the mechanisms that process DNA damage and replication challenges in coordination with the replisome to maintain genome stability (reviewed in (Cortez, 2019)). This section will discuss various sources of replication stress that threaten the fidelity of DNA replication. I will discuss how cells

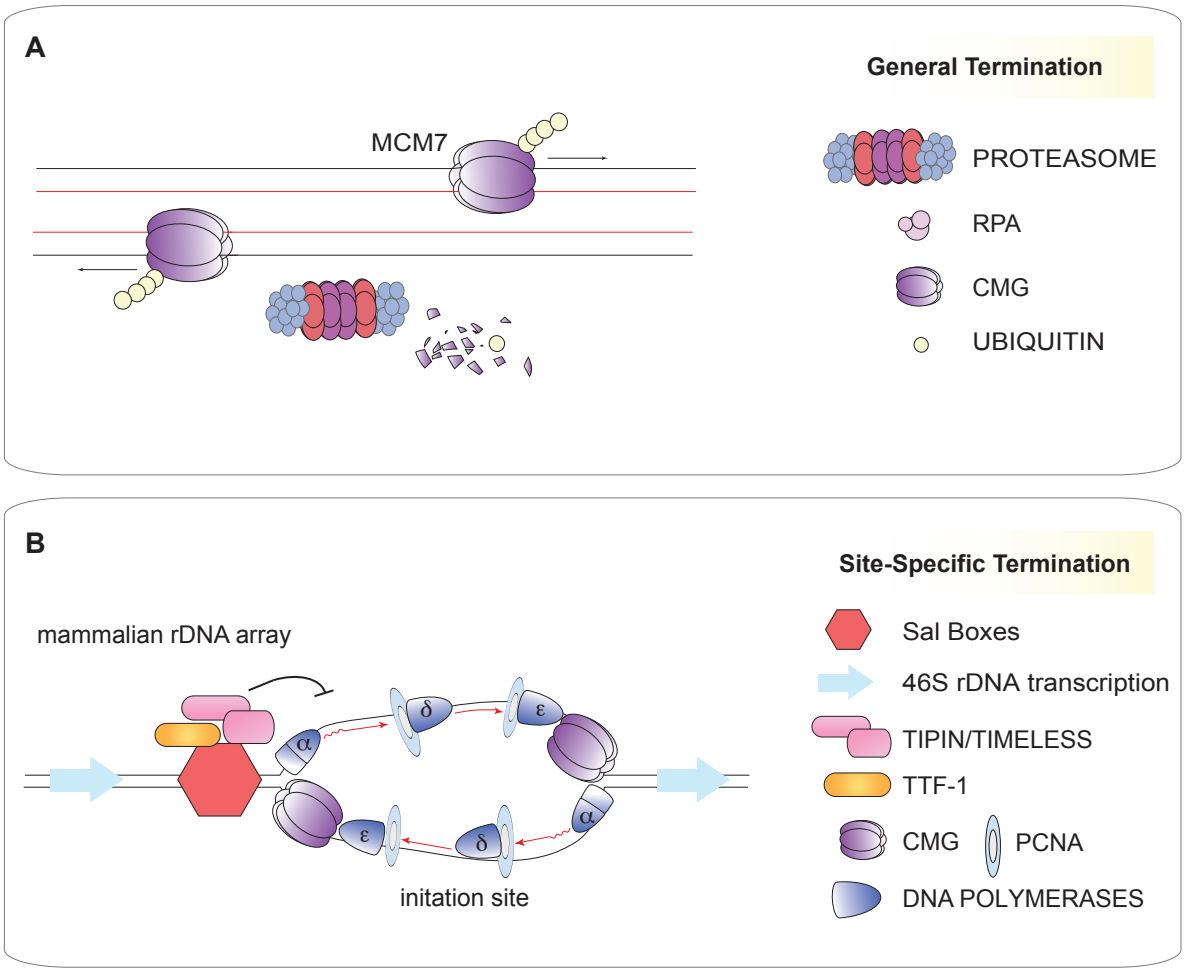

Figure 1.5. Mammalian DNA replication termination.
(A) General replication termination requires active removal of the MCM7 subunit of the CMG complex. This removal is dependent on Cullin E3 (Cullin RING Ligase 2 associated with Leucine Rich Repeats 1 ($CRL2^{Lrr1}$) in *X. laevis*)) K-48 ubiquitination and VCP/p97 extraction of MCM7. (B) Replication termination at site-specific barriers is also an active process. At the mammalian rDNA array, replication termination prevents head-on collisions between the replication and transcription machinery. Site-specific termination occurs at specific loci. In the case of the rDNA replication fork barrier, Sal boxes and flanking sequences direct the location of termination. Cis-regulatory factors, such as TTF-1 (Rtf1 in S. pombe), TIPIN, and TIMELESS, promote replication termination at these sites.

respond to these challenges, and how stalled replication forks are restarted. The inability to deal with these challenges is a genome-destabilizing event. As mentioned throughout this section, mutations in proteins involved in the processes to maintain genome stability often result in human disease.

1.3.1 Sources of replication stress

There are many endogenous sources of replication stress. Changes in the DNA template, including damaged bases, and mis-incorporated nucleotides or ribonucleotides, must be removed and the DNA strand must be repaired during DNA replication to ensure faithful transmission of the genetic material (reviewed in (Ganai and Johansson, 2016)). Bases damaged by oxidation, deamination, or alkylation, among other modifications, may induce mutation. Mis-matched nucleotides can also be incorporated into the DNA nascent strand, which occurs more frequently on the lagging-strand than the leading-strand due to Pol α's lack of exonuclease activity. Dedicated cellular pathways exists to remove these lesions outside of S phase, however, their persistence during replication presents challenges to the replicative polymerases and/or results in genomic instability and mutation. Lesions that pause the replicative polymerases and completely block replication include unrepaired damaged bases or base modifications, such as abasic sites, and larger obstacles like R-loops, transcribing RNA polymerases, unusual DNA structures, interstrand crosslinks (ICLs), and DNA-protein complexes (DPCs). While some lesions, such as ICLs and DPCs, were thought to also block the replicative helicase, evidence is accumulating to show that the helicase can bypass these lesions (Huang et al., 2013; Huang et al., 2019; Sparks et al., 2019), leaving polymerase stalling as the main challenge to overcome.

Replication stress is exogenously induced using replication stress-inducing drugs or radiation. Examples of these chemicals include hydroxyurea (HU), which depletes nucleotide pools by inhibiting ribonucleotide reductase ((Akerblom et al., 1981; Dresler and Stein, 1869; Reichard and Ehrenberg, 1983); reviewed in (Singh and Xu, 2016)); aphidicolin, which directly inhibits B-family polymerases (Baranovskiy et al., 2014; Bucknall et al., 1973; Cheng and Kuchta, 1993; Ikegami et al., 1978); Mitomycin C (MMC), and Cisplatin (Siddik, 2003), which both induce ICLs, among other chemicals. Exposure to UV radiation can inhibit replication fork progression. In response to these insults, cells have repair mechanisms to help respond, recover and resume DNA replication.

1.3.2 Aberrant incorporation of ribonucleotides

Aberrant incorporation of ribonucleotides into genomic DNA, estimating about one ribonucleotide incorporation event per ~ 0.7kb replicated DNA, is one of the largest endogenous sources of replication stress in the cell (Sparks et al., 2012). rNTPs are structurally similar to dNTP but contain an additional hydroxyl (-OH) group on the 2' position of the ribose sugar. This additional hydroxyl group makes the rNTP base far more labile and capable of generating breaks. The most abundant source of genome-

embedded ribonucleotides is from the repeated RNA priming of the lagging-strand during DNA replication (reviewed in (Kuchta and Stengel, 2010)). Cells have developed processes (described in section 1.2.5) to remove these ribonucleotides from OFs, ideally making the presence of ribonucleotides transient.

In addition to RNA primers, the replicative polymerases can incorporate rNTPs during elongation synthesis, albeit at a lower frequency than dNTPs due to their steric gate (Table 1) (Brown and Suo, 2011; Clausen et al., 2013; Goksenin et al., 2012; Nick McElhinny et al., 2010); (reviewed in (Williams et al., 2016)). An overabundance of rNTP pools relative to dNTP pools also causes DNA polymerases to incorporate rNTPs into the nascent strands (Yao et al., 2013). In eukaryotic cells, the concentrations of rNTPs are approximately two orders of magnitude higher than dNTPs (Nick McElhinny et al., 2010).

Other primases, such as Primase and DNA-directed Polymerase (PRIMPOL) (Garcia-Gomez et al., 2013) and polymerases, such as translesion synthesis (TLS) polymerases, incorporate rNTPs during DNA repair pathways (Bergoglio et al., 2003; Cavanaugh et al., 2011; Cilli et al., 2015; Crespan et al., 2016; Donigan et al., 2014; Gosavi et al., 2012; Nick McElhinny and Ramsden, 2003; Pryor et al., 2018); (reviewed in (Williams et al., 2016)). Persistence of single genome-embedded ribonucleotides causes replication slowing due to intrinsic limitations of the polymerases to synthesize across ribonucleotides efficiently (Watt et al., 2011).

1.3.3 Ribonucleotide excision repair

The ribonucleotide excision repair (RER) pathway functions to remove single DNA-embedded ribonucleotides in the genome. Biochemically, RER can be reconstituted *in vitro* with RNase H2, PCNA, Pol δ/Pol ε and Fen1/Exo1 purified from *S. cerevisiae* (Sparks et al., 2012). *In vivo*, RNase H2 activity is essential for recognizing and removing ribonucleotides from RNA-DNA hybrids to prevent the accumulation of single genome-embedded ribonucleotides (Reijns et al., 2012).

RNase H proteins were first described in 1969 as enzymes that hydrolyze the RNA strand of RNA-DNA hybrids (Stein and Hausen, 1969). In eukaryotes, there are two classes of RNase H enzymes with distinct biochemical properties and substrates: Type 1 and Type 2 (Ohtani et al., 1999). Together they are implicated in the resolution of RNA-DNA hybrids in a variety of contexts, including R-loops, OF primers, and single DNA-embedded ribonucleotides (reviewed in (Cerritelli and Crouch, 2009)).

Type 1 enzymes are designated RNase H1 in eukaryotes (RNASEHI in prokaryotes). All eukaryotic RNase H1 enzymes have highly conserved regions at their N- and C-termini separated by a variable sequence. The N-terminus contains a hybrid binding domain (HBD) showing a 25-fold preference for RNA-DNA hybrids compared to dsRNA (Nowotny et al., 2008). In humans, RNASEH1 is an endonuclease that requires

Table 1.1. Ribonucleotide Incorporation Rates

Polymerase	Ribonucleotide Incorporation Rate
Pol ε	1 rNTP per every 1250 dNTPs
Pol δ	1 rNTP per every 5000 dNTPs
Pol α	1 rNTP per every 625 dNTPs

*rates estimated in *S. cerevisiae* (reviewed in (Williams et al., 2016))

three or four consecutive DNA-embedded ribonucleotides for efficient cleavage (Nowotny et al., 2007). Type 2 enzymes are designated as RNase H2 in eukaryotes (RNASEHII in prokaryotes). Type 2 enzymes, heterotrimers in eukaryotes and monomers in prokaryotes, have a unique ability to recognize and cleave the 5'-phosphodiester bond of a single ribonucleotide embedded in a DNA strand (Eder et al., 1993). Purified RNase H2 from *Archaeoglobus fulgidus* demonstrates that RNase H2 prefers junction substrates (similar to OFs) and cleaves 5' to the ribonucleotide (Bubeck et al., 2011). While RNase H2 has some overlapping functions with RNase H1, RNase H1 is generally implicated in the removal of R-loops (Cerritelli et al., 2003; Lima et al., 2016) while RNase H2 is primarily implicated in the removal of RNA primers in OFs or single ribonucleotides (Eder and Walder, 1991; Eder et al., 1993; Murante et al., 1998; Reijns et al., 2012; Turchi et al., 1994).

In mammals, the RNase H2 complex, composed of RNASEH2A, RNASEH2B, and RNASEH2C, is essential (Reijns et al., 2012). The individual subunits of the RNase H2 complex are diverse in terms of both primary structure and function. RNASEH2A serves as the catalytic core of the complex. RNASEH2B and RNASEH2C are non-catalytic accessory subunits (Chon et al., 2009). RNASEH2B contains a PIP-box thought to localize the RNase H2 complex to PCNA and the replication fork (Bubeck et al., 2011; Chon et al., 2009) while RNASEH2C spans the interface between RNASEH2A and RNASEH2B. RNase H2 may also be recruited to the replication fork in a PCNA-independent manner (Kind et al., 2014). The RNase H2 complex, unlike RNASEH1, travels with the replication fork machinery (Alabert et al., 2014; Dungrawala et al., 2015; Wessel et al., 2019).

In *S. pombe*, neither rnh1 (RNase H1), rnh201 (RNase H2 catalytic subunit), nor the combination of both is required for growth; therefore, these genes are not essential in yeast (Ohle et al., 2016). Despite RNase H2 not being essential in yeast, unlike in metazoans, yeast models are useful to understand RNase H2's function. A separation of function mutation in RNase H2, termed the ribonucleotide excision repair defective (RED) allele (P45D/Y219A) was identified in yeast (Chon et al., 2013) and parallel mutations were made in mammalian cells (P40D/Y210A) (Uehara et al., 2018; Zimmermann et al., 2018). This mutant retains catalytic activity, albeit reduced, against RNA-DNA hybrids, but not single DNA-embedded ribonucleotides. In yeast, alleles of *rnh202* (homolog of RNASEH2B) in which expression of the proteins was restricted to either the S or G2/M phase of the cell cycle were generated (Lockhart et al., 2019). Cells with S phase-restricted expression of *rnh202* and a mutant allele of the catalytic subunit of Pol ε (*pol2M644G*), which increases the ribonucleotide incorporation rate 10x, were sensitive to hydroxyurea, whereas cells with G2/M phase-restricted expression of *rnh202* and *pol2M644G* were not, suggesting RNase H2 expression in G2/M phase, not S phase, is required to tolerate genome-embedded ribonucleotides (Lockhart et al., 2019). It is unknown whether this is also the case in mammalian cells.

In the absence of RNase H2, yeast, mice, and human cells accumulate millions of single genome-embedded ribonucleotides (Kim et al., 2011; Reijns et al., 2012; Zimmermann et al., 2018). As a compensatory mechanism, topoisomerase 1 (TOP1) processes these ribonucleotides on the leading-strand. In this reaction, the tyrosine residue of TOP1 covalently binds the 3' terminal phosphate of the ribonucleotide, forming a TOP1 cleavage complex. The TOP1-phosphate bond is prone to attack from the adjacent 2' -OH groups of the ribose moiety, resulting in TOP1 release and the creation of a 2',3' cyclic phosphate (Kim et al., 2011). This 2',3' cyclic phosphate is recognized by Poly [ADP-ribose] polymerase 1 (PARP1). Downstream processing of this 2',3' cyclic phosphate can result in gaps and double-strand breaks and consequently 2-5 nucleotide base deletions are generated (Kim et al., 2011; Sekiguchi and Shuman, 1997; Sparks and Burgers, 2015; Williams et al., 2013; Zimmermann et al., 2018).

In mice, loss of the RNase H2 complex leads to embryonic lethality, which is attributed to elevated DNA damage and reduced cellular proliferation during gastrulation (Hiller et al., 2012; Lima et al., 2016; Reijns et al., 2012). Loss of *Rnase2b,* specifically in basal cells of mouse skin epithelium, is implicated in squamous cell carcinoma (Hiller et al., 2018). In humans, pathogenic variants in any of the three RNase H2 subunits result in Aicardi-Goutières Syndrome (AGS), a disease first described in the 1980s when Jean Aicardi and Françoise Goutières reported eight children from five families with early onset encephalopathy characterized by basal-ganglia calcification, white matter abnormalities, chronic cerebrospinal fluid (CSF) lymphocytosis and raised levels of interferon alpha (IFN-α) in the CSF (Aicardi and Goutieres, 1984; Lebon et al., 1988). Since then, disease causing pathogenic variants have been identified in several genes, including all 3 subunits of *RNASEH2*, Three prime repair exonuclease 1 (*TREX1*), SAM and HD Domain Containing Deoxynucleoside Triphosphate Triphosphohydrolase (*SAMHD1*), Interferon Induced With Helicase C Domain 1 (*IFIH1)*, and Adenosine Deaminase RNA Specific (*ADAR*) (Oda et al., 2014; Rice et al., 2007; Rice et al., 2009; Rice et al., 2012). Finally, frequent deletion of RNASEH2B occurs in metastatic prostate cancer and chronic lymphocytic leukemia (Zimmermann et al., 2018). There are no known cancer associations for RNASEH2A or RNASEH2C, but The Cancer Genome Atlas and cBioPortal show that amplifications of RNASEH2A and RNASEH2C occur more frequently than deletions across various cancer types.

1.3.4 S phase-specific DNA damage responses

A universal response to replication fork stalling is often the formation of stretches of ssDNA. This ssDNA may be a result of functional polymerase-helicase uncoupling that occurs when the polymerase stalls and the replicative helicase continues to unwind dsDNA (Byun et al., 2005). RPA binds ssDNA and serves as a recruitment platform for many factors, including ATR interacting protein (ATRIP), which facilitates the association of ATR (Zou and Elledge, 2003) (Figure 1.6), a member of the phosphoinositide 3- kinase (PI3K)-related protein kinases (PIKKs) family, which includes ataxia-telangiectasia

mutated (ATM) and DNA dependent protein kinase, catalytic subunit (DNA-PKcs) (reviewed in (Saldivar et al., 2017)).

The persistence of ssDNA facilitates downstream activation of ATR (Figure 1.6). Activation of ATR requires additional proteins, TOPBP1 and ETAA1. RAD9-RAD1-HUS1 (9-1-1) complex binds at the 5'-ended ssDNA-dsDNA junction and recruits TOPBP1 for ATR activation (Delacroix et al., 2007; Lee et al., 2007a). Long patches of ssDNA facilitate recruitment of ETAA1 (through RPA binding) (Bass et al., 2016; Haahr et al., 2016) (Figure 1.6). ETAA1 and TOPBP1 function in parallel pathways to activate ATR, but recent data suggest that ETAA1 may be more important for controlling cell division processes unrelated to DNA damage response pathways, such as regulation of the spindle assembly checkpoint (Bass and Cortez, 2019).

Persistence of RPA-bound ssDNA also results in the phosphorylation of RPA. The PIKKs phosphorylate distinct sets of RPA residues in response to replication stress. ATR primarily functions to phosphorylate RPA32 on serine residue 33 (P-RPA S33). Although DNA-PKcs is classically defined as a factor important for non- homologous end joining (NHEJ) repair of double-strand breaks (DSBs), DNA-PKcs has also been implicated in the response to replication stress and functions to phosphorylate RPA32 on serine residues 4 and 8 (P-RPA S4/8) (Ashley et al., 2014; Liaw et al., 2011; Liu et al., 2012) and threonine residue 21 (P-RPA T21). Hyperphosphorylation of RPA, including P-RPA S4/8, is important for checkpoint signaling and Checkpoint Kinase 1 (CHK1) activation (Liu et al., 2012).

ATR orchestrates multiple downstream events in response to replication stress, including cell cycle arrest, global origin firing suppression, local origin activation, DNA repair, and replication fork restart. These downstream responses are largely dependent on the activation of CHK1 by ATR-dependent phosphorylation on serine residues 317 and 345 (P-CHK1 S317 and P-CHK1 S345) (Zhao and Piwnica-Worms, 2001). CHK1 facilitates several responses, including the degradation of CDC25A as previously mentioned in Section 1.2.1. (Falck et al., 2001; Sorensen et al., 2003), to inhibit DNA replication initiation globally. ATR, however, also promotes origin firing locally (Ge and Blow, 2010; Maya-Mendoza et al., 2007; Petermann and Caldecott, 2006; Petermann et al., 2006; Petermann et al., 2010b). Thus ATR's ability to suppress new origin firing distally, but activate origins locally, allows for replication to continue (reviewed in (Saldivar et al., 2017)).

1.3.5 Direct replication fork restart pathways: re-priming, translesion synthesis and template switching

When a replication fork stalls, it must be rescued by another replication fork or restarted in a timely manner to allow for the completion of DNA synthesis. Since only a portion of potential replication origins are used in a given S phase, the activation of

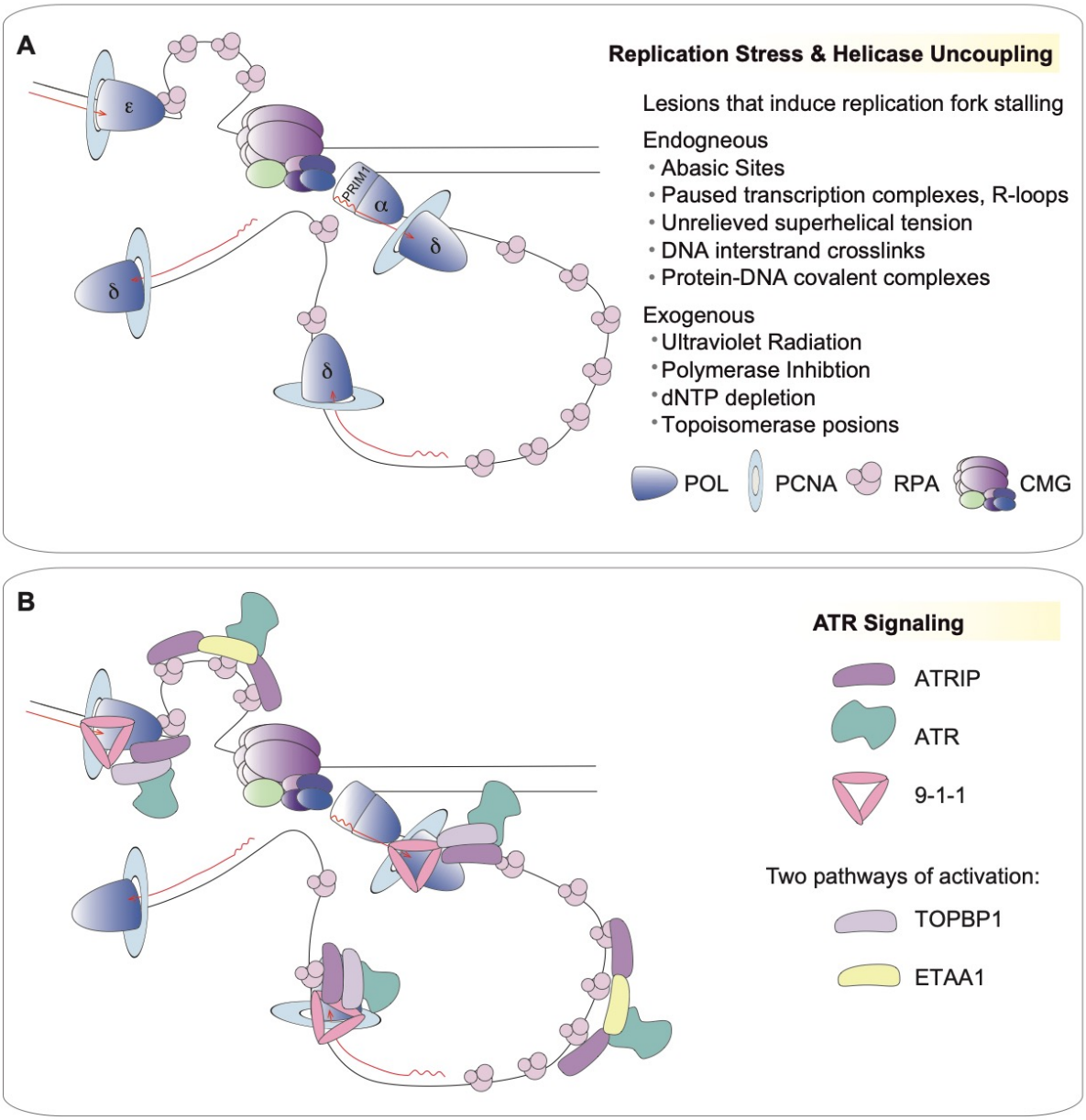

Figure 1.6. Replication stress and ATR activation.
(A) Many sources of replication stress stall replicative polymerases and completely block nascent strand synthesis. Polymerase-helicase uncoupling results in generation of ssDNA at replication forks. (B) RPA binds ssDNA and serves to recruit ATRIP. ATRIP binding facilitates ATR association, but ATR activation requires TOPBP1 or ETAA1. The 9-1-1 checkpoint complex binds at the 5'-end of the ssDNA-dsDNA junction and recruits TOPBP1 whereas RPA recruits ETAA1, localizing the activation of each to distinct regions of the replication fork. The active ATR kinase phosphorylates downstream targets to facilitate a replication stress response.

‘dormant’ origins allows for completion of DNA replication without removal of the blocking lesion, bypass of the lesion, or restart of the stalled replication fork (Ge et al., 2007). The newly fired origin completes replication upon collision with the compromised replication fork (Figure 1.7). In the event that no dormant origins are available in the region of replication stalling, an alternative pathway must be employed to restart DNA replication. I will refer to direct replication restart as the ability to restart a replication fork without disassembly of the replisome or replication fork breakage.

Several pathways have been proposed to promote direct replication restart of the compromised replication fork, including re-priming downstream of the lesion, lesion bypass with the use of translesion synthesis (TLS) polymerases, or lesion bypass via template switching (TS) (reviewed in (Berti and Vindigni, 2016; Heller and Marians, 2006; Petermann and Helleday, 2010; Yeeles et al., 2013)). Though TLS and TS can function at the replication fork itself as modes of lesion bypass, most studies address these pathways in the context of post-replicative repair.

A reversed fork substrate is an important intermediate replication structure that forms at a stalled replication fork. Fork reversal is an active remodeling of the replication fork, where the branch migrates backward to form a “chicken foot” structure and the nascent strands anneal to each other (Sogo et al., 2002). It has been hypothesized that reversed forks are intermediate replication fork structures that assist in replication fork restart upon treatment with genotoxic agents without fork breakage. For example, fork reversal can stabilize the stalled replication fork until a distal origin can rescue it. Secondly, reversed forks also provide the ability to restart replication by placing a blocking lesion back in the context of dsDNA where repair pathways can recognize and remove the lesion. Restoration of a normal fork in this context will allow replication to efficiently restart. Finally, fork reversal can allow for TS to bypass the lesion and subsequently restore and restart the replication fork.

1.3.5.1 Re-priming

Re-priming, the process of synthesizing a primer downstream of a lesion, was first conceptually proposed in studies from *Escherichia coli* that found an accumulation of ssDNA in nucleotide excision repair (NER)-deficient cells that continued to replicate following UV irradiation (Iyer and Rupp, 1971; Rupp and Howard-Flanders, 1968). Re-priming is an effective mechanism to resume synthesis directly at the replication fork, but it also leaves behind gaps of ssDNA that need to be repaired post-replicatively. The mechanistic details of re-priming in mammalian cells require further elucidation.

Re-priming is dependent on the Archaeo-Eukaryotic Primase (AEP) superfamily of proteins, which are responsible for synthesizing new primers (Figure 1.7B). In mammals, there are only two identified members of the AEP superfamily: PRIM1 (the primase catalytic subunit of DNA Polymerase α (Pol α)-primase) and PRIMPOL. The factors

Figure 1.7. Replication fork restart pathways in response to stress.
(A) ATR-dependent activation of a 'dormant' origin can rescue a stalled replication fork to allow for completion of DNA synthesis. In the absence of fork rescue, the compromised replication fork must be restarted to continue DNA synthesis. Direct replication fork restart may occur via (B) PRIM1- or PRIMPOL-dependent re-priming, (C) translesion synthesis, or (D) template switching. (E) In mammalian cells, fork reversal, mediated by HLTF, ZRANB3, SMARCAL1, FBH1, and RAD51 contributes to template switching and replication fork restart. (F) In the absence direct replication restart, replication forks may collapse. DSBs can be generated when the replisome encounters a SSB and upon nucleolytic cleavage. Replication can be restarted with the use of BIR- or HR-dependent pathways.

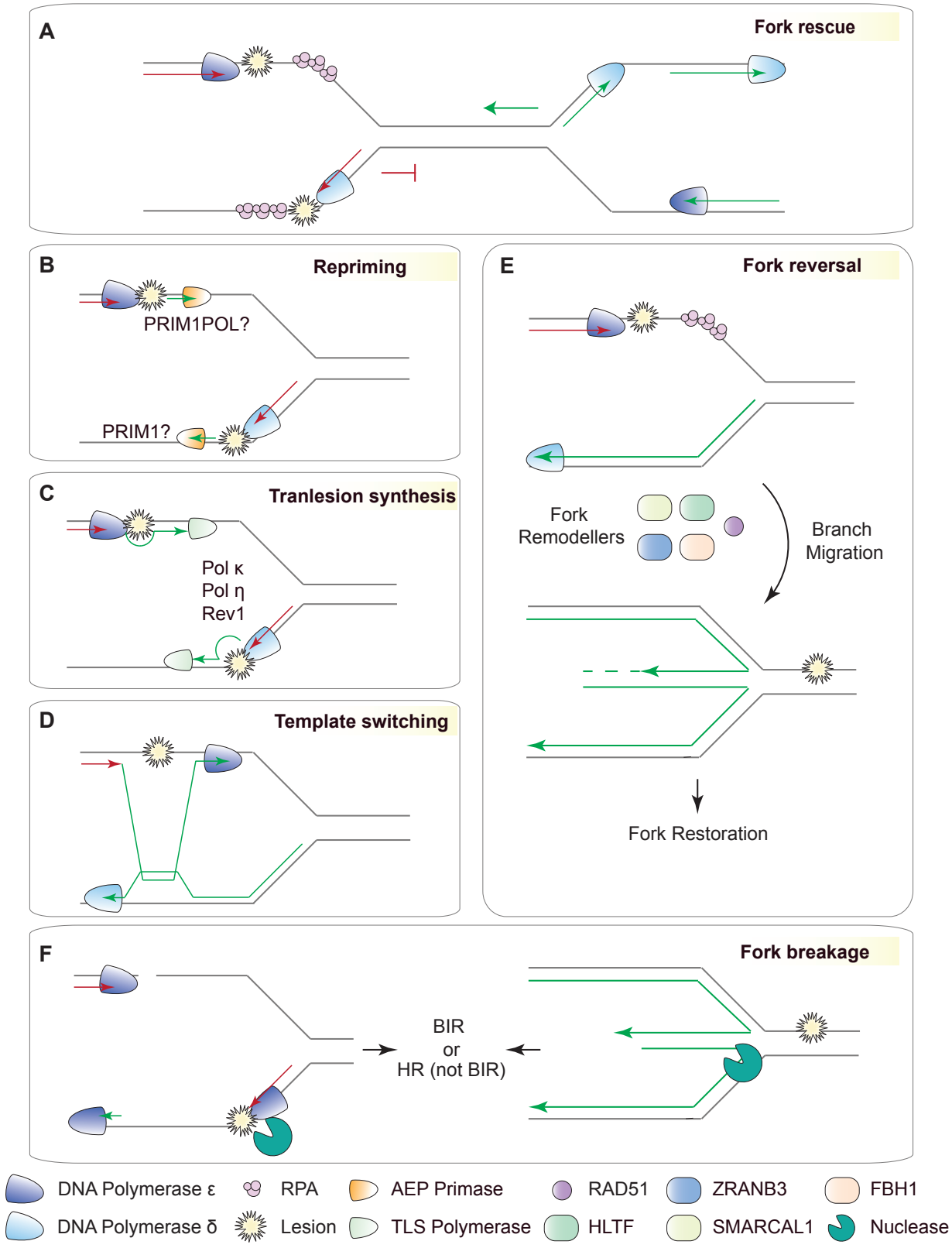
A
Fork rescue
B
Repriming
PRIM1POL?
PRIM1?
C
Tranlesion synthesis
Pol κ
Pol η
Rev1
D
Template switching
E
Fork reversal
Fork
Remodellers
Branch
Migration
Fork Restoration
F
Fork breakage
BIR
or
HR (not BIR)
DNA Polymerase ε
DNA Polymerase δ
RPA
Lesion
AEP Primase
TLS Polymerase
RAD51
HLTF
ZRANB3
SMARCAL1
FBH1
Nuclease

determining the usage of PRIM1 or PRIMPOL for re-priming may be complex, but a favorable model is that usage differs depending on the location of the lesion in either the lagging- or leading-strand template.

Evidence suggests that re-priming occurs efficiently on the lagging-strand for lesion bypass. In bacteria, abasic sites on the lagging-strand do not impede replication *in vitro* (Higuchi et al., 2003; McInerney and O'Donnell, 2004), demonstrating that the ability to synthesize a new OF is a successful method of lesion bypass and replication fork restart. In *Saccharomyces cerevisiae*, experiments that reconstitute DNA replication on templates containing blocking lesions show that lesions on the lagging-strand, but not the leading-strand, can be efficiently re-primed by Pol α-primase (Taylor and Yeeles, 2018). However, Pol α-primase-dependent re-priming on the leading-strand can occur at a subset of stalled forks (Taylor and Yeeles, 2018; Taylor and Yeeles, 2019). PRIM1 travels with the replication fork as a component of Pol α-primase and is responsible for the continued synthesis of RNA primers on the lagging-strand. Thus it is not surprising that PRIM1 functions in re-priming, specifically on the lagging-strand. In *Xenopus laevis* egg extracts, Pol α-primase is hyper-loaded at stalled replication forks by TOPBP1 (Parrilla-Castellar and Karnitz, 2003; Yan and Michael, 2009) and this hyper-loading results in a slight accumulation of small nascent DNAs (Van et al., 2010). Re-priming may also contribute to the activation of ATR by providing 5' ssDNA-dsDNA junctions (MacDougall et al., 2007; Van et al., 2010), furthering the stabilization and repair of stalled replication forks. The contribution of Pol α-primase-dependent re-priming remains to be assessed in response to replication fork stalling in mammalian cells.

Re-priming may also occur on the leading-strand. The first evidence of re-priming to restart replication on the leading-strand came from *in vitro* reconstituted DNA replication studies when it was shown the *E. coli* replisome has the inherent capacity to "skip" over multiple leading-strand lesions via re-priming (Yeeles and Marians, 2011, 2013). Unlike bacteria, biochemical studies in yeast show that re-priming by the replication fork-associated proteins, specifically Pol α-primase, on the leading-strand is inefficient (Taylor and Yeeles, 2018). Since these studies rely on biochemical reconstitution of DNA replication, it is unknown if there are other factors that promote efficient re-priming on the leading-strand. Incubation of DNA templates with human extracts show that bypass of a thymidine dimer can occur on the lagging- or leading-strand (Svoboda and Vos, 1995) suggesting there are mechanisms to bypass a lesion on the leading strand. However, restart in these extracts does not necessarily occur through re-priming as whole cell extracts contain many factors that could be related to the other pathways of restart. Recently, PRIMPOL has implicated in direct replication restart via re-priming in mammalian cells and its function may be most relevant for leading-strand lesion bypass (Bianchi et al., 2013; Garcia-Gomez et al., 2013; Mouron et al., 2013; Schiavone et al., 2016; Wan et al., 2013).

PRIMPOL is a 560 amino acid (AA) protein that contains an N-terminal AEP-like catalytic domain with the conserved I, II, III motifs and a UL52-like zinc finger that support

its polymerase and primase activities (Iyer et al., 2005; Rechkoblit et al., 2016). In addition to retaining the classical primase activity to synthesize primers using rNTPs, PRIMPOL is unique in its ability to also synthesize primers using dNTPs (Bianchi et al., 2013; Garcia-Gomez et al., 2013). The primase activity of PRIMPOL is dependent on a template T and on rATP or dATP as a starting nucleotide (Bianchi et al., 2013). *In vitro* studies also demonstrate that PRIMPOL has TLS polymerase activity (Bianchi et al., 2013; Garcia-Gomez et al., 2013; Makarova et al., 2018; Martinez-Jimenez et al., 2015; Mouron et al., 2013; Zafar et al., 2014). PRIMPOL exhibits low fidelity DNA synthesis, lacking 3'-5' exonuclease activity (Guilliam et al., 2015; Martinez-Jimenez et al., 2015; Mislak and Anderson, 2016; Zafar et al., 2014).

Cellularly the biological relevance of PRIMPOL activity remains an active area of research, especially in regard to re-priming at stalled replication forks. PRIMPOL is present in most compartments of the cell – cytosolic, nuclear and mitochondrial matrix (Garcia-Gomez et al., 2013). Cells are viable without PRIMPOL, but exhibit a growth defect (Mouron et al., 2013). Loss of PRIMPOL induces sensitivity to replication stress-inducing agents, including MMS, cisplatin and UV (Bianchi et al., 2013; Kobayashi et al., 2016), suggesting it is important in the replication stress response. In mammalian cells, PRIMPOL is crucial for restarting replication forks after exposure to UV radiation and BPDE treatment (Bianchi et al., 2013; Mouron et al., 2013; Piberger et al., 2019). Data on the role for PRIMPOL in replication fork restart after treatment with HU is contradictory in the literature with the Wan and Mouron studies, but not the Ercilla study, showing a role for PRIMPOL in replication restart after HU-induced stalling (Ercilla et al., 2019; Mouron et al., 2013; Wan et al., 2013).

Separation of function mutations for PRIMPOL activity have been helpful to decipher PRIMPOL's biological role *in vivo*. A double mutation in the zinc-finger element in the CTD (C419G/H426Y) abolishes its primase activity while preserving polymerase function (Mouron et al., 2013). Mutation of the two catalytic carboxylate residues (D114A/E116A) disrupts both catalytic activities (Bianchi et al., 2013; Garcia-Gomez et al., 2013; Mouron et al., 2013). A point mutation of Y89D retains primase activity while reducing polymerase activity (Keen et al., 2014a; Zhao et al., 2013). A mutation that retains primase activity while completely abolishing polymerase activity has not yet been identified (Keen et al., 2014b), but the identification of such a mutation would be greatly beneficial to further decipher PRIMPOL's cellular function. Complementation of PRIMPOL-deficient cells with mutant PRIMPOL cDNA constructs suggests that PRIMPOL's re-priming function, not its TLS polymerase function, is biologically relevant in regard to the replication stress response. For instance, the expression of the primase-deficient PRIMPOL constructs cannot rescue phenotypes associated with loss of PRIMPOL, including increased cell death upon treatment with replication stress-inducing agents and the inability to restart replication after replication stress (Keen et al., 2014b; Kobayashi et al., 2016; Mouron et al., 2013; Quinet et al., 2019; Schiavone et al., 2016). These data are consistent with a model where PRIMPOL restarts stalled replication forks

by re-priming downstream of a blocking lesion. Re-priming is an effective mechanism to resume replication.

1.3.5.2 Translesion synthesis

Translesion Synthesis (TLS) is a process where the replicative polymerases are replaced with TLS polymerases to insert and extend bases opposite of a given DNA lesion at the replication terminus (Figure 1.7B). Mammalian TLS polymerases include Y- (Pol η, Pol ι, Pol κ, Rev1), B- (pol ζ, composed of Rev3, Rev7, PolD2, and PolD3 (Lee et al., 2014)), A- and X-family DNA polymerases (Pol ν, Pol θ, Pol β, Pol λ, and Pol μ) family polymerases. The Y- and B-family polymerases function in lesion bypass. After the DNA lesion has been bypassed, displacement of TLS polymerases with replicative polymerases resumes high fidelity replication. Therefore, TLS polymerases possess the ability to restart a replication fork by synthesizing across damaged bases. Although TLS provides a mechanism to restart replication, it is a mutagenic process. For example, the error rate of TLS polymerases can be up to 1 in every 10^2 incorporated nucleotides compared to the replicative polymerases that make 1 error per 10^4-10^5 incorporated nucleotides (reviewed in (McCulloch and Kunkel, 2008)). It has been proposed that TLS can occur at or behind the replication fork, though the knowledge of which factors function directly at the replication fork is still limited (Diamant et al., 2012; Elvers et al., 2011; Quinet et al., 2019; Quinet et al., 2014; Tonzi et al., 2018)(reviewed in (Sale et al., 2012)).

Lesion bypass is a two-step process that includes: (1) insertion by the Y-family polymerases and (2) extension by pol ζ (Johnson et al., 2000; Lee et al., 2014) or Pol κ (Haracska et al., 2002; Jha and Ling, 2018; Washington et al., 2002). During insertion, the TLS polymerase accommodates the lesion in its active site to direct dNTP incorporation. Y-family polymerases can tolerate bulky lesions due to their capacious active sites and the absence of proofreading activity (Biertümpfel et al., 2010). Y-family polymerases are remarkably diverse in their substrate specificity and respond to particular cognate lesions (reviewed in (Sale, 2013)). For example, biochemical evidence shows Pol η can synthesize across from cyclobutane pyrimidine dimers and intra-strand crosslinks (Masutani et al., 2000; Masutani et al., 1999; McCulloch et al., 2004; Zhao et al., 2012), Pol κ across from polycyclic aromatic hydrocarbon-induced adducts, (Rechkoblit et al., 2002; Suzuki et al., 2002; Zhang et al., 2000a), and Pol ι across from 8-oxo-guananine (Tissier et al., 2000; Zhang et al., 2001; Zhang et al., 2000b), among others. Rev1 is a DNA-template dCMP transferase that can place a dCMP opposite of an abasic site (Lin et al., 1999). TLS polymerases generally tolerate bulky adducts, but Pol κ has also been shown to be required for efficient replication fork restart in response to hydroxyurea (Tonzi et al., 2018). The mechanistic details regarding how the right polymerase is selected for the target lesion are still being resolved, but this process could be dependent on the identity of the DNA lesion, specific interactions with other factors at the site of the lesion, or the availability of TLS polymerases present at a given lesion. During extension, the TLS polymerase accommodates the abnormal lesion-dNTP duplex for further synthesis.

The potential mutagenicity of the TLS polymerases necessitates their regulation, both at the recruitment and displacement level. Central to TLS regulation is the RAD18- and RAD6-dependent mono-ubiquitination of PCNA on Lys164, which increases PCNA's affinity for TLS polymerases at stalled replication forks (Hoege et al., 2002; Kannouche et al., 2004; Stelter and Ulrich, 2003). $CRL4^{Cdt2}$ and RNF8 can also catalyze mono-ubiquitination of PCNA, but may play a minor role in doing so (Terai et al., 2010; Zhang et al., 2008). PCNA is de-ubiquitinated by USP1, USP7, and USP10-dependent mechanisms (Huang et al., 2006; Kashiwaba et al., 2015; Park et al., 2014). $PCNA^{K164R/K164R}$ mutant mouse embryonic fibroblasts can still support 25-30% of TLS synthesis, suggesting there are other mechanisms to control the use of TLS polymerases (Hendel et al., 2011). This includes post-translational modifications of the TLS polymerases themselves (Bienko et al., 2005; Bienko et al., 2010) and protein interactions, such as that between PAF15 and Pol η or REV7 and TRIP13 (Clairmont et al., 2020; Povlsen et al., 2012). TLS polymerases have low processivity, which likely facilitates their removal and replacement by the replicative polymerases.

1.3.5.3 Template switching and fork reversal

Template switching (TS), first conceptually proposed in 1976 by Higgins et. al., is a homologous recombination-based method of lesion bypass that allows the replication fork to use an alternate DNA source, most commonly the newly synthesized daughter strand on the sister chromatid, as a template instead of the damaged parental strand (Figure 1.7D) (Higgins et al., 1976). Site-specific replication fork barriers, such as the Replication Termination Sequence 1 (RTS1) site in *S. pombe*, have been useful to determine the molecular mechanisms for direct replication fork restart via TS, also referred to replication-dependent recombination (RDR) or homologous recombination-restarted replication (HoRReR) (Jalan et al., 2019; Lambert et al., 2010; Lambert et al., 2005; Miyabe et al., 2015; Mizuno et al., 2009; Nguyen et al., 2015). Replication restart at the RTS1 occurs within S phase without the generation of a double-strand break (DSB) (Ahn et al., 2005; Lambert et al., 2010; Mizuno et al., 2009), but this type of restart can still be mutagenic (Iraqui et al., 2012; Lambert et al., 2010).

The data from experiments using the RTS1 site have generated hypothetical models of replication fork restart via TS. The first model proposes the stalled replication fork is regressed into a reversed fork. In a second model, the replication fork backtracks without annealing the nascent strands. Nucleolytic activities of Mre11-Rad50-Nbs1-Ctp1 and Exo1 can process either of these structures, exposing a ssDNA tail (Teixeira-Silva et al., 2017). $Rhp51^{Rad51}$ can then promote invasion of ssDNA tail into a homologous duplex to form a D-loop and subsequently, DNA Polymerase δ extends the 3' end of the invading strand (Miyabe et al., 2015). In yeast, $Rad22^{Rad52}$ functions to displace RPA and facilitates loading of $Rhp51^{Rad51}$. $Rad22^{Rad52}$ also possess its own strand annealing activity that can mediate $Rhp51^{Rad51}$-independent recombination (Lambert et al., 2010). DNA helicases,

Pfh1 and Srs2, are also required for replication restart at the RTS1 (Inagawa et al., 2009; Jalan et al., 2019; Lambert et al., 2010).

Mechanisms of TS dependent on Rad52 and Rad51 also occur in *S. cerevisiae* (Gangavarapu et al., 2007; Prakash, 1981), but experimental models often focus on TS as occurring behind the fork, necessitating bypass of the lesion by another mechanism such as re-priming (Fumasoni et al., 2015; Giannattasio et al., 2014; Vanoli et al., 2010). Much less is known about mechanisms of TS at the replication fork in *S. cerevisiae*, but if they exist, they are likely dependent on Rad5-generated intermediate structures (Blastyák et al., 2007; Minca and Kowalski, 2010).

Evidence TS as a mechanism of direct replication restart is starting to accumulate in mammalian cells but requires much further investigation. There is a RAD51-dependent mechanism of rapid fork restart that not involve the generation of a DSB, suggesting a RAD51-dependent TS mechanism exists in mammalian cells at the replication fork (Petermann et al., 2010a). Mechanisms of replication restart by TS have the potential to be error-free, but can also be a source of complex genomic rearrangements when a nascent strand invades a distal replication bubble rather than its sister chromatid (Lee et al., 2007b).

In mammalian cells, it has been proposed that fork reversal and subsequent fork restoration largely accounts for TS-dependent replication restart (Figure 1.7E). Data from electron microscopy shows fork reversal occurs in ~25% of replication forks upon exposure to a variety of replication stress-inducing agents (Zellweger et al., 2015). *In vivo* fork reversal is catalyzed by fork reversal enzymes, including SWI/SNF Related, Matrix Associated, Actin Dependent Regulator Of Chromatin, Subfamily A Like 1 (SMARCAL1), Zinc Finger RANBP2-type Containing 3 (ZRANB3), and HLTF (Bétous et al., 2012; Blastyák et al., 2010; Ciccia et al., 2012; Kile et al., 2015; Taglialatela et al., 2017; Vujanovic et al., 2017; Yuan et al., 2012) and is promoted by RAD51 recombinase (Zellweger et al., 2015). FBH1 can also catalyze fork reversal *in vivo* (Fugger et al., 2015).

The location and stability of the replisome during fork reversal is unknown. Evidence suggests that the replisome remains stably bound at sites of nascent DNA during replication fork stalling (De Piccoli et al., 2012; Dungrawala et al., 2015). Recently single-molecule analysis suggests that CMG can rapidly diffuse on dsDNA, but can transition back onto ssDNA for continued fork progression (Wasserman et al., 2019). Based on this finding, it is possible that in the event of replication fork stalling the CMG may be transitioned onto dsDNA to allow for fork reversal.

There likely exists a balance between replication fork reversal and restoration, but the mechanistic details of these processes are still being resolved (Figure 1.8). It is possible that the replication fork remodelers, SMARCAL1, ZRANB3, and HLTF, can restore a reversed fork to a replication fork as has been shown *in vitro* (Bétous et al., 2013; Chavez et al., 2018). While SMARCAL1 can restore both leading- and lagging-

Figure 1.8. Replication fork restoration pathways.
To resume DNA replication, a reversed fork can be restored to allow for bypass of a lesion. (A) Fork remodeling proteins can catalyze fork restoration. When the nascent leading-strand is longer than the nascent lagging-strand, SMARCAL1-dependent fork restoration is stimulated by RPA. HLTF and ZRANB3 can only weakly catalyze this substrate, and while they can catalyze fork restoration when the nascent lagging-strand is longer than the nascent leading-strand, this reaction is inhibited by the presence of RPA. (B) The RECQ family helicases can also promote fork restoration. RECQL1 has fork restoration activity. WRN functions epistatic with DNA2 to promote replication restart. A reversed fork processed by WRN and DNA2 can be restored through branch migration or homology-directed restoration. BLM promotes fork restoration, but the mechanistic details have yet to be determined. (C) Homology-directed restoration may rely on classical homologous recombination factors: BRCA2 and RAD51. BRCA2 functions to load RAD51 onto the ssDNA overhang and subsequently RAD51 mediates strand-invasion and D-loop formation. Whether RAD52 plays a role in fork restoration at an intact stalled replication fork is unknown.

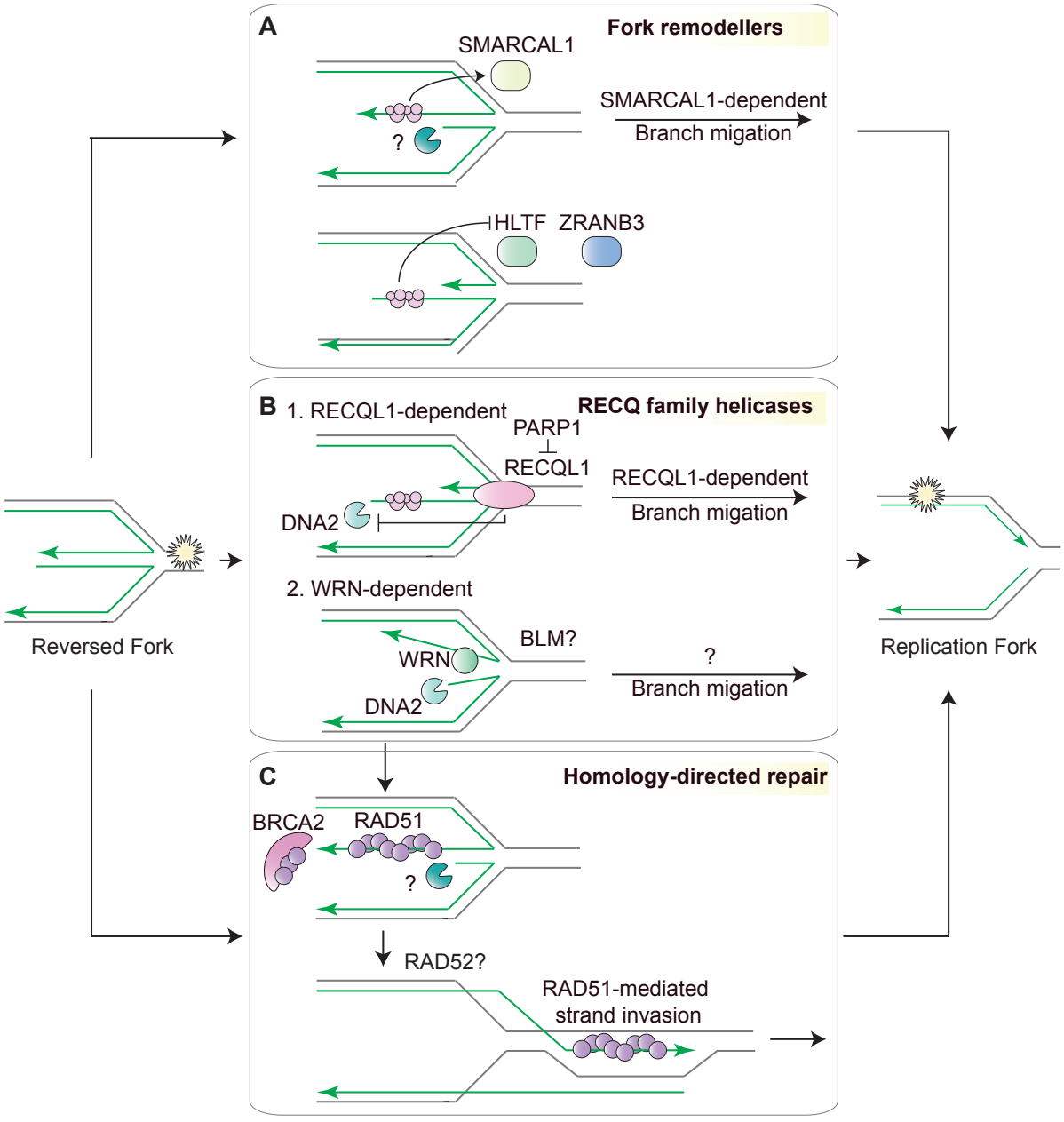
A
Fork remodellers
SMARCAL1
?
SMARCAL1-dependent
Branch migation
HLTF
ZRANB3
B
1. RECQL1-dependent
RECQ family helicases
PARP1
RECQL1
DNA2
RECQL1-dependent
Branch migation
2. WRN-dependent
BLM?
WRN
DNA2
?
Branch migation
Reversed Fork
Replication Fork
C
Homology-directed repair
BRCA2
RAD51
?
RAD52?
RAD51-mediated
strand invasion

strand gapped forks, RPA stimulates and enforces the specificity of SMARCAL1 to only restoration the fork when the nascent leading-strand is longer that the nascent lagging-strand (Bétous et al., 2013). ZRANB3 and HLTF show preference for restoration of forks where the nascent lagging-strand is longer than that of the leading-strand, but this activity is inhibited by RPA (Bétous et al., 2013; Chavez et al., 2018). This model also predicts that 5'-3' nucleolytic resection is required for SMARCAL1-dependent replication fork restoration (Bétous et al., 2013).

The RecQ family of helicases may also promote replication fork restoration. RECQL1's helicase activity promotes the restart of replication forks reversed by various types of replication stress (Berti et al., 2013; Zellweger et al., 2015). PARP PARylation inhibits RECQL1 fork restoration activity to prevent premature restart of the regressed forks (Berti et al., 2013). Another RecQ family helicase, WRN, is also required for restoration of a reversed fork, and this restoration is dependent on DNA2-mediated processing of the reversed fork (Machwe et al., 2011; Thangavel et al., 2015). RECQL1- and WRN-dependent restart likely function in independent pathways of replication fork restoration as RECQL1 limits DNA2-mediated nucleolytic resection (Thangavel et al., 2015). BLM may also function in fork restoration as it can catalyze fork restoration *in vitro* and is required for fork restart *in vivo* (Davies et al., 2004; Davies et al., 2007; Machwe et al., 2011; Sidorova et al., 2013). Other factors may also contribute to directing RecQ-dependent fork restoration. RIF1 was found to be enriched at stalled replication forks to prevent degradation of reversed forks by DNA2 and promote replication restart (Mukherjee et al., 2019). Authors propose that this mechanism preserves the reversed fork as a substrate for RECQL1-dependent fork restoration, but it remains to be tested whether RECQL1 and RIF1 are epistatic with each other. It is unclear exactly how the RecQ family helicases restart a reversed replication fork. RECQL1 may unwind the daughter strand duplex to promote branch migration-assisted re-establishment of a functional replication fork (Berti et al., 2013). Like RECQL1, BLM and WRN may also promote branch migration or, unlike RECQL1, they may promote homology-dependent repair (HDR) (Bugreev et al., 2007; Nimonkar et al., 2008; Sidorova et al., 2013; Sturzenegger et al., 2014; Thangavel et al., 2015). It is also possible that WRNIP1, WRN and DNA Polymerase δ, form a complex to promote DNA synthesis (Leuzzi et al., 2016; Tsurimoto et al., 2005).

Restoration of reversed forks is also catalyzed by proteins required for HDR, such as BRCA2, RAD51, and RAD52. Since BRCA2 and RAD51 have multiple functions at reversed fork substrates, including promoting fork reversal (RAD51) (Zellweger et al., 2015) and protecting the regressed nascent strands (BRAC2 and RAD51) (Mijic et al., 2017; Schlacher et al., 2011), teasing out their exact role in fork restoration is difficult. HDR requires much higher levels of RAD51 than those required for fork reversal or nascent strand protection (Dungrawala et al., 2017). RAD52 has been shown to promote replication fork restart after extensive (>6 hours) treatments with replication stress-inducing agents (Sotiriou et al., 2016), but not with shorter ($\leq$2 hours) treatments (Hromas

et al., 2017; Kelso et al., 2019) and thus may be unlikely that RAD52 plays a role in HDR-dependent restoration of reversed forks without the generation of a DSB.

Molecular switches exist to induce fork reversal and TS. In both yeast and mammalian cells, TS is driven by PCNA poly-ubiquitination. In yeast, PCNA poly-ubiquitination requires Rad6-Rad18 and Ubc13-Mms2-Rad5 (Branzei et al., 2008; Hoege et al., 2002; Torres-Ramos et al., 2002). Similarly, RAD6-RAD18, UBC13-MMS2 and the human ortholog of Rad5, Helicase-like Transcription Factor (HLTF), as well as SNF2 histone linker PHD RING helicase (SHPRH), are responsible for poly-ubiquitination of PCNA in mammalian cells (Lin et al., 2011; Masuda et al., 2012; Motegi et al., 2008; Unk et al., 2008; Unk et al., 2006) and this poly-ubiquitination of PCNA drives replication fork reversal (Ciccia et al., 2012).

1.3.5.4 Pathway Choice

In mammalian cells, evidence is accumulating that re-priming, TLS, and TS are independent pathways. For example, co-depletion of PRIMPOL and TLS polymerases (Pol η and pol ζ) leads to a synergistic increase in sensitivity to replication stress-inducing agents, suggesting re-priming and TLS function independently (Bianchi et al., 2013; Kobayashi et al., 2016). In addition, fork reversal (and TS) is independent of re-priming and TLS (Fumasoni et al., 2015; Piberger et al., 2019; Quinet et al., 2019). Consistent with this, Pol κ-deficiency results in nascent strand degradation in response to HU suggesting replication fork reversal (and TS) occurs in the absence of TLS (Tonzi et al., 2018). In the absence of PRIMPOL and Pol η, there is an accumulation chromatin-bound RAD51, suggesting that either fork reversal or HDR occurs in the absence of re-priming or TLS (Bianchi et al., 2013). Loss of POLDIP2 decreases the usage of TLS and increases the usage of TS (Tsuda et al., 2019). While it is clear that re-priming, TLS, and TS are independent pathways, the extent to which the pathways are interchangeable and the factors controlling pathway usage require further investigation.

The molecular mechanisms of pathway choice between re-priming, TLS, and TS are likely complex. Whether the DNA lesion is located on the leading- or lagging-strand, may direct repair. Re-priming by Pol α-primase theoretically should be able to account for the majority of lagging-strand restart as DNA Polymerase α-primase is readily available as part of the replisome. However, specific evidence of this dependence on Pol α-primase in mammalian cells has yet to be reported. On the leading-strand, the decision whether to re-prime with PRIMPOL, bypass the lesion with a specific TLS polymerase, or bypass the lesion by fork reversal and TS is more complex.

When a lesion is present on the leading-strand, PCNA modification, ubiquitination or small ubiquitin-like modification (SUMOylation), might be a central determinant for which factors are recruited to the replication fork (Masuda et al., 2018; Mohiuddin et al., 2018). As mentioned in the previous sections, PCNA mono-ubiquitination promotes TLS, whereas PCNA poly-ubiquitination promotes TS. Recent biochemical analysis suggests

a mechanism for pathway choice via distinct modes of PCNA poly-ubiquitination, including both *en bloc* transfer of a pre-formed poly-ubiquitin chain and step-by-step ubiquitin elongation processes (Masuda et al., 2018). Other factors have been shown to stimulate PCNA ubiquitination in response to specific types of damage, such as SIVA1, NBS1, FANCD2, RAD51, PARP10, and chromatin remodelers, BAF180 and ZBTB1 (Chen et al., 2016; Han et al., 2014; Kim et al., 2014; Nicolae et al., 2014; Niimi et al., 2015; Yanagihara et al., 2011). PIAS1- and PIAS4-dependent SUMOylation of PCNA can also direct repair to TS (Mohiuddin et al., 2018). The wide variety of responses that occur at stalled replication forks may be dependent on the timing of recruitment of the proteins involved and the type, location, and duration of replication stress. More work is required to understand if and how a stalled replication fork favors a certain response.

1.3.5.5 Fork Collapse

Fork collapse is defined as the formation of a DSB at the replication fork. At the replication fork, single-strand breaks (SSBs) can be converted to DSBs after fork passage (Hashimoto et al., 2011). In the absence of appropriate and timely restart of a stalled replisome, the replication fork is susceptible to breakage and double-strand breaks (DSBs) can be generated from nucleolytic cleavage (Hanada et al., 2007). This includes cleavage of reversed replication forks by MUS81 structure-specific endonuclease (MUS81) and cleavage of the nascent-nascent duplexes at a deprotected (RAD51- or BRCA2- deficient) reversed forks (Bhat et al., 2018; Schlacher et al., 2011; Schlacher et al., 2012; Wang et al., 2015a) (Figure 1.7F).

Replication forks can be restarted after breakage by homologous recombination-mediated mechanisms, including break-induced replication (BIR). BIR, a form of TS requiring replication fork breakage, resumes DNA synthesis using a modified replisome assembled on a migrating D-loop. BIR requires the presence of proteins, including POLD3 and RAD52 (Bhowmick et al., 2016; Costantino et al., 2014; Sotiriou et al., 2016). Upon DSB formation at a collapsed fork, other pathways may be employed to recover and restart replication; for example, a RAD51-dependent mechanism has been demonstrated that is distinct from classical DSB repair can also promote replication fork recovery (Petermann et al., 2010a).

1.4 The DDI-RTF2 axis

Our laboratory recently discovered a mechanism to cope with replication stress dependent on proteasomal “shuttle” proteins, DNA Damage Inducible 1 (DDI1) and DNA Damage Inducible 2 (DDI2). Proteasomal “shuttle” proteins are responsible for transporting cargo from one area in the cell to the proteasome for degradation (Elsasser et al., 2002); (reviewed in (Saeki, 2017). The loss of DDI1/2 from human cells results in a defective replication stress response, which led to the hypothesis that there are factors at the replication fork that DDI1/2 function to remove. Replication Termination Factor 2 (RTF2) was identified as one of these factors degraded in a DDI1/2- and proteasome-

dependent manner (Kottemann et al., 2018). Under normal conditions, RTF2 travels with the replication fork, but when the replication fork encounters replication stress, RTF2 must be removed to resume replication. This removal allows cells to appropriately recover from replication stress (Figure 1.9).

1.4.1 DNA Damage Inducible 1 and DNA Damage Inducible 2

DDI1 and DDI2 are paralogs, with human DDI2 sharing more similarities to *S. cerevisiae* Ddi1 (*scDdi1*; no homolog has been identified in *S. pombe)*, suggesting DDI2 likely gave rise to DDI1 through a retrotransposition event (Siva et al., 2016). DDI1 and DDI2 are "shuttle" or adaptor proteins in the same family as RAD23A and RAD23B that deliver poly-ubiquitinated substrates to the regulatory part of the 26S proteasome. Proteasomal shuttle proteins possess an N-terminal ubiquitin-like domain (UBL) that binds to the 26S proteasome and a C-terminal ubiquitin-associated domain (UBA) responsible for binding ubiquitin chains (Bertolaet et al., 2001; Kang et al., 2006). DDI1 and DDI2 both contain a conserved N-terminal UBL domain and a C-terminal retroviral aspartyl protease (RVP) domain but lack a UBA domain. However, the DDI's UBL domain facilitates binding both to ubiquitin receptors and ubiquitin, fulfilling the bifunctional requirement for shuttle proteins to transport a substrate from its original location to the proteasome for degradation (Nowicka et al., 2015) and may imply DDI1 and DDI2 dimerize.

Functionally, human DDI1 and DDI2 are not well studied. While DDI1 and DDI2 share some functional similarities with their yeast homolog, Ddi1, they are also involved in distinct processes. *sc*Ddi1 has been shown to function in cell cycle control, (Clarke et al., 2001; Liu and Xiao, 1997), endo- and exo-cytosis (Gabriely et al., 2008), and protein trafficking (Gomez et al., 2011). These functions have yet to be described for the human homologs. In addition, *Δddi*1 yeast barely exhibit sensitivity to most replication stress-inducing agents, while human cells depleted of DDI1 and DDI2 show striking sensitivity to same agents (Kottemann et al., 2018; Svoboda et al., 2019). Like human DDI1 and DDI2, *scDdi1* has been proposed to function as a proteasomal shuttle, but it responsible for degradation different substrates, including the HO nuclease (Kaplun et al., 2005) and the UFO1 protein (Ivantsiv et al., 2006; Voloshin et al., 2012).

Recent work from our laboratory discussed the importance of DDI1/2 as proteasomal shuttle proteins in mammalian cells. DDI1/2 is responsible for RTF2 degradation at the replisome under conditions of replication stress. Under conditions of DDI1/2-depletion, RTF2 is not actively removed from the replication fork and cells exhibit sensitivity, accumulation of ssDNA, deficient fork replication restart and chromosomal breakage upon treatment with drugs that induce replication fork stalling (Kottemann et al., 2018) (Figure 1.9C). These phenotypes are ameliorated upon knockdown of RTF2. Understanding if RTF2's removal is ubiquitin-dependent is an area of active research in our laboratory.

Figure 1.9. The DDI-RTF2 axis.
(A) Replication Termination Factor 2 (RTF2) travels with the replisome during unperturbed replication. The placement of RTF2 in this diagram does not represent its physical location, as there is not enough evidence to yet determine where it is located. (B) Upon replication stress, DNA Damage Inducible 1 (DDI1) and DNA Damage Inducible 2 (DDI2) are proposed to bind and remove RTF2 from the replication fork for proteasome-mediated degradation. We postulate this mechanism is ubiquitin-dependent. RTF2 removal allows for proper recovery from replication stress and replication fork restart. (C) In the absence of DDI1/2, RTF2 is stabilized at the replication fork under conditions of stress. This stabilization results in a compromised response to replication stress and an inability to restart replication.

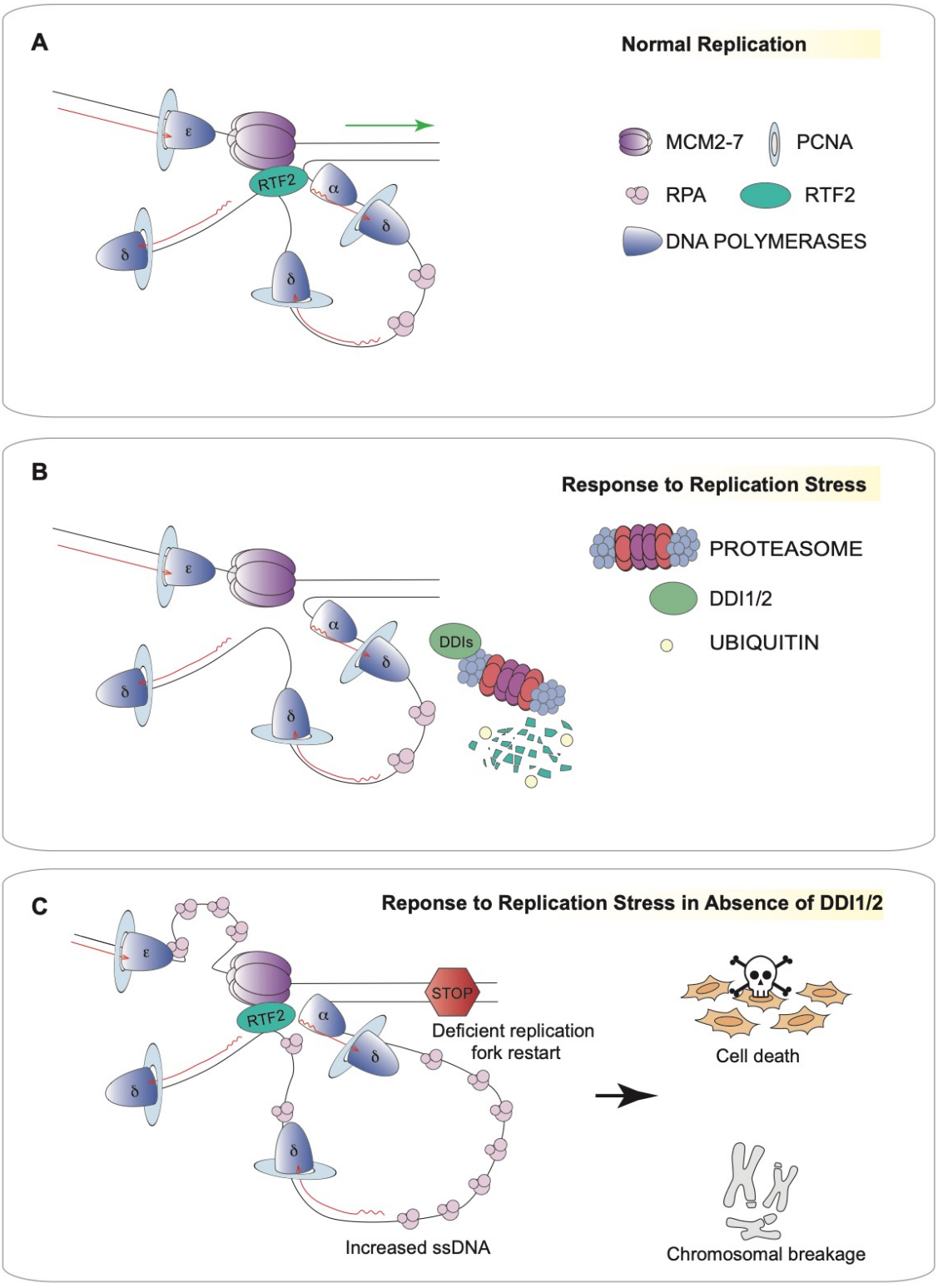
A
Normal Replication
ε
RTF2
α
δ
δ
δ
MCM2-7
PCNA
RPA
RTF2
DNA POLYMERASES
B
Response to Replication Stress
ε
α
δ
δ
δ
DDIs
PROTEASOME
DDI1/2
UBIQUITIN
C
Reponse to Replication Stress in Absence of DDI1/2
ε
RTF2
α
δ
δ
δ
STOP
Deficient replication
fork restart
Increased ssDNA
Cell death
Chromosomal breakage

1.4.2 Replication Termination Factor 2

RTF2 is well-conserved with the exception that no homolog has been identified in *S. cerevisiae.* This may explain why it has not been studied in replication since *S. cerevisiae* has been the predominant model system for mechanistic replication studies. Human RTF2 consists of 306 AAs and contains a Rtf2 domain (classified in PFAM as clan "Really Interesting New Gene (RING)" CL0229 that consist of RING/U-box-like domains) (Figure 1.10). RING/U-BOX domains are zinc fingers mainly found in E3 ubiquitin/ small ubiquitin-like modifier (SUMO)-ligases. This central domain contains a C2HC2 motif (in mammalian: C5) that most similarly resembles a SP-RING finger. In RING fingers, four cysteine residues are required to chelate one Zn^{2+} ion. Biochemical assays for the Rtf2 domain's activity remain inconclusive. Though no other domains have been formally assigned, computational analyses suggests RTF2 may also contain a SAP domain from AA position 40-90 as well as potential SUMO-interacting motifs (SIM) and SUMOylation sites. RTF2 is also predicted to contain a nuclear localization signal (NLS) in AA position 199-204 (Sontheimer, 2011).

In *S. pombe,* (*spRtf2*) Rtf2 is a 240 AA protein that lacks a portion of the C-terminus compared to mammals (Figure 1.10). In yeast, Rtf2 has primarily been implicated in mating type switching. Mating type switching is a programmed DNA rearrangement, responsible for switching the mating type of yeast to either plus (P) or minus (M). Recent evidence suggests this process requires two ribonucleotides, referred to as the imprint, that stalls replication forks initiated from a *mat1* telomere-distal origin (Figure 1.11) (reviewed in (Singh, 2019; Yamada-Inagawa et al., 2007)). This replication barrier is referred to as the mat1-pausing site (MPS1). Swi and Swi3 are implicated in pausing at the MPS1 along with Mrc1, Swi7 and Mcm10 (Dalgaard and Klar, 2000; Singh et al., 2019; Singh and Klar, 1993; Zech et al., 2015). The imprint is established in the first round of DNA replication (lagging-strand product) and in the subsequent round of DNA replication, the imprint, a single-stranded nick or gap, is converted to a DSB that triggers homologous recombination, a process that requires many more factors to determine appropriate donor selection. To optimize mating type switching, DNA replication is also blocked from the *mat1* centromere-distal origin at the RTS1 barrier and thus DNA replication proceeds unidirectionally and ensures only leading-strand synthesis reaches the imprint. If the lagging-strand encounters the imprint, a DSB would not be formed. Factors involved in termination at the RTS1 site include Rtf1, Swi1, and Swi3 (Dalgaard and Klar, 2000; Eydmann et al., 2008; Inagawa et al., 2009). Rtf2 also contributes to the site-specific replication termination at the *RTS1* site as Δ*rtf2* cells display a pausing defect, but how Rtf2 terminates replication forks is unknown (Inagawa et al., 2009). It is unclear how Rtf2's function in this system relates to RTF2's role in mammalian cells.

Δ*rtf2* yeast cells were examined to identify non-RTS1-dependent functions. Δ*rtf2* cells are not sensitive to most replication stress-inducing agents (HU, UV, camptothecin) but they display a minor sensitivity to alkylating damage (Inagawa et al., 2009). These

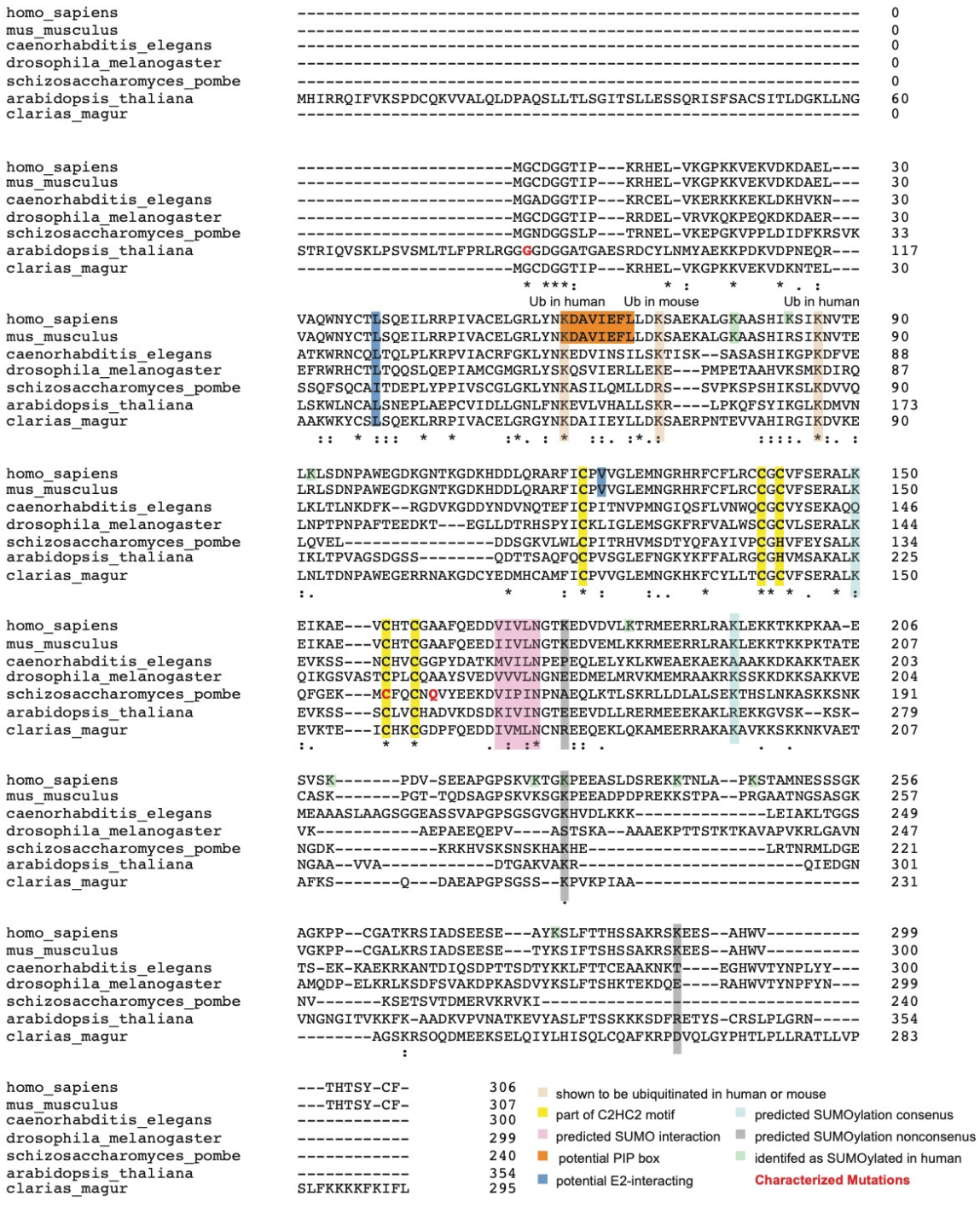

Figure 1.10. Alignment of primary sequences of RTF2 orthologs.
RTF2 is highly conserved in mammalian cells. Several key residues are highlighted as indicated in figure.

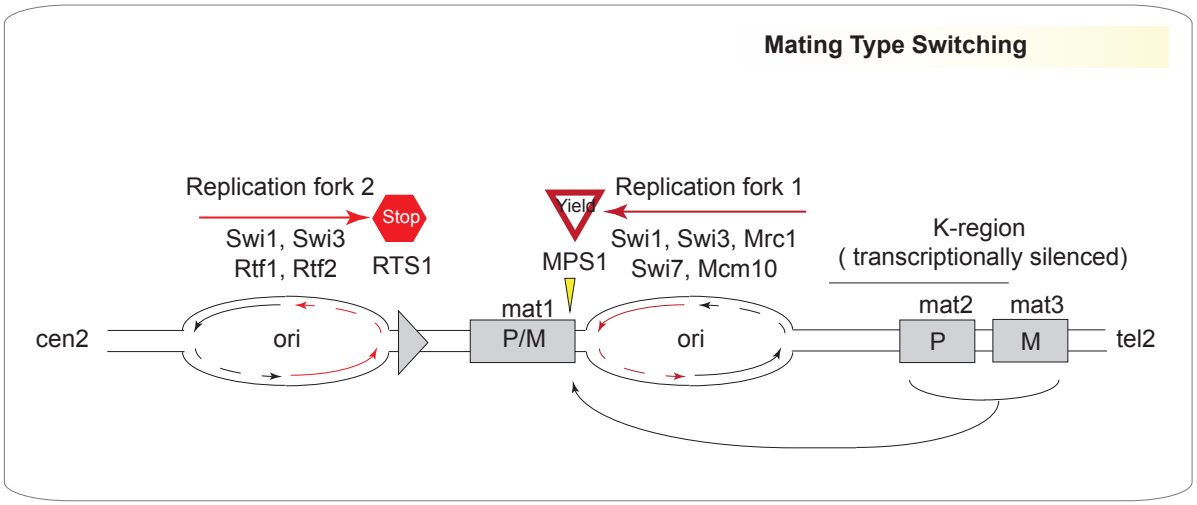

Figure 1.11. Mating type switching.
In *S. pombe*, one round of replication establishes an imprint (yellow triangle), a single strand nick of gap, whose generation may be the dependent on the synthesis of two ribonucleotides by Swi7 and Mcm10. In the second round of replication, leading-strand synthesis (from replication fork 1) stops at this modification, converting the single-stranded nick or gap into an one-ended DSB. The stalling at the MPS1 site is dependent on Swi1, Swi3, and Mrc1. The resulting free DNA end invades the silent cassette containing the information for the opposite mating type. D-loop formation allows for extension of this locus to resolve recombination. DNA replication proceeding from the mat1 centromere-distal side (replication fork 2) is stopped to optimize this process. Swi1, Swi3, Rtf1 and Rtf2 have been implicated in DNA replication termination at the RTS1. This block ensures that leading-strand encounters the imprint, allowing for DSB formation.

results suggest in yeast, Rtf2 plays a minor role at replication forks stalled at damaged bases. Rtf2 and PCNA were shown to interact (albeit weakly and transiently) with yeast-two hybrid assays and immunoprecipitations (Inagawa et al., 2009). This interaction may suggest that Rtf2 localizes to the replication fork. Mammalian RTF2 also contains a region that resembles a non-canonical PIP (Figure 1.10), but the function of this region has yet to be empirically tested.

Unrelated to DNA replication, Rtf2 has been implicated in RNA splicing in *Arabidopsis thaliana (*atRTF2). atRtf2 has an N-terminal extension of 80 AA that is only weakly conserved on the AA sequence level. This N-terminal domain is important for plant viability (Sasaki et al., 2015). A role for atRTF2 in pre-mRNA splicing was identified using a green fluorescent protein (GFP)-dependent splicing assay. In addition, RNA sequencing (RNA-seq) in the *Rtf2* null mutants reveals increased intron retention consistent with genome-wide splicing defects (Sasaki et al., 2015). Since atRTF2's function in RNA splicing is dependent on the N-terminal domain that is not conserved in higher eukaryotes this may be a plant-specific role of RTF2.

Strikingly, except for our recent report (Kottemann et al., 2018), there have been no functional studies of RTF2 in mammalian cells. Screens using Clustered regularly interspaced short palindromic repeats (CRISPR) or RNA inference (RNAi) methodologies indicate that RTF2 is essential in cells (Fraser et al., 2000; Hart et al., 2015; Wang et al., 2015b).

1.5 Objectives

While it is clear that the DDI-RTF2 axis is important for the cellular response to replication stress, little is known about the mechanistic details surrounding this pathway. Despite identifying RTF2 as a component of the mammalian replisome, it remains unexplored why RTF2 travels with the replication fork but is removed upon replication stress. Perturbations in replication and the response to replication stress have been consistently linked to human health and therapeutics. Dissecting the function of RTF2 may be clinically relevant.

The objectives of this study are: (1) to understand the endogenous function of RTF2 at the replication fork, (2) to determine why RTF2 must be removed from the replisome upon replication stress and, (3) to uncover how removal of RTF2 promotes recovery from replication stress.

Chapter 2: RTF2 is necessary for *in vivo* viability, cellular proliferation, and DNA replication

2.1 Introduction

While RTF2 has been identified at the replication fork (Alabert et al., 2014; Dungrawala et al., 2015; Kottemann et al., 2018; Wessel et al., 2019), the function of RTF2 in mammalian cells has not been systematically characterized. Loss-of-function genetic approaches are powerful tools to interrogate the function of a gene. Thus, the strategy to understand the role of RTF2 on an organismal and cellular level relied on the creation of a loss-of-function model. In this section, the experimental approach, based on mouse genetics, to develop a system whereby RTF2 expression can be removed in a conditional manner is described. Phenotypes, especially DNA replication defects, of mice and cells devoid of RTF2 were examined and the results of these studies are reported here.

2.2. Results

2.2.1 RTF2 is necessary for *in vivo* viability and cellular proliferation

A conditional RTF2 knockout (KO) model was generated in *Mus musculus*. Mouse embryonic stem cells (mESCs) carrying a *Rtf2*$^{tm1a(KOMP)Wtsi}$ allele (Knockout Mouse Project (KOMP) repository) were injected into albino embryos to generate chimeric mice (Figure 2.1). The presence of this allele, *Rtf2*$^{tm1a(KOMP)Wtsi}$*,* referred to as *Rtf2*^{stop}, was confirmed with long range polymerase chain reactions (PCRs) on genomic DNA isolated from the mESCs, followed by Sanger sequencing of the amplified products (Figure 2.1). Chimeras with greater than 50% black coat color were bred against C57BL6/J (Jackson Labs) mice to generate *Rtf2*$^{+/stop}$ mice. These mice were subsequently bred with mice expressing recombinase flippase (Flp) and mice expressing Causes recombination (Cre) recombinase, to generate *Rtf2*$^{+/\Delta exon3}$ mice with germline deletion of exon 3. The loss of exon 3 will herein be referred to as *Rtf2*$^{-}$ as this loss is predicted to result in early truncation of the *Rtf2* transcript (Figure 2.1). The presence of *Rtf2*$^{+}$*, Rtf2*^{stop}*, Rtf2*^{lox}*,* and *Rtf2*$^{-}$ alleles were identified and confirmed in genomic DNA extracted from mouse tail tips with genotyping PCRs (Figure 2.2).

Heterozygous intercrosses (*Rtf2*$^{+/-}$ x *Rtf2*$^{+/-}$) were performed to determine the Mendelian ratios of the offspring. Ninety-eight pups were obtained from nineteen crosses, averaging 5.2 pups per litter (44.4% female, 55.5% male). Of ninety-eight progeny analyzed, no homozygous *Rtf2*$^{-/-}$ pups or embryos at 10.5 days post coitum (dpc) or beyond were observed (Figure 2.3A). In addition, *Rtf2*$^{-/-}$ blastocysts isolated on 3.5 dpc and grown over several days *in vitro* did not hatch (Figure 2.3D). These results indicate RTF2 is essential for embryonic development.

Rtf2$^{+/-}$ mice did not display any visible defects and were born at the expected Mendelian ratios (Figure 2.3A). No differences in growth, as assessed by body weight, were observed between wild type (*Rtf2*$^{+/+}$) and heterozygous (*Rtf2*$^{+/-}$) mice (Figure 2.4).

Figure 2.1. Schematic of conditional *Rtf2* knockout allele in *Mus musculus*.
(A) mESCs from the KOMP repository containing a *Rtf2* allele targeted with a Lac operon Z (LacZ) and Neomycin resistance (NeoR) selection cassette flanked by flippase recognition target (FRT) sites in between exon 2 and exon 3. Exon 3 is flanked by locus of X(cross)-over in P1 (loxP) sites. This allele is designated $Rtf2^{stop}$ as it has potential to disrupt the *Rtf2* gene. The selection cassette can be removed with Flp expression to generate a $Rtf2^{lox}$ allele. Exon 3 can then be removed with Cre expression, herein referred to as $Rtf2^{-}$. Removal of exon 3 is predicted to result in a truncated protein at AA 57. There are no common alternative splice variants of *Mus musculus* RTF2. The next methionine to start a new transcript is located at AA 128. Expression of this N-terminally truncated transcript would lack the C-terminus including the first cysteine of RTF2's predicted functional C2HC2 RING motif (cysteine residues are present at AA positions: 121, 140, 142, 157 and 159). We expect this transcript is degraded by nonsense mediated decay. (B) The presence of the targeted RTF2 allele in mESCs was confirmed using long-range PCRs performed on genomic DNA. 5' sequence: Forward primer in exon 1 and reverse primer flanking in the first FRT sequence and subsequent genomic sequence (light gray). 3' sequence: Forward primer flanking the LacZ cassette and subsequent genomic sequence and reverse primer downstream of the 3' LoxP site (dark gray). Sanger sequencing of PCR products confirmed the presence of the FRT and LoxP sites (not shown). (C) A grade "A" chimera male mouse (indicated) with greater than 90% of black coat color was mated with two C57BL6/J females to produce $Rtf2^{+/stop}$ mice.

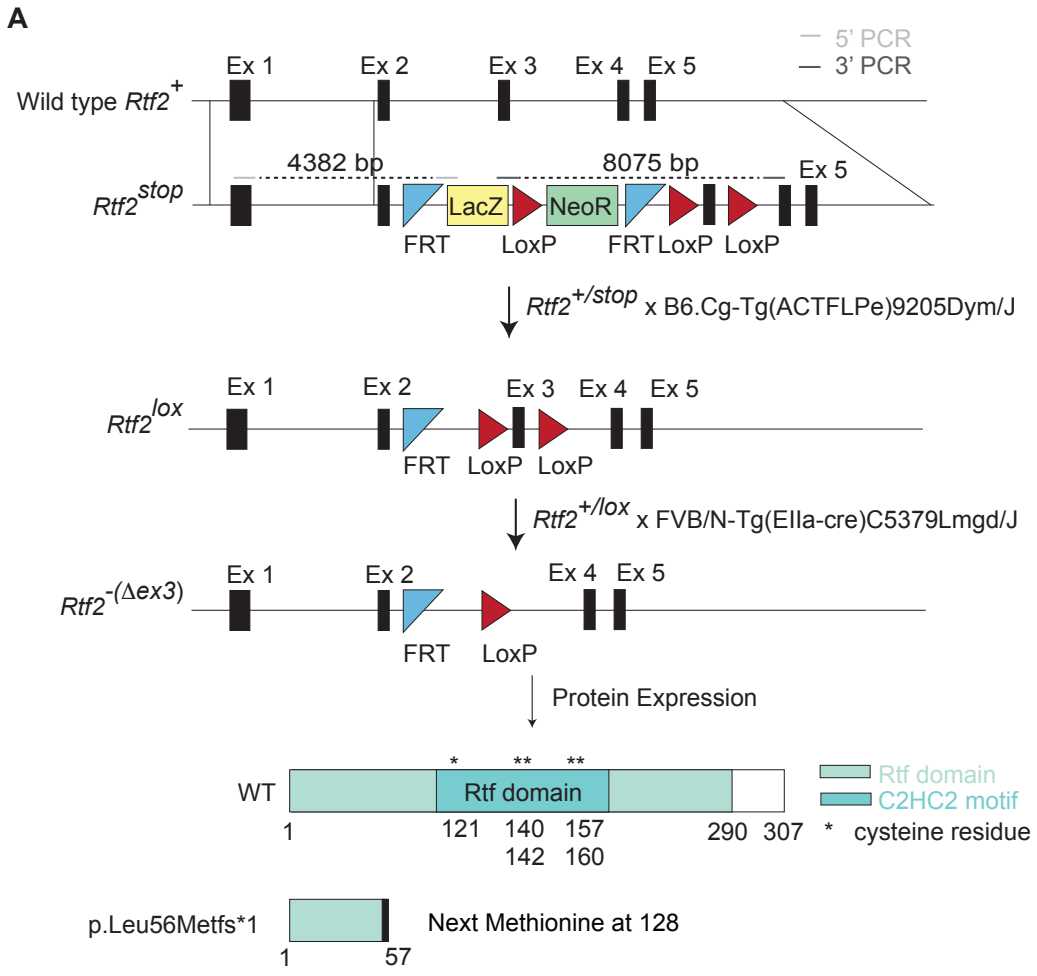
A
5' PCR
3' PCR
Ex 1
Ex 2
Ex 3
Ex 4
Ex 5
Wild type Rtf2+
4382 bp
8075 bp
Rtf2stop
LacZ
NeoR
FRT
LoxP
FRT
LoxP
LoxP
Rtf2+/stop x B6.Cg-Tg(ACTFLPe)9205Dym/J
Rtf2lox
Rtf2+/lox x FVB/N-Tg(EIIa-cre)C5379Lmgd/J
Rtf2-(Δex3)
Protein Expression
WT
Rtf domain
C2HC2 motif
cysteine residue
1
121
140
142
157
160
290
307
p.Leu56Metfs*1
Next Methionine at 128
57

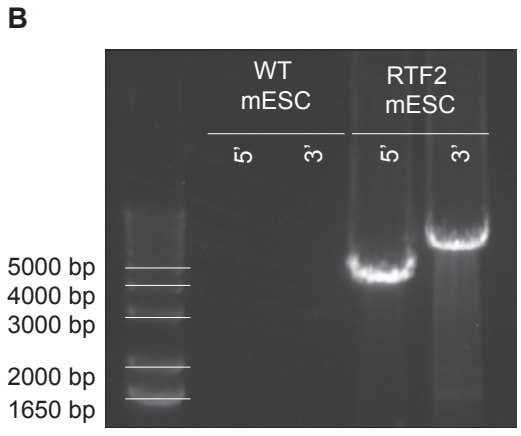
B
WT mESC
RTF2 mESC
5'
3'
5'
3'
5000 bp
4000 bp
3000 bp
2000 bp
1650 bp

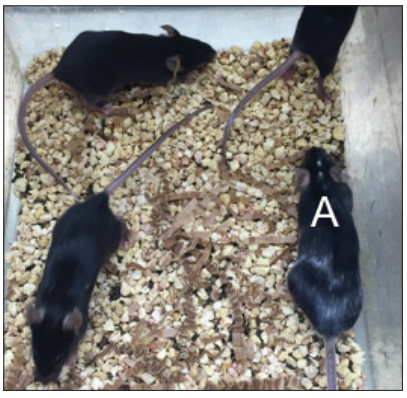
C
A

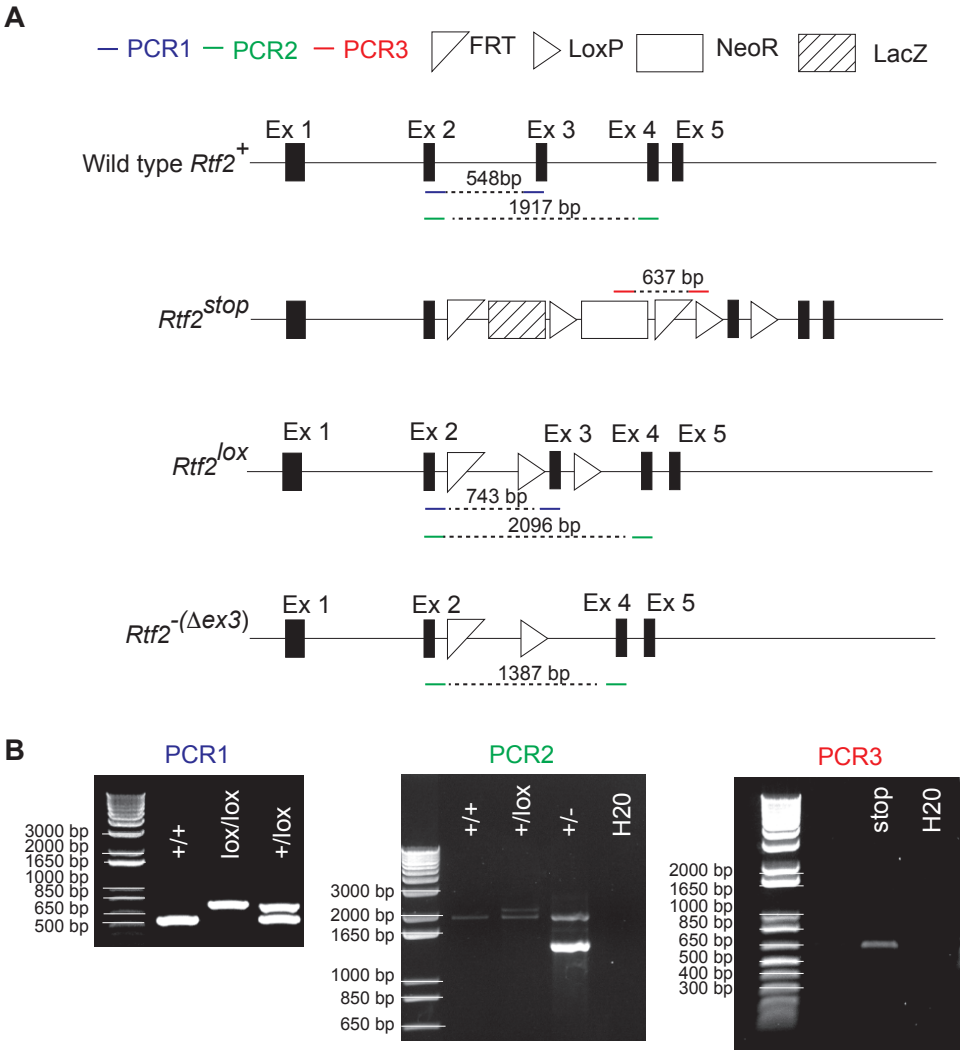

Figure 2.2. Confirmation of targeted *Rtf2* alleles.
(A) Schematic of *Rtf2* allele indicating genotyping primers and predicted product sizes. (B) Representative genotyping PCR products run on 0.8% agarose gel and stained with EtBr. PCR1 discriminates between $Rtf2^{+}$ and $Rtf2^{lox}$ alleles (blue); PCR 2 discriminates between $Rtf2^{+}/Rtf2^{lox}$ and $Rtf2^{-}$ alleles (green); PCR3 detects the presence of the $Rtf2^{stop}$ allele (red).

Figure 2.3. The loss of RTF2 in mice results in early embryonic lethality.
(A) *Rtf2*$^{+/-}$ mice were intercrossed. Of ninety-eight pups, no viable *Rtf2*$^{-/-}$ mice were born. These results significantly differ from the expected Mendelian ratios of 25% *Rtf2*$^{+/+}$, 50% *Rtf2*$^{+/-}$, and 25% *Rtf2*$^{-/-}$, when assessed with a chi-squared test. In addition, no *Rtf2*$^{-/-}$ embryos from 10.5 to 14.5 dpc were genotyped. Chi-square and p-values indicated. (B) Uterine horns from *Rtf2*$^{+/-}$ females mated with *Rtf2*$^{+/-}$ males on indicated dpc. Arrows indicate resorbed embryos. Genotypes of embryos indicated on right. (C) *Rtf2*$^{+/stop}$ mice were intercrossed. Of thirty-six pups, no *Rtf2*$^{stop/stop}$ mice were born. These results significantly differ from the expected Mendelian ratios of 25% *Rtf2*$^{+/+}$, 50% *Rtf2*$^{+/stop}$, and 25% *Rtf2*$^{stop/stop}$ when assessed with a chi-squared test. Chi-square and p-values indicated. (D) Blastocysts were isolated at E3.5 and grown *in vitro* over the course of four days. Images were taken each day. The number of hatched blastocysts for each given *Rtf2* genotype is listed on the right.

A

♀ *Rtf2*$^{+/-}$ x ♂ *Rtf2*$^{+/-}$

Age (dpc)	Number	*Rtf2*$^{+/+}$	*Rtf2*$^{+/-}$	*Rtf2*$^{-/-}$
10.5	8	1 (12.5%)	7 (87.5%)	0 (0.0%)
12.5	7	4 (57.1%)	3 (42.9%)	0 (0.0%)
13.5	8	4 (50.0%)	4 (50.0%)	0 (0.0%)
14.5	6	2 (33.3%)	4 (66.7%)	0 (0.0%)
Pups	98	34 (34.7%)	64 (65.3%)	0 (0.0%)

Expected Mendelian Ratios (*Rtf2*$^{+/+}$:*Rtf2*$^{+/-}$:*Rtf2*$^{-/-}$ of 1:2:1) : χ^2 value: 32.78, p-value: <0.00001

If *Rtf2*$^{-/-}$ lethal, Mendelian Ratios (*Rtf2*$^{+/+}$:*Rtf2*$^{+/-}$ of 1:2): χ^2 value: 0.08 p-value: 0.78

B

Rtf2:
1: +/-
2: +/+
3: +/-
4: +/+
5: +/+
6: +/-

Rtf2:
1: +/-
2: +/-
3: +/+
4: +/-
5: +/-
6: +/-

C

♀ *Rtf2*$^{+/stop}$ x ♂ *Rtf2*$^{+/stop}$

Age (dpc)	Number	*Rtf2*$^{+/+}$	*Rtf2*$^{+/stop}$	*Rtf2*$^{stop/stop}$
Pups	34	16 (47.1%)	18 (52.9%)	0 (0.0%)

Expected Mendelian Ratios (*Rtf2*$^{+/+}$:*Rtf2*$^{+/stop}$:*Rtf2*$^{stop/stop}$ of 1:2:1) : χ^2 value: 15.18 p-value: <0.001

If *Rtf2*$^{stop/stop}$ lethal, Mendelian Ratios (*Rtf2*$^{+/+}$:*Rtf2*$^{+/stop}$ of 1:2): χ^2 value: 2.88 p-value: 0.09

D

16 (47.1%) 18 (52.9%) 0 (0.0%)

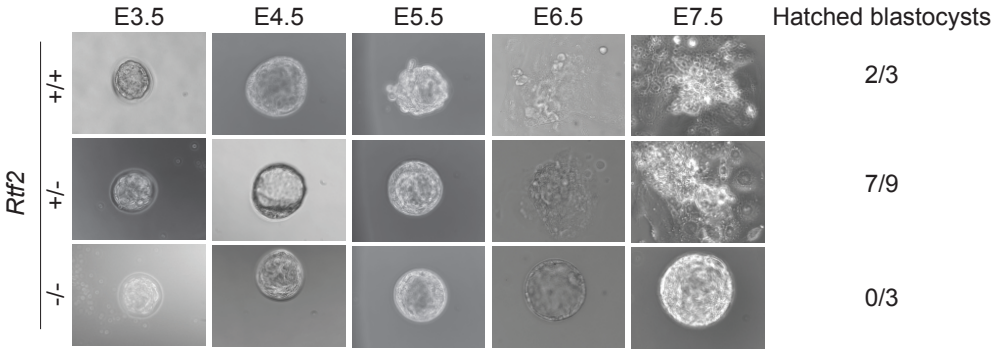

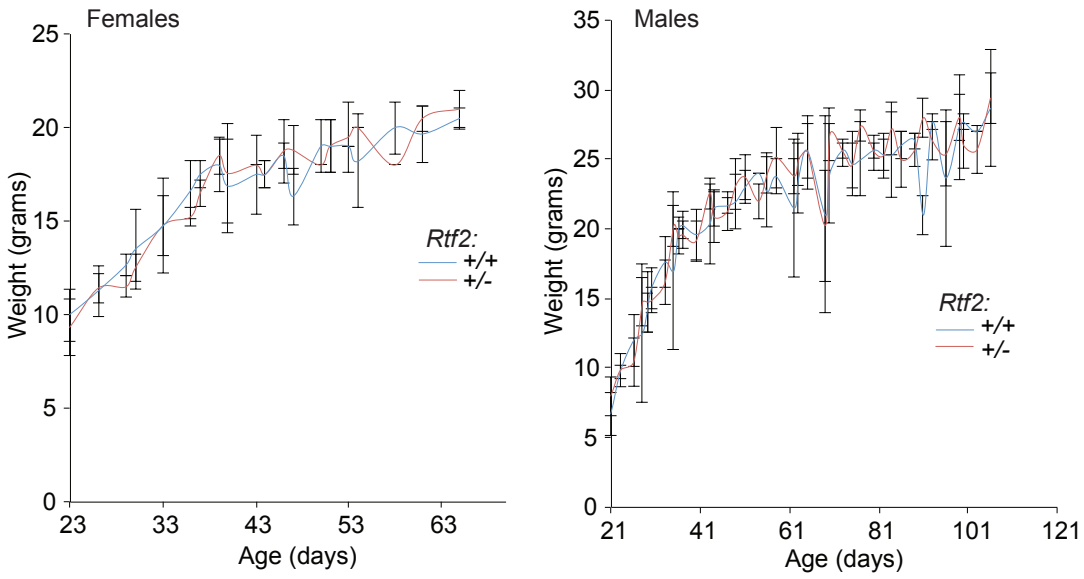

Figure 2.4. *Rtf2* heterozygous mice do not display growth defects.
Rtf2$^{+/+}$ mice and *Rtf2*$^{+/-}$ were weighed at given days. There are no statistically significant changes between the genotypes. For each point, n≥2 mice. n for given genotypes, male *Rtf2*$^{+/+}$ = 14, male *Rtf2*$^{+/-}$ = 34, female *Rtf2*$^{+/+}$ = 15 and female *Rtf2*$^{+/-}$ = 21.

Based on the hypothesis that the selection cassette may partially disrupt the *Rtf2* allele, *Rtf2*$^{+/stop}$ mice were intercrossed to examine the Mendelian ratios of hypomorphic mice. Hypomorphic *Rtf2*$^{stop/stop}$ mice were also inviable (Figure 2.3C).

Since we could not study other phenotypes associated with loss of RTF2 *in vivo,* a conditional cell culture system was generated. *Rtf2*$^{+/+}$, *Rtf2*$^{+/lox}$, *Rtf2*$^{lox/lox}$ and *Rtf2*$^{-/lox}$ mouse embryonic fibroblasts (MEFs) were isolated from the appropriate crosses. Multiple MEF lines from individual mothers were isolated and used as biological replicates. Primary, SV40 Large T antigen (SV40)-immortalized and *Rtf2*$^{-/-}$ clonal cell lines generated from SV40-immortalized *Rtf2*$^{-/lox}$ MEFs after infection with pMMP Hit & Run Cre recombinase were characterized. Despite RTF2 being essential in mice, RTF2-null clonal cell lines were isolated and this isolation was dependent on the SV40-immortalization. These clones grew very slowly and displayed phenotypes consistent with the bulk populations of RTF2-deficient cells as discussed below.

To ablate RTF2 in MEFs, cells were transduced with a retrovirus expressing Cre recombinase (pMMP Hit & Run Cre or pWZL Cre-hygro). Post-infection, RTF2 expression was barely detectable by western blot or quantitative reverse transcription PCR (RT-qPCR) in *Rtf2*$^{-/lox}$ and *Rtf2*$^{lox/lox}$ MEFs, demonstrating inducible loss of RTF2 (Figure 2.5A-D). *Rtf2*$^{+/lox}$ MEFs expressed intermediate levels of RTF2 (Figure 2.5A-D). These data support that *Rtf2* expression is abrogated in the *Rtf2* mouse model. RTF2-deficient MEFs were transduced with a wild type mouse *Rtf2* (*mRtf2*) cDNA. Cells lacking RTF2 exhibited a significant growth defect that was rescued upon expression of the wild type *mRtf2* cDNA (Figure 2.6A-C). Based on the *in vivo* and *in vitro* data, we conclude RTF2 is required for cellular and organismal growth.

Cells without RTF2 exhibited abnormal nuclear morphology, including multinucleated cells and cells with multiple micronuclei (Figure 2.7A,B). To examine the source of these abnormal nuclei, GFP-H2B was expressed in RTF2-deficient cells and imaged every 5 minutes (Figure 2.7C). This revealed that the abnormal nuclei are likely a result of inappropriate cell division as there was an increase in abnormal mitoses (Figure 2.7C,D). Cells without RTF2 also took about 10-15 minutes longer to complete mitosis than wild type cells. The accumulation of abnormal nuclei was suppressed by treatment with RO-3306, a potent specific inhibitor of CDK1 (Vassilev et al., 2006) that traps the cells in G2 and prevents them from entering M phase (Figure 2.7E). This data suggest that the increase in abnormal nuclei is a result of aberrant cellular division.

2.2.2 RTF2 is necessary for efficient DNA replication

Given that RTF2 is identified as a component of the replisome, (Alabert et al., 2014; Dungrawala et al., 2015; Kottemann et al., 2018; Wessel et al., 2019), we hypothesized that RTF2 functions in DNA replication. Cell cycle profiles were assessed after labeling *Rtf2* MEFs with 5-Ethynyl-2-deoxyuridine (EdU), a thymidine analog (Figure 2.8). In

Figure 2.5. Induction of RTF2 loss in MEFs.
(A) Immunoblot showing that cell lysates isolated from primary MEFs infected with pMMP Hit & Run Cre recombinase retrovirus (96 hours post-infection) lack RTF2 expression. (B) Representative RT-qPCR of relative *Rtf2* mRNA transcript levels in primary MEFs using primers flanking exons 5 and 6. Cell lysates were prepared 96 hours post-infection with pMMP Hit & Run Cre recombinase. Expression was normalized against *β-actin*. Error bars indicate standard deviation. (C) Immunoblot showing cell lysates isolated from SV40-immortalized MEFs expressing cDNA for HA-FLAG-empty-vector (+ EV) or HA-FLAG-mouse-RTF2 (+ mRTF2) infected with pWZL Cre-hygro retrovirus (96 hours post-infection). (D) Representative RT-qPCR of relative *Rtf2* mRNA transcript levels in SV40-immortalized MEFs 72 hours post infection with pWZL Cre-hygro retrovirus. Expression was normalized against *β-actin*. Error bars indicate standard deviation. (E) Immunoblot showing that cell lysates isolated from SV40-immortalized *Rtf2*$^{-/-}$ + EV MEF clones lack RTF2 expression compared to *Rtf2*$^{-/-}$ + mRTF2 MEF clones. Clones were isolated from *Rtf2*$^{-/lox}$ MEFs infected with pMMP Hit & Run Cre. After infection, cells were single cell cloned and stable *Rtf2*$^{-/-}$ MEF clones were obtained. These clones were infected with indicated HA-FLAG-tagged retroviruses. (F) Representative RT-qPCR of relative *Rtf2* mRNA transcript levels in SV40-immortalized *Rtf2*$^{-/-}$ MEF clones + EV or + mRTF2. Expression was normalized against *β-actin*. Error bars indicate standard deviation.

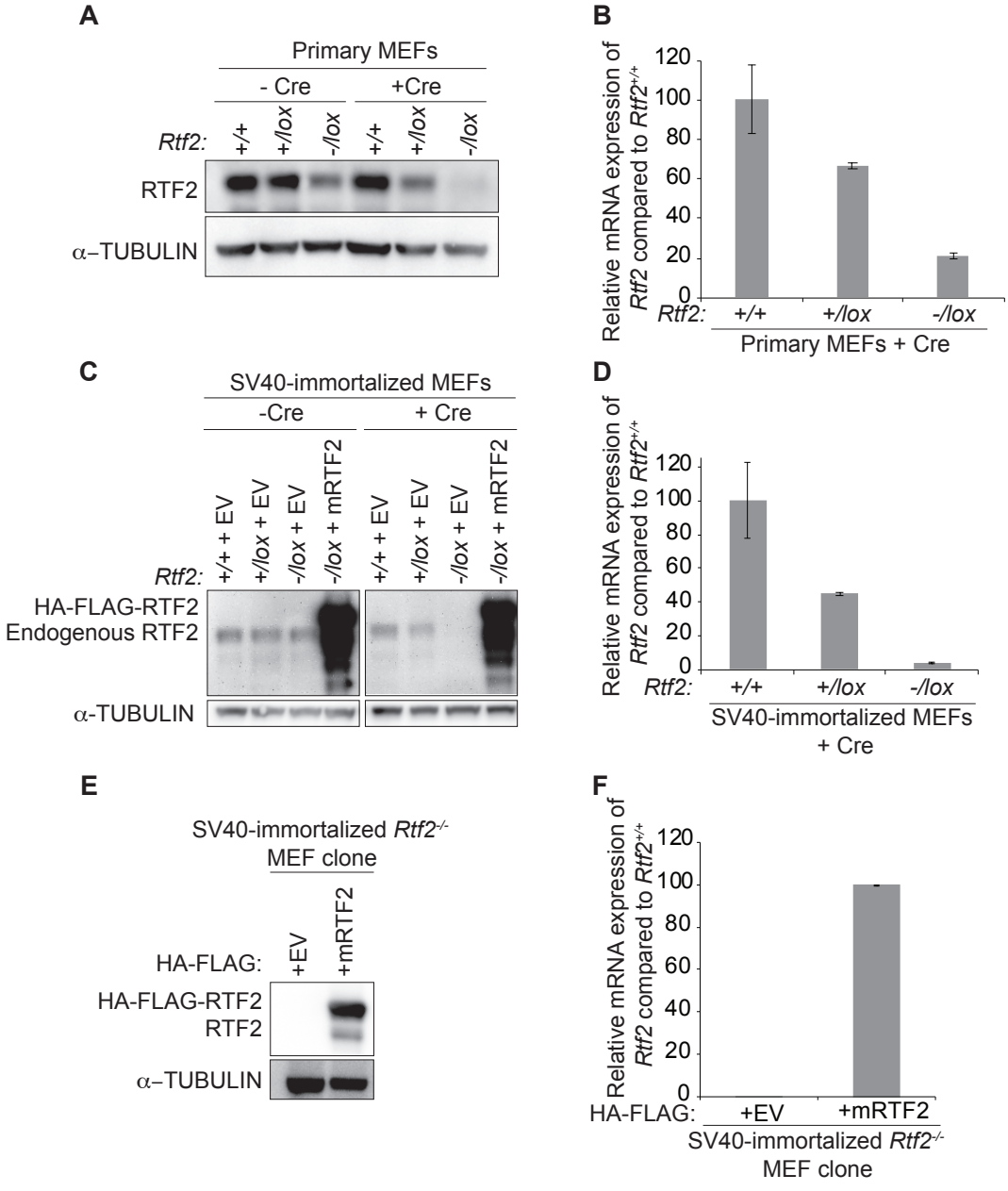
A
Primary MEFs
- Cre
+Cre
Rtf2:
+/+
+/lox
-/lox
+/+
+/lox
-/lox
RTF2
α–TUBULIN
B
Relative mRNA expression of Rtf2 compared to Rtf2+/+
120
100
80
60
40
20
0
Rtf2:
+/+
+/lox
-/lox
Primary MEFs + Cre
C
SV40-immortalized MEFs
-Cre
+ Cre
+/+ + EV
+/lox + EV
-/lox + EV
-/lox + mRTF2
+/+ + EV
+/lox + EV
-/lox + EV
-/lox + mRTF2
Rtf2:
HA-FLAG-RTF2
Endogenous RTF2
α-TUBULIN
D
Relative mRNA expression of Rtf2 compared to Rtf2+/+
120
100
80
60
40
20
0
Rtf2:
+/+
+/lox
-/lox
SV40-immortalized MEFs
+ Cre
E
SV40-immortalized Rtf2-/-
MEF clone
+EV
+mRTF2
HA-FLAG:
HA-FLAG-RTF2
RTF2
α–TUBULIN
F
Relative mRNA expression of Rtf2 compared to Rtf2+/+
120
100
80
60
40
20
0
HA-FLAG:
+EV
+mRTF2
SV40-immortalized Rtf2-/-
MEF clone

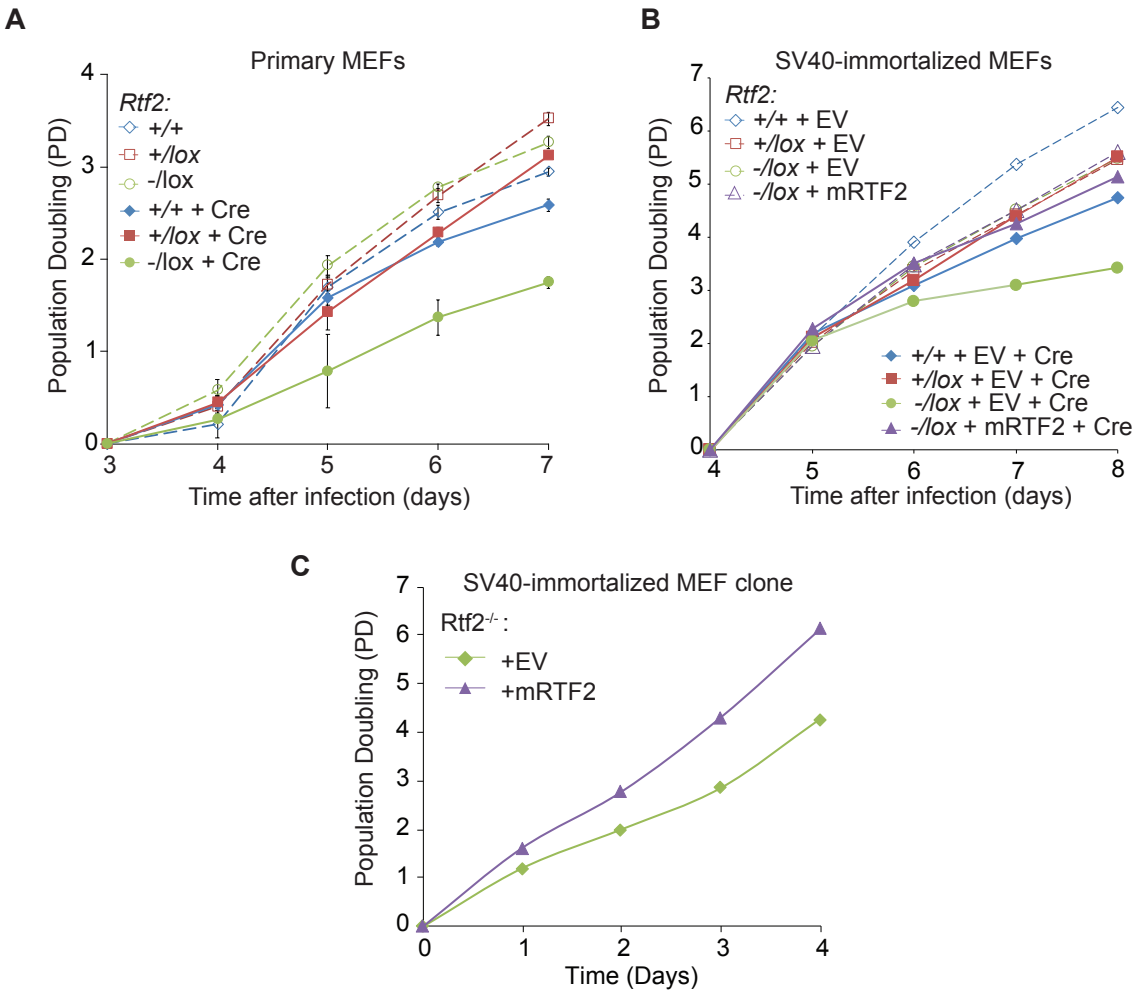

Figure 2.6. Loss of RTF2 induces a growth defect *in vitro*.
(A) Representative growth curves of primary MEFs with or without infection of Hit & Run Cre recombinase retrovirus. 50,000 cells of the indicated genotypes were plated per well of a 6-well dish. Cells were counted on subsequent days. Error bars indicate standard deviation. (B) Representative growth curves of SV40-immortalized MEFs expressing cDNA for HA-FLAG-empty-vector (+ EV) or HA-FLAG-mouse-RTF2 (+ mRTF2) infected with pWZL Cre-hygro retrovirus. 25,000 cells of indicated genotypes were plated per well of a 6-well dish. Cells were counted on subsequent days. (C) Representative growth curves of SV40-immortalized *Rtf2*$^{-/-}$ MEF clones + EV or + mRTF2. 25,000 cells of indicated genotypes were plated per well of a 6-well. Cells were counted on subsequent days.

Figure 2.7. RTF2-deficient cells have abnormal nuclei as a result of defective mitoses.
(A) Representative images of DAPI-stained nuclei in SV40-immortalized MEFs after infection with pWZL Cre-hygro (120 hours). (B) Quantification of abnormal DAPI-stained nuclei in images shown in A. Averages plotted from three biological replicates. Error bars indicate standard deviation. (C) Representative mitoses from SV40-immortalized Rtf2$^{-/lox}$ MEFs after infection with pWZL Cre-hygro (120 hours). Top panel represents a normal mitosis. Bottom three panels represent examples of mitoses generating micronuclei, nuclear holes and binucleated cells. (D) SV40-immortalized MEFs expressing GFP-H2B. Cells were imaged every 5 minutes for 24 hours. Quantification of abnormal mitoses. (E) Representative images of DAPI-stained nuclei in SV40-immortalized MEFs after infection with pWZL Cre-hygro (120 hours) were treated with CDK1 inhibitor (RO-3306) for an additional 24 hours to prevent mitosis and collected 144 hours post-Cre infection. (F) Quantification of abnormal DAPI-stained nuclei in images shown in E. Averages plotted from two biological replicates.
Error bars indicate standard deviation.

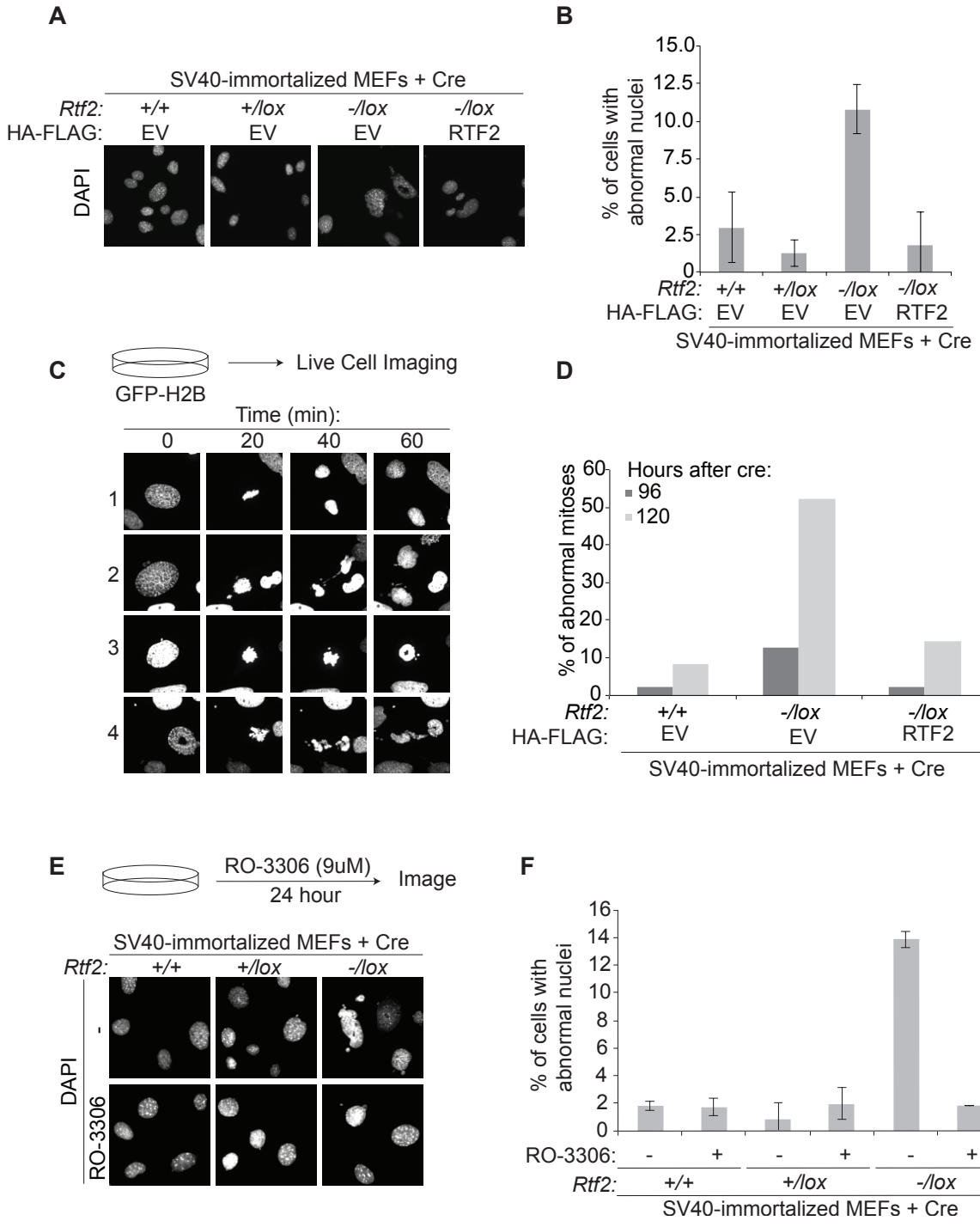
A
SV40-immortalized MEFs + Cre
Rtf2: +/+ +/lox -/lox -/lox
HA-FLAG: EV EV EV RTF2
DAPI
B
% of cells with abnormal nuclei
15.0
12.5
10.0
7.5
5.0
2.5
0
Rtf2: +/+ +/lox -/lox -/lox
HA-FLAG: EV EV EV RTF2
SV40-immortalized MEFs + Cre
C
GFP-H2B
Live Cell Imaging
Time (min):
0 20 40 60
1
2
3
4
D
% of abnormal mitoses
Hours after cre:
96
120
60
50
40
30
20
10
0
Rtf2: +/+ -/lox -/lox
HA-FLAG: EV EV RTF2
SV40-immortalized MEFs + Cre
E
RO-3306 (9uM)
24 hour
Image
SV40-immortalized MEFs + Cre
Rtf2: +/+ +/lox -/lox
DAPI
-
RO-3306
F
% of cells with abnormal nuclei
16
14
12
10
8
6
4
2
0
RO-3306: - + - + - +
Rtf2: +/+ +/lox -/lox
SV40-immortalized MEFs + Cre

Figure 2.8. RTF2-deficient cells exhibit an S phase defect.
(A) Representative cell cycle profiles from flow cytometry of primary MEFs after infection with Hit & Run Cre recombinase retrovirus (72 hours). Cells were pulsed with EdU for one hour prior to collection and fixation. Newly replicated DNA is represented on the y-axis in logarithmic scale. Total DNA content is represented on the x-axis in linear scale. Percentage of cells in S phase is shown in the top left corner of each plot. (B) Representative cell cycle profiles from flow cytometry of SV40-immortalized MEFs expressing cDNA for HA-FLAG-empty-vector (+ EV) or HA-FLAG-mouse-RTF2 (+ mRTF2) infected with pWZL Cre-hygro retrovirus (120 hours post-infection). (C) Mean G1, S, and G2 populations from B. Error bars represent standard deviation; n=3, biological replicates.

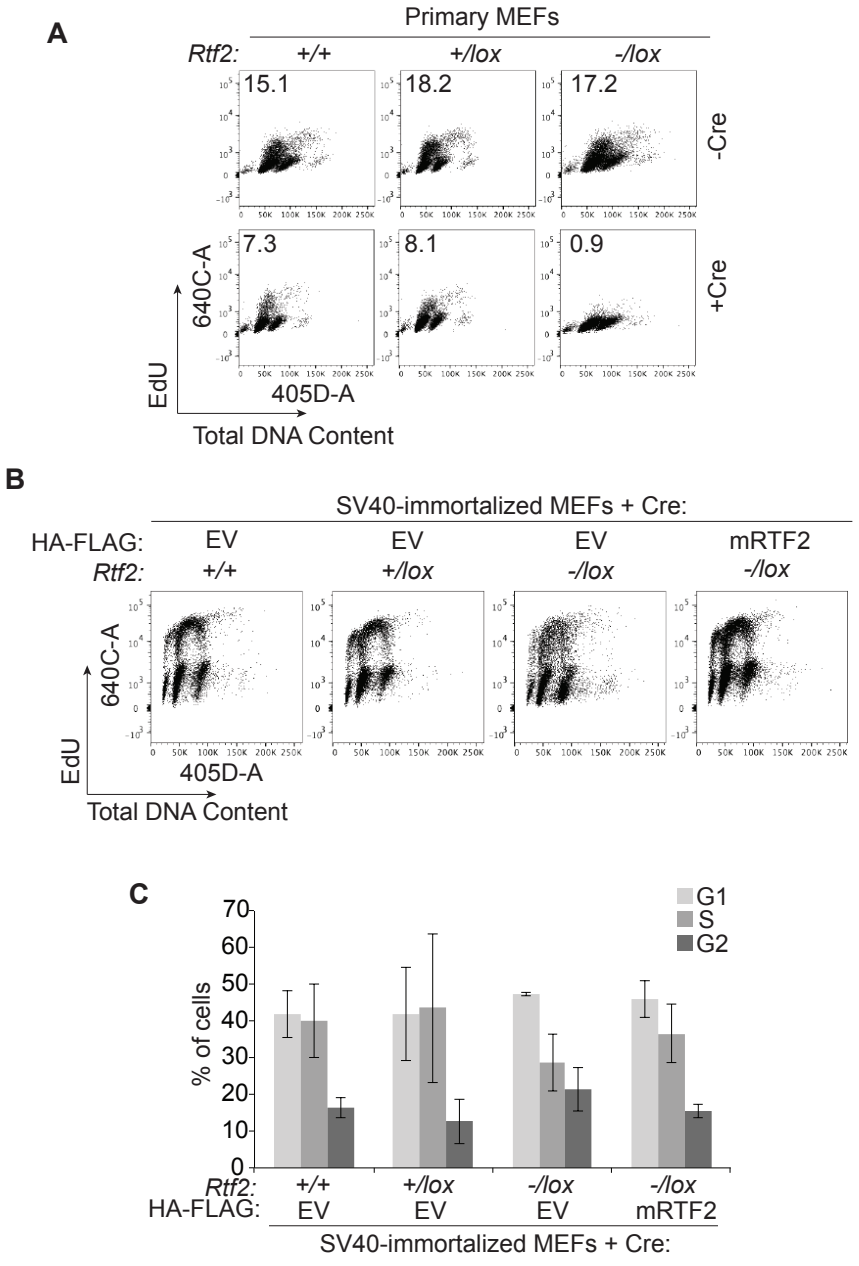
A
Primary MEFs
Rtf2:
+/+
+/lox
-/lox
15.1
18.2
17.2
-Cre
7.3
8.1
0.9
+Cre
640C-A
EdU
405D-A
Total DNA Content
B
SV40-immortalized MEFs + Cre:
HA-FLAG:
EV
EV
EV
mRTF2
Rtf2:
+/+
+/lox
-/lox
-/lox
640C-A
EdU
405D-A
Total DNA Content
C
G1
S
G2
% of cells
70
60
50
40
30
20
10
0
Rtf2:
+/+
+/lox
-/lox
-/lox
HA-FLAG:
EV
EV
EV
mRTF2
SV40-immortalized MEFs + Cre:

primary RTF2-deficient cells, there was a significant decrease in the S phase (EdU positive) population (Figure 2.8A). In SV40-immortalized cells, RTF2-deficient cells exhibited a population that did not reach peak EdU intensity, incorporating less EdU at a comparable total DNA content in mid-S (Figure 2.8B). The SV40-immortalized RTF2-null cells showed a decrease in the percentage of cells in the S phase population and an increase in the G2 population, but neither of these changes reached statistical significance (Figure 2.8C). While the cell cycle profiles were different between primary and immortalized, there was a consistent S phase defect. To further assess the S phase population, cells were grown on coverslips and pulsed with EdU for one hour (Figure 2.9). Cre-infected *Rtf2*$^{-/lox}$ EdU positive cells exhibited a significant decrease in mean nuclear gray value of EdU (Figure 2.9). Together these data suggest a defect in DNA synthesis.

To examine this S phase defect at a single-molecule level, replication forks lengths were directly assessed using DNA combing (Figure 2.10A). A significant decrease in replication fork tract length was observed in RTF2-deficient cells and this defect could be complemented upon expression of a *mRtf2* cDNA (Figure 2.10B-D). This defect was more pronounced in the RTF2-deficient primary MEFs; replication tract lengths were approximately 40% shorter in RTF2-deficient primary MEFs compared wild type cells and tract lengths were approximately 25% shorter in RTF2-deficient SV40-immortalized MEFs compared to wild type cells. Replication without RTF2 was slower and inter-origin distance was decreased (Figure 2.11A), but the replication forks around origins were symmetrical (Figure 2.11B), suggesting that replication forks are stable without of RTF2.

While expression of a wild type *Rtf2* cDNA complemented the replication defect, we wanted to test the necessity of key residues, specifically the cysteines in RTF2's RING domain, in the observed replication function. Expression of *Rtf2* cDNA constructs with mutation of a single cysteine residue of the RING motif to alanine (C121A, C140A, C142A, or C160A) complemented the replication defect, whereas mutation of two or more cysteine residues to alanine did not (C140A/C142A, C121A/C160A, C121A/C140A/C142A, C121A/C140A/C142A/C157A, C121A/C140A/C142A/C157A/ C160A, C121A/C140A/ C142A/C160A (Figure 2.12), suggesting the RING domain, particularly its ability to use four cysteines to chelate an Zn^{2+} ion, is important for RTF2's function in DNA replication.

Previous reports in *Arabidopsis thaliana* suggest RTF2 has a role in intron retention (Sasaki et al., 2015). Using paired-end RNA-seq, we did not detect any significant changes in global intron retention, defined as the percent of reads mapping to introns (Figure 2.13A). Single-ended RNA-seq also did not show a large difference in the transcriptional profile of RTF2-deficient MEFs as only 64 genes were significantly differentially expressed (Figure 2.13B).

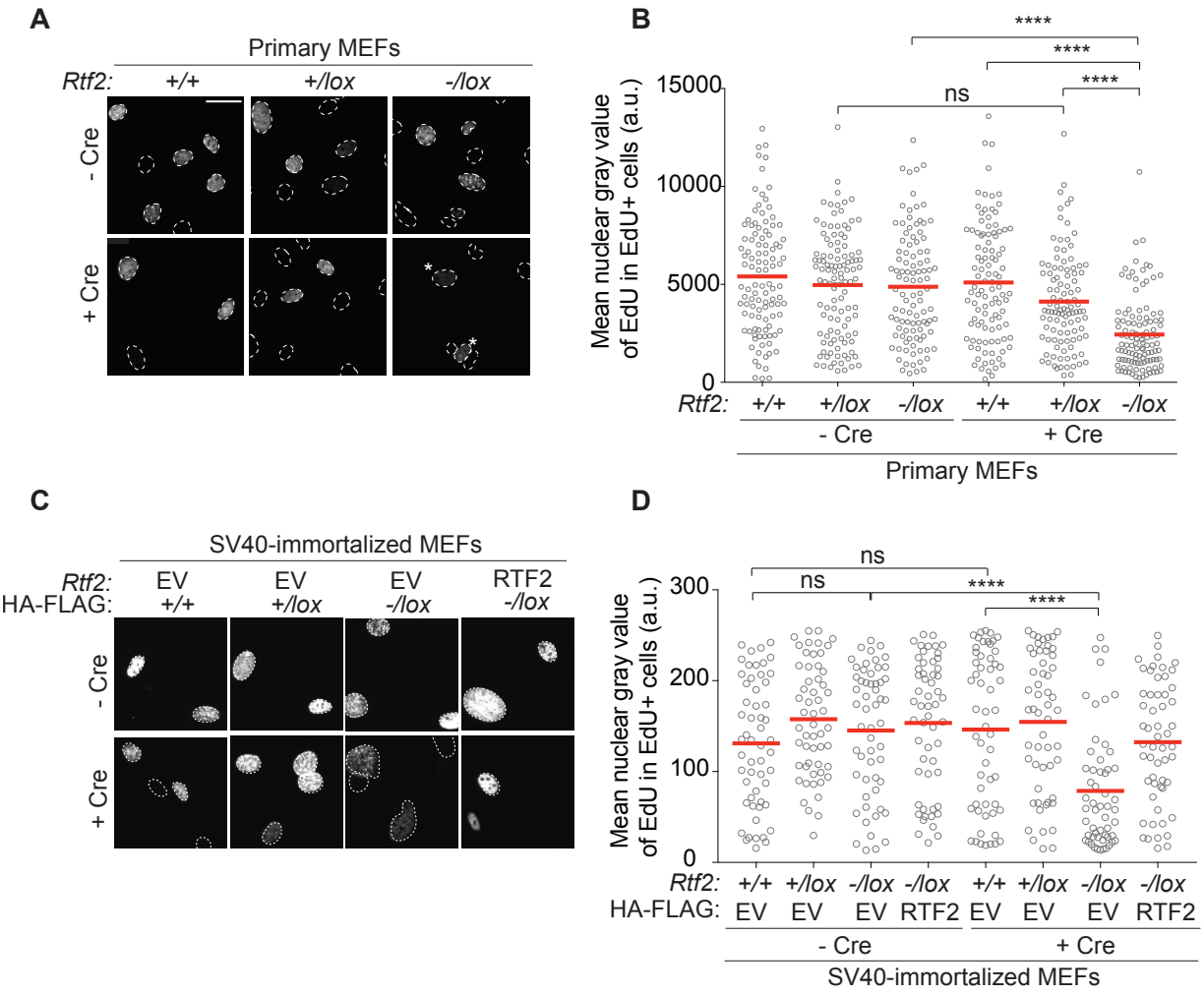

Figure 2.9. Loss of RTF2 results in decreased DNA synthesis.
(A) Representative immunofluorescence images cells in primary MEFs after infection with Hit & Run Cre recombinase retrovirus (72 hours). Cells were pulsed with EdU for 1 hour prior to fixation. Nuclei are outlined in dashed lines based on DAPI staining. * indicated EdU positive cells in the *Rtf2*$^{-/lox}$ + Cre sample. (B) Representative quantification of mean nuclear gray value of EdU from EdU positive cells from A. Each dot represents Edu positive one cell. Mean for each sample shown with red line. n>100 for each sample. ****P <0.0001, ns, not significant, Kruskal-Wallis ANOVA with a Dunn's post-test. (C) Representative immunofluorescence images as described in A in SV40-immortalized MEFs expressing cDNA for HA-FLAG-empty-vector (+ EV) or HA-FLAG-mouse-RTF2 (+ mRTF2) after infection with pWZL Cre-hygro retrovirus (120 hours). (D) Representative quantification of mean nuclear gray value of EdU from EdU positive cells from C. Each dot represents one EdU positive cell. Mean for each sample shown with red line. n=55 for each sample.
****P <0.0001, ns, not significant, Kruskal-Wallis ANOVA with a Dunn's post-test.

Figure 2.10. RTF2 is necessary for normal DNA replication speed.
(A) Experimental schematic of DNA combing. Cells were labeled with IdU for 30 minutes, washed, and then labeled with CldU for 30 minutes. Cells were then collected, and DNA was combed onto silanized glass coverslips, fixed, denatured and immunodetected. Progressing forks are defined as those that have both IdU and CldU incorporation as seen on the left. (B) Representative experiment showing replication tract lengths of progressing fork species from primary MEFs after infection with Hit & Run Cre recombinase retrovirus (72 hours). Each dot represents one replication tract. Mean tract length and fork speeds using a conversion factor of 2kb/μm/minute are listed above each sample. Each dot represents one replication tract. Mean for each sample shown with red line. n=200 for each sample. ****P<0.0001, ns, not significant, Kruskal-Wallis ANOVA with a Dunn's post-test. (C) Representative experiment showing replication tract lengths of progressing forks from SV40-immortalized MEFs expressing cDNA for HA-FLAG-empty-vector (+ EV) or HA-FLAG-mouse-RTF2 (+ mRTF2) after infection with pWZL Cre-hygro retrovirus (120 hours). Each dot represents one replication tract. Mean for each sample shown with red line. n>200 for each sample. ****P<0.0001, ns, not significant, Kruskal-Wallis ANOVA with a Dunn's post-test. (D) Representative experiment showing replication tract lengths of progressing forks from SV40-immortalized *Rtf2*$^{-/-}$ MEF clones + EV or + mRTF2. Each dot represents one replication tract. Mean for each sample shown with red line. n>300 for each sample. ****P<0.0001, ns, not significant, t-test.

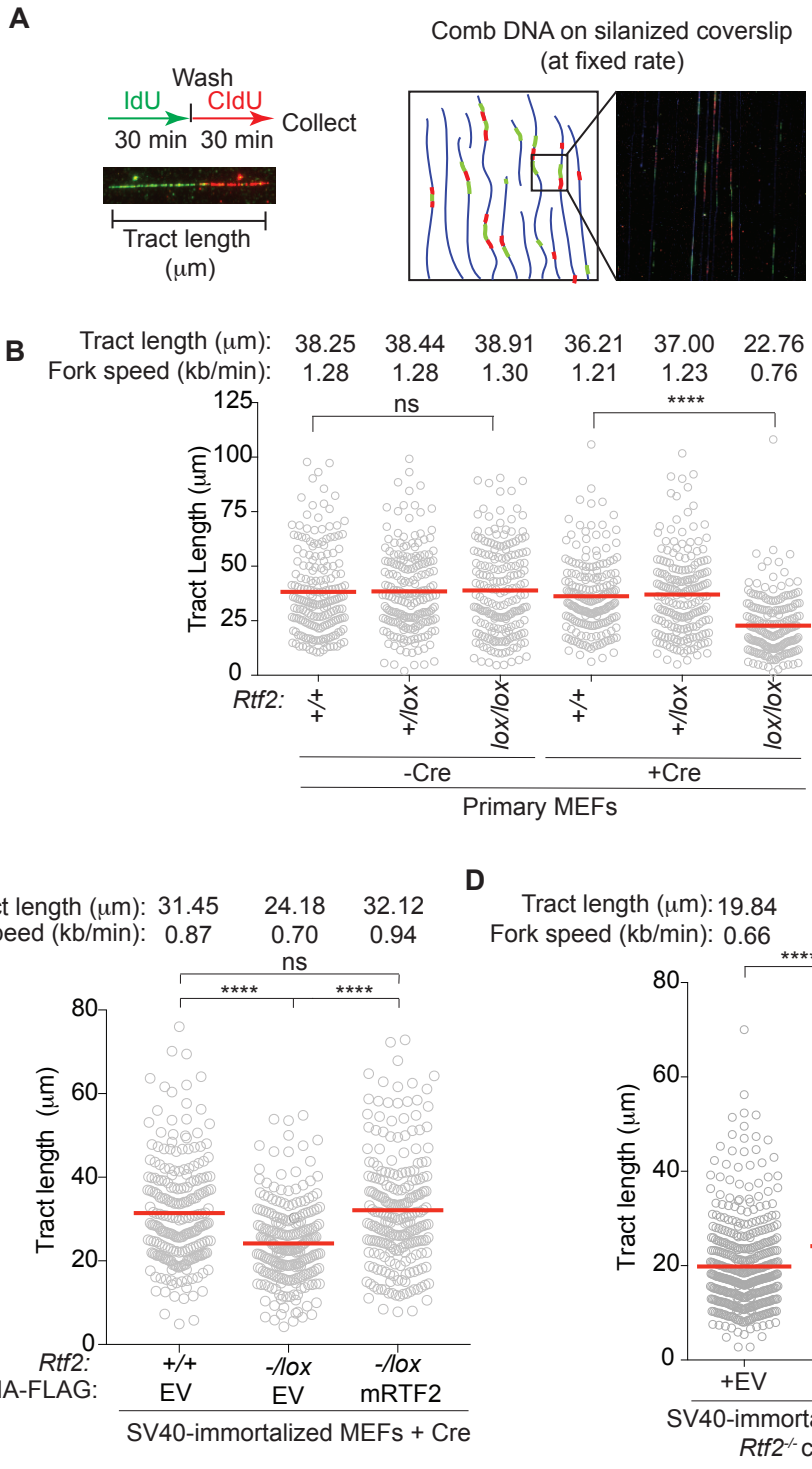
A
Wash
IdU
CldU
Collect
30 min 30 min
Tract length (μm)
Comb DNA on silanized coverslip (at fixed rate)
B
Tract length (μm): 38.25 38.44 38.91 36.21 37.00 22.76
Fork speed (kb/min): 1.28 1.28 1.30 1.21 1.23 0.76
ns
****
Tract Length (μm)
125
100
75
50
25
0
Rtf2: +/+ +/lox lox/lox +/+ +/lox lox/lox
-Cre
+Cre
Primary MEFs
C
Tract length (μm): 31.45 24.18 32.12
Fork speed (kb/min): 0.87 0.70 0.94
ns
****
****
Tract length (μm)
80
60
40
20
0
Rtf2: +/+ -/lox -/lox
HA-FLAG: EV EV mRTF2
SV40-immortalized MEFs + Cre
D
Tract length (μm): 19.84 24.48
Fork speed (kb/min): 0.66 0.82
****
Tract length (μm)
80
60
40
20
0
+EV +mRTF2
SV40-immortalized MEF
Rtf2-/- clone

Figure 2.11. RTF2-deficiency affects inter-origin distances, but not replication fork symmetry.
(A) Representative experiment showing the length of inter-origin distances (IOD) measured within replication clusters from primary MEFs after infection with Hit & Run Cre recombinase retrovirus (72 hours). Mean for each sample shown with red line. n>30 for each sample. *P<0.05, **P<0.01, ns, not significant, Kruskal-Wallis ANOVA with a Dunn's post-test. (B) Representative experiment showing fork symmetry from primary MEFs after infection with Hit & Run Cre recombinase retrovirus (72 hours). Replication initiation sites were identified as species where the second label (CldU) flanks the first label (IdU). Left fork length is plotted against right fork length. Lines represent arbitrary cutoffs for replication forks with symmetry less than 2 and greater than 0.5. Percentages in the bottom right corner represent the percentage of asymmetrical forks.

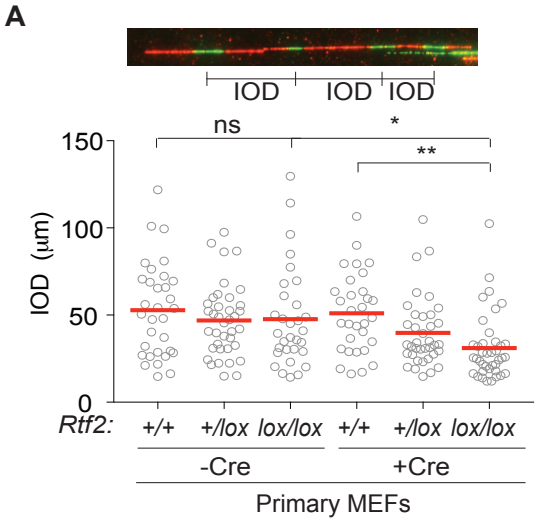
A
IOD
IOD
IOD
ns
*
**
150
100
50
0
IOD (μm)
Rtf2:
+/+
+/lox
lox/lox
+/+
+/lox
lox/lox
-Cre
+Cre
Primary MEFs

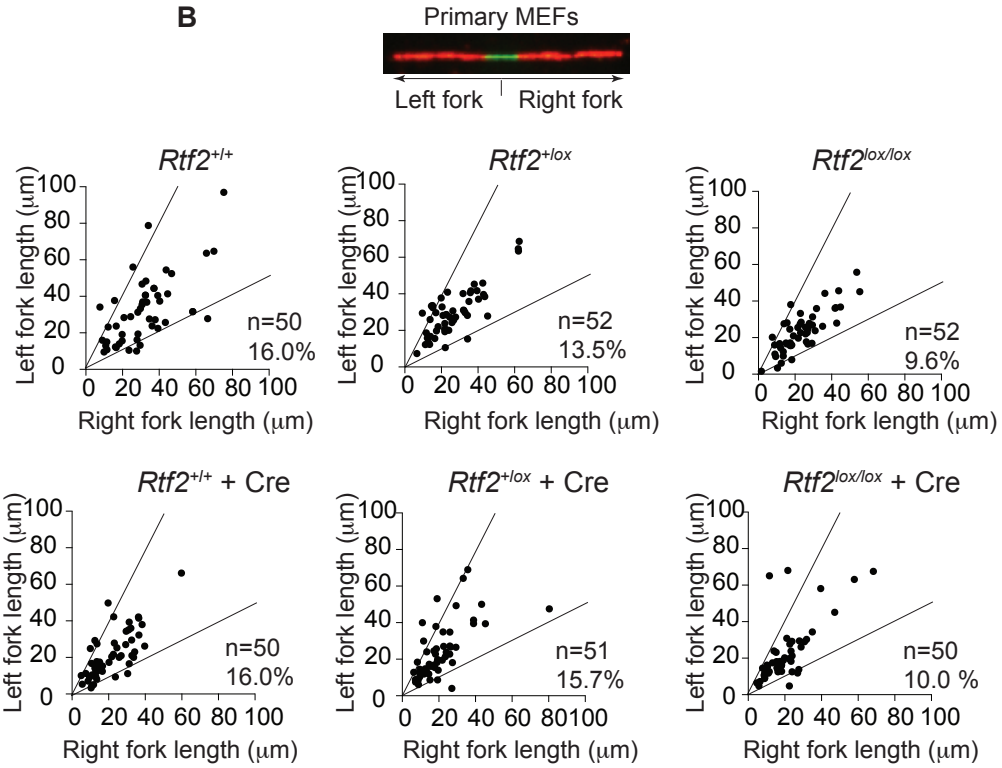
B
Primary MEFs
Left fork
Right fork
Rtf2+/+
Rtf2+lox
Rtf2lox/lox
Left fork length (μm)
Right fork length (μm)
n=50
16.0%
n=52
13.5%
n=52
9.6%
Rtf2+/+ + Cre
Rtf2+lox + Cre
Rtf2lox/lox + Cre
n=50
16.0%
n=51
15.7%
n=50
10.0 %

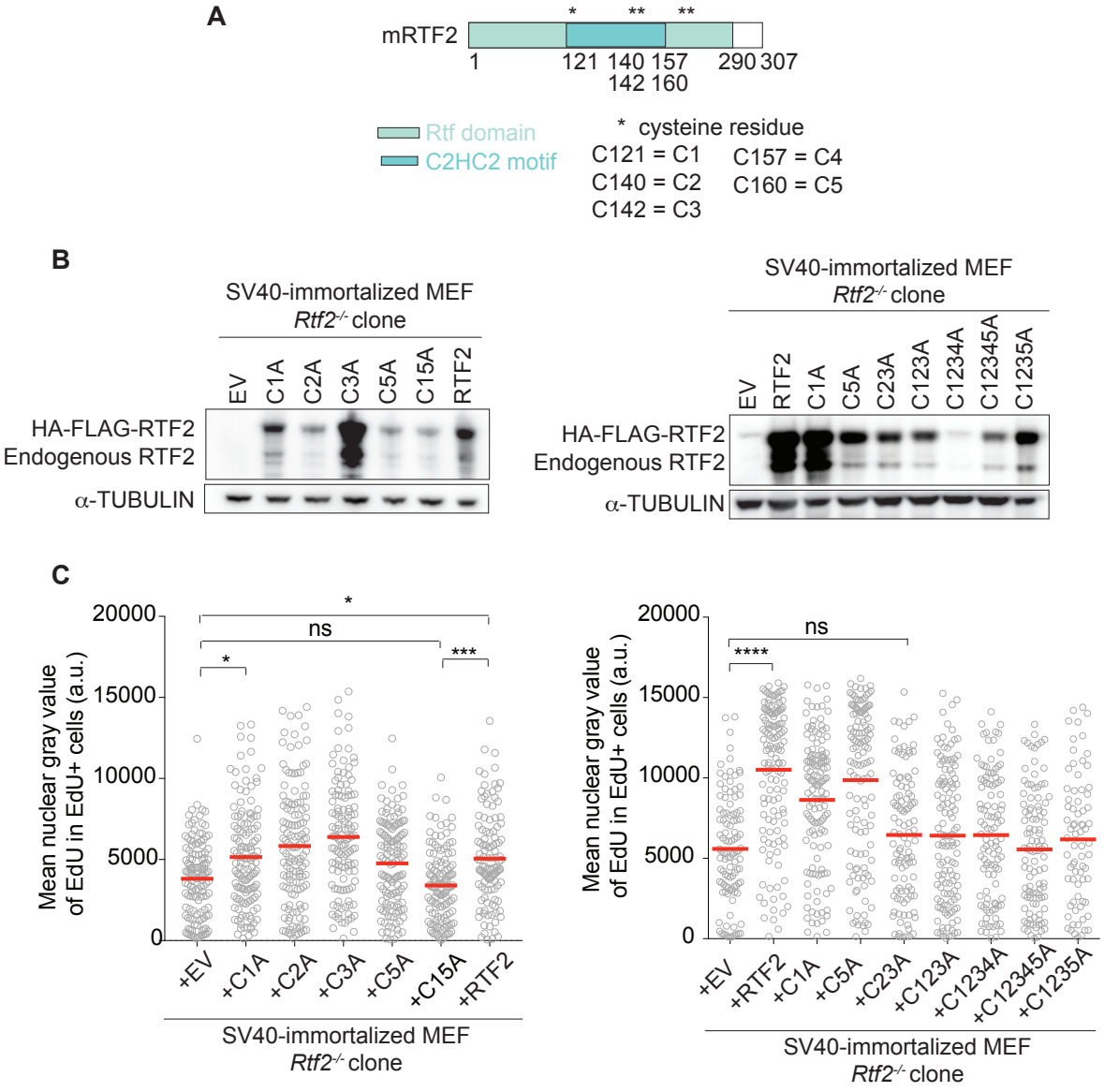

Figure 2.12. RTF2's RING domain is necessary for DNA replication.
(A) Schematic of RTF2 protein. Mouse and human RTF2 contain 5 cysteines that are predicted to function as part of the RING domain. These cysteine residues were mutated to alanine residues in various combinations. C1A represents C121A where as C23A represents C140A/C142A, etcetera. (B) Representative immunoblots of whole cell lysates isolated from SV40-immortalized *Rtf2*$^{-/-}$ MEF clones expressing indicated mRTF2 mutant constructs. (C) Representative quantification of mean nuclear gray value of EdU from EdU positive cells in SV40-immortalized *Rtf2*$^{-/-}$ MEF clones expressing indicated RTF2 RING mutant constructs. Each dot represents one EdU positive cell. Mean for each sample shown with red line. n>60 for each sample.
****P <0.0001. ns, not significant, Kruskal-Wallis ANOVA with a Dunn's post-test.

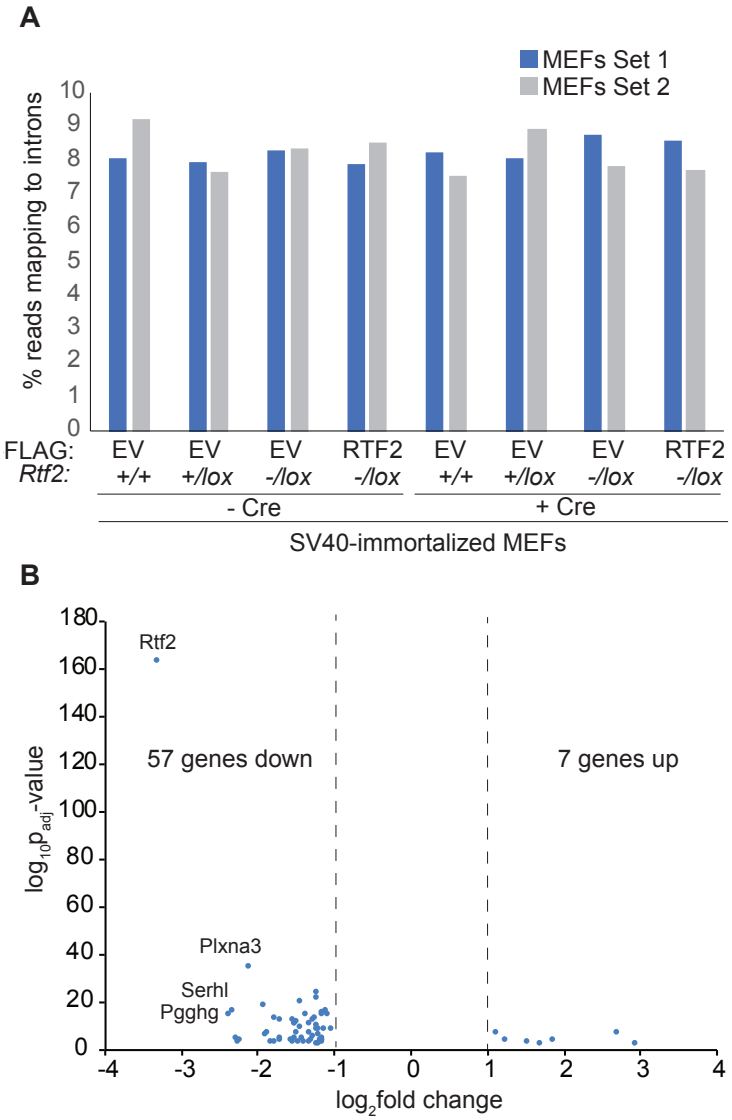

Figure 2.13. RTF2-deficient MEFs do not display global intron retention or gene expression defects.

(A) Percent of reads from paired-end RNA-seq mapping to introns. Genotypes are indicated for SV40-immortalized MEFs expressing cDNA for HA-FLAG-empty-vector (+ EV) or HA-FLAG-mouse-RTF2 (+ mRTF2) after infection with pWZL Cre-hygro retrovirus (120 hours). (B) Volcano plot showing $\log_{10}$p-values against $\log_2$fold change for the significant differentially expressed genes as calculated by DESeq2. Genes with $\log_2$fold change >1 and $p_{adjusted}$-value <0.05 averaged across the two sets of SV40-immortalized MEFs are shown. These results indicate 57 genes significantly downregulated and 7 genes significantly upregulated. n=3 for each set of MEFs, biological replicate. Comparison is between aligned single-end reads from *Rtf2*$^{+/+}$ and *Rtf2*$^{-/lox}$ SV40-immortalized MEFs infected with Hit & Run pMMP Cre retrovirus (72 hours).

2.3 Summary of Findings and Outlook

Together, these data demonstrate the importance of RTF2 for organismal viability, cellular proliferation, and DNA replication. The results from attempting to generate a mouse model indicate RTF2 is required very early in development. Since we were unable to isolate any normal proliferating *Rtf2*$^{-/-}$ blastocysts, RTF2 is likely required in the first few cell cycles. However, an increased sample size of blastocysts is needed to determine statistical significance. While Cre recombinase was expressed in mice from the ubiquitous EIIa promoter, the model was established in a manner to allow for deletion of RTF2 in specific tissues in the future. Mice expressing Cre driven from tissue-specific promoters are commercially available. Those of interest include the K14 (expression in all basal cells of skin epithelium including hair follicles) or Vav (expression in hematopoietic lineages) promoters. K14-driven Cre expression may help to assess RTF2's contribution to squamous cell carcinoma as has been published for RNase H2 (Hiller et al., 2018). Vav-driven Cre expression will determine if there is a defect without RTF2 in the hematopoietic compartment, where cells are highly proliferative and heavily rely on DNA replication.

There were no striking phenotypes associated with decreased levels of RTF2, as both *Rtf2*$^{+/-}$ mice and *Rtf2*$^{+/-}$ cells retained similar phenotypes to *Rtf2*$^{+/+}$ genotypes, suggesting that RTF2 is not haploinsufficient. The cell may need minimal levels of RTF2 to sustain normal proliferation and DNA replication rates. Transient knockdown of RTF2 with short-interfering RNAs (siRNAs) did not elicit growth and replication defects (data not shown), suggesting that very little RTF2 is necessary for cellular viability.

The phenotypes were consistent across different isolations of MEFs as well as between primary, immortalized, and clonal MEF lines. The immortalization with SV40, however, did lessen the replication defect. SV40-LT is a helicase that mediates viral DNA replication and its overexpression could impact general DNA replication (Borowiec et al., 1990; Cheng et al., 2009; Li et al., 2003a). RTF2-deficient cells may progress through mitosis, despite not being able to complete it appropriately, because of the SV40-immortalization which inhibits p53. The abnormal nuclear morphology in RTF2-deficient cells could be a result of premature mitotic entry with under-replicated and DNA damage. The cellular growth defect seen without RTF2 could be attributed to two possible causes: (1) decreased proliferation rate and/or (2) increased cell death. Slower replication fork speeds in the absence of RTF2 may contribute to a decreased proliferation rate. We cannot rule out the possibility that cell death also contributes to the slow growth as we have not examined the activation of programmed cell death pathways.

Single-molecule DNA fiber visualization assays have proven to be a powerful tool in mammalian cells to address fundamental replication processes. Two predominant methods are currently used in the field, but they have several differences. In the first method, DNA fibers, a cell mixture is dropped onto glass slides and lysed. The slides are then tilted to stretch the DNA. In the second method, cells are embedded in agarose plugs before lysis and proteinase K digestion. After melting and digesting the plugs, 'naked'

DNA is stretched at a fixed rate onto glass slides. The main difference in the DNA fiber technique is the lack of proteinase K digestion and a fixed stretching factor. This means that chromatin is present, which can influence DNA stretching, and stretching is variable between slides. DNA combing removes the confounding artifacts associated with the presence of chromatin and ensures a constant stretching rate. The work presented in this thesis solely employed the use of the DNA combing technique.

We observed a decrease of replication fork speed concurrent with decreased inter-origin distance (increased origin firing) and fork symmetry in RTF2-deficient cells. Increased origin firing could be a passive response to replication slowing. The increase in replication origin firing did not fully compensate for the slow replication speed, as the EdU immunofluorescence and cell cycle assays both show a bulk decrease in EdU intensity. The symmetry of the replication forks around origins implies the replication fork slowing is not the outcome of a stochastic impediment to replication. This makes it unlikely the slow replication in RTF2-deficient cells is a result of collision with the transcription machinery.

While the data presented here indicate the importance of RTF2's RING-finger domain, it remains unclear what functional activity this domain performs to maintain RTF2's role in DNA replication. The data presented are consistent with the hypothesis that any four of the five cysteine residues in the RTF2 RING-finger domain are required for RTF2's replication function. The data showing that single cysteine mutations (C121A, C160A or C140A, C142A) rescue the replication defect whereas combined double mutations (C121A/C160A or C140A/C142A) do not establish the requirement for four cysteines. The ability to complement the replication defect is not dependent upon the variability in expression levels of these constructs. This is most clearly demonstrated with a comparison between the expression of the C140A mutant construct and the C121A/C160A mutant construct. Both constructs are expressed at similarly low levels, but the single mutant rescues the replication defect whereas the double mutant does not. Understanding the function of this RING finger will require further biochemical analysis.

These results also indicate that there is not an RNA splicing defect in the absence of RTF2, in contrast to the role for RTF2 in RNA splicing reported in *A. thaliana*. We cannot exclude the possibility that some individual transcripts may be alternatively spliced, but there was no evidence that global changes were occurring. The RNA-seq results indicated specific genes were differentially regulated; however, there were no observable patterns, either based on chromosomal location or gene ontology, among the significant differentially expressed transcripts.

Chapter 3. RTF2's function during unperturbed replication is dependent on RNase H2

3.1 Introduction

Experiments described in the previous chapter indicate a role for RTF2 in normal DNA replication, but the mechanism of RTF2 function at the replication fork is unknown. In this chapter, discovery-based approaches were used to determine where and how RTF2 contributes to replisome function, including an examination of the changes in proteome of replication forks in the absence of RTF2 and the proteins directly interacting with RTF2. Together these data sets suggest that a complex previously identified at the replication fork, RNase H2 (Alabert et al., 2014; Dungrawala et al., 2015; Wessel et al., 2019), could be important for RTF2's function during replication. In this chapter, we explore this possibility and address the necessity of RNase H2 for normal DNA replication as well as the convergence of the phenotypes in cells deficient for RNase H2 or RTF2.

3.2 Results

3.2.1 RTF2 interacts with and recruits RNase H2 to the replication fork

To identify the mechanism behind the observed replication defect in RTF2-deficient cells, we employed isolation of proteins on nascent DNA (iPOND) (Dungrawala and Cortez, 2015; Sirbu et al., 2013) to examine the changes in the proteome at the replication fork in the absence of RTF2. Cells were pulsed with EdU, based on timing normalized for DNA replication tract lengths (Figure 3.1A) and the proteome associated with the nascent DNA was examined using liquid chromatography-mass-spectrometry (LC-MS). While peptides corresponding to replisome components, such as the MCM2-7 complex and PCNA, were identified, no peptides from the RNase H2 complex were detected in RTF2-null MEFs (Figure 3.1B). To validate RNase H2's dependence on RTF2 for replisome localization, nascent DNA proximity ligation assay (nPLA), a method to detect the presence of proteins at nascent DNA, was used (Taglialatela et al., 2017). nPLA showed a decrease of RNASEH2A, the catalytic subunit, at the replication fork in the absence of RTF2 (Figure 3.1C,D). Total levels of RNase H2 remained unchanged in cells lacking RTF2 by western or RT-qPCR (Figure 3.2), suggesting that RTF2 is necessary for RNase H2's presence at replication forks.

To catalog RTF2's network of protein interactions, several LC-MS-based discovery experiments were performed (Figure 3.3). This included immunoprecipitation of two different RTF2 constructs: (1) exogenous overexpression of N-terminal GFP-tagged RTF2 cDNA (Figure 3.3A) or (2) CRISPR-generated N-terminal GFP-tagged RTF2 cDNA construct incorporated at the *Rtf2* locus to replace the endogenous gene (Figure 3.3C-G, Sunandini Sridhar). LC-MS-based analysis of the RTF2-immunoprecipitated lysate yielded identification of many interacting factors (Figure 3.3B, H). Components of the MCM helicase and RPA also co-immunoprecipitated with RTF2, confirming RTF2's

A

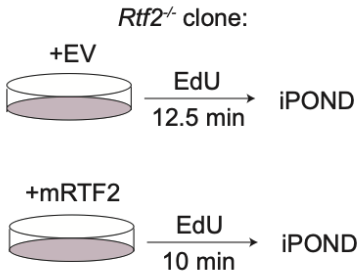

C

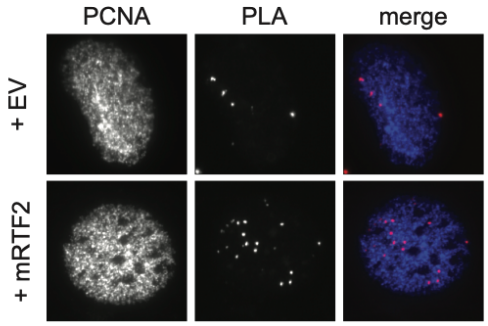

B

	#PSM	
Rtf2$^{-/-}$ clone:	+EV	+mRTF2
MCM2	14	17
MCM3	28	35
MCM4	24	29
MCM5	28	27
MCM6	31	34
MCM7	22	21
PCNA	75	50

	#PSM	
Rtf2$^{-/-}$ clone:	+EV	+mRTF2
RTF2	0	16
RNASEH2A	0	5
RNASEH2B	0	5
RNASEH2C	0	1

D

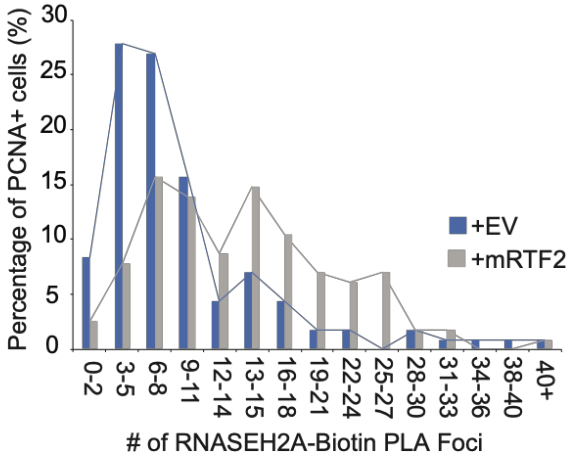

Figure 3.1. RTF2-deficient MEFs exhibit a concurrent loss of RNase H2 from the replication fork.

(A) Schematic depicting iPOND experimental setup. Cells were pulsed with EdU for differential times to normalize replication tract lengths. (B) Peptide Spectral Match values from SV40-immortalized *Rtf2*$^{-/-}$ MEF clones expressing cDNA for HA-FLAG-empty-vector (+ EV) or HA-FLAG-mouse-RTF2 (+ mRTF2). (C) Representative images from PCNA-stained nascent proximity ligation assay (nPLA). This assay has been optimized to detect the amount of protein at the replication fork by labeling with short pulses of EdU. *Rtf2*$^{-/-}$ + mRTF2 MEFs were labeled for 4.5 minutes and *Rtf2*$^{-/-}$ + EV MEFs were labeled for 6 minutes with EdU to normalize replication tracts. EdU was biotin-clicked and coverslips were incubated with mouse anti-biotin and rabbit anti-RNASEH2A. Antibody-coupled sense and anti-sense probes are detect the light chains of rabbit and mouse IgG, respectively. PLA signal represents RNASEH2A co-localizing with nascent DNA based on probe proximity. Cells were co-stained with PCNA to determine actively replicating cells. (D) Quantification of RNASEH2A-Biotin Foci in PCNA positive cells. Cells were binned by the number of foci and percentage of cells in each bin is plotted.

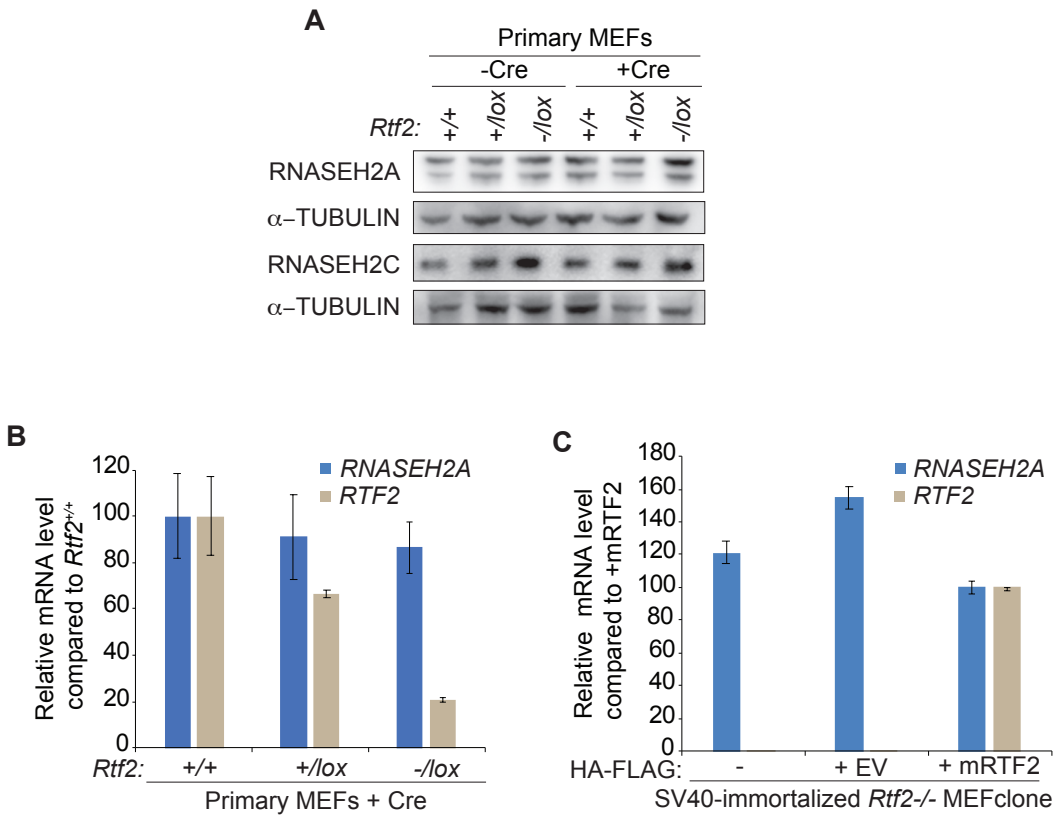

Figure 3.2. Total RNase H2 levels are unchanged in RTF2-deficient cells.
(A) Immunoblot of whole cell lysates isolated from primary MEFs infected with Hit & Run Cre recombinase retrovirus (72 hours) showing RNASEH2A and RNASE2C protein levels. (B,C) RT-qPCR analysis of mouse *Rnaseh2a* or mouse *Rtf2* expression in indicated cells normalized to *β-actin* expression. Error bars represent standard deviation.

Figure 3.3. RTF2 interacts with components of the replication fork and the RNase H2 complex.
(A) Immunoprecipitation with GFP from HEK 293Ts expressing GFP-Empty Vector (+ EV) or GFP-human-RTF2 (+ hRTF2). The GFP-hRTF2 construct is predicted to be 63.8 kDa. (B) GFP was immunoprecipitated from the chromatin fraction of cell lysates with GFP nanobodies isolated from cells in A. Peptide Spectral Match count (#PSM) and Area Under the Curve (AUC) from LC-MS for given proteins averaged across two biological replicates. (C) Schematic of CRISPR-Cas9 targeting of a plasmid containing homology arms to the 5' and 3' untranslated region's (UTR) of *Rtf2* flanking a *GFP-AID-hRTF2* cDNA at the endogenous *RTF2* locus in HEK 293Ts. sgRNAs were designed to cut within the 5' and 3' UTRs. Successfully edited clones were isolated. (D) Genotyping analysis of wild type and CRISPR-Cas9 targeted GFP-AID-RTF2 HEK 293Ts. Schematic represents genotyping primers that were used to amplify the endogenously tagged locus; Forward primer recognizes RTF2 promoter region upstream to the GFP-AID-hRTF2 insert and reverse primer recognizes an RTF2 exonic region. The primer pair amplifies a wild type RTF2 allele of 1124 bp and the GFP-tagged allele of 2571 bp. (E) Flow cytometry analysis of wild type and CRISPR-Cas9 targeted GFP-AID-RTF2 HEEK293Ts. (F) Representative immunofluorescence of CRISPR-Cas9 targeted GFP-AID-RTF2 293Ts. Cells were fixed and stained with anti-GFP antibodies. (G) Immunoprecipitation with GFP antibodies from wild type and CRISPR-Cas9 targeted GFP-AID-RTF2 HEK 293Ts. Membranes were immunoblotted with RTF2 antibody. The GFP-AID-hRTF2 construct is predicted to be 90.5 kDa. (H) GFP was immunoprecipitated with GFP antibodies from wild type and CRISPR-Cas9 targeted GFP-AID-RTF2 HEK 293Ts in C-F. #PSM and AUC from LC-MS for given proteins averaged across two biological replicates.

A

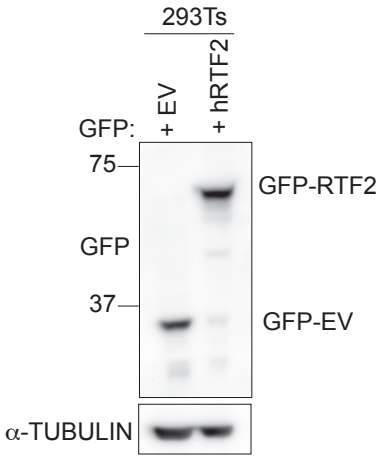

B

	IP: GFP			
	#PSM		AUC	
	GFP-EV	GFP-RTF2	GFP-EV	GFP-RTF2
RTF2	0	30	0.00	4.48E9
GFP-RTF2	0	60.5	0.00	4.97E9
RNASEH2A	0	1.5	0.00	4.96E7
RNASEH2C	0	0.5	0.00	9.88E6
MCM2	7.5	13.5	3.16E7	9.58E7
MCM3	7.5	14.5	1.518E7	6.26E8
MCM4	11	13.5	4.72E7	1.98E8
MCM5	3.5	3	5.76E7	7.25E7
MCM6	4	17	2.03E7	8.84E7
MCM7	7.5	16	5.21E7	1.79E8
PCNA	3.5	7	5.17E7	1.62E8
RPA70	3.5	8	3.10E7	7.07E7
RPA32	4.5	7	4.40E7	1.28E8
RPA14	0.5	2.5	9.22E7	2.31E8

C

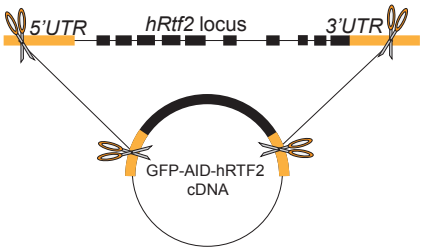

D

E

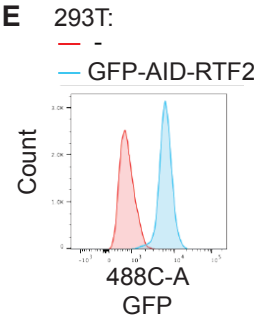

F

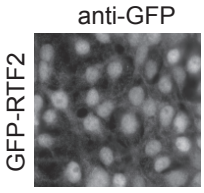

G

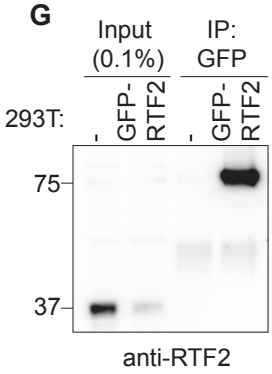

H

	IP: GFP			
	#PSM		AUC	
	293T	GFP-AID-RTF2	293T	GFP-AID-RTF2
RTF2	0	7.5	0.00	2.97E7
RNASEH2A	0.5	1.5	0.00	1.50E7
MCM2	0.5	2.5	9.84E5	6.14E6
MCM3	0	2.5	0.00	1.13E7
MCM4	0.5	1.5	2.69E6	1.15E7
MCM5	0.5	1.5	0.00	1.36E7
MCM6	0.5	4.5	2.14E6	9.14E6
MCM7	2	5	6.10E6	1.70E7
PCNA	5.5	7.5	9.25E7	2.31E8
RPA70	1	4	0.00	2.97E7
RPA32	0	1	0.00	9.70E6
RPA14	0	0.5	0.00	5.62E6
SAE1	0.5	3.5	0.00	2.71E7

presence at the replication fork. RNASEH2A was also among one of the top unique interactors of RTF2 identified by co-immunoprecipitation followed by LC-MS and was not detected in controls. These interactions, confirmed with co-immunoprecipitations followed by western blots, were not sensitive to benzonase treatment, a nuclease that hydrolyzes dsDNA, suggesting that the interactions are not mediated through both proteins binding to DNA (Figure 3.4). WAPL, a component of cohesion at the replication fork, did not co-immunoprecipitate with RTF2 indicating the specificity of the identified RTF2-RNASEH2A interaction (Figure 3.4).

To biochemically test these interactions, His14-GFP-hRTF2 and His14-SUMO-hRTF2 constructs were expressed in *E. coli* and purified (Figure 3.5A-C). The His14-SUMO-hRTF2 construct exhibited fewer degradation products and, therefore, was chosen for further purification. The His14-SUMO tag was cleaved with Ubiquitin-like-specific protease 1 (Ulp1) and untagged RTF2 was purified with size exclusion chromatography followed by an additional step where the supernatant was run over a His-affinity gel column to remove any free His14-SUMO or undigested His14-SUMO-hRTF2. RTF2 eluted with a high 260 peak on size-exclusion chromatography suggesting RTF2 may bind DNA or RNA (data not shown). *In vitro* biochemical immunoprecipitations show interaction between hRTF2 and the hMCM2-7 complex (Gift from the late J. Hurwitz) that is not dependent on DNA (Figure 3.5D). The FLAG beads-only control immunoprecipitation results in some background signal, which necessitates further examination of this interaction (Figure 3.5D).

3.2.2 Similar phenotypes in the absence RTF2 or RNase H2

We hypothesize that loss of RNase H2 from the replication fork in RTF2-deficient cells leads to the replication defect characterized in Chapter 2. To examine if the loss of RNase H2 is responsible for the phenotypes seen in RTF2-deficient MEFs, replication was assayed in cells deficient for RNASEH2A, the catalytic subunit of RNase H2. Like RTF2-deficient cells, RNASEH2A knockout (KO) HCT116 *p53*$^{-/-}$ cells, RNASEH2A KO HeLa cells (Zimmermann et al., 2018), and BJ cells depleted of RNASEH2A with siRNAs exhibited phenotypes consistent with the replication defect observed in RTF2-null cells, including slow growth, a significant decrease in mean nuclear gray value of EdU and shorter replication fork track lengths (Figure 3.6). Expression of a wild type *RNASEH2A* cDNA rescues the decreased mean nuclear gray value in HeLa RNASEH2A KO cells to levels comparable to those observed in wild type cells (Figure 3.6A,C, Nicolas Blobel complemented the RNASEH2A KO cells). Knockdown of RNASEH2A in RTF2-null cells did not further diminish the mean nuclear gray of EdU, indicating that RNase H2 and RTF2 may function in the same pathway in regard to DNA replication (Figure 3.6G,H).

We next sought to assess whether RTF2-deficient cells exhibit phenotypes consistent with RNase H2 deficiency. An increased single genome-embedded ribonucleotide burden is observed in *Rnaseh2b*$^{-/-}$*p53*$^{-/-}$ MEF cells (Reijns et al., 2012).

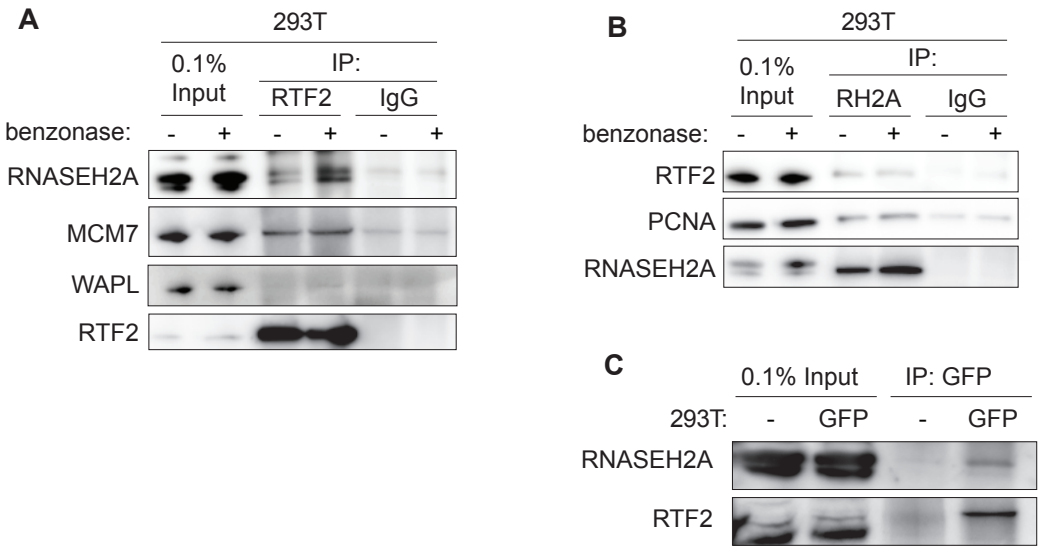

Figure 3.4. Validation of RTF2 interactions by western blot.
(A) Immunoblots from co-immunoprecipitations in HEK 293Ts with an RTF2 antibody. (B) Immunoblots from co-immunoprecipitations in HEK 293Ts with an RNASEH2A antibody. (C) Immunoblots from co-immunoprecipitations in wild type and CRISPR-Cas9 targeted GFP-AID-RTF2 HEK 293Ts. GFP-AID-RTF2 was immunoprecipitated with a GFP antibody.

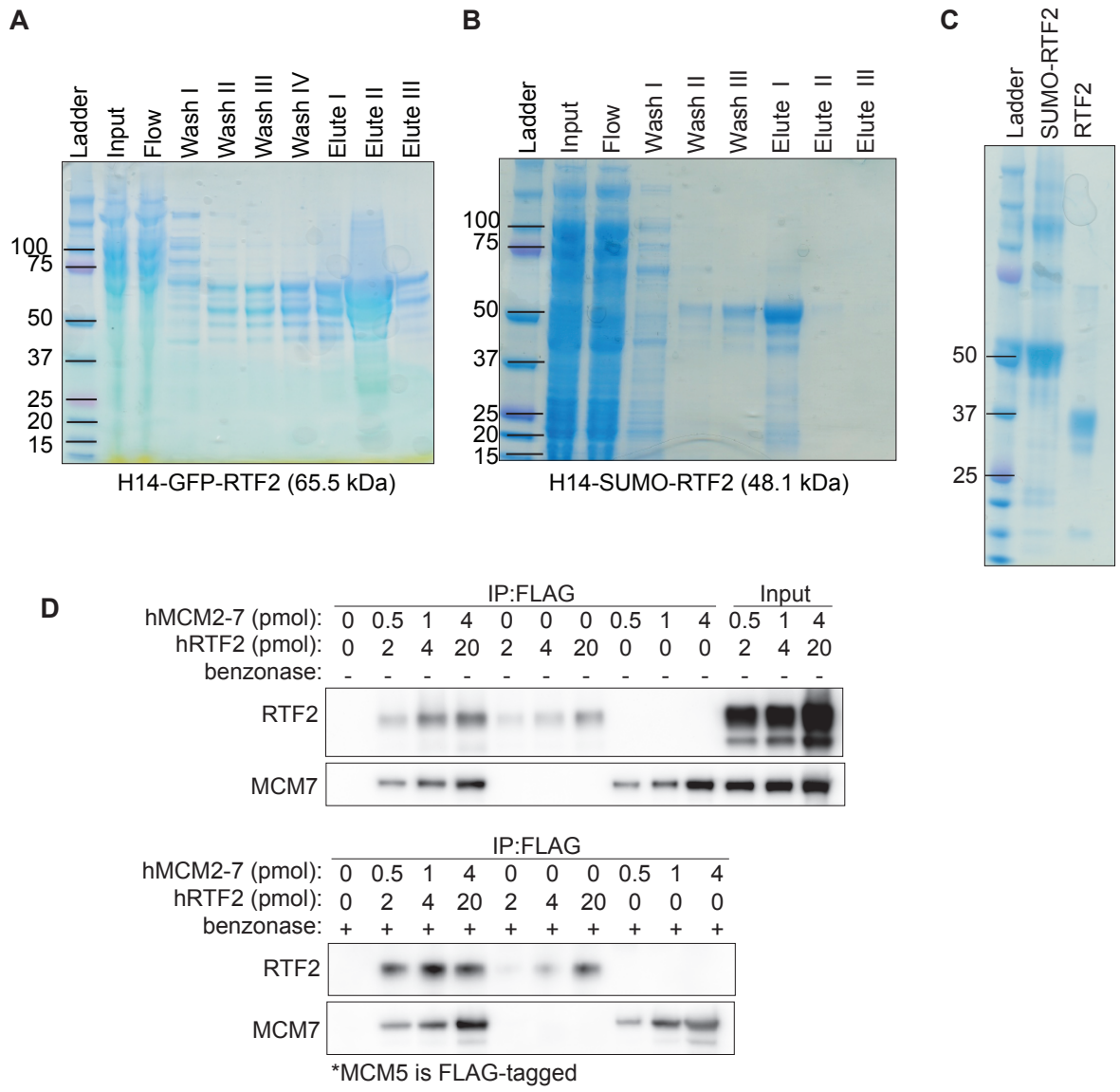

Figure 3.5. Biochemical reconstitution of RTF2 interaction with the MCM complex. (A) Coomassie stained acrylamide gel showing expression from *E. coli* cells and purification of Histidine 14-GFP-RTF2 construct. (B) Coomassie stained acrylamide gel showing expression and purification of His14-SUMO-RTF2 construct. (C) Coomassie stained acrylamide gel showing purification of His14-SUMO-RTF2 construct before and after Ulp1 digestion, size-exclusion chromatography and column clean-up. (D) Biochemical co-immunoprecipitations. RTF2 and MCM7 are detected with antibodies. MCM5 is flag tagged.

Figure 3.6. Loss of RNase H2 results in replication elongation defect.
(A) Immunoblot of RNASEH2A expression in whole cell lysates of indicated cells. (B) Growth curves of indicated cells. 50,000 cells of indicated genotypes were plated per well of a 6-well dishes in triplicate. Cells were counted on subsequent days. Error bars represent standard deviation. (C) Mean nuclear gray value of EdU in EdU positive cells in indicated cells. Cells were pulsed with EdU for 1 hour prior to fixation. Each dot represents one EdU positive cell. Mean for each sample shown with red line. n>100 for each sample. ****$P < 0.0001$, t-test (HCT116) or Kruskal-Wallis ANOVA with a Dunn's post-test (HeLa). (D) Replication tract lengths in CRISPR-edited HeLa cells. Each dot represents one replication tract. Mean for each sample shown with red line. Fork speeds using a conversion factor of 2kb/μm/minute are listed above each sample. n>140 for each sample. ****$P < 0.0001$, Kruskal-Wallis ANOVA with a Dunn's post-test. (E) RT-qPCR analysis of human *RNASEH2A* expression in indicated cells normalized to *GAPDH* expression. Error bars represent standard deviation. (F) Mean nuclear gray value of EdU in EdU positive cells in BJ cells transfected with indicated siRNAs. Cells were pulsed with EdU for 1 hour prior to fixation. Each dot represents one EdU positive cell. Mean for each sample shown with red line. n>100 for each sample. ****$P < 0.0001$, Kruskal-Wallis ANOVA with a Dunn's post-test. (G) RT-qPCR analysis of mouse *Rnaseh2* expression in indicated cells normalized to *β-actin* expression. Error bars represent standard deviation. (H) Mean nuclear gray value of EdU in EdU positive cells in SV40-immortalized *Rtf2*$^{-/-}$ MEF clones transduced with indicated shRNAs. Cells were pulsed with EdU for 1 hour prior to fixation. Each dot represents one EdU positive cell. Mean for each sample shown with red line. n>100 for each sample. ns = not significant, Kruskal-Wallis ANOVA with a Dunn's post-test.
RH2A = RNASEH2A, P = Parental, WT = wildtype, EV = empty vector, Luc = Luciferase, NT = Non-targeting

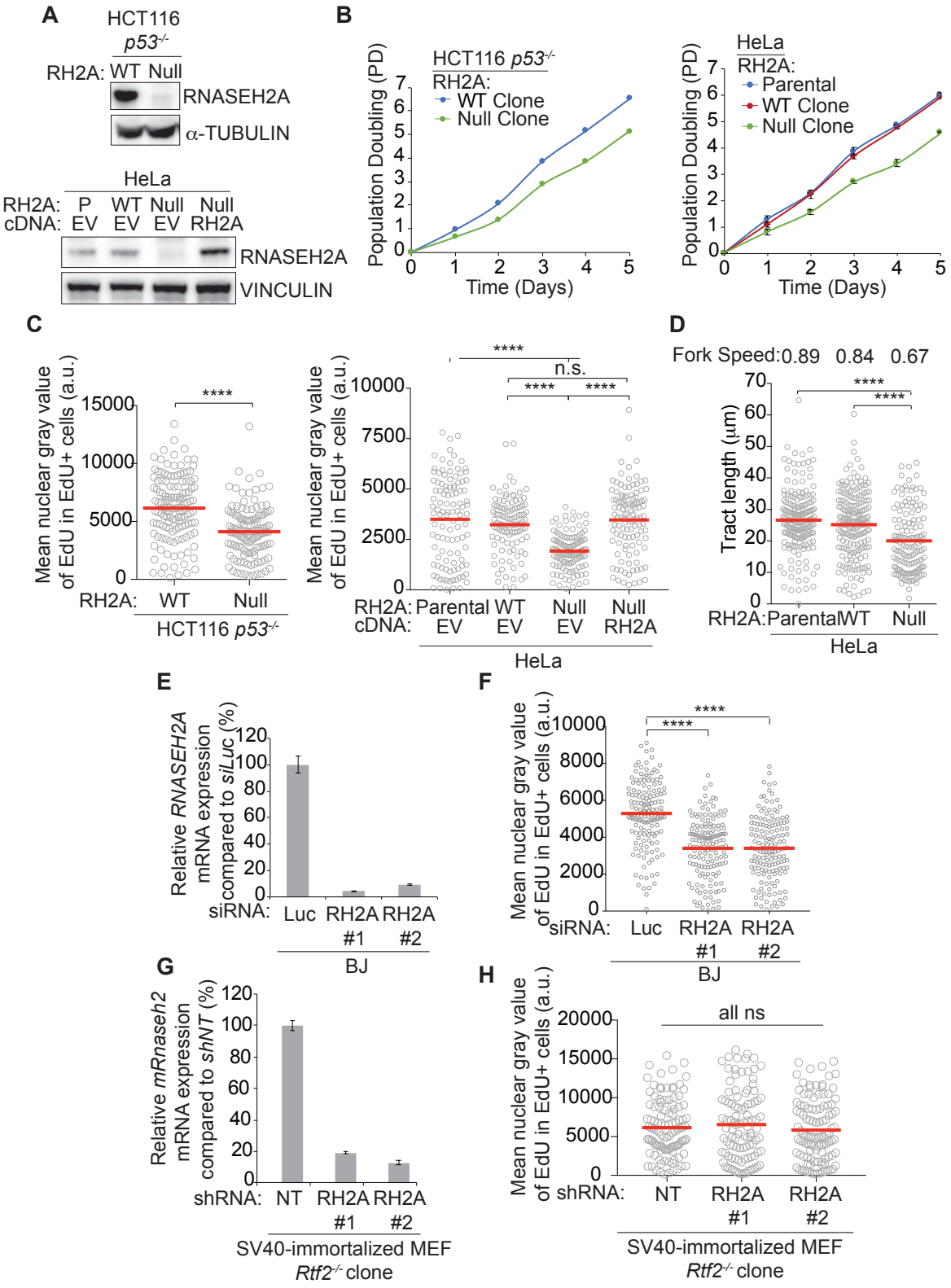
A
HCT116 p53-/-
RH2A: WT Null
RNASEH2A
α-TUBULIN
HeLa
RH2A: P WT Null Null
cDNA: EV EV EV RH2A
RNASEH2A
VINCULIN
B
HCT116 p53-/-
RH2A:
WT Clone
Null Clone
Population Doubling (PD)
Time (Days)
HeLa
RH2A:
Parental
WT Clone
Null Clone
Population Doubling (PD)
Time (Days)
C
Mean nuclear gray value of EdU in EdU+ cells (a.u.)
****
RH2A: WT Null
HCT116 p53-/-
Mean nuclear gray value of EdU in EdU+ cells (a.u.)
****
n.s.
****
****
RH2A: Parental WT Null Null
cDNA: EV EV EV RH2A
HeLa
D
Fork Speed: 0.89 0.84 0.67
Tract length (μm)
****
****
RH2A: Parental WT Null
HeLa
E
Relative RNASEH2A mRNA expression compared to siLuc (%)
siRNA: Luc RH2A #1 RH2A #2
BJ
F
Mean nuclear gray value of EdU in EdU+ cells (a.u.)
****
****
siRNA: Luc RH2A #1 RH2A #2
BJ
G
Relative mRnaseh2 mRNA expression compared to shNT (%)
shRNA: NT RH2A #1 RH2A #2
SV40-immortalized MEF
Rtf2-/- clone
H
Mean nuclear gray value of EdU in EdU+ cells (a.u.)
all ns
shRNA: NT RH2A #1 RH2A #2
SV40-immortalized MEF
Rtf2-/- clone

The persistence of genome-embedded ribonucleotides causes replication-dependent DNA damage as a result of inappropriate TOP1-processing. In the absence of RNase H2, TOP1-dependent processing induces poly-ADP-ribosylation and increased γH2AX staining (Kim et al., 2011; Niu et al., 2016; Reijns et al., 2012; Sparks and Burgers, 2015; Williams et al., 2013; Zimmermann et al., 2018) (Figure 3.7A). Similarly, cells without RTF2 exhibited increased poly-ADP-ribosylation (Figure 3.7B,C) and increased S phase-specific γH2AX staining (Figure 3.7D,E).

3.3 Summary of Findings and Outlook

iPOND is a powerful tool to identify changes at the replication fork and the ability to compare data from iPOND with another discovery data set, the proteome associated with RTF2, allowed for systematic filtering of factors that may be regulated by RTF2 at the replication fork. The combination of these techniques allowed for the identification of RNase H2 as a potential effector of RTF's function during DNA replication.

While LC-MS and co-immunoprecipitation analyses indicated that RTF2 and RNASEH2A interact, these studies would also benefit from biochemical evidence. It is unknown whether this interaction is direct or indirect. An indirect interaction could be mediated through another protein and if this is the case, it would be important to identify this intermediary. LC-MS analysis also revealed an increased number of peptides from the MCM2-7 complex associating with RTF2 and biochemical evidence suggested that this interaction may be direct. It is tempting to hypothesize that the interaction of RTF2 with the MCM2-7 complex localizes RTF2 to the replication fork. These studies would benefit from mutational analysis to pinpoint the residues necessary for the interaction.

We purified human RTF2 to use for biochemical experiments. hRTF2 was expressed and purified in *E. coli*. The stability of hRTF2 was augmented with the addition of a SUMO tag. While the purification yielded a reasonably clean fraction, a contaminating band around 70 kDa still remained after Upl1 digestion, size-exclusion, and column clean-up (Figure 3.5C). The identity of this contaminating band could be a common bacterial chaperone, and if so, additional ATP and KCl washes may remove it. The ability to purify RTF2 extends to other species, as we have also purified *X. laevis* RTF2 (data not shown). Purification of xRTF2 was used to immunize a rabbit and generate an xRTF2-specific antibody that could be used to deplete RTF2 from cell-free xenopus extracts used to reconstitute DNA replication *in vitro* (Lebofsky et al., 2009) and study DNA replication without RTF2. Purification of specific RTF2 mutants would further elucidate how RTF2 functions at the replisome.

As introduced in Chapter 1, RNase H2 is thought to be recruited to the replication fork through RNASEH2B's PIP-box (Bubeck et al., 2011). There may be an additional mechanism for RNase H2 recruitment to the replication fork independent of RNASEH2B's PIP box (Kind et al., 2014). Our results suggest RTF2 is needed to support RNase H2's

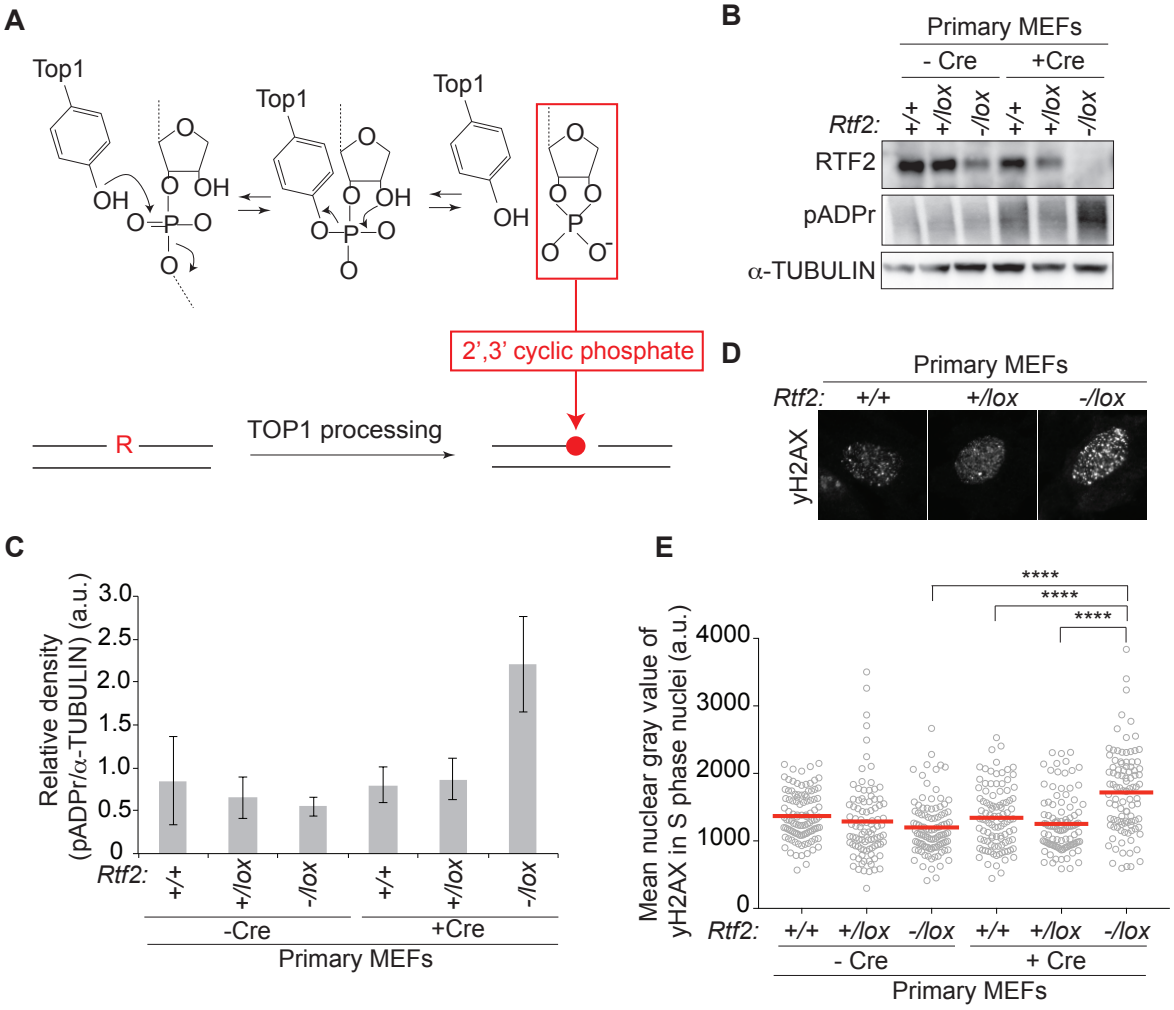

Figure 3.7. RTF2-deficient cells exhibit increased DNA damage consistent with the persistence of genome-embedded ribonucleotides.

(A) Schematic of TOP1-mediated ribonucleotide processing in the absence of RNase H2. (B) Representative immunoblot of whole cell lysates in primary MEFs infected with Hit & Run Cre (72 hours) showing poly-ADP-ribosylation. (C) Average densitometry plots from 3 experiments. Error bars represent standard deviation; n=3, biological replicates. (D) Representative immunofluorescent images of γH2AX staining in of primary MEFS after infection with Hit & Run Cre (72 hours). (E) Mean nuclear gray value of γH2AX from D. Cells were labeled with EdU 1 hour prior to fixation and stained with Click-It EdU Alexa-488 to determine the cells in S phase. Each dot represents one cell. Mean for each sample shown with red line. n>90 per sample. ****$P < 0.0001$, Kruskal-Wallis ANOVA with a Dunn's post-test.

localization to the replication fork. Whether RTF2 and PCNA cooperate or function independently to support RNase H2 localization to the replisome has yet to be determined.

Our data suggest that the RNase H2 complex is necessary for normal replication speed, however, whether catalytic activity against RNA-DNA hybrids or single DNA-embedded ribonucleotides is required for RNase H2's function in DNA replication is under ongoing investigation. Expression of an RNASEH2A (P40D/Y210A) ribonucleotide excision repair defective (RED) mutant cDNA, which cannot excise single DNA-embedded ribonucleotides, but cleaves RNA-DNA hybrids cannot rescue the PARPi sensitivity of RNASEH2A KO cells. This model suggests that PARPi sensitivity is the result of PARP1 trapping on TOP1-processed single genome-embedded ribonucleotides (Zimmermann et al., 2018). If single genome-embedded ribonucleotides are responsible for the replication slowing, expression of an RNASEH2A RED or an RNASEH2A (D34A/D169A) Catalytic Dead mutant cDNA would not rescue the replication defect in RNASEH2A KO cells.

RTF2-deficient and RNase H2-deficient cells share similar DNA damage phenotypes, including increased poly-ADP-ribosylation, and S phase-specific γH2AX. We speculate these phenotypes are a result of DNA-embedded ribonucleotides. TOP1-dependent processing of ribonucleotides in the absence of RNase H2 could be the cause of the poly-ADP-ribosylation and γH2AX. Knockdown of TOP1 in an RTF2-deficient background would determine the causal relationship if γH2AX and pADPr levels returned to normal. Unresolved DNA damage in RNase H2-deficient cells may result in the formation of micronuclei. Micronuclei, which arise during mitosis from lagging chromosomal DNA and chromatin bridges, are sufficient to activate the cGAS/STING pathways in these cells (Bartsch et al., 2017; Mackenzie et al., 2016; Mackenzie et al., 2017). This is hypothesized to contribute to the etiology of AGS, a disease caused by pathogenic variants in any of the RNase H2 subunits that presents with severe inflammatory responses (Bartsch et al., 2017; Mackenzie et al., 2016; Mackenzie et al., 2017). It should be determined if the cGAS/STING pathway is active in the absence of RTF2 as abnormal nuclei and mitotic defects were observed in the absence of RTF2 as presented in Chapter 2.

Loss of *Rtf2* or *Rnaseh2b* (resulting in loss of the entire complex) results in embryonic lethality in mice (Reijns et al., 2012), indicating *Rtf2, Rnaseh2a, Rnaseh2b,* and *Rnaseh2c* are essential genes. The embryonic lethality associated with the loss of RNase H2 occurs later than that associated with the loss of RTF2. This suggests there could be other functions for RTF2 outside of its role in regulating RNase H2 levels at the replication fork and that role still needs to be studied. In the next chapter, I will further study RTF2's function in regulating RNase H2 levels at the replisome and I will genetically place RNase H2 in the DDI1/RTF2 pathway.

Chapter 4: Coordination of RTF2, RNase H2, and PRIM1 in the replication stress response and replication fork restart

4.1 Introduction

Recent single-molecule DNA fiber analysis suggests many additional factors function in direct replication restart from HU. For example, BAP1 promotes replication restart by recruiting INO80 as INO80 is required for replication restart (Lee et al., 2019; Vassileva et al., 2014). In yeast, Ino80 facilitates PCNA ubiquitination (Falbo et al., 2009), but whether INO80 has a similar function requires in mammals further examination. Another studied observed that EXD2-deficient cells exhibit inefficient fork restart (Nieminuszczy et al., 2019), but how exactly EXD2 facilitates fork restart is unknown. Studies from our laboratory indicate DDI1/2-mediated removal of RTF2 from the replication fork is also required for fork restart in response to HU-induced stalling (Kottemann et al., 2018). When DDI1 and DDI2 are depleted, cells exhibit an abnormal replication stress response due to the stabilization of RTF2 at the stalled replication fork (Kottemann et al., 2018). In this chapter, we explore how DDI1/2 and RTF2 coordinate replication fork restart.

Given the data in Chapter 3 indicating RTF2 interacts with RNase H2 and is necessary to localize RNase H2 to the replication fork, we hypothesized that the inability to recover from replication stress in the absence of DDI1/2 is also due to the stabilization of RNase H2 at stalled replication forks. This led us to assess the function of RNase H2 during the replication stress response. As RNase H2 is a ribonuclease H, its preferred substrates are DNA-embedded ribonucleotides, such as single ribonucleotides, R-loops or RNA primers. Since RNA-dependent priming is required for normal replication, we hypothesize that RNA primers are also important for restarting stalled replication forks and that inappropriate stabilization of RNase H2 at stalled replication forks may result in the hydrolysis of these primers. This led us to consider the contribution of RNA primases for replication restart in the DDI-RTF2 pathway was also assessed. The results of these studies are reported here.

4.2 Results

4.2.1 Regulation of RNase H2 coordinates the response to replication stress.

Identification of the interaction between RNase H2 and RTF2 and loss of RNase H2 from the replication fork upon removal of RTF2 led us to examine whether RNase H2 was also a mediator of the response to replication stress. DDI1/2-depleted cells show increased sensitivity to replication stress-inducing agents, including HU, aphidicolin, MMC and gemcitabine that can be rescued by RTF2 depletion (Kottemann et al., 2018). We tested if knockdown of RNase H2 using siRNAs against the catalytic subunit, *RNASEH2A*, could rescue the replication stress phenotypes associated with DDI1/2-deficiency. Indeed, knockdown of RNASEH2A rescued the sensitivity of DDI1/2-depleted cells to increasing doses of HU to the same degree as *siRTF2* transfection (Figure 4.1A).

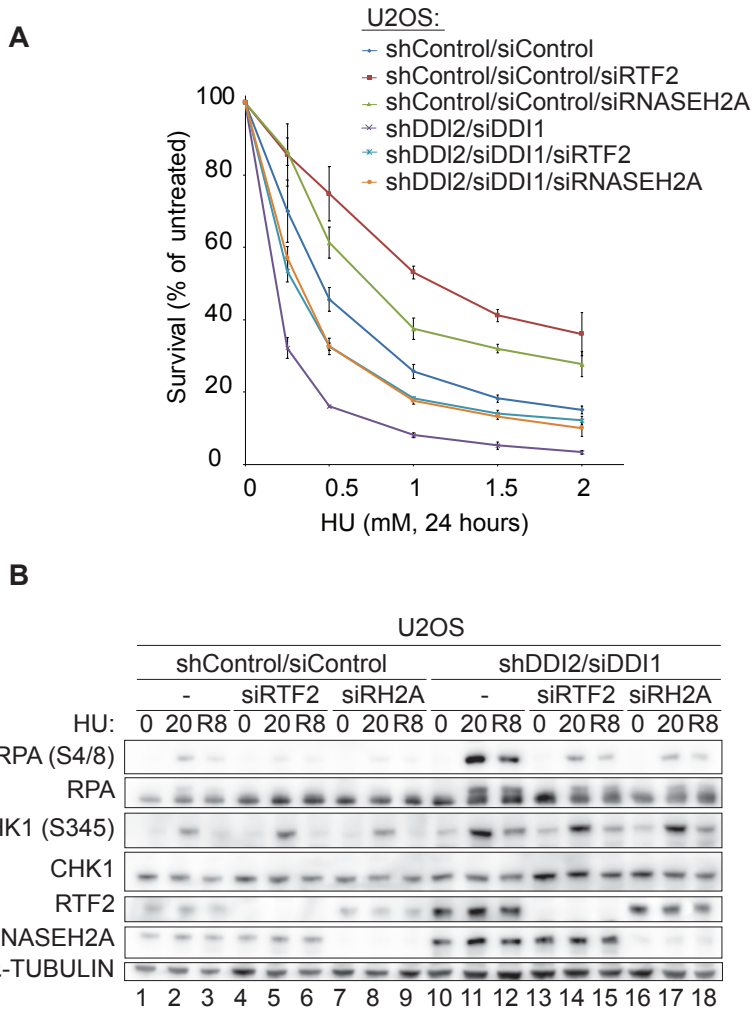

Figure 4.1. RNase H2 knockdown rescues the cellular sensitivity and increased P-RPA S4/8 signal observed upon treatment with replication stress-inducing drugs in the absence of DDI1/2 .

(A) Graph showing survival of U2OS cells transduced or transfected with indicated shRNA and siRNA, respectively, and treated with indicated HU doses. Cells were treated 72 hours after transfection for 24 hours prior to release into fresh medium. Error bars represent standard deviation. (B) Immunoblots of whole cell lysates isolated from U2OS cells transduced or transfected with indicated RNAi reagent and treated with 0.5 mM HU (72 hours prior to the start of the experiment). 0 = untreated, 20 = 20 hour treatment, R8 = 20 hour treatment followed by 8 hour release into fresh media. Immunoblots show loss of RTF2 and RNASEH2A in indicated siRNA lanes (Lanes 4-6 and 13-15 for RTF2, Lanes 7-9 and 16-18 for RNASEH2A).

RH2A = RNASEH2A.

Cells depleted of DDI1/2 also display an increase in ssDNA formation as shown by elevated BrdU signal under non-denaturing conditions, higher chromatin-associated RPA staining, and elevated P-RPA S4/8 signaling during low dose HU treatment (0.5 mM), which slows the replication fork without completely stopping it (Kottemann et al., 2018). Using these conditions, knockdown of DDI1/2 induced phosphorylation of P-RPA S4/8 (Figure 4.1B, Lane 11 and 12) that was suppressed upon knockdown of RNASEH2A (Figure 4.1B, Lane 17 and 18). The extent of this suppression was similar to that seen when RTF2 was depleted in the DDI1/2-deficient background (Figure 4.1B, Lane 14 and 15). The increased P-CHK1 S345 in DDI1/2-depleted cells was unchanged upon knockdown of either RTF2 or RNASEH2A in the DDI1/2-deficient settings (Figure 4.1B).

In single-molecule DNA fiber assays, DDI1/2-depleted cells exhibited a decrease in the percentage of forks that restart as well as a decrease in the efficiency of restart (the length of the replication tract after restart) after release from HU treatment (Kottemann et al., 2018). Here, we assessed replication restart defects using a modified DNA combing assay. Cells are labeled with two uniquely detectable thymidine analogs (IdU and CldU) for different times, where the second analog (CldU) is pulsed twice as long as the first (IdU) (Figure 4.2A). To assess replication restart efficiency after stress, replication forks are then completely stalled with a high dose of HU (4 mM) between the first (IdU) and second labels (CldU). Following removal of HU, the tract length of the second analog (CldU) is measured and compared to the tract length of the first analog (IdU) as a proxy for replication restart efficiency (Figure 4.2A). The expected ratio of the thymidine analogs (CldU:IdU) without HU treatment is 2 whereas DDI1/2-depleted cells show a reduction in this ratio upon release from treatment with HU, indicating a replication fork restart defect. The fork restart defect observed upon treatment with HU in DDI1/2-depleted cells is rescued upon knockdown of RNASEH2A to the same extent as knockdown of RTF2 (Figure 4.2C). Control experiments did not indicate any differences in replication restart efficiency without HU treatment (Figure 4.2B).

As discussed in Chapter 1, one consequence of an inability to restart replication forks is replication fork collapse and breakage. If unresolved, these breaks can contribute to an increase in chromosome breaks, which can be visualized in metaphase spreads. Highly damaged metaphases were observed in DDI1/2-deficient cells when grown in the presence of HU or aphidicolin (Kottemann et al., 2018). Knockdown of RNASEH2A, like knockdown of RTF2, suppressed the chromosome breaks observed with depletion of DDI1/2 (Figure 4.3).

Since RNase H2-deficiency rescued the replication stress-induced phenotypes associated with DDI1/2 deficiency, we next tested whether the other member of the ribonuclease H family, RNASEH1, could also function in the response to replication stress. Knockdown of RNASEH1 in a DDI1/2-deficient background could not fully suppress the induction of P-RPA S4/8 (Figure 4.4A) nor rescue the decreased fork restart efficiency (Figure 4.4B) despite knockdown to approximately 10% of wild type levels (Figure 4.4C).

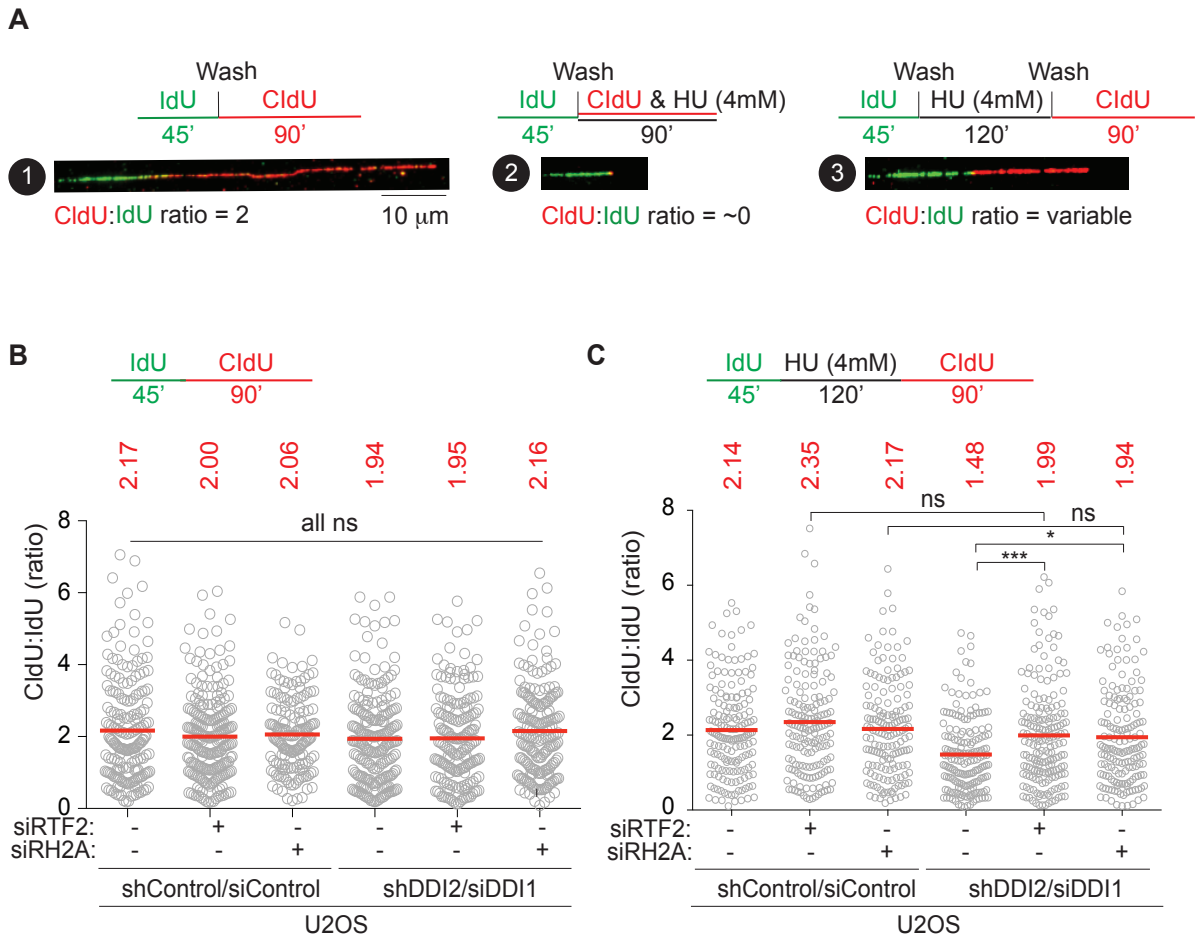

Figure 4.2. DDI1/2 promote efficient replication restart by modulating RNase H2 levels.

(A) Experimental schematic and representative images of fork restart assay assessed using DNA combing using thymidine analogs, IdU and CldU. (1) Given the pulse of the second label, CldU, is twice as long as the first, IdU, the expected ratio of the CldU:IdU analogs without HU treatment is 2. (2) During 4 mM HU treatment, all progressing replisomes are stalled. Co-incubation of CldU with HU shows that there is no new DNA synthesis. (3) Upon removal of HU, the length of the second label, CldU, can be compared to that of the first label, IdU, as a proxy for replication restart efficiency. (B,C) Ratio of CldU to IdU tract lengths in U2OS cells transduced or transfected with indicated RNAi reagent (72 hours prior to the start of the experiment). Labeling schematic indicated above plots. Each dot represents one replication tract. Mean ratios indicated above each sample and with red lines. n>150 for each sample. Outliers removed with ROUT (1%). *P < 0.05, ***P<0.001 ns, not significant, Kruskal-Wallis ANOVA with a Dunn's post-test. RH2A = RNASEH2A.

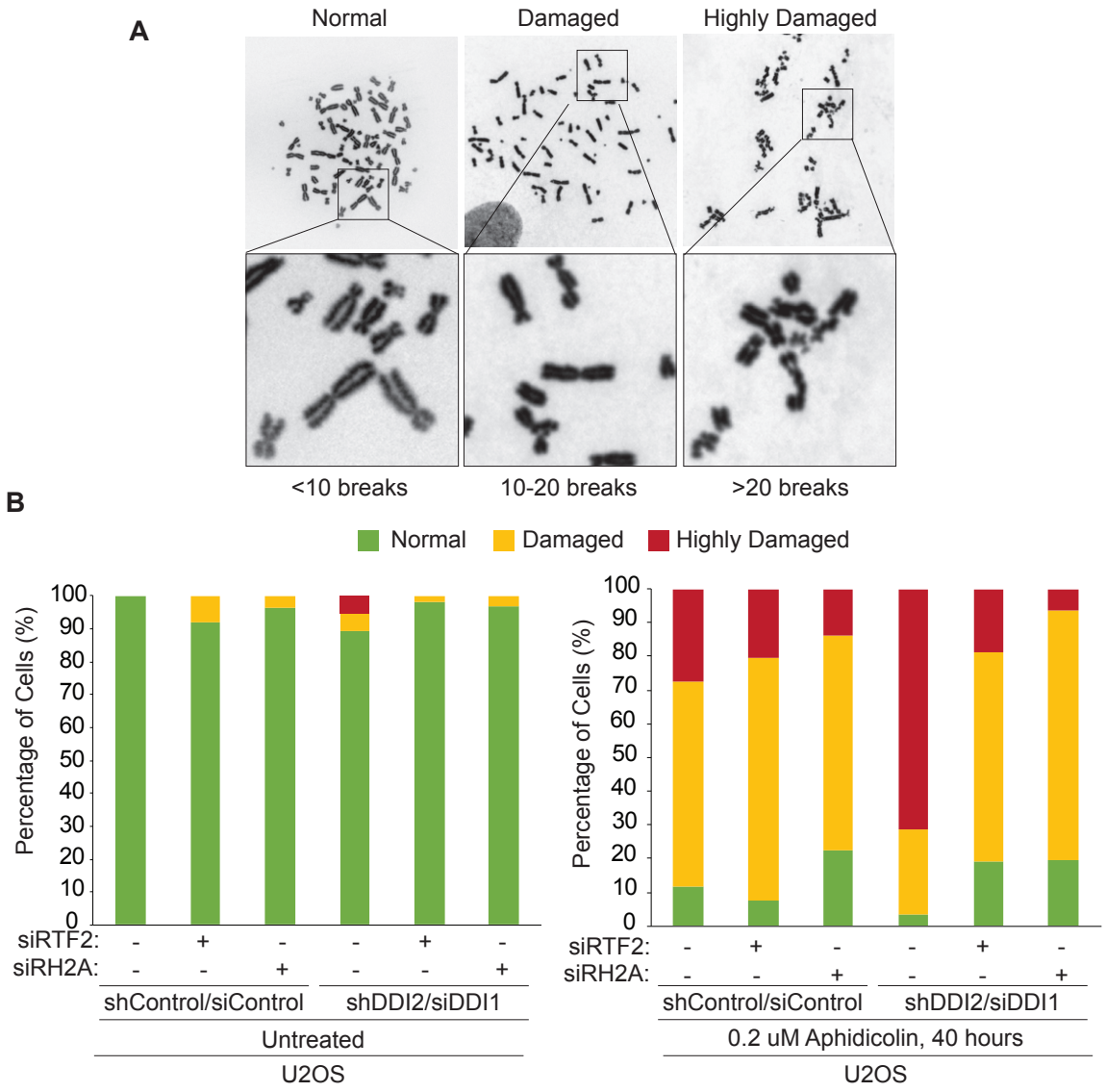

Figure 4.3. RNase H2 deficiency rescues genome stability in the absence of DDI1/2. (A) Representative DNA metaphase spreads from U2OS cells after replication in the presence of low-dose aphidicolin for 40 hours. Metaphase spreads were categorized into three classes of breakage severity normal (<10 breaks); damaged (10-20 breaks); and highly damaged/uncountable (>20 breaks). (B) Representative quantification of the percentage of metaphase spreads in each category described in A in U2OS cells transduced or transfected with indicated RNAi reagents (112 hours prior to the start of the experiment). n>50 for metaphases scored in each sample.

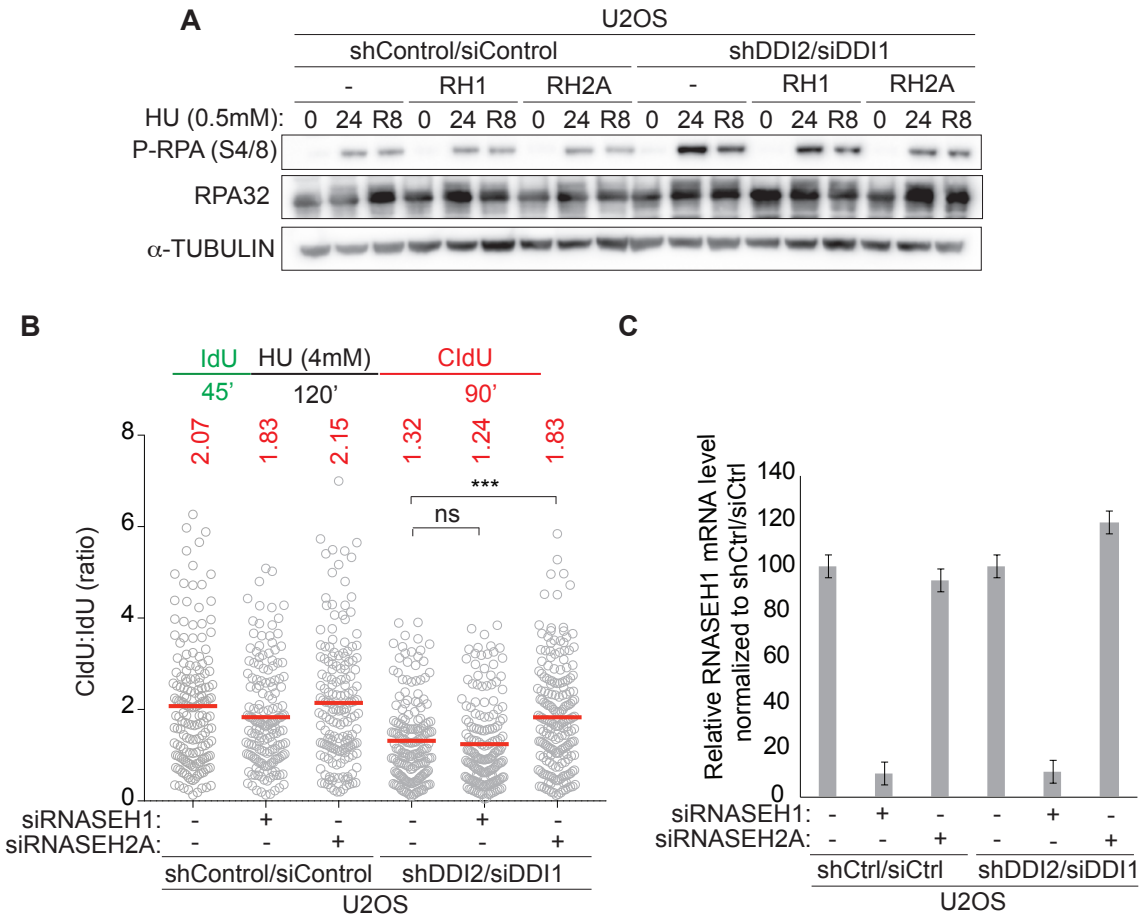

Figure 4.4. RNase H1 knockdown does not rescue phenotypes associated with DDI1/2-deficiency .

(A) Immunoblots of whole cell lysates isolated from U2OS cells transduced or transfected with indicated RNAi reagents (72 hours prior to the start of the experiment) and treated with 0.5 mM HU. 0 = untreated, 24 = 24 hour treatment, R8 = 24 hour treatment followed by 8 hour release into fresh media. (B) Ratio of CldU tract to IdU tract lengths in U2OS cells transduced or transfected with indicated RNAi reagents (72 hours prior to the start of the experiment). Labeling schematic indicated above plot and means indicated above each sample. n>150 for each sample. Outliers removed with ROUT (1%).***P < 0.001, ns, not significant, Kruskal-Wallis ANOVA with a Dunn's post-test. (C) RT-qPCR analysis of *RNASEH1* expression in indicated cells normalized to *GAPDH* expression. Error bars represent standard deviation.

Ctrl = Control, RH1 = RNASEH1, RH2A = RNASEH2A.

Given RNASEH2A or RTF2 knockdown rescued the phenotypes associated with DDI1/2 depletion, we examined if this decreased response and increased ability to recover from replication stress in the absence of RTF2 was also observed with normal DDI1/2 levels. Depletion of RNASEH2A or RTF2 resulted in cellular resistance to HU (Figure 4.1A) and decreased HU-induced P-RPA S4/8 compared to wild type cells (Figure 4.1B, Lane 2 compared to Lane 5 or 7). Knockdown of RTF2 also induced cellular resistance to various replication stress-inducing drugs, including HU, aphidicolin, and MMC (Figure 4.5A), and increased entry into S phase after release from a high dose of HU (Figure 4.5B,C). Cells depleted of RTF2 also exhibited an increased ability to replicate in the presence of aphidicolin, MMC and cisplatin (Figure 4.5D, experiment performed by Molly Kottemann). These data suggest that RTF2 functions across multiple types of replication stress.

4.2.2 Primase promotes replication restart after release from replication stress

Our results indicate that RNase H2's removal from the replication fork mediates recovery from replication stress in DDI1/2-depleted cells, but the underlying reason for RNase H2's removal is unknown. We hypothesized that the inability to recover from replication stress is due to RNase H2 activity at stalled replication forks. A plausible substrate for RNase H2 activity at stalled replication forks is an RNA-DNA hybrid, for example, an RNA primer that might be necessary to resume replication. The ability of RNASEH2A knockdown to rescue DDI1/2-deficient phenotypes could be due to stabilization of priming events. To test this hypothesis, we systematically examined the contribution of the two AEP primases, PRIMPOL and PRIM1, in this pathway.

Cells depleted of PRIMPOL alone exhibited an increase in P-RPA S4/8 signal after an 24 hour low-dose HU (0.5mM) treatment (Figure 4.6A). Levels of P-RPA S4/8 in DDI1/2-depleted cells were unchanged with co-depletion of PRIMPOL (Figure 4.6A). Interestingly, knockdown of PRIMPOL did not have an effect on the efficiency of replication fork restart after release from HU (Figure 4.6B,C), in contrast to its role in fork restart after UV (Figure 4.6D, Cayla Broton) (Bianchi et al., 2013; Mouron et al., 2013; Wan et al., 2013).

Next, we examined the role of PRIM1 in response to replication stress. An increased P-RPA S4/8 signal was induced in cells with knockdown of PRIM1 during an 24 hour low-dose HU (0.5mM) treatment (Figure 4.7A). The appearance of this P-RPA S4/8 signal exhibited slower accumulation compared to the signal observed when DDI1/2 were depleted (Figure 4.7A). This slower induction of P-RPA S4/8 signal was also seen upon co-depletion of PRIM1 and DDI1/2 (Figure 4.7A). Although cells depleted of PRIM1 maintained a normal ratio of CldU:IdU in untreated conditions (Figure 4.7B), after release from HU-induced stalling cells depleted of PRIM1 exhibited a decreased fork restart efficiency (Figure 4.7B,C). Knockdown of PRIM1 also reverted the rescue of RTF2 or RNASEH2A knockdown in DDI1/2-depleted cells (Figure 4.7C). Given the length of in

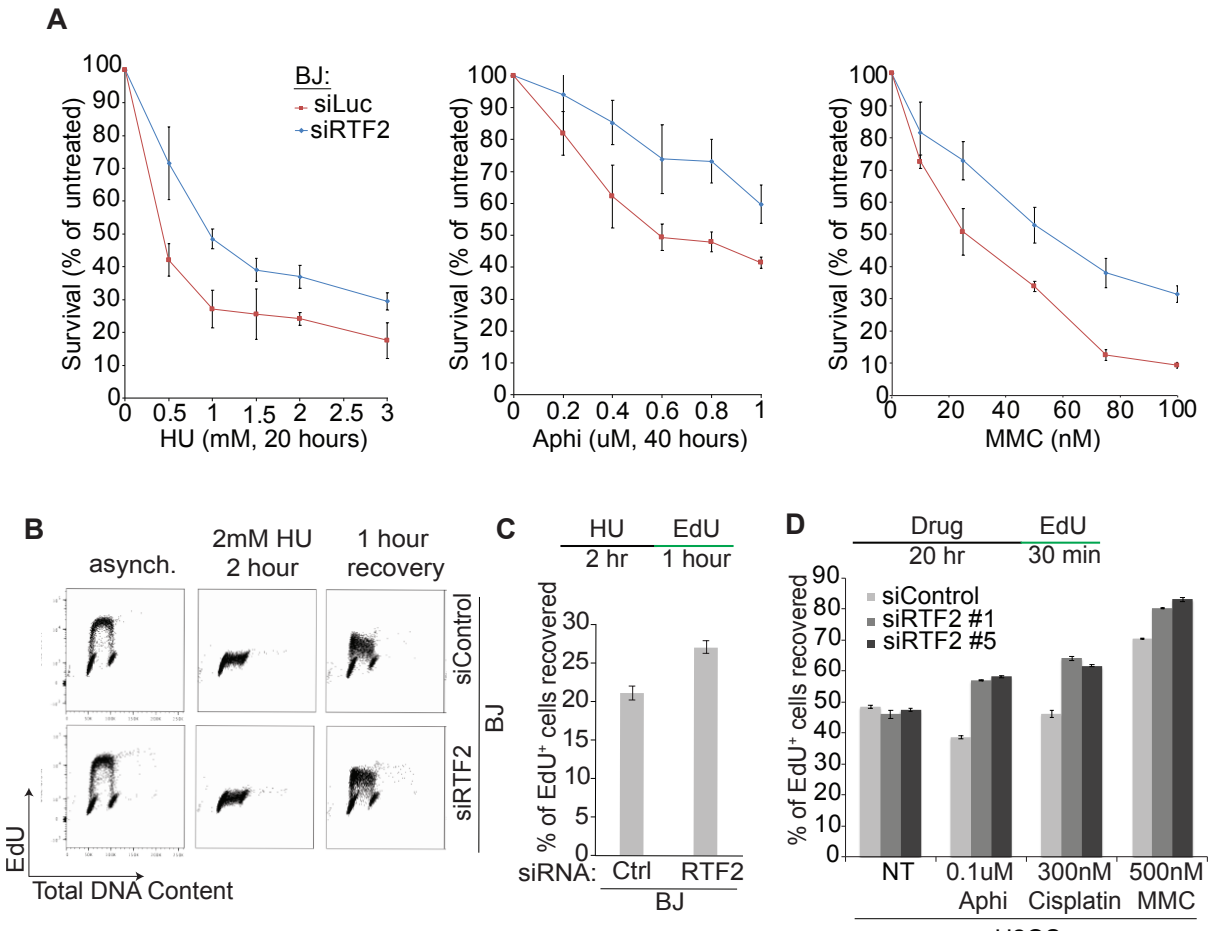

Figure 4.5. Depletion of RTF2 mitigates response to a variety of replication stress-inducing drugs.

(A) Cellular survival of BJ cells transfected with siRNA reagents (72 hours prior to the start of the experiment) and treated with indicated drugs. (B) Representative cell cycle profiles from flow cytometry of BJ cells transfected with indicated RNAi reagents (72 hours prior to the start of the experiment). Asynchronous cells were pulsed with EdU for one hour prior to collection and fixation (left panel). Cells treated with 2 mM HU (2 hours) were pulsed with EdU in the final hour of treatment (middle panel). After cells were pulsed with 2 mM HU (2 hours), the HU was washed off and cells were pulsed with EdU in fresh media for one hour (right panel). Newly replicated DNA is represented on the y-axis in logarithmic scale. Total DNA content is represented on the x-axis. (C) Bar graph showing percentage of EdU positive cells after recovery from HU in B. Error bars represent standard deviation. (D) Bar graphs representing EdU positive populations of cell cycle profiles from flow cytometry in U2OS cells transfected with indicated RNAi reagents (72 hours prior to the start of the experiment) and treated with indicated drugs for 20 hours prior to release into fresh media with EdU for 30 minutes. Error bars represent standard deviation.

NT = not treated, Aphi = aphidicolin, MMC = mitomycin C.

Figure 4.6. Knockdown of PRIMPOL elicits increase in P-RPA S4/8 signal without displaying a replication fork restart efficiency defect in response to hydroxyurea. (A) Immunoblot of whole cell lysates isolated from U2OS cells with indicated RNAi reagents (72 hours prior to the start of the experiment) treated with 0.5 mM hydroxyurea. 0 = untreated, 24 = 24 hour treatment, R8 = 8 hours post hydroxyurea removal. (B) Ratio of CldU to IdU tract lengths in indicated U2OS cells. Labeling schematic indicated above plots. Each dot represents one replication tract. Mean ratios indicated above each sample and shown with red line. n>150 for each sample. Outliers removed with ROUT (1%). ****P<0.0001, ns, not significant, Kruskal-Wallis ANOVA with a Dunn's post-test. (C) RT-qPCR analysis of *PRIMPOL* expression in indicated cells normalized to *GAPDH* expression. Error bars represent standard deviation. (D) Percentage of forks that restart after UV treatment. Percentage of fork rescue was calculated as restarted fork/(restarted forks + stalled forks). n>250. Ctrl = Control, RH2A = RNASEH2A.

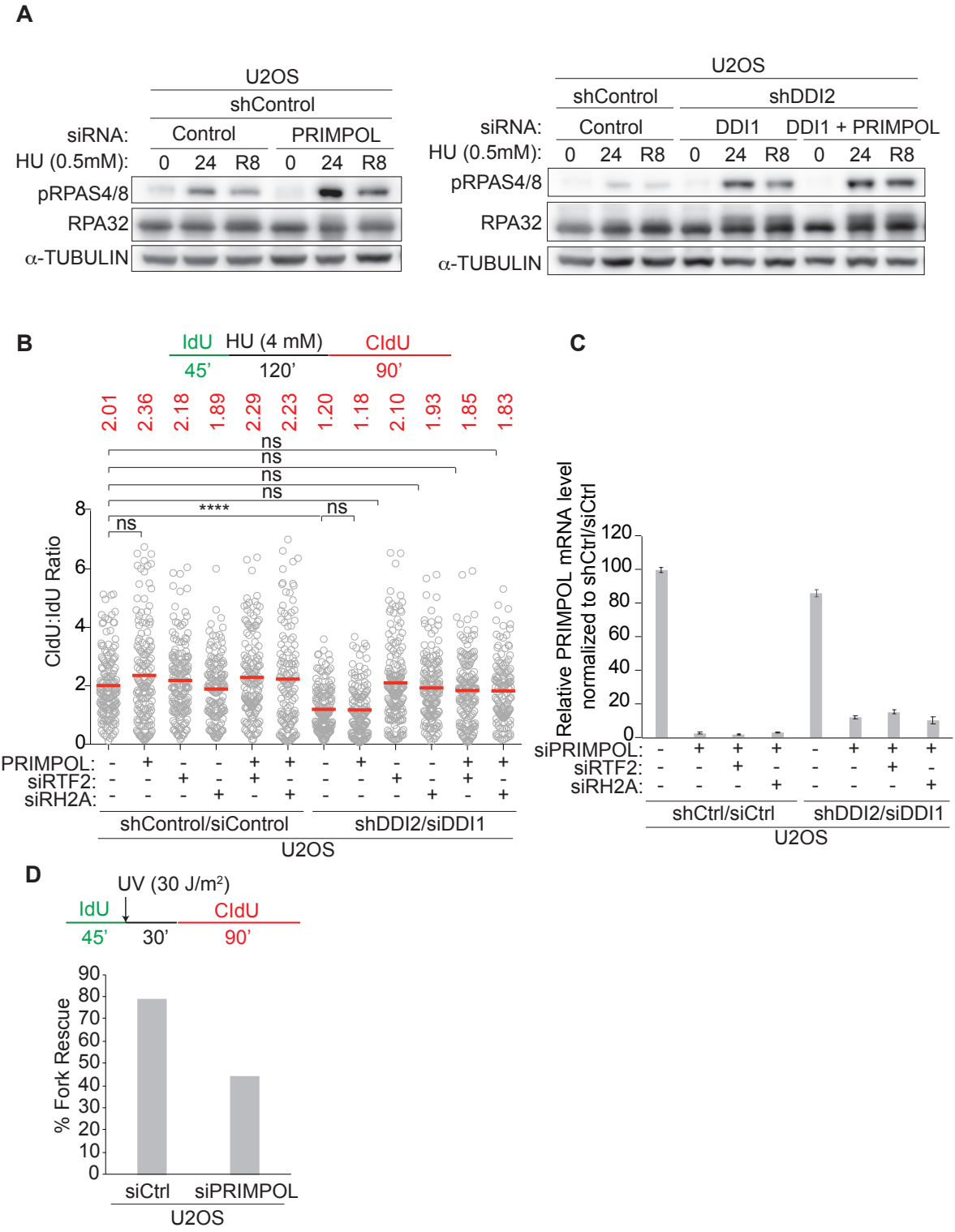
A
U2OS
shControl
siRNA:
Control
PRIMPOL
HU (0.5mM):
0 24 R8 0 24 R8
pRPAS4/8
RPA32
α-TUBULIN
U2OS
shControl
shDDI2
siRNA:
Control
DDI1
DDI1 + PRIMPOL
HU (0.5mM):
0 24 R8 0 24 R8 0 24 R8
pRPAS4/8
RPA32
α-TUBULIN
B
IdU
HU (4 mM)
CldU
45'
120'
90'
2.01 2.36 2.18 1.89 2.29 2.23 1.20 1.18 2.10 1.93 1.85 1.83
ns
****
CldU:IdU Ratio
siPRIMPOL:
siRTF2:
siRH2A:
shControl/siControl
shDDI2/siDDI1
U2OS
C
Relative PRIMPOL mRNA level normalized to shCtrl/siCtrl
siPRIMPOL:
siRTF2:
siRH2A:
shCtrl/siCtrl
shDDI2/siDDI1
U2OS
D
UV (30 J/m²)
IdU
CldU
45'
30'
90'
% Fork Rescue
siCtrl
siPRIMPOL
U2OS

Figure 4.7. Knockdown of PRIM1, the catalytic subunit of primase, causes inefficient fork restart.
(A) Immunoblot of whole cell lysates isolated from U2OS cells with indicated RNAi reagents (72 hours prior to the start of the experiment) treated with 0.5 mM hydroxyurea. 0 = untreated, 24 = 24 hour treatment, R8 = 8 hours post hydroxyurea removal. (B,C) Ratio of CldU to IdU tract lengths in indicated U2OS cells. Labeling schematic indicated above plot. Each dot represents one replication tract. Mean ratios indicated above each sample and shown with red line. n>150 for each sample. Outliers removed with ROUT (1%). *P<0.05, ***P < 0.001, ****P<0.0001, ns, not significant, Kruskal-Wallis ANOVA with a Dunn's post-test. (D) RT-qPCR analysis of *PRIM1* expression in indicated cells normalized to *GAPDH* expression. Error bars represent standard deviation.
Ctrl = Control, RH2A = RNASEH2A.

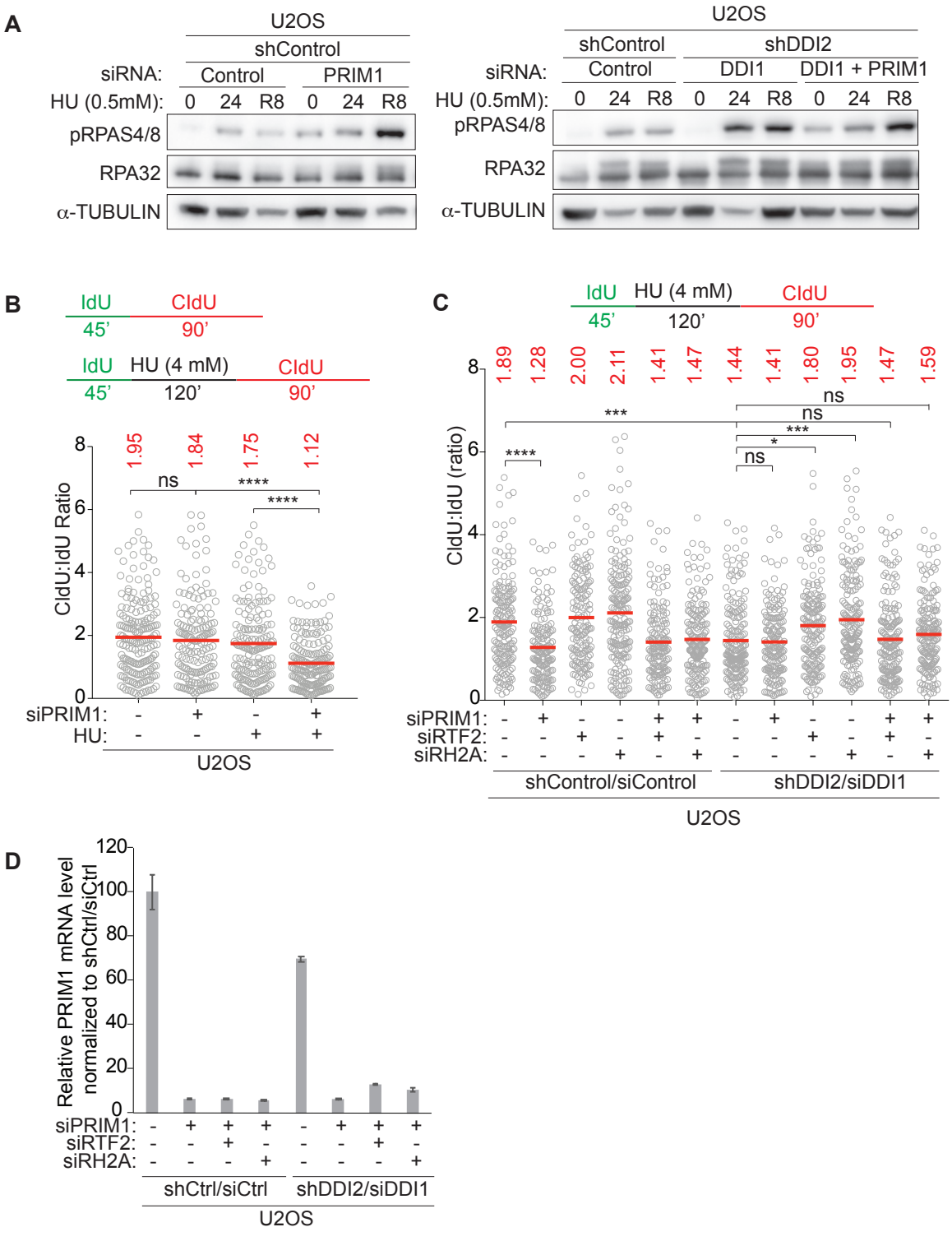
A
U2OS
shControl
siRNA:
Control
PRIM1
HU (0.5mM):
0 24 R8 0 24 R8
pRPAS4/8
RPA32
α-TUBULIN
U2OS
shControl
shDDI2
siRNA:
Control
DDI1
DDI1 + PRIM1
HU (0.5mM):
0 24 R8 0 24 R8 0 24 R8
pRPAS4/8
RPA32
α-TUBULIN
B
IdU
CldU
45'
90'
IdU
HU (4 mM)
CldU
45'
120'
90'
CldU:IdU Ratio
1.95
1.84
1.75
1.12
ns
****
****
siPRIM1:
HU:
U2OS
C
IdU
HU (4 mM)
CldU
45'
120'
90'
CldU:IdU (ratio)
1.89
1.28
2.00
2.11
1.41
1.47
1.44
1.41
1.80
1.95
1.47
1.59
***
ns
ns
***
*
ns
****
siPRIM1:
siRTF2:
siRH2A:
shControl/siControl
shDDI2/siDDI1
U2OS
D
Relative PRIM1 mRNA level
normalized to shCtrl/siCtrl
siPRIM1:
siRTF2:
siRH2A:
shCtrl/siCtrl
shDDI2/siDDI1
U2OS

knockdown and HU-treatment, these results are confounded by PRIM1's essential role DNA replication. To resolve the issues associated with RNAi modification of PRIM1, several orthogonal approaches, including conditional inhibition or inducible degradation of PRIM1, were employed to determine PRIM1's function in replication restart and contribution to the DDI-RTF2 pathway.

First, we inhibited primase using with Vidarabine-TP, a compound that structurally resembles adenosine 5' monophosphate but where the ribose 3' hydroxyl group is in the *ara* orientation (Holzer et al., 2019; Parker and Cheng, 1987; Yoshida et al., 1985) (Figure 4.8A). Vidarabine-TP inhibited replication restart efficiency in wild type cells at high concentrations (50-100 μM) but did not affect replication restart efficiency at low concentrations (10 μM) (Figure 4.8B). Low concentrations of Vidarabine-TP reverted the rescue of replication restart by *siRTF2* or *siRNASEH2A* in the DDI1/2-depleted setting (Figure 4.8C).

Next, an auxin-inducible degron (AID) system was employed to partially degrade PRIM1 in a relatively short period of 30 minutes (Figure 4.9). The AID system co-opts a unique plant degradation mechanism, reliant on the plant hormone auxin. Auxin binds the F-box transport inhibitor response 1 (TIR) protein and promotes the interaction with the E3 ubiquitin ligase SCF complex, which are universally found in eukaryotes. SCF-TIR1 recruits an E2 ubiquitin conjugating enzyme that polyubiquitylates the degron, resulting in rapid degradation by the 26S proteasome (Nishimura et al., 2009) (Figure 4.9A). The endogenous PRIM1 locus was biallelically replaced with a PRIM-AID-mClover allele using CRISPR (obtained from Nanda Sasi, de Lange lab). A doxycycline-induced HA-TIR1 cDNA construct was retrovirally expressed in these cells. The PRIM1-AID system was optimized to induce a mild reduction (about 20%) in PRIM1 expression (Figure 4.9B,C). This reduction resulted in a significant replication fork restart defect, but not a global replication defect (Figure 4.9B-D). Slight changes in the length of the first thymidine analog, IdU, did not account for the differences in the CldU:IdU ratios (Figure 4.9E). To understand the genetic interaction of PRIM1 with the DDI-RTF2 pathway, DDI1/2 were depleted in RPE PRIM-AID-mClover cells (Figure 4.10). No further reduction in replication restart efficiency was observed upon combined reduction of PRIM1 and DDI1/2 levels (Figure 4.10). However, depletion of PRIM1 reverted the rescue of replication restart by *siRTF2* or *siRNASEH2A* treatment in the DDI1/2-depleted setting (Figure 4.10), suggesting that PRIM1 and RTF2/RNASEH2A are working in the same pathway.

These results lead us to consider a model in which a competition occurs between PRIM1 and RNase H2 at stalled replication forks, where PRIM1 synthesizes the same RNA primer RNase H2 degrades. We hypothesized that increasing the local concentration of PRIM1 could outcompete RNase H2 and overcome the fork restart defect in DDI1/2-depleted cells. To test this hypothesis, PRIM1 was over-expressed in U2OS cells using a lentivirus carrying a HA-FLAG- PRIM1 cDNA construct. The expression of PRIM1 from this vector was very high compared to endogenous expression

Figure 4.8. Primase inhibition results in defective replication restart.
(A) Schematic of Vidarabine 5'-monophosphate structure compared to adenosine 5'-monophosphate. (B) Ratio of CldU to IdU tract lengths in indicated U2OS cells. Increasing concentrations of Vidarabine-TP were added during the 90-minute CldU pulse. Labeling schematic indicated above plots. Each dot represents one replication tract. Mean ratios indicated above each sample and shown with red line. n>150 for each sample. Outliers removed with ROUT (1%). ****P<0.0001, ns, not significant, Kruskal-Wallis ANOVA with a Dunn's post-test. (C) Ratio of CldU to IdU tract lengths in indicated U2OS cells. Vidarabine-TP was added during the 90 minute CldU pulse in all samples. Each dot represents one replication tract. Mean ratios indicated above each sample and shown with red line. n>150 for each sample. Outliers removed with ROUT (1%). ns, not significant, Kruskal-Wallis ANOVA with a Dunn's post-test.
V-TP = Vidarabine-TP.

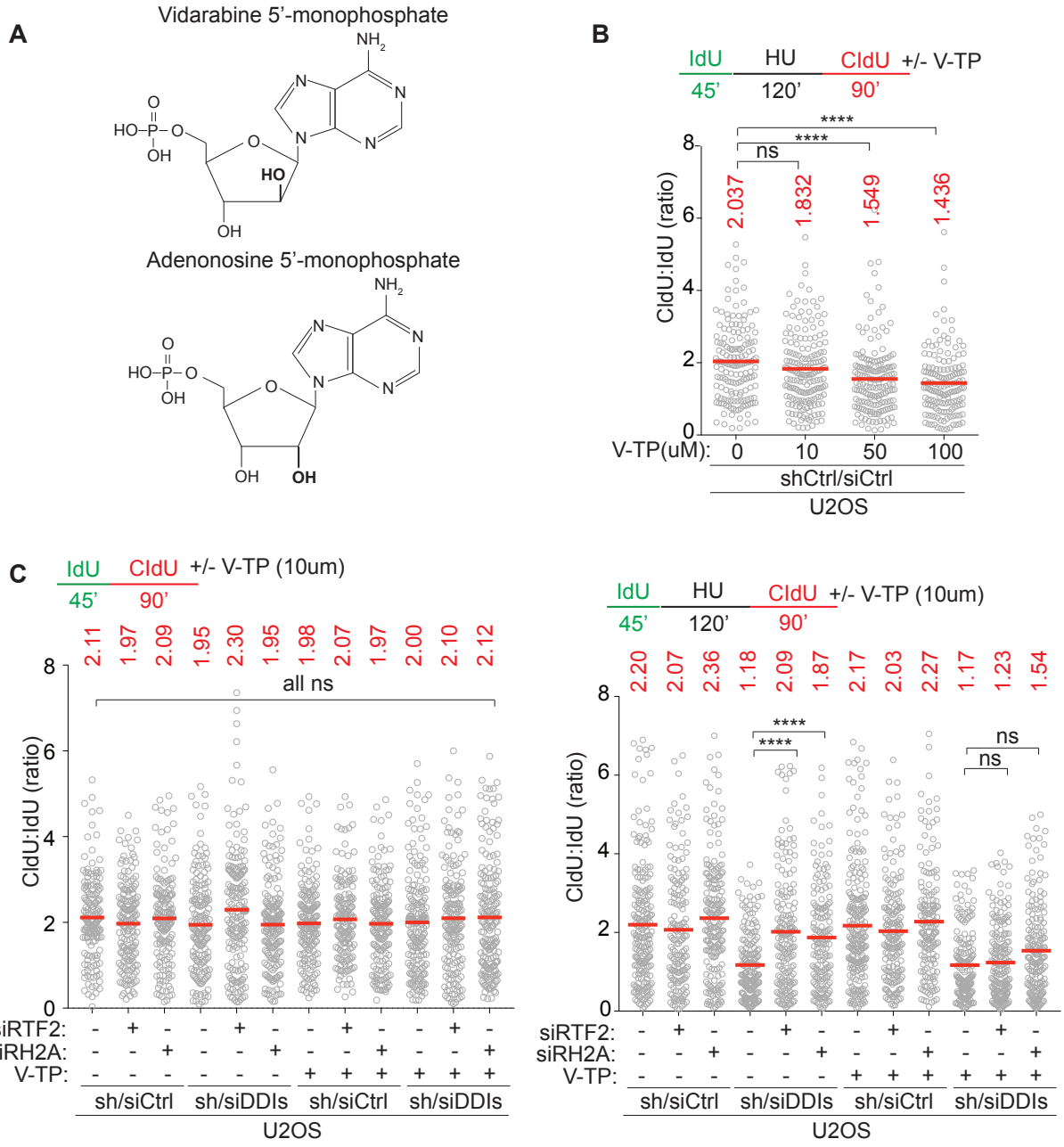
A
Vidarabine 5'-monophosphate
Adenonosine 5'-monophosphate
B
IdU
HU
CldU +/- V-TP
45'
120'
90'
CldU:IdU (ratio)
2.037
1.832
1.549
1.436
ns
****
****
V-TP(uM): 0 10 50 100
shCtrl/siCtrl
U2OS
C
IdU
CldU +/- V-TP (10um)
45'
90'
2.11 1.97 2.09 1.95 2.30 1.95 1.98 2.07 1.97 2.00 2.10 2.12
all ns
CldU:IdU (ratio)
siRTF2:
siRH2A:
V-TP:
sh/siCtrl
sh/siDDIs
sh/siCtrl
sh/siDDIs
U2OS
IdU
HU
CldU +/- V-TP (10um)
45'
120'
90'
2.20 2.07 2.36 1.18 2.09 1.87 2.17 2.03 2.27 1.17 1.23 1.54
****
****
ns
ns
CldU:IdU (ratio)
siRTF2:
siRH2A:
V-TP:
sh/siCtrl
sh/siDDIs
sh/siCtrl
sh/siDDIs
U2OS

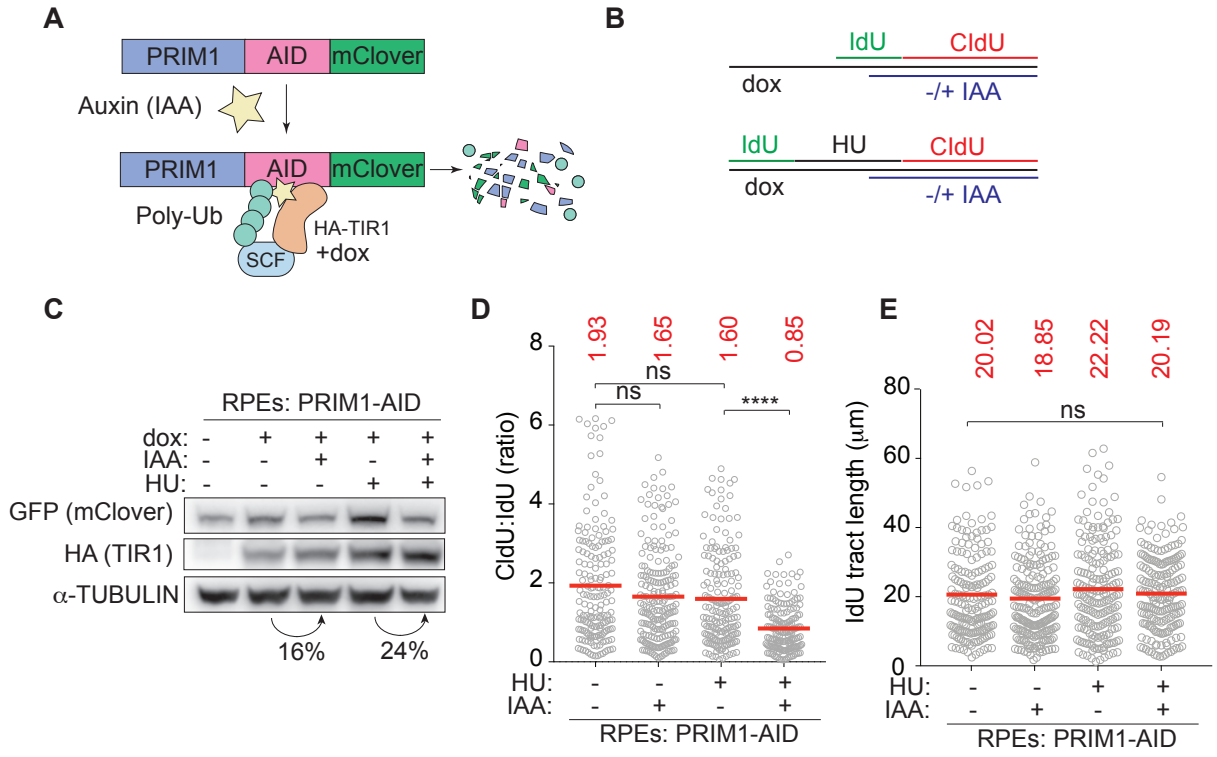

Figure 4.9. Auxin-inducible degradation of PRIM1 results in defective fork restart
(A) Schematic of PRIM1-tagged auxin-induced degron system in RPE-hTERT *p53*$^{-/-}$, *pRb*$^{-/-}$ cells. HA-TIR1 expression is under the control of a doxycycline-inducible promoter. (B) Labeling schematic of PRIM1-AID system with combing labeling. Cells were treated with doxycycline 4 hours and 15 minutes prior to collection. Cells were pulsed as indicated with drugs according to the schematic for the following times: IdU for 45 minutes, 4 mM HU for 120 minutes, CldU for 90 minutes, IAA for 120 minutes. (C) Immunoblot of whole cell lysates isolated from RPE cells with indicated treatments 0.5 mM HU. Percent decrease in PRIM1-AID-mClover signal by densitometry is indicated. (D) Ratio of CldU to IdU tract lengths in indicated RPE cells. Each dot represents one replication tract. Mean ratios indicated above each sample and shown with red line. n>150 for each sample. Outliers removed with ROUT (1%). *P<0.05, ****P<0.0001, ns, not significant, Kruskal-Wallis ANOVA with a Dunn's post-test. (E) IdU lengths in indicated RPE cells. Each dot represents one replication tract. Mean ratios indicated above each sample and shown with red line. n>150 for each sample. *P<0.05, ns, not significant, Kruskal-Wallis ANOVA with a Dunn's post-test.
dox = doxycycline.

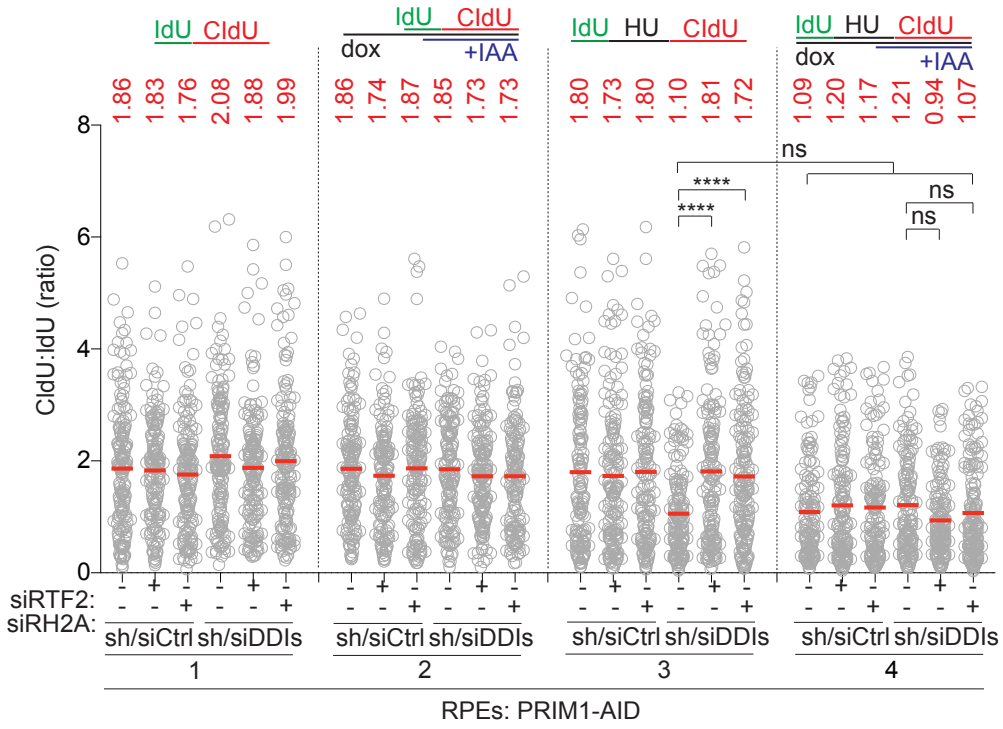

Figure 4.10. Genetic interaction between PRIM1 and the DDI-RTF2 pathway during replication restart.

Ratio of CldU to IdU tract lengths in indicated RPE cells. Labeling schematic of PRIM1-AID system with combing labeling indicated above. Cells were pulsed with indicated drugs for the following times: doxycycline for 4 hours and 15 minutes, IdU for 45 minutes, 4 mM HU for 120 minutes, CldU for 90 minutes, IAA for 120 minutes. Each dot represents one replication tract. Mean ratios indicated above each sample and shown with red line. n>140 for each sample. Outliers removed with ROUT (1%). ****P<0.0001, ns, not significant, Kruskal-Wallis ANOVA with a Dunn's post-test.

Ctrl = Control, RH2A = RNASEH2A.

(Figure 4.11A). Over-expression of PRIM1 rescued the replication restart defect seen upon depletion of DDI1/2 (Figure 4.11B). These results suggest there is competition between PRIM1 and RNase H2 at stalled replication forks.

4.3 Summary of Findings and Outlook

The results in this chapter indicate that removal of RNase H2 from the replication fork is necessary to promote replication restart when DDI1/2 are depleted and suggest that inappropriate enzymatic activity of RNase H2 at a stalled replication fork is detrimental to recovery from replication stress. Knockdown of RNase H2 rescued DDI1/2-deficient phenotypes to the same extent as RTF2 knockdown, suggesting that RTF2 and RNase H2 function in the same pathway to ameliorate the phenotypes associated with DDI1/2-deficiency.

The replication stress phenotypes presented in this chapter are consistent with those previously published for cells depleted of DDI1/2 (Kottemann et al., 2018). Since our DNA combing studies yielded the same results as those published using DNA fibers (Kottemann et al., 2018), this suggests that the phenotype is not dependent on changes in chromatin structure. One benefit of these single-molecule techniques is that they provide a means to directly assess nascent synthesis changes that rapidly occur in response to replication stress. Replication stress in this chapter was mostly modeled with HU treatment, but there are indications that removal of RTF2 (and RNase H2) could be a universal response to a variety of replication stress-inducing agents (Figure 4.5) and we propose that this removal is necessary for replication through genomic regions with high levels of endogenous replication stress.

As discussed in Chapter 3, RNase H2's localization to the replication fork may be dependent on the RNASEH2B's PIP box. Knockdown of RNASEH2B in a DDI1/2-depleted background should be assessed for the ability to rescue the phenotypes associated with DDI1/2-deficiency. If RNASEH2B knockdown rescues these phenotypes, an siRNA-resistant RNASEH2B PIP box mutant (FF>AA) could be expressed in DDI1/2-depleted cells treated with siRNASEH2B to evaluate the contribution of PCNA-localization in retaining RNASEH2B at the replication fork. If the PIP box does not contribute to RNase H2's localization in the absence of DDI1/2, expression of this mutant would not rescue the phenotypes associated with DDI1/2-depletion as RNASEH2B would still be retained at the replisome. However, if the PIP box is required, the expression of this mutant would still rescue the phenotypes associated with the depletion of DDI1/2.

Similar to the question asked in Section 3.3 regarding the RNase H2 activity necessary for the normal replication phenotype, it is unknown whether RNase H2's inappropriate activity at a stalled replication fork is against single DNA-embedded ribonucleotides or longer RNA-DNA hybrids, such as RNA primers. Since our data indicate restart is dependent on PRIM1, it is most likely that RNase H2 is removing RNA

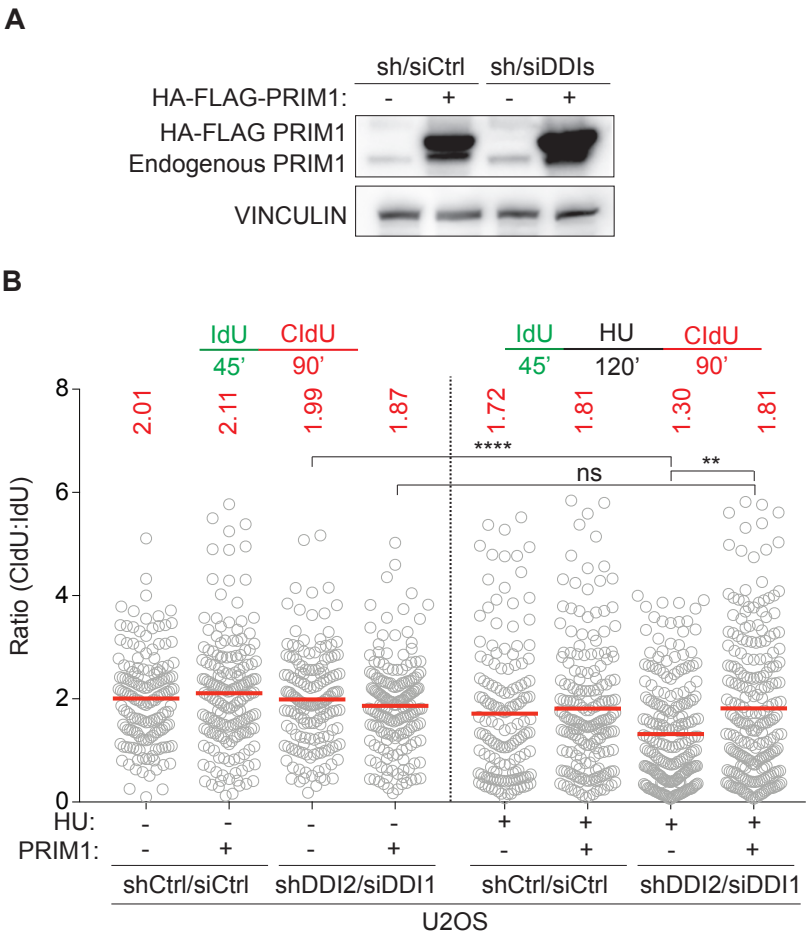

Figure 4.11. Overexpression of PRIM1 rescues replication restart deficiency associated with DDI1/2 depletion.

(A) Immunoblot of whole cell lysates isolated from U2OS cells indicating PRIM1 expression levels. (B) Ratio of CldU to IdU tract lengths in indicated U2OS cells Each dot represents one replication tract. Mean ratios indicated above each sample and shown with red line. n>150 for each sample. Outliers identified and removed with ROUT (1%). **P<0.01, ****P<0.0001, ns, not significant, Kruskal-Wallis ANOVA with a Dunn's post-test.

Ctrl = Control

primers. We propose that expression of an siRNA-resistant RNASEH2A mutant that cannot excise single DNA-embedded ribonucleotides (RED mutant) should still rescue the DDI1/2-associated phenotype when RNASEH2A is depleted whereas expression of a catalytically inactive RNASEH2A mutant will not. These hypotheses are currently being tested.

The cleavage of RNA-DNA hybrids at stalled replication forks appears to be a specific function of RNase H2 as depletion of RNASEH1 did not rescue the fork restart defect associated with DDI-deficiency. The difference in dependency of RNase H enzymes could be due to a difference in RNASEH1's localization. RNASEH1 has not been identified as part of the replisome, therefore, it may not be located in a location to interfere with replication restart. To test this hypothesis, replication restart defects could be assessed in a system where RNASEH1 is artificially tethered to the replication fork.

Our results show cells depleted of PRIMPOL did not exhibit replication restart defects after HU-induced stalling, indicating there is not a primary role for PRIMPOL in this type of restart. These results are in accordance with those from the Ercilla study, but not the Wan and Mouron studies (Ercilla et al., 2019; Mouron et al., 2013; Wan et al., 2013). The Ercilla study used siRNAs to examine PRIMPOL function in RPE-hTERT cells, whereas Wan et al. used stably selected shRNAs in HeLa cells and Mouron et al. used inducible shRNAs in HeLa cells and PRIMPOL KO MEFs. Though not entirely clear why, the differences in cell lines and methods of depletion may explain why some studies show a role for PRIMPOL in replication restart after HU-induced stalling and others do not.

We did observe an accumulation of P-RPA S4/8 when PRIMPOL was depleted, implying there is a contribution of PRIMPOL to the replication stress response, though this contribution does not occur immediately at the replication fork. These results collectively suggest that PRIMPOL functions behind the replication fork to promote gap fill-in as a secondary response to replication stress. Recently, PRIMPOL was shown to be upregulated after treatment with a high dose of cisplatin and this upregulation helped cells to recover from a second dose of cisplatin (Quinet et al., 2019), further supporting the hypothesis that PRIMPOL is a secondary responder.

PRIM1 is essential for replication and thus assessing PRIM1's function in replication restart is difficult. While collectively the data suggest a primary role for PRIM1 in replication fork restart, there are caveats to some of our approaches. For example, siRNAs to PRIM1 may have unintended consequences, especially over a long experimental time frame. Knockdown of an essential gene in DNA replication may explain the different dynamics in HU-induced P-RPA S4/8 accumulation in cells depleted of PRIM1 compared to cells depleted of DDI1/2. Moreover, while chemical inhibition using Vidarabine-TP is specific to the primase, it is not selective and may have off-target effects on other polymerases, including the replicative polymerases. The PRIM1-AID system is beneficial because it can reduce levels of PRIM1 specifically in a relatively short amount of time, but it is unknown which pools of PRIM1 are affected, those that are free in

solution, those that are bound to the replication fork, or both. Knowing which pools of PRIM1 are selectively degraded would help to interpret our results. Both RNAi- and AID-meditated depletion of PRIM1 could also result in the loss of other Pol α-primase components. Examining PRIM2, POLA1, and POLA2 levels are necessary to determine the specificity of PRIM1 depletion. However, this multi-pronged experimental approach augments confidence in the result that there is a greater reliance on PRIM1 during replication restart than during general DNA replication.

Our results suggest that PRIM1 and RNASEH2A compete at the replication fork for an RNA substrate, likely the RNA primer. The results that low doses of Vidarabine-TP do not inhibit replication restart efficiency but revert the rescue of RTF2 or RNASEH2A were initially perplexing but fit this competition model. The PRIM1 overexpression experiments are also consistent with this hypothesis. Biochemical experiments where the concentrations of PRIM1 and RNase H2 could be titrated will be useful to test this model.

The experiments examining the role of PRIM1 in replication fork restart suggest that PRIM1 is functioning in a pathway epistatic with DDI1/2, RTF2, and RNase H2. Since re-priming is occurring directly at the replication fork, PRIM1-dependent replication restart is likely a rapid process. PRIM1-dependent replication restart would be an efficient first-line mechanism of restart because the required machinery is already present in the replisome and immediately available for use. The DDI1/2 removal of RTF2 and RNase H2 from the replication fork is likely also a rapid mechanism.

Chapter 5: Discussion

5.1 The DDI-RTF2 axis

5.1.1 A general model for the DDI-RTF2 axis

DNA replication is vital for the propagation of the genetic material from one cell to the next, but DNA replication faces many obstacles to complete accurate and timely duplication of the genome. Here we present DDI1/2 and RTF2 as being indispensable for DNA replication and recovery from replication stress. Our data support a model whereby the DDI-RTF2 axis dynamically regulates RNase H2 at the replication fork to control the excision of genome-embedded ribonucleotides. During unperturbed DNA replication, RNase H2 travels with the replisome to remove excess ribonucleotides (Figure 5.1A). This ensures that replication proceeds normally as DNA-embedded ribonucleotides induce DNA damage and slow the replisome. On the other hand, when the replication fork stalls, RNase H2 must be removed to allow for proper replication restart (Figure 5.1B). The inability to remove RNase H2 (in a DDI1/2-depleted setting) results in cellular sensitivity, an accumulation of ssDNA, deficient fork restart and chromosomal breakage upon treatment with drugs that induce replication stress. We show that replication fork restart is dependent on PRIM1, leading to a model whereby inappropriate retention of RNase H2 at the replication fork degrades PRIM1-synthesized RNA primers that are necessary for restart.

Our experiments modeled replication stress with exogenous agents, including HU and aphidicolin. Future experiments will be important to determine the endogenous function for this pathway, such as hard-to-replicate areas of the genome. These areas include centromeres, telomeres, and replication fork barriers around the rDNA locus. We hypothesize that the removal of RTF2 and RNase H2 will be important at these hard-to-replicate regions where the replication fork may stall.

5.1.2 Replication stress response pathway choice

As discussed in Chapter 1, direct replication restart of a compromised replication fork can be achieved by re-priming downstream of the lesion, lesion bypass with the use of TLS polymerases, or lesion bypass via template switching. Our data are consistent with a direct re-priming mechanism to allow for replication restart at sites of replication stalling. We show that restart after HU is dependent on PRIM1 and not on PRIMPOL. Though we did not observe any contribution of PRIMPOL in replication fork restart after release from HU, we did, however, observe a replication fork restart defect for PRIMPOL in response to UV radiation as previously reported (Bianchi et al., 2013; Mouron et al., 2013; Wan et al., 2013). Thus, PRIMPOL-dependent re-priming is relevant to restart replication in response to UV radiation-induced fork stalling, but not HU-induced fork stalling. This implies that there are mechanisms to control which primase is selected for re-priming.

Figure 5.1. Our model of the DDI-RTF2 axis at the replication fork.
(A) During normal replication, RTF2 travels with the replication fork. We propose that this keeps RNase H2 at the replication fork to remove recently incorporated genomic ribonucleotides. Without RTF2, RNase H2 is lost from the replication fork and ribonucleotides are abnormally incorporated into DNA accumulating over several rounds of replication. Slower replication may be a result of incompetent OF maturation, the inability of the polymerases to synthesize across ribonucleotides efficiently, and/or the induction of DNA damage responses. (B) Under replication stress, DDI1 and DDI2 remove RTF2 from the replisomes which also results in loss of RNase H2 allowing cells to efficiently restart replication PRIM1-dependent manner. If RTF2 and RNase H2 are not removed, replication forks cannot restart resulting in increased ssDNA and genomic instability. We propose there is a competition between PRIM1 and RNase H2, which regulates the synthesis and degradation of the RNA primer. Several possibilities are drawn for where PRIM1 may be located because it is not known where PRIM1 and RNase H2 are acting.
*The placement of RTF2 in this diagram does not represent its physical location, as there is not enough evidence to yet determine where it is located.

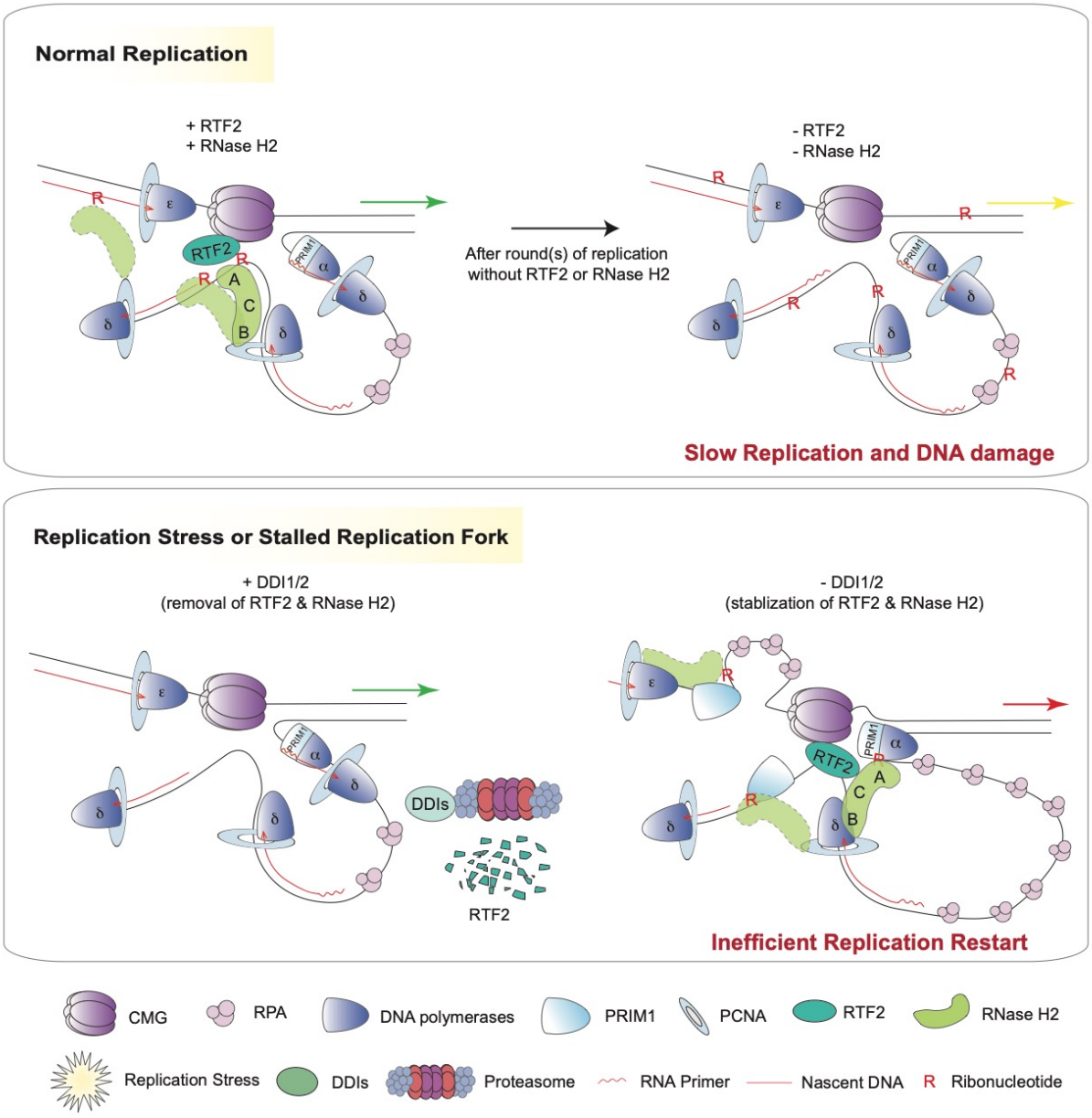
Normal Replication
+ RTF2
+ RNase H2
After round(s) of replication
without RTF2 or RNase H2
- RTF2
- RNase H2
Slow Replication and DNA damage
Replication Stress or Stalled Replication Fork
+ DDI1/2
(removal of RTF2 & RNase H2)
- DDI1/2
(stablization of RTF2 & RNase H2)
DDIs
RTF2
Inefficient Replication Restart
CMG
RPA
DNA polymerases
PRIM1
PCNA
RTF2
RNase H2
Replication Stress
DDIs
Proteasome
RNA Primer
Nascent DNA
R
Ribonucleotide

Why there is a difference in dependency on PRIM1 or PRIMPOL for direct re-priming to rescue DNA synthesis is currently unknown. As discussed in Chapter 4, differences in dependency could be based on the timing of protein recruitment to the replisome. Our data suggest PRIM1 direct re-priming in response to HU occurs rapidly at the replication fork, whereas PRIMPOL response is temporally distal to promote gap fill-in. Since PRIMPOL has not been identified as part of the replisome (Wessel et al., 2019), PRIMPOL's recruitment may be slower in comparison to PRIM1's recruitment as PRIM1 is constitutively present at the replication fork. Differences in dependency may also be related to the differential roles of the primases on the lagging or leading-strand. Since there is a greater reliance on PRIM1 during DNA replication on the lagging-strand due to the confined nature of DNA synthesis, we speculate PRIM1-dependent restart is a lagging stand specific recovery pathway. It is possible that PRIM1 is recruited to the leading-strand upon replication fork stalling, but it is more likely re-priming on the leading-strand favors the use of PRIMPOL, especially when there is a blocking lesion. A leading-strand role for PRIMPOL would be consistent with our results and the published data (Bianchi et al., 2013; Mouron et al., 2013; Wan et al., 2013).

Experimentally deciphering the differences in responses on the leading and lagging-strands is complex. While DNA combing is a powerful technique, it does not allow for specific strand visualization. Coupling of leading and lagging-strand synthesis has been proposed in *E. coli* and T4 bacteriophage (Graham et al., 2017; Lee et al., 1998). If this is also true in mammalian cells, a defect in either the leading- or lagging-strand coupling would result in overall fork dysfunction and prevent the visualization of a defect in one strand by DNA combing. If strand coupling does not occur in mammalian cells, differences between the leading- and lagging-strand would result in bimodal DNA combing data sets. Dissection of the differences in response to replication stress between the leading- and lagging-strand remains an area for further investigation and could require single-molecule biochemical assays.

Selection of which primase is employed to restart replication occurs within the direct re-priming pathway, but other pathways, including TLS and fork reversal, have also been described as important for direct replication restart. While TLS polymerases are typically studied for their role in bypassing bulky lesions to resume DNA synthesis, recently Pol κ has shown to be required for efficient replication fork restart in response to HU (Tonzi et al., 2018). Pol κ-deficiency also results in nascent strand degradation in response to HU suggesting replication fork reversal may occur without Pol κ (Tonzi et al., 2018). This phenotype is different from DDI1/2-depleted cells, as we observe defective fork restart efficiency, but not nascent strand degradation (Kottemann et al., 2018). If and how DDI-RTF2-dependent replication restart after HU-induced stalling coordinates with Pol κ-dependent replication restart has yet to be assessed.

Evidence is accumulating that replication fork remodeling, particularly fork reversal, can function to promote template switching and restart replication after HU. DNA translocases including SMARCAL1, ZRANB3, and HTLF as well as RAD51 (Bétous et

al., 2012; Blastyák et al., 2010; Ciccia et al., 2012; Taglialatela et al., 2017; Vujanovic et al., 2017; Yuan et al., 2012; Yusufzai and Kadonaga, 2008, 2010) are implicated in the catalysis of fork reversal. Understanding whether or not these proteins function epistatically with the DDI-RTF2 axis will be important to determine the relationship between re-priming and fork reversal.

The factors governing direct restart pathway choice during restart are still unclear. We propose a model where PRIM1-mediated re-priming disfavors the use of TLS polymerases and template switching. Efficient re-priming has been proposed to act in opposition to fork reversal (Fumasoni et al., 2015; Quinet et al., 2019), but more work is needed to address the genetic interplay between re-priming and fork reversal as mechanisms of direct replication restart. There is no available DNA template on a reversed fork capable of being primed that would promote restart since reversed forks are double-stranded. This further supports the idea that re-priming and fork reversal are separate pathways of direct replication fork restart. As discussed in Chapter 1, the ubiquitin status of PCNA may direct pathway choice. The mechanism by which stalled replication forks restart may also be dependent on the timing of recruitment of the proteins involved and the type, location, and duration of replication stress.

The accumulation of ssDNA at stalled replication forks activates ATR. In response to replication stress, depletion of DDI1/2 generates large stretches of ssDNA, as measured by increased P-RPA S4/8 signal (Kottemann et al., 2018). The location of this ssDNA is unknown, but we hypothesize it accumulates at stalled replication forks. The observation of increased P-CHK1 S345 signal when DDI1/2 are depleted may indicate that this ssDNA activates ATR, as phosphorylation of CHK1 on S345 is an ATR-dependent event. Interestingly, the induction of P-CHK1 S345 in DDI1/2-depleted cells is not suppressed upon knockdown of RTF2 or RNase H2, despite a reduction in ssDNA, as measured by the decrease in P-RPA S4/8 signal. Since ATR signaling is intact upon depletion of RTF2 or RNase H2, these data could suggest that there is an independent mode of ATR activation that is unrelated to the R-RPA S4/8 signal when DDI1/2 are deficient. It is also possible that activation of ATR signaling associated with DDI1/2 repression is due to the accumulation of ssDNA whereas the activation of ATR signaling in the absence of RTF2 or RNase H2 is due to the generation of additional 5’ ssDNA-dsDNA TOPBP1-binding sites by PRIM1-dependent RNA priming and extension. These two alternate possibilities remain to be tested.

5.1.3 PRIM1-dependent priming and re-priming at the replication fork

PRIM1 is required during general DNA replication, but we observed there is an even greater reliance on PRIM1 during replication stress as discussed in Chapter 4. Our results lead to several questions regarding the nature of RNA priming during DNA replication. First, why is there an increased dependency on PRIM1 during replication fork restart as opposed to during continuous replication? Second, how does RNase H2 ensure that ribonucleotides are not retained in the nascent daughter strand without disrupting

normal PRIM1-dependent priming events at the replication fork? Third, is it physically possible for RNase H2 to access the RNA primer in the Pol α-primase complex?

One hypothesis to resolve the difference in PRIM1 dependency is that replication fork stalling allows RNase H2 to access substrates that would not be available if the replication fork is moving at a consistent rate. For example, replication fork stalling could allow for the Pol α-primase to be dynamically overturned at the replication fork, exposing the RNA primer for RNase H2 degradation**.** If Pol α-primase remains stably bound during continuous replication, the RNA primer would not be exposed. A recent single-molecule biochemical study may support this hypothesis. It shows that Pol α-primase can be stably bound to the replisome when no excess Pol α-primase molecules are available in solution (Lewis et al., 2019). When concentrations of Pol α-primase are high and excess molecules are available, Pol α-primase molecules can be rapidly exchanged (Lewis et al., 2019). If replisomes moving continually have limited availability of Pol α-primase molecules and if stalled replisomes have an excess availability of Pol α-primase molecules, this could explain the why RNase H2 can degrade RNA primers in the 'stalled' but not 'moving' state. At high concentrations of Pol α-primase, the authors also observed two molecules of Pol α-primase present at the replication fork (Lewis et al., 2019). The biological relevance of the second bound Pol α-primase molecule is unknown, but the authors suggest examining whether this second bound Pol α-primase molecule allows for efficient bypass across replication obstacles. Increasing the number of Pol α-primase molecules at the replication fork may fit with our hypothesis that competition occurs between RNase H2 and PRIM1 at stalled replication forks.

Another possibility to resolve why there is an increased dependency on PRIM1 during replication stress is that PRIM1 is acting outside of the Pol α-primase complex at a stalled replication fork. While PRIM1 is normally studied as a component of the primosome, PRIM1 has biochemical RNA primase activity without the other Pol α-primase components (PRIM2, POLA1, POLA2) (Schneider et al., 1998). It is possible that additional PRIM1 molecules are recruited to the replication fork upon stalling to synthesize RNA primers that are extended by any of the replicative polymerases. This could be tested by examining whether specific inhibition or targeted degradation of POLA1, the catalytic subunit of Pol α, results in a replication fork restart defect. If inhibition of POLA1 does not trigger a fork restart defect, it would suggest that PRIM1 is acting outside of the Pol α-primase complex. These "non-classical" PRIM1-synthesized RNA primers may be the relevant substrate required for replication restart and are susceptible to RNase H2 degradation. This would potentially explain why the localization of RNase H2 at the replication fork does not interfere with normal DNA replication.

If PRIM1 is acting as part of the Pol α-primase complex during direct replication restart, it would have to be possible for RNase H2 to access the RNA primer for degradation if the RNA primer is the target of RNase H2's activity. It is not clear from structural data whether RNase H2 can physically contact an RNA primer in the Pol α-primase complex. PRIM1 continually establishes three hydrogen bonds with the growing

3’- rNTP end of the RNA primer, but this is a relatively weak association of PRIM1 with the RNA-DNA heteroduplex. The helical CTD of PRIM2 forms thirteen hydrogen bonds with the template, the majority of which are located near the RNA-DNA junction, and six hydrogen bonds with the 5’ triphosphate of the RNA primer, resulting in a very stable association. There appear to be no other contacts between PRIM2 and the RNA primer except for a stacking interaction between His-303 and the base of the 5’ rNTP (Baranovskiy et al., 2016a; Baranovskiy et al., 2016b). Therefore, the majority of the interactions between primase and the RNA primer are found on the 3’ and 5’ ends of the RNA primer, leaving the middle of a 9 mer primer exposed (Baranovskiy et al., 2016a; Baranovskiy and Tahirov, 2017; Baranovskiy et al., 2016b). It is tempting to speculate that the open architecture of the primase/DNA-RNA complex, where contacts with both the minor and major grooves are absent, could leave primers susceptible to nuclease activity especially when the replisome is stalled. However, the mechanism of intramolecular transfer may shield primers from nucleolytic degradation. The hypothesis that RNase H2 could access and degrade these RNA primers remains to be empirically tested.

There are many species of RNA-DNA hybrids, including R-loops, RNA primers, or single DNA-embedded, that could be the substrate of RNase H2 at a stalled replication fork. Based on the results showing a dependence on PRIM1 for replication restart, we hypothesize RNA primers are the predominant substrate which RNase H2 degrades at a stalled replication fork. RNase H2-dependent removal of the PRIM1-synthesized RNA primers would result in replication fork stalling. Removal of R-loops would logically promote, not prevent, replication restart because R-loops can block the replication machinery. Thus, RNase H2 is likely not removing R-loops at stalled replication forks as their presence would prevent replication restart. It is possible single DNA-embedded ribonucleotides could be RNase H2’s substrate and the experiments proposed in Chapter 4 to examine the RNase H2 separation of function mutant that does not have catalytic activity against single-embedded ribonucleotides while retaining activity against longer RNA-DNA hybrids, will help to identify the substrate of RNase H2 at stalled replication forks.

5.1.4 RNase H2 processing of genome-embedded ribonucleotides during normal DNA replication

RNase H2-dependent removal of RNA-DNA hybrids is vital for normal DNA replication. The RNA-DNA substrate processed by RNase H2 during unperturbed DNA replication may be different from that which is removed during stalled replication. Here I will discuss which RNA-DNA hybrid species, whether R-loops, RNA primers, or single DNA-embedded, is most likely removed by RNase H2 during normal DNA replication. R-loops are a source of replication stress and, therefore, RNase H2-dependent removal of these lesions would promote normal DNA replication. The accumulation of R-loops would result in fork asymmetry (Gan et al., 2011). However, RTF2-deficient cells do not exhibit fork asymmetry, indicating that the replication forks are stable even without the presence

of RTF2 and RNase H2. Therefore, our data are inconsistent with R-loops being the substrate RNase H2 processes during normal DNA replication. RNase H2-dependent removal of RNA primers required for normal DNA synthesis would be unfavorable during normal DNA replication. Thus, we suspect RNA primers are not the substrates that RNase H2 removes during normal DNA replication. Loss of RNase H2-mediated removal of single genome-embedded ribonucleotides could explain the replication slowing and DNA damage phenotypes observed in the absence of RTF2. During normal DNA replication, we favor a model where RNase H2 catalyzes the removal of single DNA-embedded ribonucleotides. This will be tested with experiments examining the RNASEH2A separation of function mutant as described in Chapter 3.

Our observation of replication slowing when RNase H2 is lost from the replication fork suggests DNA-embedded ribonucleotides disrupt DNA replication. How does the accumulation of ribonucleotides behind the replication fork result in slower replication? One hypothesis is that inefficient removal of RNA primers during Okazaki fragment maturation interferes with Pol δ progression and synthesis on the lagging-strand, resulting in a strand-specific replication slowing. A second possibility is that multiple rounds of replication result in the accumulation of single genome-embedded ribonucleotides. These ribonucleotides may accumulate from several sources, including incorporation by the DNA polymerases, inefficient Okazaki fragment maturation, and/or DNA repair (Bergoglio et al., 2003; Brown and Suo, 2011; Cavanaugh et al., 2011; Cilli et al., 2015; Clausen et al., 2013; Crespan et al., 2016; Donigan et al., 2014; Gosavi et al., 2012; Nick McElhinny and Ramsden, 2003; Nick McElhinny et al., 2010; Pryor et al., 2018). These ribonucleotides remain in the genome in the absence of RNase H2. In this setting, replication slowing is the result of an intrinsic inability of the polymerases to synthesize across a ribonucleotide at an efficient rate as it is known that high levels of ribonucleotides in the template strand impedes replication fork progression (Watt et al., 2011). Finally, TOP1 can compensate for the loss of RNase H2 and remove genome-embedded ribonucleotides (Kim et al., 2011; Sekiguchi and Shuman, 1997; Sparks and Burgers, 2015; Williams et al., 2013; Zimmermann et al., 2018). TOP1-dependent removal of ribonucleotides generates DNA lesions, stimulates PARP1 activity, and induces poly-ADP-ribosylation, all of which may hinder the replisome. Therefore, in the absence of RNase H2, the presence of single-embedded ribonucleotides in the genome may also induce replication slowing as the result of inappropriate TOP1-dependent removal of ribonucleotides.

5.1.5 Regulation of RTF2, RNase H2, and other nucleases at the replication fork

Our data indicate that RTF2 and RNase H2 travel with the replisome and are required during normal replication but must be removed upon replication stress. We do not fully understand the mechanisms that exist to regulate RTF2 and RNase H2's localization, retention, and removal at the replication fork.

How RTF2 is normally recruited to the replication fork is unknown. Our results suggest RTF2 could be recruited through interaction with the MCM2-7 complex. If residues essential for the interaction are identified and mutated, future experiments could determine whether RTF2 is recruited to the replication fork without MCM2-7 interaction. These experiments would resolve the function that the MCM2-7 complex has in the recruitment of RTF2 to the replication fork. It is also possible that RTF2 is recruited to the replication fork via PCNA. RTF2 contains a “non-canonical” PIP box sequence (Figure 1.10), however, we have not been able to observe a strong, reproducible interaction between RTF2 and PCNA. If an RTF2 cDNA carrying a mutation in RTF2’s putative PIP box cannot be recruited to the replication fork, this may indicate that PCNA mediates RTF2 localization. The function of PCNA in recruitment of RTF2 to the replication fork requires further investigation.

The nature of DDI1/2-dependent removal of RTF2 during replication stress also requires further exploration. The ability of DDI1 and DDI2 to shuttle RTF2 to the proteasome likely requires ubiquitination of RTF2. If, where, and how RTF2 becomes ubiquitinated during replication stress is an area of active investigation in our laboratory. Identifying the specific E3 ligase responsible for ubiquitinating RTF2 and the specific RTF2 residues that become modified will provide opportunities to modulate this pathway. RTF2 contains a RING domain, which we have shown to be important for RTF2’s function in unperturbed DNA replication. It has been speculated that this domain could have E3 ubiquitin or SUMO ligase activity (Inagawa et al., 2009). So far the function of this domain has not been biochemically tested. If this domain is shown to have E3 activity, it is possible that RTF2 could ubiquitinate itself

Similarly, further investigation is required to understand the regulation of RNase H2 levels at the replication fork. Localization of RNase H2 at the replication fork can be facilitated by PCNA-dependent (RNASEH2B’s PIP Box) (Bubeck et al., 2011), PCNA-independent (via RNASEH2A) (Kind et al., 2014), or an RTF2-dependent mechanism. The coordination between these pathways is unknown. Our results indicate RNase H2 is lost from the replication fork specifically but retained on the whole-cell level in the absence of RTF2. Cells depleted of RTF2 provide a way to study the loss of RNase H2 in DNA replication without confounding effects from complete cellular loss of RNase H2.

Though our data suggest RTF2 sustains levels of RNase H2 at the replication fork, the mechanism by which RTF2 provides this regulation is unknown. Future experiments will be important to determine whether the interaction between RTF2 and RNase H2 is direct or indirect. Identifying whether the interaction is direct can provide insight into the mechanism of RTF2 regulation of RNase H2 at the replication fork. If direct, it will be important to determine which component of the RNase H2 complex mediates the interaction. Systematic truncation mutations of RTF2 and RNase H2 subunits could identify the required regions for the interaction and lend further insight into the mechanism of RNase H2 regulation by RTF2. If the RTF2 and RNase H2 interaction is indirect, there

could exist a mediator protein of this interaction. PCNA, which interacts with RNASEH2B's PIP box and is a central hub in DNA replication, could be one such factor.

Since we have identified RTF2 RING mutants that do not rescue the replication defect, these mutants could be assessed for their ability to bind to the RNase H2 complex. If the mutants retain the ability to bind RNase H2, this would suggest that there is some other active function associated with this domain to sustain RNase H2 levels at the replication fork. As previously stated, this domain could have ubiquitin or SUMO ligase activity, but this remains to be functionally tested. If one of these biochemical activities exists, it is possible that RTF2 regulates RNase H2 via post-translational modification.

In addition to RNase H2, other nucleases travel with the replisome and have specific roles to maintain general DNA replication. For example, multiple nucleases, including FEN1, DNA2, and EXO1, are implicated in OF maturation and processing RNA primers on the lagging-strand. Without these nucleolytic activities, DNA damage ensues. Poly(ADP-Ribose) polymerase functions to sense unprocessed and un-ligated OFs in cells (Hanzlikova et al., 2018), which is consistent with data that loss of RNase H2 or FEN1 inhibition is synthetically lethal with PARP inhibitors (Hanzlikova et al., 2018; Zimmermann et al., 2018). Since the induction of DNA damage in the absence of RTF2 is likely due to RNase H2 loss from the replication fork, it remains to be determined whether RTF2 loss is also synthetically lethal with PARP inhibition.

Based on our data regarding the regulation of RNase H2 at the replication fork, we speculate that the activity of other nucleases involved in OF maturation, including that of FEN1, DNA2, or EXO1, may need to be regulated at stalled replication forks. Upon EXO1 depletion, we observed partial suppression of the increased P-RPA S4/8 signal associated with DDI1/2-depletion (data not shown). FEN1 and DNA2 knockdown alone induced P-RPA S4/8 making any DDI1/2 co-depletion studies uninterpretable (data not shown). EXO1 has 5' to 3' exonuclease activity as well as RNase H activity (Lee and Wilson, 1999; Orans et al., 2011; Qiu et al., 1999a). Unrestrained EXO1 activity has also been implicated in nascent DNA resection at reversed forks (Lemaçon et al., 2017). Since we do not observe DNA resection in DDI1/2-depleted cells (Kottemann et al., 2018), we think this activity of EXO1 is irrelevant in our system. EXO1, DNA2, and FEN1's role in direct replication restart requires further investigation.

The main replisome components are stable upon replication stress (Dungrawala et al., 2015), but it is becoming increasingly evident that accessory factors are dynamically altered upon replication fork stalling. Certain factors are restrained, such as DNA2, MRE11, and EXO1, by replication fork protection activities of BRCA1, BRCA2, or RAD51 (Lemaçon et al., 2017; Schlacher et al., 2011; Schlacher et al., 2012; Wang et al., 2015a). Our work suggests that removal of nucleases may also be vital to replication fork protection as we hypothesize ubiquitin-mediated removal of RTF2 results in RNase H2 removal from the replication fork. Future work will be important to address a more complete profile of the proteasomal shuttle-dependent protein turnover events at the DNA

replication fork during normal replication and during recovery from replication stress. Turnover events provide a rapid mechanism of responding to DNA insults. By understanding the complex dynamics and regulation of supportive replisome-associated proteins, in addition to the major components, we will have a more complete picture of replication stress responses.

5.1.6 Clinical implications of the DDI-RTF2 axis

The results from these studies have implications for human health. First, these data may provide a better understanding of AGS, a disease associated with mutations in any of the RNase H2 subunits. AGS has been a useful diagnostic label, but a larger umbrella grouping of Mendelian disorders associated with an up-regulation of type I INF signaling has been proposed, termed “type I interferonopathies" (reviewed in (Crow, 2011)). The type I INF response seen in patients with mutations in RNase H2 is also demonstrated in hypomorphic mouse models (Mackenzie et al., 2016; Pokatayev et al., 2016). It is hypothesized that cytosolic nucleic acid species, reminiscent of viral nucleic acids, stimulate type I INF expression resulting in AGS pathogenesis (Gunther et al., 2015; Mackenzie et al., 2017); (reviewed in (Rodero and Crow, 2016)). Given RTF2-deficient cells exhibit similar mitotic defects to RNase H2-deficient cells, a type I INF response should be examined in the *Rtf2* mouse model driven by tissue-specific promoters, such as the Vav promoter, discussed in Chapter 2. Further work to address the origin of the cytosolic nucleic acids that stimulate type I INF and how this stimulation leads to pathogenesis is of the utmost importance to understanding the disease etiology of type I interferonopathies.

Our data suggest that mutations in RTF2 could lead to type I interferonopathies. To date, there are no characterized human mutations in RTF2 and thus any disease phenotype is unknown. Upon pursuit of these experiments, RTF2 had not yet been studied in the mammalian system and thus more work is needed to understand RTF2’s relevance to human health. Eleven of the eighteen genes associated with type I interferonopathies have known roles in nucleic acid metabolism and signaling (reviewed in (Rodero and Crow, 2016)). Interestingly, patients with splicing mutations in POLA1, the catalytic subunit of Pol α, are diagnosed with X-linked reticulate pigmentary disorder (XLPDR), a primary immunodeficiency with auto-inflammatory features. This disorder is characterized as a type I interferonopathies despite presenting distinctly from the other type I interferonopathies (Starokadomskyy et al., 2016). It will be interesting to follow how this umbrella grouping of Mendelian disorders grows and whether it will include the addition of more proteins involved in the DDI-RTF2 axis.

Genome instability also drives cancer development and therapy resistance. Understanding the regulation and consequences of genomic ribonucleotides continues to be a relevant topic for cancer development as deficiencies in RNASEH2B are associated with metastatic prostate cancer and chronic lymphocytic leukemia in humans (Zimmermann et al., 2018) and drive the development of squamous cell carcinomas in

mice (Hiller et al., 2018). Since genome-embedded ribonucleotides are a source of PARP-trapping lesions, it has been suggested that PARP inhibitors may be of therapeutic value in RNASEH2B-deficient cancers. Future studies may be important to determine RTF2's contribution to cancer development.

Targeting DNA replication and replication stress pathways in cancer cells has been the mainstay of cancer treatments. In the 1940s, the discovery of nitrogen mustard, an alkylating agent, began the first wave of chemotherapeutics targeting DNA replication. Since then, targeted therapies inhibiting specific factors in the DNA damage and replication stress response have been developed and are being examined in clinical trials. For example, an ATR kinase inhibitor, AZD6738, is currently being tested in multiple clinical trials. Inhibition of the DDI-RTF2 axis may also prove useful to sensitize cancer cells to ATR or CHK1 inhibitors if ATR signaling is independent of the DDI-RTF2 axis. It has been shown that the depletion of PRIM1 using RNAi is synthetic lethal with ATR or CHK1 inhibitors (Job et al., 2018). The increased reliance on PRIM1 during replication restart after stress, as opposed to during unperturbed replication, may allow for specific synergistic effects with the ATR and CHK1 inhibitors. Counter to this notion, the CRISPR-mediated loss of RNase H2 is also synthetic lethal with ATR inhibition (Wang et al., 2018). These data are contradictory given our results that PRIM1 and RNase H2 compete, rather than synergize, with each other. The also of either PRIM1 or RNase H2 results in genome instability, which may explain why they are both synthetic lethal with ATR inhibition. However, these published data also use methods that strongly abrogate or remove essential genes and would benefit from studies using specific inhibitors. Our data support the development of DDI1/2 or PRIM1 inhibitors for future studies to determine if this is a viable therapeutic avenue.

5.2 Concluding remarks

This work was pursued under the hypothesis that by studying proteins of unknown function at the replication fork, we would reveal interesting, previously undescribed, biological mechanisms. We found a novel pathway dependent on DDI1/2 and RTF2 that intersects with known proteins, RNase H2 and PRIM1, but reveals new insights about their regulation and function in DNA replication and the replication stress response. There are still many uncharacterized genes and new roles for known genes that remain to be discovered, especially in regard to DNA replication and repair. These types of studies are vitally important to understanding human biology.

Chapter 6: Experimental Procedures

6.1 General procedures

6.1.1 Generation of Rtf2 mouse strains, husbandry, and genotyping

mESCs containing the *Rtf2* gene targeting construct (*Rtf2*$^{tm1a(KOMP)Wtsi}$) were obtained from the UCDavis KOMP Repository. The Rockefeller transgenics facility injected targeted mESCs into C57BL/6J blastocysts to generate chimeras. *Rtf2*$^{+/stop}$ mice were mated with mice expressing Flp (Rodriguez et al., 2000) to generate *Rtf2*$^{+/lox}$ mice. *Rtf2*$^{+/lox}$ mice were then mated with mice expressing Cre recombinase from a ubiquitous EIIa promoter (Lakso et al., 1996). All of the animals were handled according to the Rockefeller University Institutional Animal Care and Use Committee protocols. See Table 6.1 for summary of mouse strains.

Mouse tail tips were obtained from pups at day 21. Tails were lysed in DirectPCR Lysis Reagent (Mouse Tail) supplemented with 0.2 mg/mL proteinase K according to manufacturer's protocol. 0.2-1.0 µL of lysate was used for 20 µL PCR reaction. GoTaq® DNA polymerase master mix was used for PCRs with appropriate primers. Sanger sequencing was performed at GeneWiz. See Table 6.3 for mESC long range genotyping primers and Table 6.4 for mouse genotyping primers.

6.1.2 Mammalian cell culture

Mouse embryonic fibroblasts (MEFs) were isolated on embryonic day 13.5 from crosses of *Rtf2*$^{+/lox}$ and *Rtf2*$^{+lox}$ mice (*Rtf2*$^{+/+}$, *Rtf2*$^{+/lox}$, and *Rtf2*$^{lox/lox}$ MEFs) and crosses of *Rtf2*$^{+/lox}$ and *Rtf2*$^{+/-}$ mice (*Rtf2*$^{+/+}$, *Rtf2*$^{+/lox}$, *Rtf2*$^{+/-}$, and *Rtf2*$^{-/lox}$ MEFs). MEFs were expanded to obtain cells for early passage primary cell stocks and to immortalize cells with a retrovirus expressing SV40 (Zhu et al., 1991). Experiments were conducted with littermate MEFs. Multiple MEF lines from individual mothers were isolated and used in replicate experiments. *Rtf2*$^{-/-}$ clonal cell lines were also generated from SV40-immortalized *Rtf2*$^{-/lox}$ MEFs after infection with pMMP Hit & Run Cre recombinase.

Primary MEFs and BJ foreskin fibroblasts (transformed by HPV16 E6E7 expression and/or immortalized by expression of catalytic subunit of human telomerase (hTERT)) were maintained in DMEM, supplemented with 15% (v/v) fetal bovine serum (FBS), 1X MEM non-essential AA, 2 mM L-alanyl-L-glutamine dipeptide, and 100U/mL penicillin-streptomycin. MEFs virally transformed with SV40, HEK 293T cells, U2OS cells (as described in Kottemann et al.) and HeLa cells (Jackson lab) were maintained in DMEM supplemented with 10% FBS and the additional supplements described above. RPE *p53*$^{-/-}$, *pRb*$^{-/-}$, PRIM1-AID-mClover cells (de Lange lab) were maintained in DMEM/F12 supplemented with 10% FBS and the additional supplements described above. HCT-116 *p53*$^{-/-}$ cells were maintained in McCoy's 5A media supplemented with 10% FBS and the additional supplements described above. Upon confluence, cells were dissociated with trypsin and a fraction of the cells were passaged into a new dish. Cells

were cryopreserved in their respective media supplemented with 10 % DMSO. See Table 6.2 for summary of cell types.

6.1.3 Growth and sensitivity assays

For growth assays, 2×10^4 - 3×10^4 cells were plated in each well of a 6-well plate in triplicate. Wells were counted on subsequent days. Population doublings were calculated using the following formula: 3.32 x [log(the number of cell harvested)–log(the initial number of cells plated)]

For sensitivity assays, $2.5 \times 10^4 – 4.5 \times 10^4$ cells were plated in each well of a 6-well plate in triplicate. The following day drugs were added at indicated concentrations. After 5-6 days in culture, cells were passaged once at appropriate ratios. Cells were counted when untreated wells reached near confluence around 7-9 days. The cell numbers at each dose of drug were divided by the cell number in the untreated sample to calculate the percent survival.

6.1.4 RNA preparation, reverse transcription, and real-time quantitative PCR

Total messenger RNA was extracted from cells using RNeasy Plus Mini Kit. RNA was reverse transcribed using the SuperScript™ III First-Strand Synthesis System. The relative transcript levels of genes of interest were determined by RT-qPCR using Platinum™ SYBR™ Green SuperMix-UDG. All kits were used according to manufacturer's protocol. Reactions were run and analyzed on Applied Biosystems™ QuantStudio™ 12K Flex system. See Table 6.5 for RT-qPCR primers.

6.1.5 Plasmid generation and mutagenesis

cDNA from MEFs or BJ cells was PCR amplified with primers containing attB sites. attB-PCR products were cloned using the Gateway® system into pDONOR223 with BP Clonase II Enzyme Mix. pDONR223 derivatives with inserted cDNAs (pENTR vectors) were cloned into destination vectors with LR clonase II Enzyme Mix. RTF2 RING mutants were generated with QuikChange Multi Site-Directed Mutagenesis Kit in pENTR plasmids. Mutagenesis was confirmed with Sanger sequencing (GeneWiz) prior to cloning into destination vectors with LR clonase II. Reactions were transformed into chemically competent DH5-α or Stlb3 *E. coli* cells and plated onto Luria-Bertani (LB)/agar plates with the appropriate bacterial selection (kanamycin (50 µg/ml), spectinomycin (50 µg/mL), chloramphenicol (25 µg/ml), or ampicillin (100 µg/ml)). Clones were mini-prepped and sequences were confirmed with Sanger sequencing (GeneWiz). Correctly identified clones were maxi-prepped and ethanol precipitated for sterile tissue culture use. See Table 6.6 for Gateway primers, Table 6.7 for mutagenesis primers and Table 6.10 for a list of plasmids with details regarding individual vectors.

6.1.6 Transductions

cDNAs were delivered by retroviral or lentiviral transduction after packaging in HEK 293T cells. $5x10^6$ were plated the evening before transfection. DNA and viral packaging vectors were transfected into cells with TransIT-293 transfection reagent according to the manufacturer's protocol. The next day, media was changed and another 24 hours later, viral supernatants were harvested every 12 hours and filtered (0.45 µM). pWZL Cre-hygro and pMMP Hit & Run Cre viral supernatants were provided by the de Lange lab. Target cells were infected with viral supernatants supplemented with 4 µg/mL polybrene. Stably expressing cells were selected with the appropriate agent ((puromycin (0.5-2 µg/ml), hygromycin (100 µg/ml), blasticidin (600 µg/ml), neomycin (600 µg/ml)). See Table 6.10 for a list of plasmids.

6.1.7 Generation of GFP-AID-RTF2 endogenously tagged HEK 293Ts

The pUC19-EGFP-AID-hRTF2 donor construct was generated with classical and In-Fusion® HD cloning techniques. hRTF2 was amplified with BamHI and NotI digestion sites and ligated into the pcDNA5-FRT-TO-EGFP-AID backbone. Using this as a PCR template, a GFP-AID-hRTF2 construct was amplified with primers compatible for In-Fusion. 5' and 3' UTR regions of RTF2 were also amplified with primers compatible with In-Fusion. Subsequently purified PCR products from these reactions were cloned into a HindIII- and EcoRI-digested pUC19 backbone with In-Fusion®, generating a donor construct containing homolog arms in the 5' UTR and 3' UTR and a cDNA for GFP-AID-RTF2. HEK 293Ts were transfected TransIT-293 with this donor construct, a guide RNA-Cas9 construct and a single guide RNA construct in a 1:1:1 ratio. Cells were grown for 48-72 hours before sorting for GFP+ populations. GFP+ populations were sub-cloned for single cell clones. These clones were verified for integration of the GFP-AID-RTF2 cDNA into the endogenous *Rtf2* locus. See Table 6.8 for CRISPR cloning primers.

6.1.8 Immunoblotting

If cells were counted upon collection, an equal number of cells was lysed by resuspension in an equal volume (100 µL per $1x10^6$ cells) of hot Laemmli buffer (Bio-Rad). If cells could not be counted upon collection, whole cell lysates were prepared by lysing cells in homemade Laemmli buffer (4% SDS, 20% glycerol, 0.125 M Tris-HCl (pH=6.8)). Samples were either sonicated or passed through a tuberculin needle 10 times. Protein concentration was determined by Lowry protein assay prior to addition of 2-mercaptoethanol (10% final concentration) and bromophenol blue (0.004% final concentration). Subsequently, samples were boiled for 5 minutes. Equal amounts of protein were separated by sodium dodecyl sulfate polyacrylamide gel electrophoresis (SDS-PAGE) on precast 4–12% Bis-Tris gels. Membranes were blocked for one hour in

5% milk in TBST (10 mM Tris-HCl (pH=7.5), 150 mM NaCl, 0.1% Tween 20) and incubated in primary antibodies for 2 hours at room temperature or overnight at 4°C. Membranes were sufficiently washed in TBST (3x 10 minutes) before being incubated with horseradish peroxidase (HRP)-conjugated secondary antibodies for 1 hour at room temperature detected by enhanced chemiluminescence. Membranes were visualized with either ImageQuantLAS 4000 or Azure c300 imaging systems. See Table 6.11 for list of antibodies.

6.1.9 Immunofluorescence and nascent proximity ligation assay

For EdU staining, cells were grown on round micro glass coverslips and pulsed with EdU (10 μM) for one hour prior to being washed in 1X phosphate buffered saline (PBS) and fixed in 3.7% (v/v) formaldehyde in PBS at room temperature for 10 minutes. Coverslips were washed and permeabilized in 0.5% (v/v) Triton X-100 in PBS. Coverslips were incubated in blocking buffer (either 5% (v/v) FBS in PBS or 3% (w/v) bovine serum albumin (BSA) in PBS) for 30 minutes at room temperature. Coverslips were stained with Click-iT™ EdU Alexa Fluor™ 488 Imaging Kit according to manufacturer's protocol. Coverslips were mounted on glass microscope slides with DAPI Fluoromount-G®.

For γH2AX staining, cells were grown on round micro glass coverslips, washed, fixed, and permeabilized as above. Coverslips were incubated with primary antibodies in blocking buffer for two hours at room temperature or overnight at 4°C. Coverslips were washed with blocking buffer and then incubated with secondary antibodies. Coverslips were washed 3x 5 minutes with PBS, dried, and mounted on glass microscope slides with DAPI Fluoromount-G®.

For nascent PLA staining, cells were grown on round micro glass coverslips and pulsed with EdU prior to being washed in ice cold PBS, pre-extracted in cold cytoskeleton buffer (10 mM PIPES pH=6.8, 100 mM NaCl, 300 mM sucrose, 3 mM MgCl2, 1 mM EGTA, 0.5% (v/v) Triton X-100) for 5 minutes, and cold cytoskeleton stripping buffer (10 mM Tris HCl (pH=7.4), 10 mM NaCl, 3 mM MgCl2, 1% (v/v) Tween 20, 0.5% (w/v) sodium deoxycholate) for 5 minutes. Coverslips were fixed, permeabilized and blocked as above. Coverslips were incubated for 30 minutes in homemade Click-iT reaction cocktail (PBS, Biotin azide (10 μM), (+) Sodium L-ascorbate (10 mM), Copper (II) sulfate pentahydrate (10 mM)). Coverslips were washed and incubated with the PCNA antibody in blocking buffer for two hours at room temperature. Coverslips were washed again and incubated with a secondary antibody. Coverslips were washed and incubated with PLA primary antibodies overnight at 4°C. The next day the PLA reaction (DuoLink®) was completed according to the manufacturer's protocol. Coverslips were mounted on glass microscope slides with DAPI Fluoromount-G®. Slides were imaged Inverted Olympus IX-71 DeltaVision Image Restoration Microscope or Axio Observer.A1 fluorescence microscope. See Table 6.11 for list of antibodies.

6.1.10 Cell cycle and flow cytometry

Exponentially growing cells were labeled with EdU one hour prior to collection and fixation. Cell cycle was performed with Click-iT™ EdU Alexa Fluor™ 647 Flow Cytometry Assay Kit per the manufacturer's protocol. Total DNA content was stained with FxCycle™ Violet. Stained cells were analyzed on a BD Accuri™ C6 or BD™ LSR II cytometers. Data were analyzed with FlowJo software.

6.1.11 Silanization of coverslips and DNA combing

Silanized coverslips were either purchased from GenomicVision or prepared in-house according to Gallo et al (Gallo et al., 2016) with modification of the plasma cleaning step, where we used Gatan Model 950 Advanced Plasma System for 10 minutes with atmospheric air. Mirco-slide holders were made at Rockefeller's Precision Fabrication Facility.

For DNA combing, exponentially growing cells were labeled with IdU (100 μM) followed by CldU (100 μM). Stocks of IdU were solubilized in sodium hydroxide (NaOH) and stocks of CldU were solubilized in ammonium hydroxide (NH_4OH) to concentrations of 10mM and stored in -20°C until use. Labelled cells were collected and washed in ice cold PBS. Cells were resuspended in 45 μL resuspension buffer (PBS, 0.2% sodium azide). An equal volume of 2% agarose (low melt, Mb grade) melted in PBS was equilibrated at 55°C and added to cells. The 90 μL slurry was solidified in plug molds for 15 minutes at 4°C. Agarose plugs were then injected into digestion buffer (1 mg/mL proteinase K, 1% N-Lauroylsarcosine, 0.2% sodium deoxycholate, 100 mM EDTA, 10 mM Tris-HCl (pH 7.5)) and incubated overnight at 55°C. Plugs were washed for at least 3 x 1 hour each in 15 mL of wash buffer (10mM Tris-HCl, 1mM EDTA, 100 mM NaCl) before melting in round bottom tubes filled with 1 mL combing buffer (50 mM MES monohydrate, pH=5.6) at 68°C for 20 minutes. After melting, tubes were gently transferred to a 42°C heat block. After 10 minutes, 1.5 μL β-agarase was added without mixing and incubated overnight at 42°C. The following morning, DNA was gently poured into disposable DNA reservoirs pre-filled with an additional 1.2 mL of combing buffer. DNA was combed onto silanized coverslips using the Molecular Combing System (Genomic Vision). Slides were dried for 2 hours at 65°C. Slides were denatured (0.5M NaOH, 1 M NaCl) for 8 minutes, followed by dehydration in 70%, 90% and 100% ethanol (5 minutes each). Slides were blocked for 1 hour in 5% FBS in PBS. Slides were incubated with primary antibodies overnight at 4°C or 2 hours at room temperature, washed and incubated with secondary antibodies for 1 hour at room temperature. Slides were mounted with Fluoromount-G®. Fibers were imaged, stitched, and measured. See Table 6.11 for list of antibodies.

6.1.12 RNA sequencing and analysis

Total messenger RNA was extracted using RNeasy Plus Mini Kit. RNA was DNase treated prior to submission to Rockefeller University's genomic core where it was prepped for sequencing. Libraries for intron retention were prepared using rRNA depletion and run on NextSeq 500 High Output for 75 base pair paired end reads. Libraries for transcript analysis were prepared using standard Illumina sequencing primers and run on NextSeq 500 High Output for 75 base pair single reads. For intron retention analysis, raw reads were aligned to the mouse genome (mm10) with Stand NGS's software. Percentage of reads mapping to introns was from determined post-alignment statistics. For mRNA transcript analysis, raw reads were aligned to the mouse genome and analyzed by Tom Carroll at Rockefeller University's Bioinformatics core using the NGSpipeR package. Differential expression was determined with DESeq2.

6.1.13 Isolation of proteins on nascent DNA (iPOND)

Exponentially growing cells were pulsed with EdU for differential times to yield similar labeled lengths of nascent DNA. iPOND was performed as previously described (Dungrawala and Cortez, 2015). Lysates were incubated with streptavidin-coupled magnetic beads overnight at 4°C on the nutator. Eluate was run 1 cm into a 4%–12% Bis-Tris gel and submitted for LC-MS analysis at Rockefeller University's Proteomics Core.

6.1.14 Co-immunoprecipitations

Endogenous co-immunoprecipitations were performed on HEK 293Ts seeded the previous day at a concentration of $10 \times 10^6 – 20 \times 10^6$ cells per 15 cm. One 15 cm dish was collected for each sample. Cells were treated one hour prior to collection with 2 µM MG-132. Cells were then washed 1x with cold PBS and scraped into 50 mL conicals. Cells were spun at 500xg for 5 min. Cells were subsequently washed twice with cold PBS. Cells were lysed in 1 mL of cold lysis buffer (50 mM HEPES (pH=7.5), 150 mM NaCl, 2 mM MgCl2, 0.1% Tween 20, 1x Phosphatase inhibitor cocktail II, 1x protease inhibitor cocktail, 2 mg/mL N-ethylmaleimide). Cells were sonicated on ice three times at 15A for 15 seconds. 1 µL of benzonase was added to samples prior to sonication. Lysates were spun at 28,000xg for 15 minutes. 50 µL of supernatant was reserved for input. Remaining supernatant was incubated with antibodies and Protein A-coupled magnetic beads (6 µg of antibody: 10 µL of Protein A beads) per sample. Normal mouse or rabbit IgG was used for antibody controls. Lysates were incubated at 4°C for 2 hours on nutator and then washed three times in 1 mL lysis buffer (5 minutes each on nutator). Beads were then boiled for 5 minutes in 25 µL Laemmli and run on 4-12% Bis-Tris SDS-PAGE gel. Membranes were subject to standard immunoblotting detection methods described in section 6.1.8.

GFP co-immunoprecipitations were performed on endogenously tagged HEK 293Ts seeded the previous day at a concentration of $10 \times 10^6 – 20 \times 10^6$ cells per 15 cm. Five 15 cm dishes were collected per sample. Lysates were prepared as above, and

supernatants were incubated with GFP-rabbit antibody coupled M270 epoxy beads for 2 hours at 4°C. GFP co-immunoprecipitations were performed on HEK 293Ts over-expressed either GFP-EV or GFP-hRTF2 cDNAs seeded the previous day at a concentration of 10 x 10^6 – 20 x 10^6 cells per 15 cm. Five 15 cm dishes were collected per sample. Chromatin extracts were isolated as previously described (Mendez and Stillman, 2000)and supernatants were incubated with GFP-nanobody coupled M270 epoxy beads for 2 hours at 4°C. anti-GFP (rabbit) antibodies or anti-GFP nanobodies were coupled to M270 epoxy beads according to manufacturer's protocol. See Table 6.11 for list of antibodies.

6.1.15 Protein biochemistry

hRTF2 was cloned into expression constructs pSKA002 (HIS14-eGFP-Protease 3 site), pSKA004 (HIS14-Protease 3 site), pSKA008 (HIS14-SUMO) (Gift from Sebastian Klinge) using classical cloning techniques (BamHI and NotI hRTF2 primers were used as in section 6.1.7). These constructs were transformed in B21 (DE3)-Codon Plus-RIL chemically competent cells. Colonies containing expression vector were grown overnight in 10 mL culture with chloramphenicol (25 µg/ml) and kanamycin (50 µg/ml). Using 10 mL start culture, 1 L of LB (no antibiotics) was inoculated and grown to an OD600 = 1. Culture was then induced with 1 mM IPTG and grow overnight at 20°C. Culture was collected, spun and resuspend in 15 mL lysis Buffer (250 mM NaCl, 10 mM imidazole, 100 mM KCl, 10% glycerol, 0.5% Triton-X100, 1 mg/mL Lysozyme, 0.2 mM PMSF). Lysate was sonicated with macro-tip at 15 A for 30 seconds (3x). Supernatant was incubated with His-binding resin for 30 minutes before transferring to column. Column was washed twice with 6 column volumes and once with 3 column volumes (wash buffer: 50 mM sodium phosphate buffer (pH=8), 250 mM NaCl, 30 mM imidazole). Column was eluted with three times with 1 column volume. (elution buffer: 50 mM Sodium phosphate buffer (pH=8), 250 mM NaCl, 250 mM imidazole). Sample of eluate was run on gel and stained with Coomassie to determine protein containing fractions. Eluates were dialyzed overnight at 4°C (50 mM sodium phosphate buffer (pH=7.4), 250 mM NaCl) to remove imidazole. Eluates were then digested with Ulp1 overnight at 4°C and size excluded on the Äkta pure system with Hiload 16/60 Superdex 75 column. Additional clean-up was performed by running sample over the His-binding resin. Purified RTF2 was filtered through 0.22 µm filter to sterilize prior to freezing with 10% glycerol. See Table 6.10 for a list of plasmids.

To assess purified RTF2 interaction with the MCM2-7 complex, hRTF2 and the hMCM2-7 complex (where MCM5 is FLAG tagged) were incubated together at 4°C for 2 hours in mixing buffer (20 mM HEPES, pH=7.5, 1 mM DTT, 0.01% NP-40, 5% glycerol, 0.1 mg/mL BSA, 1x cOmplete protease inhibitor, 50 mM NaCl; 50uL total reaction). Benzonase can be added at final concentration of 1 uL per 1 mL of mixing buffer. After mixing, additional 1uL of 5M NaCl was added to each reaction to increase final NaCl concentration to 150 mM. 2 uL of FLAG M2 magentic beads were added to each reaction and incubated 4°C for 1 hour. After one hour, beads were washed with 1 mL wash buffer (20 mM HEPES, pH=7.5, 1 mM DTT, 0.01% NP-40, 5% glycerol, 1x cOmplete protease

inhibitor, 150 mM NaCl) for 5 minutes. Washes were repeated four times before proteins were eluted in 20uL Laemmli buffer at 100°C for 5 minutes. Lysates were subjected to standard immunoblotting techniques descried in 6.1.8.

6.1.16 siRNA transfections

Cells were transfected with pools of 3 siRNAs against DDI1 as previously published (Kottemann et al., 2018). For PRIM1 and PRIMPOL, pools of 3 siRNAs were used. For RNASEH2 and RTF2 depletion, a single siRNA was used. Cells were transfected using Lipofectamine™ RNAiMAX Transfection Reagent according to manufacturer's instructions with the exception that siRNA-lipid complexes were added to the well and then cells were seeded on top of complexes. Knockdown was measured by RT-qPCR or western blot. See Table 6.9 for RNAi sequences.

6.1.17 Live cell imaging

Cells were infected with retrovirus carrying a GFP-H2B cDNA. Exponentially growing cells were infected with Cre, seeded in 35 mm glass bottom dishes and imaged every five minutes using Olympus CellVoyager.

6.1.18 Metaphase spreads

Cells were treated for 40 hours with aphidicolin. In the final 90 minutes of treatment, cells were co-incubated with colcemid (0.1 µg/mL). Cells were harvested and incubated in 5 mL 0.075 M KCL for 10 minutes before being fixed with the addition of 1 mL methanol and acetic acid (3:1). Cells were resuspend in 10 mL of methanol and acetic acid (3:1) overnight at 4°C. Cells were dropped onto wet slides and dried at 42°C for at least one hour before staining with 8% (v/v) KaryoMAX™ Giemsa in 1x Gurr buffer for three minutes, washing in 1x Gurr buffer for three minutes, washing in water for three minutes, and drying. Dry slides were then imaged on the Metasystems Metafer slide scanning platform.

6.1.19 Quantification and statistical analysis

Images were captured with default microscope software. All statistical analysis was completed using GraphPad Prism software. Image quantification was completed with FIJI software.

6.2 Key Resources

6.2.1 Mouse strains

Table 6.1. Mouse strains		
MOUSE STRAIN	**SOURCE**	**IDENTIFIER**
Rtf2$^{tm1a(KOMP)wtsi}$	This paper	
B6.Cg Tg(ACTFLPe)9205Dym/J	Jackson Laboratories	005703
B6.FVB/N-Tg(Ella-cre)C5379Lmgd/J	Jackson Laboratories	003314
C57BL/6J	Jackson Laboratories	000664

6.2.2 Mammalian cell lines

Table 6.2. Mammalian cell lines		
CELL LINE	**SOURCE**	**IDENTIFIER**
Human: HEK 293T	ATCC	
Human: HEK 293T endogenously GFP-tagged RTF2	This paper	N/A
Human: BJ-hTERT-E6/7, male	Smogorzewska Lab	
Human: U2OS, female	ATCC	HTB-96
Human: RPE *p53$^{-/-}$, pRb$^{-/-}$,* PRIM1-AID-mClover	de Lange Lab	
Human: HeLa (HeLa Parental, HeLa WT Clone, HeLa RNASEH2A KO Clone), female	Durocher and Jackson Labs	
Human: HCT-116 *p53$^{-/-}$* (HCT-116 *p53$^{-/-}$* WT Clone, HCT-116 *p53$^{-/-}$* RNASEH2A KO Clone)		
Mouse: RTF2 MEFs (*Rtf2$^{+/+}$, Rtf2$^{+/lox}$, Rtf2$^{-/lox}$,* and *Rtf2$^{lox/lox}$*)	This paper	N/A
KOMP mES cells Rtf2$^{tm1a(KOMP)wtsi}$	KOMP	MGI code: 1913654

6.2.3 Oligonucleotides

Table 6.3. mESC long range genotyping primers		
Oligonucleotide	**VENDOR**	**IDENTIFIER**
mESCs Cassette 3' Universal Forward cacacctccccctgaacctgaaac	IDT	KOMP
mESCs Cassette 5' Universal Reverse ggtggtgtgggaaagggttcgaag	IDT	KOMP
mESCs Cassette GF3 gccgaagaaggtcgagaaggtcag	IDT	KOMP
mESCs Cassette GR3 cgaatctctccacctgctcaatccag	IDT	KOMP

Table 6.4. RTF2 mouse genotyping primers		
Oligonucleotide	**VENDOR**	**IDENTIFIER**
Genotyping_PCR1_Fwd gcctgtgagcttggcaggta	IDT	This Paper
Genotyping_PCR1_Rev aggggaagacctgactgtgt	IDT	This Paper
Genotyping_PCR2_Fwd gcctgtgagcttggcaggta	IDT	This Paper
Genotyping_PCR2_Rev agcctgagctctgtcacatt	IDT	This Paper
Genotyping_PCR3_Fwd gatattgctgaagagcttgg	IDT	This Paper
Genotyping_PCR3_Rev gaagttatctcgacgaagttc	IDT	This Paper

Table 6.5. RT-qPCR primers		
Oligonucleotide	**VENDOR**	**IDENTIFIER**
Mouse *Rtf2* RT-qPCR Forward gaagtgtgtcacacgtgtgg	IDT	This Paper
Mouse *Rtf2* RT-qPCR Reverse tttcttttccagcttggccc	IDT	This Paper
Human *RTF2* RT-qPCR Forward tgctgaagacaaggatggag	IDT	Kottemann et al
Human *RTF2* RT-qPCR Reverse tgaaacagactctgctgcct	IDT	Kottemann et al.
Mouse *Rnaseh2a* RT-qPCR Forward gcatctttgccaaggtggcc	IDT	This Paper
Mouse *Rnaseh2a* RT-qPCR Reverse ggtcttgggatcattgggat	IDT	This Paper
Human *RNASEH2A* RT-qPCR Forward gctgaaagtggcagactcaa	IDT	This Paper
Human *RNASEH2A* RT-qPCR Reverse caggttgtatttgacccgcc	IDT	This Paper
Human *RNASEH1* RT-qPCR Forward aggaatcggcgtttactggg	IDT	This Paper
Human *RNASEH1* RT-qPCR Reverse aggctgcatgaatttccgc	IDT	This Paper
Human *DDI1* RT-qPCR Forward tggaacacaacgtgctacct	IDT	Kottemann et al.
Human *DDI1* RT-qPCR Reverse atctgtctgggggctgtct	IDT	Kottemann et al.
Human *DDI2* RT-qPCR Forward cgatgtagtgtgtgtgtactgc	IDT	Kottemann et al.
Human *DDI2* RT-qPCR Reverse ccagtgaggtagattctttaccactt	IDT	Kottemann et al.
Human *GAPDH* RT-qPCR Forward ggtcggagtcaacggattt	IDT	This Paper
Human *GAPDH* RT-qPCR Reverse gccccacttgattttggag	IDT	This Paper
Mouse β-actin RT-qPCR Forward ctaaggccaaccgtgaaaag	IDT	Thongthip et al.
Mouse β-actin RT-qPCR Reverse accagaggcatacagggaca	IDT	Thongthip et al.
Human *PRIM1* Forward RT-qPCR gacagagcattgaaggagga	IDT	This Paper
Human *PRIM1* Reverse RT-qPCR cgtcttgaccacccttttaca	IDT	This Paper
Human *PRIMPOL* Forward RT-qPCR ggcacttcagtagaaaccat	IDT	This Paper
Human *PRIMPOL* Reverse RT-qPCR cgccgaattcctcctttaat	IDT	This Paper

Table 6.6. Gateway cloning primers		
Oligonucleotide	**VENDOR**	**IDENTIFIER**
attB human RNASEH2A Forward ggggacaagtttgtacaaaaaagcaggcttcatggatctcagcgagctgga	IDT	This Paper
attB human RNASEH2A Reverse ggggaccactttgtacaagaaagctgggtctagaggctggttgctgact	IDT	This Paper
attB mouse RTF2 Forward ggggacaagtttgtacaaaaaagcaggcttcatgggttgcgacggaggcac	IDT	This Paper
attB mouse RTF2 Reverse ggggaccactttgtacaagaaagctgggttcagaagcagtaggatgtgt	IDT	This Paper
attB human PRIM1 Forward ggggacaagtttgtacaaaaaagcaggcttcatggagacgtttgacccccac	IDT	This Paper
attB human PRIM1 Reverse ggggaccactttgtacaagaaagctgggtttatttctcaaggaaaattt	IDT	This Paper

Table 6.7. Mutagenesis primers		
Oligonucleotide	**VENDOR**	**IDENTIFIER**
Mouse_RTF2_C121A_Mutagenesis agcgcggttcatcgcccctgtggtgggc	IDT	This Paper
Mouse_RTF2_C160A_Mutagenesis tggaaggcagccccagccgtgtgacacacttc	IDT	This Paper
Mouse_RTF_C140,142A_Mutagenesis gttttgcttcctccgatgcgccggtgctgtgttttctgaacgcgcc	IDT	This Paper
Mouse_RTF2_C157A_Mutagenesis gagataaaagctgaagtggctcacacgtgtggggctgc	IDT	This Paper
Mouse_RTF2_C140A_Mutagenesis gttttgcttcctccgatgc**gcc**ggttgtgtgttttctgaa	IDT	This Paper

Table 6.8. CRISPR cloning primers		
Oligonucleotide	**VENDOR**	**IDENTIFIER**
RTF2 5'BamHI aaaaggatcccatgggttgcgacggggga	IDT	This Paper
RTF2 3'NotI aaaagcggccgctcagaagcagtaggacgtgtgg	IDT	This Paper
hRTF 5' UTR Fwd INFUSION accatgattacgccaagcttactcttggaacgggcatggc	IDT	This Paper
hRTF 5' UTR Rev INFUSION tcctcgcccttgctcaccatcgcaggacgggagtcagagc	IDT	This Paper
GFP Fwd INFUSION atggtgagcaagggcgagga	IDT	This Paper
hRTF rev INF gagcggtggcagtgcgggcttcagaagcagtaggacgtgt	IDT	This Paper
hRTF 3' UTR Fwd INF agcccgcactgccaccgctc	IDT	This Paper
hRTF 3' UTR Rev INF aacgacggccagtgaattctaacttataggcagataaaat	IDT	This Paper

Table 6.9. siRNAs and shRNAs		
Oligonucleotide	**VENDOR**	**IDENTIFIER**
Luciferase siRNA	Thermo Fischer	12935146
hRNASEH1 siRNA 1 gggaaagaggugaucaacatt	Ambion	s48356
hRNASEH1 siRNA 2 cagacaguauguuuacgautt	Ambion	s48357
hRNASEH1 siRNA 3 cgggauuuauaggcaauatt	Ambion	s48358
hRNASEH2A siRNA 1 caaugaucccaagacaaatt	Ambion	s20656
hRNASEH2A siRNA 2 ccaccgauauuuccuggaatt	Ambion	s20657
hRTF2 siRNA 1 caaagaugccgucauugaatt	Ambion	s226737
hPrim1 siRNA 1 gaaccagagauuauaagaatt	Ambion	s11050
hPrim1 siRNA 2 caucgucucuggguauauutt	Ambion	s11051
hPrim1 siRNA 3 caacuacgguggagugauatt	Ambion	s10052
hPrimpol siRNA 1 ggcuauugauagaguuaaatt	Ambion	s11053
hPrimpol siRNA 2 ccacgaagaagagaucauatt	Ambion	s11054
hPrimpol siRNA 3 ggaucuccuucgauuuagatt	Ambion	s11055
hDDI1 siRNA1 ccggagacaucaauguuccaucgat	ThermoFisher	HSS181016
hDDI1 siRNA 2 ggaaauuacacauucagucauggat	ThermoFisher	HSS140552
hDDI1 siRNA 3 ccggagacaucaauguuccaucgat	ThermoFisher	HSS140553
hDDI2 shRNA uggaaaucgauacagcuca	Open Biosystems	V3LHS_328065
mRNASEH2A shRNA #1 ccgggctcgattacaacagcactttctcgagaaagtgctgttgtaatcgagctttttg	MilliporeSigma	TRC0000119585
mRNASEH2A shRNA #2 ccggcgggtcgttgtcgtctgagttctcgagaactcagacgacaacgacccgtttttg	MilliporeSigma	TRC0000119584

6.2.4 Plasmids

Table 6.10. Plasmids

Plasmids	**VENDOR**	**IDENTIFIER**
Gateway Entry Vectors		
pDONOR233; spectinomycin resistant; Gateway	Smogorzewska Lab	Smogorzewska Lab
pENTR-EV; spectinomycin resistant; Gateway	Smogorzewska Lab	Smogorzewska Lab
pENTR-HA-FLAG-mRTF2; spectinomycin resistant; Gateway	This paper	This paper
pENTR-HA-FLAG-mRTF2_C121A; spectinomycin resistant; Gateway	This paper	This paper
pENTR-HA-FLAG-mRTF2_C140A; spectinomycin resistant; Gateway	This paper	This paper
pENTR-HA-FLAG-mRTF2_C142A; spectinomycin resistant; Gateway	This paper	This paper
pENTR-HA-FLAG-mRTF2_C160A; spectinomycin resistant; Gateway	This paper	This paper
pENTR-HA-FLAG-mRTF2_C140A_C142A; spectinomycin resistant; Gateway	This paper	This paper
pENTR-HA-FLAG-mRTF2_C121A_C160A; spectinomycin resistant; Gateway	This paper	This paper
pENTR-HA-FLAG-mRTF2_ C121A_ C140A_C142A; spectinomycin resistant; Gateway	This paper	This paper
pENTR-HA-FLAG-mRTF2_ C121A_ C140A_C142A_C157A; spectinomycin resistant; Gateway	This paper	This paper
pENTR-HA-FLAG-mRTF2_ C121A_C140A_C142A_C157A_C160A; spectinomycin resistant; Gateway	This paper	This paper
pENTR-HA-FLAG-mRTF2_ C121A_C140A_C142A_C160A; spectinomycin resistant; Gateway	This paper	This paper
pENTR-RNASEH2A; spectinmycin resistant; Gateway	This paper	This paper
pENTR-hPRIM; spectinmycin resistant; Gateway	This paper	This paper

Retroviral expression vectors		
PEA59-EV-dest (destination vector); chloramphenicol and ampicillin resistant; Gateway	Smogorzewska Lab	Smogorzewska Lab
PEA59-EV-puro; ampicillin resistant; retroviral; Gateway	Smogorzewska Lab	Smogorzewska Lab
PEA59-HA-FLAG-mRTF2-puro; retroviral; ampicillin resistant; Gateway	This paper	This paper
PEA59-HA-FLAG-mRTF2_C121A-puro; retroviral; ampicillin resistant; Gateway	This paper	This paper
PEA59-HA-FLAG-mRTF2_C140A-puro; ampicillin resistant; retroviral; Gateway	This paper	This paper
PEA59-HA-FLAG-mRTF2_C142A-puro; ampicillin resistant; retroviral; Gateway	This paper	This paper
PEA59-HA-FLAG-mRTF2_C160A-puro; ampicillin resistant; retroviral; Gateway	This paper	This paper
PEA59-HA-FLAG-mRTF2_C140A_C142A-puro; ampicillin resistant; retroviral; Gateway	This paper	This paper
PEA59-HA-FLAG-mRTF2_C121A_C160A-puro; ampicillin resistant; retroviral; Gateway	This paper	This paper
PEA59-HA-FLAG-mRTF2_ C121A_ C140A_C142A-puro; ampicillin resistant; retroviral; Gateway	This paper	This paper
PEA59-HA-FLAG-mRTF2_ C121A_ C140A_C142A_C157A-puro; ampicillin resistant; retroviral; Gateway	This paper	This paper
PEA59-HA-FLAG-mRTF2_ C121A_C140A_C142A_C157A_C160A-puro; ampicillin resistant; retroviral; Gateway	This paper	This paper
PEA59-HA-FLAG-mRTF2_ C121A_C140A_C142A_C160A-puro; ampicillin resistant; retroviral; Gateway	This paper	This paper
pMSCVpuro-DEST (destination vector); chloramphenicol and ampicillin resistant; Gateway	Addgene	Plasmid# 119745
pMSCVpuro -EV	This Paper	This Paper
pMSCVpuro -RNASEH2A	This Paper	This Paper
MSCV_PM_shRNA_Control_puro	Smogorzewska Lab	Smogorzewska Lab
MSCV_PM_shRNA_shDDI2_puro	Smogorzewska Lab	Smogorzewska Lab
MSCV-GFP-H2B-hygro	Smogorzewska Lab	Smogorzewska Lab

pMMP Hit & Run Cre; retroviral; self-excising	Smogorzewska Lab	NA
pWZL Cre-hygro; retroviral	Smogorzewska Lab	NA
Lentiviral expression vectors		
CMV-HA-FLAG-Dest; destination vector; chloramphenicol and ampicillin resistant; Gateway	Smogorzewska Lab	Smogorzewska Lab
CMV-HA-FLAG-hPRIM1-puro; lentiviral; ampicillin resistant; Gateway	This paper	This paper
CMV-EV-puro; lentiviral; ampicillin resistant; Gateway	This paper	This paper
pLKO.1 shRNASEH2A #1_puro; ampicillin resistant	MilliporeSigma	SHCLNG-NM_027187, TRC0000119585
pLKO.1 shRNASEH2A #2_puro; ampicillin resistant	MilliporeSigma	SHCLNG-NM_027187, TRC0000119584
pLKO.1 shRNA Control Plasmid puro; ampicillin resistant;	MilliporeSigma	SHC002
CRISPR generation of GFP-AID-RTF2 HEK 293Ts		
pcDNA5-FRT-TO-EGFP-AID	Addgene	Plasmid #80075
MLM3636	Addgene	Plasmid #43860
MLM3636 5' UTR_1 sequence acgctaggcgcggcgtagcg	This Paper	This Paper
px330	Addgene	Plasmid # 42230
px330 3'UTR_1 atgtgaggcgtgtcggttcc	This Paper	This Paper
pUC19-5UTR-GFP-AID-hRTF2-3UTR Homology Donor Construct	This Paper	This Paper
Protein Biochemistry		
PSKA002 HIS14-SUMO-MCS Expression Vector	Klinger Lab	Klinger Lab
PSKA002 HIS14-SUMO-RTF2	This paper	This paper
PSKA008 HIS14-GFP-MCS-Expression Vector	Klinger Lab	Klinger Lab
PSKA008 HIS14-GFP-RTF2	This paper	This paper
Packaging Constructs		

VSV-G; retroviral packaging	Smogorzewska Lab	Smogorzewska Lab
Gagpol; retroviral packaging	Smogorzewska Lab	Smogorzewska Lab
pMD2.G (VSV-G envelope expressing plasmid); lentiviral packaging	Addgene	#12259
psPAX2; lentiviral packaging	Addgene	#12260

6.2.5 Antibodies

Table 6.11. Antibodies

ANTIBODY	SOURCE	IDENTIFIER
Primary Antibodies		
Mouse IgG	Santa Cruz	Cat# sc-2025, RRID:AB_737182
Mouse monoclonal anti-α-tubulin (clone DM1A), WB:1:5000	MilliporeSigma	Cat# T9026, RRID:AB_477593
Mouse monoclonal anti-γH2AX Ser139 (clone JBW301), IF 1:2000	MilliporeSigma	Cat# 05-636, RRID:AB_309864
Mouse monoclonal anti-biotin, IF: 1:2000	Jackson ImmunoResearch	Cat# 200-002-211, RRID:AB_2339006
Mouse monoclonal anti-BrdU (B44), combing: 1:10	BD Biosciences	Cat# 347580, RRID:AB_400326
Mouse monoclonal anti-CHK1, WB:1:1000	MilliporeSigma	Cat # C9358, RRID:AB_259159
Mouse monoclonal anti-Poly (ADP-Ribose) Polymer antibody [10H], WB:1:100	Abcam	Cat # ab14459, RRID:AB_301239
Mouse monoclonal anti-PCNA (PC10), WB: 1:1000,	Santa Cruz	Cat# sc-56, RRID:AB_628110
Mouse monoclonal anti-RNASEH2A, WB:1:500	Santa Cruz	Cat# sc-515475
Mouse monoclonal anti-RTF2 (clone OTI1E8), WB: 1:1000	LS Bio	Cat# LS-C340588
Mouse Monoclonal anti-vinculin, Unconjugated, Clone hVIN-1	MilliporeSigma	Cat# V9131, RRID:AB_477629
Mouse monoclonal anti-WAPL (A-7), WB: 1:500	Santa Cruz	Cat# sc-365189, RRID:AB_10708870
Rabbit IgG	Santa Cruz	Cat# sc-2027, RRID:AB_737197
Rat monoclonal anti-BrdU [BU1/75 (ICR1)], combing: 1:20	Abcam	Cat# ab6326, RRID:AB_305426
Rabbit monoclonal anti-MCM7 (D10A11) XP, WB: 1:1000	Cell Signaling	Cat# 3735S, RRID:AB_2142705
Rabbit polyclonal anti-c20orf43 (RTF2), WB: 1:500	Novus	Cat# NBP2-30645
Rabbit polyclonal anti-GFP	Smogorzewska Lab	Kotteman et al.
Rabbit polyclonal anti-GFP	Abcam	Cat# ab290 RRIDL AB_303395

Rabbit polyclonal anti-RNASEH2A	Abcam	Cat# ab83943, RRID:AB_1861175
Rabbit polyclonal anti-RNASEH2C	AbClonal	Cat# A13884, RRID:AB_2760737
Rabbit polyclonal anti-phospho-CHK1 (S345), WB:1:1000	Cell Signaling Technology	Cat# 2341, RRID:AB_330023
Rabbit polyclonal anti-phospho-RPA32 (S4/8), WB:1:1000	Bethyl	Cat# A300-245A, RRID:AB_210547
Rabbit polyclonal anti-PRIM1	Proteintech	Cat # 10773-1-AP RRID:AB_2237549
Rabbit polyclonal anti-RPA32, WB 1:2000	Bethyl	Cat# A300-244A, RRID:AB_185548
Secondary Antibodies		
Goat Anti-Mouse IgG H&L Cross-Absorbed (Alexa Fluor® 488), IF:1:1000, combing:1:100	ThermoFisher	Cat# A-11029, RRID:AB_2534088
Goat Anti-Mouse IgG H&L Cross-Absorbed (Alexa Fluor® 647), combing:1:100	ThermoFisher	Cat# A-21235, RRID:AB_2535804
Goat Anti-Rabbit IgG H&L (Alexa Fluor® 488)	ThermoFisher	Cat# A-11008, RRID:AB_143165
Goat Anti-Rat IgG H&L Cross-Absorbed (Alexa Fluor® 594), IF:1:1000, combing:1:100	ThermoFisher	Cat# A-11007, RRID:AB_10561522
Peroxidase-AffiniPure Goat Anti-Mouse IgG (H + L) antibody, WB:1:2000	Jackson ImmunoResearch Labs	Cat# 115-035-003, RRID:AB_10015289
Peroxidase-AffiniPure Goat Anti-Rabbit IgG (H + L) antibody, WB:1:2000	Jackson ImmunoResearch Labs	Cat# 115-035-144,

6.2.6 Reagents

Table 6.12. Reagents

REAGENT/KIT	SOURCE	IDENTIFIER
General Chemicals		
2-mercaptoethanol	MilliporeSigma	Cat# M3148
2-propanol	ThermoFisher	Cat# A416
3-Indoleacetic acid	MilliporeSigma	Cat# I3750-5G-A
5'-cholor-2'-deoxyuridine (CldU)	MilliporeSigma	Cat# C6891
5-ethynyl-2'-deoxyuridine (EdU)	ThermoFisher	Cat# A10044
5'-iodo-2'-deoxyuridine (IdU)	MilliporeSigma	Cat# I7125
Acetic Acid	ThermoFisher	Cat# A38
Acteone	ThermoFisher	Cat# A18
Agar, Bacto	VWR	Cat# 90000-762
Agarose, Low melt	Bio-Rad	Cat# 1613111
Agarose, SeaKem® LE	Lonza	Cat# 50004
Ammonium hydroxide	ThermoFisher	Cat# 15633520
Ampicillin	MilliporeSigma	Cat# A9518
Aphidicolin	MilliporeSigma	Cat# A0781
Blasticidin S HCl	ThermoFisher	Cat# R21001
Boric Acid	ThermoFisher	Cat# A73500
Bovine serum albumin	MilliporeSigma	Cat# A3059
Bromophenol Blue	Sigma	Cat# B8026
Chlorampenicol	MilliporeSigma	Cat# C0378
Chloroform	ThermoFisher	Cat# C298
Colcemid	MilliporeSigma	Cat# 234109
cOmplete™, EDTA-free Protease Inhibitor Cocktail	MilliporeSigma	Cat# 11873580001
DMSO	MilliporeSigma	Cat# D2650
EDTA	MilliporeSigma	Cat# E5134
EGTA	ThermoFisher	Cat# O2783
Ethanol, 200 proof, molecular grade	ThermoFisher	Cat# 22-032-601
Formaldehyde	ThermoFisher	Cat# F1635
Formamide	ThermoFisher	Cat# BP228100
FxCycle™ Violet Stain	ThermoFisher	Cat# F10347
Geneticin (Neomycin)	ThermoFisher	Cat# 10131035
Glycerol	ThermoFisher	Cat# G33500
H2O, molecular grade	VWR	Cat# 71002-726
HEPES	MilliporeSigma	Cat# H3375
Heptane	MilliporeSigma	Cat# 246654
Hydrochloric acid	ThermoFisher	Cat# A144S
Hydroxyurea	MilliporeSigma	Cat# H8627
Hygromycin B	ThermoFisher	Cat# 10687-010

Imidazole	MilliporeSigma	Cat# I5513
IPTG	MilliporeSigma	Cat# I6758
Kanamycin	MilliporeSigma	Cat# K1876
MES monohydrate	MilliporeSigma	Cat# 69889
Methanol	ThermoFisher	Cat# A412
Mitomycin C	MilliporeSigma	Cat# M4287
MG-132	MilliporeSigma	Cat#474790
MgCl2	MilliporeSigma	Cat# M2670
N-ethylmaleimide	MilliporeSigma	Cat# E3876
N-Lauroylsarcosine sodium salt	MilliporeSigma	Cat# 61745
Phenol:Chloroform:Isoamylalcohol (25:24:1)	MilliporeSigma	Cat# P2069
Phosphatase Inhibitor Cocktail I	MilliporeSigma	Cat# 524624
Phosphatase Inhibitor Cocktail II	MilliporeSigma	Cat# 524625
PIPES	MilliporeSigma	Cat# P6757
PMSF	MilliporeSigma	Cat# 10837091001
Polybrene (Hexadimethrine bromide)	MilliporeSigma	Cat# 28728-55-4
Potassium Chloride	ThermoFisher	Cat# P2173
Proteinase K	MilliporeSigma	Cat# 3115879001
Puromycin Dihydrochloride	MilliporeSigma	Cat# P8833
Spectinomycin	MilliporeSigma	Cat# S9007
Sodium Acetate	ThermoFisher	Cat# S209500
Sodium Azide	MilliporeSigma	Cat# S2002
Sodium Chloride	ThermoFisher	Cat# S271
Sodium Deoxycholate	MilliporeSigma	Cat# D6750
Sodium dodecyl sulfate	MilliporeSigma	Cat# L4390
Sodium hydroxide	ThermoFisher	Cat# S318500
Sodium Phosphate Dibasic Heptahydrate	ThermoFisher	Cat# BP331500
Sodium Phosphate Monobasic Monohydrate	ThermoFisher	Cat# S369
Sucrose	ThermoFisher	Cat# S53
Tris Base	ThermoFisher	Cat# BP152
Triton X-100	MilliporeSigma	Cat# T8787
Trypsin	ThermoFisher	Cat# 25200-056
Tryptone	ThermoFisher	Cat# BP1421
Tween 20	ThermoFisher	Cat# BP337
Yeast Extract	ThermoFisher	Cat# BP1422
Enzymes		
BamHI	NEB	Cat# R3136
Beta-agarase	NEB	Cat# M0392
Benzonase	MilliporeSigma	Cat# E1014
DNase	ThermoFisher	EN0531
NotI	NEB	Cat# M0288

RNASEHII	NEB	Cat# M0288
ThermoPol® Reaction Buffer Pack	NEB	Cat# B9004
Genotyping (related to 6.1.1)		
1 Kb Plus DNA Ladder	ThermoFisher	Cat# 10787018
DirectPCR Lysis Reagent (Mouse Tail)	Viagen Biotech	Cat #102-T
GoTaq® DNA polymerase master mix	Promega	Cat# M7833
Mammalian cell culture (related to 6.1.2)		
DMEM	ThermoFisher	Cat# 11965-092
DMEM/F12	ThermoFisher	Cat# 11330-032
Fetal Bovine Serum (FBS)	R&D Systems	Cat# S11150
GlutaMAX™	ThermoFisher	Cat# 35050061
McCoy's 5A	ThermoFisher	Cat# 16600082
MEM non-essential AA 100X)	ThermoFisher	Cat# 11140076
Penicillin-streptomycin	ThermoFisher	Cat# 15140122
RNA preparation, reverse transcription and RT-qPCR (related to 6.1.4)		
RNeasy Plus Mini Kit	Qiagen	Cat# 74134
Platinum SYBR Green SuperMix-UDG	ThermoFisher	Cat# 11733046
SuperScript™ III First-Strand Synthesis	ThermoFisher	Cat# 18080051
Platinum SYBR Green SuperMix-UDG	ThermoFisher	Cat# 11733046
Plasmid generation and mutagenesis (related to 6.1.5)		
Chemically competent DH5-α *E. coli*	Smogorzewska Lab	
Chemically competent Stlb3 *E. coli*	Smogorzewska Lab	
BP Clonase II Enzyme Mix	ThermoFisher	Cat# 11789020
GenElute HP Plasmid DNA Maxiprep Kit	MilliporeSigma	Cat# NA0310
LR Clonase II Enzyme Mix	ThermoFisher	Cat# 11791100
Multi-Site Directed Mutagenesis Kit	Agilent	Cat# 200514
QIAprep Spin Miniprep Kit	Qiagen	Cat# 27106
PBS (10x)	ThermoFisher	Cat# 20012050
Transductions (related to 6.1.6)		
TransIT-293	MirusBio LLC	Cat# MIR2700
Generation of GFP-AID-RTF2 endogenously tagged HEK 293T (related to 6.1.7)		
In-Fusion® HD Cloning Plus	Clontech	Cat# 638917
Immunoblotting (related to 6.1.8)		

DC™ Protein Assay	Bio-Rad	Cat# 5000111
NuPAGE™ 4-12% Bis-Tris Midi Protein Gels, 20- or 26-well, w/adapators	ThermoFisher	Cat# WG1402A Cat# WG1403A
NuPAGE™ 4-12% Bis-Tris Mini Protein Gels, 10-well	ThermoFisher	Cat# NP0321
NuPAGE™ MOPS SDS Running Buffer (20X)	ThermoFisher	Cat# NP0001
NuPAGE™ Transfer Buffer	ThermoFisher	Cat# NP0006
Western Lighting Plus-ECL, Enhanced Chemiluminescence Substrate	PerkinElmer	Cat# NEL104001
Immunofluorescence (related to 6.1.9)		
Biotin azide	ThermoFisher	Cat# B10184
(+)-sodium L-ascorbate	MilliporeSigma	Cat# A7631
Click-iT™ EdU Alexa Fluor™ 488 Imaging Kit	ThermoFisher	Cat# C10337
Copper (II) sulfate pentahydrate	ThermoFisher	Cat# C489
DAPI Fluoromount-G®	SouthernBiotech	Cat# 0100-20
DuoLink® In Situ PLA Anti-mouse MINUS probe	MilliporeSigma	Cat# DUO92004
DuoLink ®In Situ PLA Anti-rabbit PLUS probe	MilliporeSigma	Cat# DUO92002
DuoLink® In Situ Detection Reagents Orange	MilliporeSigma	Cat# DUO92007
DuoLink® In Situ Wash Buffers	MilliporeSigma	Cat# DUO82049
Micro Cover Glasses, Round, No. 1.5 12 mm	ThermoFisher	Cat# 1254581
Flow cytometry (related to 6.1.10)		
Click-iT™ EdU Alexa Fluor™ 647 Flow Cytomtery Kit	ThermoFisher	Cat# C10419
DNA Combing (related to 6.1.11)		
Combicoverslips	GenomicVision	Cat# COV-002-RUO
Disposable Reservoirs	GenomicVision	Cat# RES-001
FiberPrep® (DNA Extraction Kit)	GenomicVision	Cat# EXTR-001
Fluoromount-G®	SouthernBiotech	Cat# 0100-01
Micro Cover Glasses, Square, No. 1.5, 22x22	ThermoFisher	Cat# 12-541-BP
Octenyltrichlorosilane, mixture of isomers	MilliporeSigma	Cat# 539279
Co-immunoprecipitations (related to 6.1.14)		

Dynabeads™ M-270 Epoxy	ThermoFisher	Cat# 14301
Dynabeads™ MyOne™ Streptavidin C1	ThermoFisher	Cat# 65001
Dynabeads™ Protein A	ThermoFisher	Cat# 10001D
Protein biochemistry (related to 6.1.15)		
Anti-FLAG® M2 Magnetic beads	MilliporeSigma	Cat# M8823
BL21-CodonPlus (DE3)-RIL Competent Cells	Aglient	Cat# 230240
HIS-Select® HF Nickel Affinity Gel	MilliporeSigma	Cat# H0537
InstantBlue	Expedeon	Cat# ISB1L
Laemmli 2x Concentrate	MilliporeSigma	Cat# S3401
Lysozyme	MilliporeSigma	Cat# L6876
siRNA transfections (related to 6.1.17)		
Lipofectamine RNAiMAX Transfection Reagent	ThermoFisher	Cat# 13778-150
Metaphase spreads (related to 6.1.18)		
Gurr Buffer Tablets	ThermoFisher	Cat# 10582013
KaryoMAX™ Giemsa Stain Solution	ThermoFisher	Cat# 10092013

6.2.7 Equipment

Table 6.13. Equipment		
EQUIPMENT	**SOURCE**	**IDENTIFIER**
General Lab Equipment		
Nanodrop 2000c Spectrophotometer	ThermoFisher, Smogorzewska Lab	ND-2000C
PowerPac™ Basic Power Supply	Bio-Rad, Smogorzewska Lab	Cat# 1645050
Thermocycler	Bio-Rad, Smogorzewska Lab	C1000
Wide Mini ReadySub-Cell GT Cell	Bio-Rad, Smogorzewska Lab	Cat# 1704489
Mammalian cell culture/ Growth and sensitivity assays (related to 6.1.2 and 6.1.3)		
Z2™ Coulter Counter® Analyzer	Beckman Coulter, Smogorzewska Lab	Cat# 6605700
RNA preparation, reverse transcription and RT-qPCR (related to 6.1.4)		
Applied Biosystems™ QuantStudio™ 12K Flex	ThermoFisher, Rockefeller Genomics Resource Center	Cat# 4471087
Immunoblotting (related to 6.1.8)		
Azure c300 Chemiluminescent Western Blot Imaging System	Azure Biosystems, Smogorzewska Lab	Cat# c300
Criterion™ Vertical Electrophoresis Cell	Bio-Rad, Smogorzewska Lab	Cat# 1656001
ImageQuantLAS 4000	GE Healthcare Life Science, Nussenzweig Lab	Cat# 28955810
XCell SureLock™ Mini-Cell	ThermoFisher, Smogorzewska Lab	Cat#EI0001
Immunofluorescence (related to 6.1.9)		
Axio Observer.A1 fluorescence microscope, equipped with a Pan-Apochromat 63X NA-1.4 oil objective and Axio CCD camera	Carl Zeiss, Smogorzewska Lab	NA

Flow cytometry (related to 6.1.10)		
BD Accuri™ C6	Becton Dickinson, Rockefeller Flow Cytometry Resource Center	NA
BD FACSAria™ II	Becton Dickinson, Rockefeller Flow Cytometry Resource Center	NA
BD™ LSR II	Becton Dickinson, Rockefeller Flow Cytometry Resource Center	NA
DNA Combing (related to 6.1.11)		
Branson 2800 liquid sonicator	ThermoFisher, Smogorzewska Lab	Cat# 15-336-126
FiberComb® (Molecular Combing System)	GenomicVision, Smogorzewska Lab	Cat# MCS-001
Gatan Model 950 Advanced Plasma System	Gatan, Rockefeller Cyro-EM Resource Center	
Inverted Olympus IX-71 DeltaVision Image Restoration Microscope, equipped with 60x oil objective and pco.edge sCOS camera	Applied Precision, Rockefeller Bioimaging Resource Center	NA
RNA sequencing (related to 6.1.12)		
NextSeq 500	Illumina, Rockefeller Genomics Resource Center	NA
Protein Biochemistry (related to 6.1.15)		
Äkta pure system	GE LifeSciences, Klinge Lab	NA
HiLoad 16/60 Superdex 75	GE LifeSciences, Klinge Lab	NA
Live Cell Imaging (related to 6.1.17)		
Olympus CellVoyager CV1000	Olympus, Rockefeller Bioimaging Resource Center	NA

Metaphase Spreads (related to 6.1.18)		
Humidifier	Smogorzewska Lab	NA
Metafer Slide Scanning Platform	MetaSystem, Smogorzewska Lab	NA

Chapter 7: References

Ahn, J.S., Osman, F., and Whitby, M.C. (2005). Replication fork blockage by RTS1 at an ectopic site promotes recombination in fission yeast. The EMBO journal *24*, 2011-2023.

Aicardi, J., and Goutieres, F. (1984). A progressive familial encephalopathy in infancy with calcifications of the basal ganglia and chronic cerebrospinal fluid lymphocytosis. Annals of neurology *15*, 49-54.

Akerblom, L., Ehrenberg, A., Gräslund, A., Lankinen, H., Reichard, P., and Thelander, L. (1981). Overproduction of the free radical of ribonucleotide reductase in hydroxyurea-resistant mouse fibroblast 3T6 cells. Proceedings of the National Academy of Sciences of the United States of America *78*, 2159-2163.

Alabert, C., Bukowski-Wills, J.C., Lee, S.B., Kustatscher, G., Nakamura, K., de Lima Alves, F., Menard, P., Mejlvang, J., Rappsilber, J., and Groth, A. (2014). Nascent chromatin capture proteomics determines chromatin dynamics during DNA replication and identifies unknown fork components. Nature cell biology *16*, 281-293.

Ashley, A.K., Shrivastav, M., Nie, J., Amerin, C., Troksa, K., Glanzer, J.G., Liu, S., Opiyo, S.O., Dimitrova, D.D., Le, P.*, et al.* (2014). DNA-PK phosphorylation of RPA32 Ser4/Ser8 regulates replication stress checkpoint activation, fork restart, homologous recombination and mitotic catastrophe. DNA repair *21*, 131-139.

Ayyagari, R., Gomes, X.V., Gordenin, D.A., and Burgers, P.M.J. (2003). Okazaki fragment maturation in yeast. I. Distribution of functions between FEN1 AND DNA2. The Journal of biological chemistry *278*, 1618-1625.

Bae, S.-H., Bae, K.-H., Kim, J.-A., and Seo, Y.-S. (2001). RPA governs endonuclease switching during processing of Okazaki fragments in eukaryotes. Nature *412*, 456-461.

Bae, S.H., and Seo, Y.S. (2000). Characterization of the enzymatic properties of the yeast dna2 Helicase/endonuclease suggests a new model for Okazaki fragment processing. The Journal of biological chemistry *275*, 38022-38031.

Bai, L., Yuan, Z., Sun, J., Georgescu, R., O'Donnell, M.E., and Li, H. (2017). Architecture of the Saccharomyces cerevisiae Replisome. Advances in experimental medicine and biology *1042*, 207-228.

Bailey, R., Priego Moreno, S., and Gambus, A. (2015). Termination of DNA replication forks: "Breaking up is hard to do". Nucleus *6*, 187-196.

Balakrishnan, L., and Bambara, R.A. (2013). Okazaki fragment metabolism. Cold Spring Harbor perspectives in biology *5*.

Ballabeni, A., Melixetian, M., Zamponi, R., Masiero, L., Marinoni, F., and Helin, K. (2004). Human geminin promotes pre-RC formation and DNA replication by stabilizing CDT1 in mitosis. The EMBO journal *23*, 3122-3132.

Baranovskiy, A.G., Babayeva, N.D., Suwa, Y., Gu, J., Pavlov, Y.I., and Tahirov, T.H. (2014). Structural basis for inhibition of DNA replication by aphidicolin. Nucleic acids research *42*, 14013-14021.

Baranovskiy, A.G., Babayeva, N.D., Zhang, Y., Gu, J., Suwa, Y., Pavlov, Y.I., and Tahirov, T.H. (2016a). Mechanism of Concerted RNA-DNA Primer Synthesis by the Human Primosome. The Journal of biological chemistry *291*, 10006-10020.

Baranovskiy, A.G., and Tahirov, T.H. (2017). Elaborated Action of the Human Primosome. Genes *8*.

Baranovskiy, A.G., Zhang, Y., Suwa, Y., Gu, J., Babayeva, N.D., Pavlov, Y.I., and Tahirov, T.H. (2016b). Insight into the Human DNA Primase Interaction with Template-Primer. The Journal of biological chemistry *291*, 4793-4802.

Bartsch, K., Knittler, K., Borowski, C., Rudnik, S., Damme, M., Aden, K., Spehlmann, M.E., Frey, N., Saftig, P., Chalaris, A.*, et al.* (2017). Absence of RNase H2 triggers generation of immunogenic micronuclei removed by autophagy. Human molecular genetics *26*, 3960-3972.

Bass, T.E., and Cortez, D. (2019). Quantitative phosphoproteomics reveals mitotic function of the ATR activator ETAA1. The Journal of cell biology *218*, 1235-1249.

Bass, T.E., Luzwick, J.W., Kavanaugh, G., Carroll, C., Dungrawala, H., Glick, G.G., Feldkamp, M.D., Putney, R., Chazin, W.J., and Cortez, D. (2016). ETAA1 acts at stalled replication forks to maintain genome integrity. Nature cell biology *18*, 1185-1195.

Bell, S.P., and Dutta, A. (2002). DNA replication in eukaryotic cells. Annual review of biochemistry *71*, 333-374.

Bell, S.P., and Kaguni, J.M. (2013). Helicase loading at chromosomal origins of replication. Cold Spring Harbor perspectives in biology *5*.

Bell, S.P., and Stillman, B. (1992). ATP-dependent recognition of eukaryotic origins of DNA replication by a multiprotein complex. Nature *357*, 128-134.

Bergoglio, V., Ferrari, E., Hubscher, U., Cazaux, C., and Hoffmann, J.S. (2003). DNA polymerase beta can incorporate ribonucleotides during DNA synthesis of undamaged and CPD-damaged DNA. Journal of molecular biology *331*, 1017-1023.

Berti, M., Ray Chaudhuri, A., Thangavel, S., Gomathinayagam, S., Kenig, S., Vujanovic, M., Odreman, F., Glatter, T., Graziano, S., Mendoza-Maldonado, R.*, et al.* (2013). Human RECQ1 promotes restart of replication forks reversed by DNA topoisomerase I inhibition. Nature structural & molecular biology *20*, 347-354.

Berti, M., and Vindigni, A. (2016). Replication stress: getting back on track. Nature structural & molecular biology *23*, 103-109.

Bertolaet, B.L., Clarke, D.J., Wolff, M., Watson, M.H., Henze, M., Divita, G., and Reed, S.I. (2001). UBA domains of DNA damage-inducible proteins interact with ubiquitin. Nat Struct Biol *8*, 417-422.

Bétous, R., Couch, F.B., Mason, A.C., Eichman, B.F., Manosas, M., and Cortez, D. (2013). Substrate-selective repair and restart of replication forks by DNA translocases. Cell reports *3*, 1958-1969.

Bétous, R., Mason, A.C., Rambo, R.P., Bansbach, C.E., Badu-Nkansah, A., Sirbu, B.M., Eichman, B.F., and Cortez, D. (2012). SMARCAL1 catalyzes fork regression and Holliday junction migration to maintain genome stability during DNA replication. Genes & development *26*, 151-162.

Bhat, K.P., Krishnamoorthy, A., Dungrawala, H., Garcin, E.B., Modesti, M., and Cortez, D. (2018). RADX Modulates RAD51 Activity to Control Replication Fork Protection. Cell reports *24*, 538-545.

Bhowmick, R., Minocherhomji, S., and Hickson, I.D. (2016). RAD52 Facilitates Mitotic DNA Synthesis Following Replication Stress. Molecular cell *64*, 1117-1126.

Bianchi, J., Rudd, S.G., Jozwiakowski, S.K., Bailey, L.J., Soura, V., Taylor, E., Stevanovic, I., Green, A.J., Stracker, T.H., Lindsay, H.D.*, et al.* (2013). PrimPol bypasses UV photoproducts during eukaryotic chromosomal DNA replication. Molecular cell *52*, 566-573.

Bienko, M., Green, C.M., Crosetto, N., Rudolf, F., Zapart, G., Coull, B., Kannouche, P., Wider, G., Peter, M., Lehmann, A.R.*, et al.* (2005). Ubiquitin-binding domains in Y-family polymerases regulate translesion synthesis. Science (New York, NY) *310*, 1821-1824.

Bienko, M., Green, C.M., Sabbioneda, S., Crosetto, N., Matic, I., Hibbert, R.G., Begovic, T., Niimi, A., Mann, M., Lehmann, A.R.*, et al.* (2010). Regulation of translesion synthesis DNA polymerase eta by monoubiquitination. Molecular cell *37*, 396-407.

Biertümpfel, C., Zhao, Y., Kondo, Y., Ramón-Maiques, S., Gregory, M., Lee, J.Y., Masutani, C., Lehmann, A.R., Hanaoka, F., and Yang, W. (2010). Structure and mechanism of human DNA polymerase eta. Nature *465*, 1044-1048.

Blastyák, A., Hajdú, I., Unk, I., and Haracska, L. (2010). Role of double-stranded DNA translocase activity of human HLTF in replication of damaged DNA. Molecular and cellular biology *30*, 684-693.

Blastyák, A., Pintér, L., Unk, I., Prakash, L., Prakash, S., and Haracska, L. (2007). Yeast Rad5 protein required for postreplication repair has a DNA helicase activity specific for replication fork regression. Molecular cell *28*, 167-175.

Boehm, E.M., Gildenberg, M.S., and Washington, M.T. (2016). The Many Roles of PCNA in Eukaryotic DNA Replication. The Enzymes *39*, 231-254.

Boos, D., Sanchez-Pulido, L., Rappas, M., Pearl, L.H., Oliver, A.W., Ponting, C.P., and Diffley, J.F. (2011). Regulation of DNA replication through Sld3-Dpb11 interaction is conserved from yeast to humans. Current biology : CB *21*, 1152-1157.

Boos, D., Yekezare, M., and Diffley, J.F.X. (2013). Identification of a Heteromeric Complex That Promotes DNA Replication Origin Firing in Human Cells. Science (New York, NY) *340*, 981.

Borowiec, J.A., Dean, F.B., Bullock, P.A., and Hurwitz, J. (1990). Binding and unwinding--how T antigen engages the SV40 origin of DNA replication. Cell *60*, 181-184.

Bowers, J.L., Randell, J.C., Chen, S., and Bell, S.P. (2004). ATP hydrolysis by ORC catalyzes reiterative Mcm2-7 assembly at a defined origin of replication. Molecular cell *16*, 967-978.

Branzei, D., Vanoli, F., and Foiani, M. (2008). SUMOylation regulates Rad18-mediated template switch. Nature *456*, 915-920.

Bravo, R., Frank, R., Blundell, P.A., and Macdonald-Bravo, H. (1987). Cyclin/PCNA is the auxiliary protein of DNA polymerase-delta. Nature *326*, 515-517.

Brown, J.A., and Suo, Z. (2011). Unlocking the sugar "steric gate" of DNA polymerases. Biochemistry *50*, 1135-1142.

Bubeck, D., Reijns, M.A., Graham, S.C., Astell, K.R., Jones, E.Y., and Jackson, A.P. (2011). PCNA directs type 2 RNase H activity on DNA replication and repair substrates. Nucleic acids research *39*, 3652-3666.

Bucknall, R.A., Moores, H., Simms, R., and Hesp, B. (1973). Antiviral effects of aphidicolin, a new antibiotic produced by Cephalosporium aphidicola. Antimicrobial agents and chemotherapy *4*, 294-298.

Bugreev, D.V., Yu, X., Egelman, E.H., and Mazin, A.V. (2007). Novel pro- and anti-recombination activities of the Bloom's syndrome helicase. Genes & development *21*, 3085-3094.

Byrnes, J.J., Downey, K.M., Black, V.L., and So, A.G. (1976). A new mammalian DNA polymerase with 3' to 5' exonuclease activity: DNA polymerase δ. Biochemistry *15*, 2817-2823.

Byun, T.S., Pacek, M., Yee, M.C., Walter, J.C., and Cimprich, K.A. (2005). Functional uncoupling of MCM helicase and DNA polymerase activities activates the ATR-dependent checkpoint. Genes & development *19*, 1040-1052.

Cavanaugh, N.A., Beard, W.A., Batra, V.K., Perera, L., Pedersen, L.G., and Wilson, S.H. (2011). Molecular insights into DNA polymerase deterrents for ribonucleotide insertion. The Journal of biological chemistry *286*, 31650-31660.

Cayrou, C., Coulombe, P., Vigneron, A., Stanojcic, S., Ganier, O., Peiffer, I., Rivals, E., Puy, A., Laurent-Chabalier, S., Desprat, R.*, et al.* (2011). Genome-scale analysis of metazoan replication origins reveals their organization in specific but flexible sites defined by conserved features. Genome research *21*, 1438-1449.

Cerritelli, S.M., and Crouch, R.J. (2009). Ribonuclease H: the enzymes in eukaryotes. The FEBS journal *276*, 1494-1505.

Cerritelli, S.M., Frolova, E.G., Feng, C., Grinberg, A., Love, P.E., and Crouch, R.J. (2003). Failure to produce mitochondrial DNA results in embryonic lethality in Rnaseh1 null mice. Molecular cell *11*, 807-815.

Chavez, D.A., Greer, B.H., and Eichman, B.F. (2018). The HIRAN domain of helicase-like transcription factor positions the DNA translocase motor to drive efficient DNA fork regression. The Journal of biological chemistry *293*, 8484-8494.

Chen, J.Z., Qiu, J., Shen, B., and Holmquist, G.P. (2000). Mutational spectrum analysis of RNase H(35) deficient Saccharomyces cerevisiae using fluorescence-based directed termination PCR. Nucleic acids research *28*, 3649-3656.

Chen, X., Bosques, L., Sung, P., and Kupfer, G.M. (2016). A novel role for non-ubiquitinated FANCD2 in response to hydroxyurea-induced DNA damage. Oncogene *35*, 22-34.

Cheng, C.H., and Kuchta, R.D. (1993). DNA polymerase epsilon: aphidicolin inhibition and the relationship between polymerase and exonuclease activity. Biochemistry *32*, 8568-8574.

Cheng, J., DeCaprio, J.A., Fluck, M.M., and Schaffhausen, B.S. (2009). Cellular transformation by Simian Virus 40 and Murine Polyoma Virus T antigens. Semin Cancer Biol *19*, 218-228.

Cho, W.H., Kang, Y.H., An, Y.Y., Tappin, I., Hurwitz, J., and Lee, J.K. (2013). Human Tim-Tipin complex affects the biochemical properties of the replicative DNA helicase and DNA polymerases. Proceedings of the National Academy of Sciences of the United States of America *110*, 2523-2527.

Choe, K.N., and Moldovan, G.L. (2017). Forging Ahead through Darkness: PCNA, Still the Principal Conductor at the Replication Fork. Molecular cell *65*, 380-392.

Chon, H., Sparks, J.L., Rychlik, M., Nowotny, M., Burgers, P.M., Crouch, R.J., and Cerritelli, S.M. (2013). RNase H2 roles in genome integrity revealed by unlinking its activities. Nucleic acids research *41*, 3130-3143.

Chon, H., Vassilev, A., DePamphilis, M.L., Zhao, Y., Zhang, J., Burgers, P.M., Crouch, R.J., and Cerritelli, S.M. (2009). Contributions of the two accessory subunits, RNASEH2B and RNASEH2C, to the activity and properties of the human RNase H2 complex. Nucleic acids research *37*, 96-110.

Chowdhury, A., Liu, G., Kemp, M., Chen, X., Katrangi, N., Myers, S., Ghosh, M., Yao, J., Gao, Y., Bubulya, P.*, et al.* (2010). The DNA unwinding element binding protein DUE-B interacts with Cdc45 in preinitiation complex formation. Molecular and cellular biology *30*, 1495-1507.

Church, D.M., Goodstadt, L., Hillier, L.W., Zody, M.C., Goldstein, S., She, X., Bult, C.J., Agarwala, R., Cherry, J.L., DiCuccio, M.*, et al.* (2009). Lineage-specific biology revealed by a finished genome assembly of the mouse. PLoS biology *7*, e1000112.

Ciccia, A., Nimonkar, A.V., Hu, Y., Hajdu, I., Achar, Y.J., Izhar, L., Petit, S.A., Adamson, B., Yoon, J.C., Kowalczykowski, S.C*., et al.* (2012). Polyubiquitinated PCNA recruits the ZRANB3 translocase to maintain genomic integrity after replication stress. Molecular cell *47*, 396-409.

Cilli, P., Minoprio, A., Bossa, C., Bignami, M., and Mazzei, F. (2015). Formation and Repair of Mismatches Containing Ribonucleotides and Oxidized Bases at Repeated DNA Sequences. The Journal of biological chemistry *290*, 26259-26269.

Clairmont, C.S., Sarangi, P., Ponnienselvan, K., Galli, L.D., Csete, I., Moreau, L., Adelmant, G., Chowdhury, D., Marto, J.A., and D'Andrea, A.D. (2020). TRIP13 regulates DNA repair pathway choice through REV7 conformational change. Nature cell biology *22*, 87-96.

Clarke, D.J., Mondesert, G., Segal, M., Bertolaet, B.L., Jensen, S., Wolff, M., Henze, M., and Reed, S.I. (2001). Dosage suppressors of pds1 implicate ubiquitin-associated domains in checkpoint control. Molecular and cellular biology *21*, 1997-2007.

Clausen, A.R., Lujan, S.A., Burkholder, A.B., Orebaugh, C.D., Williams, J.S., Clausen, M.F., Malc, E.P., Mieczkowski, P.A., Fargo, D.C., Smith, D.J*., et al.* (2015). Tracking replication enzymology in vivo by genome-wide mapping of ribonucleotide incorporation. Nature structural & molecular biology *22*, 185-191.

Clausen, A.R., Zhang, S., Burgers, P.M., Lee, M.Y., and Kunkel, T.A. (2013). Ribonucleotide incorporation, proofreading and bypass by human DNA polymerase delta. DNA repair *12*, 121-127.

Clijsters, L., and Wolthuis, R. (2014). PIP-box-mediated degradation prohibits re-accumulation of Cdc6 during S phase. Journal of cell science *127*, 1336-1345.

Cook, J.G., Chasse, D.A., and Nevins, J.R. (2004). The regulated association of Cdt1 with minichromosome maintenance proteins and Cdc6 in mammalian cells. The Journal of biological chemistry *279*, 9625-9633.

Cook, J.G., Park, C.H., Burke, T.W., Leone, G., DeGregori, J., Engel, A., and Nevins, J.R. (2002). Analysis of Cdc6 function in the assembly of mammalian prereplication complexes. Proceedings of the National Academy of Sciences of the United States of America *99*, 1347-1352.

Cooper, G. (2000). The Cell: A Molecular Approach, Vol Vol. 2nd edition (Sinauer Associates).

Copeland, W.C., and Wang, T.S. (1993). Enzymatic characterization of the individual mammalian primase subunits reveals a biphasic mechanism for initiation of DNA replication. The Journal of biological chemistry *268*, 26179-26189.

Cortez, D. (2019). Replication-Coupled DNA Repair. Molecular cell *74*, 866-876.

Costa, A., Renault, L., Swuec, P., Petojevic, T., Pesavento, J.J., Ilves, I., MacLellan-Gibson, K., Fleck, R.A., Botchan, M.R., and Berger, J.M. (2014). DNA binding polarity, dimerization, and ATPase ring remodeling in the CMG helicase of the eukaryotic replisome. eLife *3*, e03273.

Costantino, L., Sotiriou, S.K., Rantala, J.K., Magin, S., Mladenov, E., Helleday, T., Haber, J.E., Iliakis, G., Kallioniemi, O.P., and Halazonetis, T.D. (2014). Break-induced replication repair of damaged forks induces genomic duplications in human cells. Science (New York, NY) *343*, 88-91.

Coulombe, P., Nassar, J., Peiffer, I., Stanojcic, S., Sterkers, Y., Delamarre, A., Bocquet, S., and Méchali, M. (2019). The ORC ubiquitin ligase OBI1 promotes DNA replication origin firing. Nature communications *10*, 2426.

Crespan, E., Furrer, A., Rösinger, M., Bertoletti, F., Mentegari, E., Chiapparini, G., Imhof, R., Ziegler, N., Sturla, S.J., Hübscher, U.*, et al.* (2016). Impact of ribonucleotide incorporation by DNA polymerases β and λ on oxidative base excision repair. Nature communications *7*, 10805.

Crow, Y.J. (2011). Type I interferonopathies: a novel set of inborn errors of immunity. Annals of the New York Academy of Sciences *1238*, 91-98.

Dalgaard, J.Z., and Klar, A.J. (2000). swi1 and swi3 perform imprinting, pausing, and termination of DNA replication in S. pombe. Cell *102*, 745-751.

Dalgaard, J.Z., and Klar, A.J. (2001). A DNA replication-arrest site RTS1 regulates imprinting by determining the direction of replication at mat1 in S. pombe. Genes & development *15*, 2060-2068.

Davies, S.L., North, P.S., Dart, A., Lakin, N.D., and Hickson, I.D. (2004). Phosphorylation of the Bloom's syndrome helicase and its role in recovery from S-phase arrest. Molecular and cellular biology *24*, 1279-1291.

Davies, S.L., North, P.S., and Hickson, I.D. (2007). Role for BLM in replication-fork restart and suppression of origin firing after replicative stress. Nature structural & molecular biology *14*, 677-679.

de Laat, W.L., Appeldoorn, E., Sugasawa, K., Weterings, E., Jaspers, N.G., and Hoeijmakers, J.H. (1998). DNA-binding polarity of human replication protein A positions nucleases in nucleotide excision repair. Genes & development *12*, 2598-2609.

De Piccoli, G., Katou, Y., Itoh, T., Nakato, R., Shirahige, K., and Labib, K. (2012). Replisome stability at defective DNA replication forks is independent of S phase checkpoint kinases. Molecular cell *45*, 696-704.

Delacroix, S., Wagner, J.M., Kobayashi, M., Yamamoto, K., and Karnitz, L.M. (2007). The Rad9-Hus1-Rad1 (9-1-1) clamp activates checkpoint signaling via TopBP1. Genes & development *21*, 1472-1477.

Delmolino, L.M., Saha, P., and Dutta, A. (2001). Multiple mechanisms regulate subcellular localization of human CDC6. The Journal of biological chemistry *276*, 26947-26954.

Dewar, J.M., Budzowska, M., and Walter, J.C. (2015). The mechanism of DNA replication termination in vertebrates. Nature *525*, 345-350.

Dewar, J.M., Low, E., Mann, M., Raschle, M., and Walter, J.C. (2017). CRL2(Lrr1) promotes unloading of the vertebrate replisome from chromatin during replication termination. Genes & development *31*, 275-290.

Dewar, J.M., and Walter, J.C. (2017). Mechanisms of DNA replication termination. Nature reviews Molecular cell biology *18*, 507-516.

Diamant, N., Hendel, A., Vered, I., Carell, T., Reissner, T., de Wind, N., Geacinov, N., and Livneh, Z. (2012). DNA damage bypass operates in the S and G2 phases of the cell cycle and exhibits differential mutagenicity. Nucleic acids research *40*, 170-180.

Donigan, K.A., McLenigan, M.P., Yang, W., Goodman, M.F., and Woodgate, R. (2014). The steric gate of DNA polymerase iota regulates ribonucleotide incorporation and deoxyribonucleotide fidelity. The Journal of biological chemistry *289*, 9136-9145.

Dresler, W.F.C., and Stein, R. (1869). Ueber den Hydroxylharnstoff. Justus Liebigs Annalen der Chemie *150*, 242-252.

Dungrawala, H., Bhat, K.P., Le Meur, R., Chazin, W.J., Ding, X., Sharan, S.K., Wessel, S.R., Sathe, A.A., Zhao, R., and Cortez, D. (2017). RADX Promotes Genome Stability and Modulates Chemosensitivity by Regulating RAD51 at Replication Forks. Molecular cell *67*, 374-386.e375.

Dungrawala, H., and Cortez, D. (2015). Purification of proteins on newly synthesized DNA using iPOND. Methods in molecular biology (Clifton, NJ) *1228*, 123-131.

Dungrawala, H., Rose, K.L., Bhat, K.P., Mohni, K.N., Glick, G.G., Couch, F.B., and Cortez, D. (2015). The Replication Checkpoint Prevents Two Types of Fork Collapse without Regulating Replisome Stability. Molecular cell *59*, 998-1010.

Eder, P.S., and Walder, J.A. (1991). Ribonuclease H from K562 human erythroleukemia cells. Purification, characterization, and substrate specificity. The Journal of biological chemistry *266*, 6472-6479.

Eder, P.S., Walder, R.Y., and Walder, J.A. (1993). Substrate specificity of human RNase H1 and its role in excision repair of ribose residues misincorporated in DNA. Biochimie *75*, 123-126.

Elledge, S.J. (1996). Cell Cycle Checkpoints: Preventing an Identity Crisis. Science *274*, 1664.

Elsasser, S., Gali, R.R., Schwickart, M., Larsen, C.N., Leggett, D.S., Müller, B., Feng, M.T., Tübing, F., Dittmar, G.A.G., and Finley, D. (2002). Proteasome subunit Rpn1 binds ubiquitin-like protein domains. Nature cell biology *4*, 725-730.

Elvers, I., Johansson, F., Groth, P., Erixon, K., and Helleday, T. (2011). UV stalled replication forks restart by re-priming in human fibroblasts. Nucleic acids research *39*, 7049-7057.

Ercilla, A., Feu, S., Aranda, S., Llopis, A., Brynjólfsdóttir, S.H., Sørensen, C.S., Toledo, L.I., and Agell, N. (2019). Acute hydroxyurea-induced replication blockade results in replisome components disengagement from nascent DNA without causing fork collapse. Cellular and Molecular Life Sciences.

Evrin, C., Clarke, P., Zech, J., Lurz, R., Sun, J., Uhle, S., Li, H., Stillman, B., and Speck, C. (2009). A double-hexameric MCM2-7 complex is loaded onto origin DNA during licensing of eukaryotic DNA replication. Proceedings of the National Academy of Sciences of the United States of America *106*, 20240-20245.

Eydmann, T., Sommariva, E., Inagawa, T., Mian, S., Klar, A.J.S., and Dalgaard, J.Z. (2008). Rtf1-mediated eukaryotic site-specific replication termination. Genetics *180*, 27-39.

Fairman, M.P., and Stillman, B. (1988). Cellular factors required for multiple stages of SV40 DNA replication in vitro. The EMBO journal *7*, 1211-1218.

Falbo, K.B., Alabert, C., Katou, Y., Wu, S., Han, J., Wehr, T., Xiao, J., He, X., Zhang, Z., Shi, Y.*, et al.* (2009). Involvement of a chromatin remodeling complex in damage tolerance during DNA replication. Nature structural & molecular biology *16*, 1167-1172.

Falck, J., Mailand, N., Syljuasen, R.G., Bartek, J., and Lukas, J. (2001). The ATM-Chk2-Cdc25A checkpoint pathway guards against radioresistant DNA synthesis. Nature *410*, 842-847.

Fraser, A.G., Kamath, R.S., Zipperlen, P., Martinez-Campos, M., Sohrmann, M., and Ahringer, J. (2000). Functional genomic analysis of C. elegans chromosome I by systematic RNA interference. Nature *408*, 325-330.

Fugger, K., Mistrik, M., Neelsen, K.J., Yao, Q., Zellweger, R., Kousholt, A.N., Haahr, P., Chu, W.K., Bartek, J., Lopes, M.*, et al.* (2015). FBH1 Catalyzes Regression of Stalled Replication Forks. Cell reports *10*, 1749-1757.

Fujita, M., Yamada, C., Goto, H., Yokoyama, N., Kuzushima, K., Inagaki, M., and Tsurumi, T. (1999). Cell cycle regulation of human CDC6 protein. Intracellular localization, interaction with the human mcm complex, and CDC2 kinase-mediated hyperphosphorylation. The Journal of biological chemistry *274*, 25927-25932.

Fumasoni, M., Zwicky, K., Vanoli, F., Lopes, M., and Branzei, D. (2015). Error-free DNA damage tolerance and sister chromatid proximity during DNA replication rely on the Polα/Primase/Ctf4 Complex. Molecular cell *57*, 812-823.

Gabriely, G., Kama, R., Gelin-Licht, R., and Gerst, J.E. (2008). Different domains of the UBL-UBA ubiquitin receptor, Ddi1/Vsm1, are involved in its multiple cellular roles. Molecular biology of the cell *19*, 3625-3637.

Gallo, D., Wang, G., Yip, C.M., and Brown, G.W. (2016). Analysis of Replicating Yeast Chromosomes by DNA Combing. Cold Spring Harbor Protocols *2016*, pdb.prot085118.

Gambus, A., Jones, R.C., Sanchez-Diaz, A., Kanemaki, M., van Deursen, F., Edmondson, R.D., and Labib, K. (2006). GINS maintains association of Cdc45 with MCM in replisome progression complexes at eukaryotic DNA replication forks. Nature cell biology *8*, 358-366.

Gan, W., Guan, Z., Liu, J., Gui, T., Shen, K., Manley, J.L., and Li, X. (2011). R-loop-mediated genomic instability is caused by impairment of replication fork progression. Genes & development *25*, 2041-2056.

Ganai, R.A., and Johansson, E. (2016). DNA Replication-A Matter of Fidelity. Molecular cell *62*, 745-755.

Gangavarapu, V., Prakash, S., and Prakash, L. (2007). Requirement of RAD52 Group Genes for Postreplication Repair of UV-Damaged DNA in <em>Saccharomyces cerevisiae</em&gt. Molecular and cellular biology *27*, 7758.

Garcia-Gomez, S., Reyes, A., Martinez-Jimenez, M.I., Chocron, E.S., Mouron, S., Terrados, G., Powell, C., Salido, E., Mendez, J., Holt, I.J*., et al.* (2013). PrimPol, an archaic primase/polymerase operating in human cells. Molecular cell *52*, 541-553.

Garg, P., Stith, C.M., Sabouri, N., Johansson, E., and Burgers, P.M. (2004). Idling by DNA polymerase delta maintains a ligatable nick during lagging-strand DNA replication. Genes & development *18*, 2764-2773.

Ge, X.Q., and Blow, J.J. (2010). Chk1 inhibits replication factory activation but allows dormant origin firing in existing factories. The Journal of cell biology *191*, 1285-1297.

Ge, X.Q., Jackson, D.A., and Blow, J.J. (2007). Dormant origins licensed by excess Mcm2-7 are required for human cells to survive replicative stress. Genes & development *21*, 3331-3341.

Georgescu, R., Yuan, Z., Bai, L., de Luna Almeida Santos, R., Sun, J., Zhang, D., Yurieva, O., Li, H., and O'Donnell, M.E. (2017). Structure of eukaryotic CMG helicase at a replication fork and implications to replisome architecture and origin initiation. Proceedings of the National Academy of Sciences of the United States of America *114*, E697-e706.

Gerber, J.-K., Gögel, E., Berger, C., Wallisch, M., Müller, F., Grummt, I., and Grummt, F. (1997). Termination of Mammalian rDNA Replication: Polar Arrest of Replication Fork Movement by Transcription Termination Factor TTF-I. Cell *90*, 559-567.

Giannattasio, M., and Branzei, D. (2019). DNA Replication Through Strand Displacement During Lagging Strand DNA Synthesis in Saccharomyces cerevisiae. Genes *10*.

Giannattasio, M., Zwicky, K., Follonier, C., Foiani, M., Lopes, M., and Branzei, D. (2014). Visualization of recombination-mediated damage bypass by template switching. Nature structural & molecular biology *21*, 884-892.

Giordano-Coltart, J., Ying, C.Y., Gautier, J., and Hurwitz, J. (2005). Studies of the properties of human origin recognition complex and its Walker A motif mutants. Proceedings of the National Academy of Sciences of the United States of America *102*, 69-74.

Goksenin, A.Y., Zahurancik, W., LeCompte, K.G., Taggart, D.J., Suo, Z., and Pursell, Z.F. (2012). Human DNA polymerase epsilon is able to efficiently extend from multiple consecutive ribonucleotides. The Journal of biological chemistry *287*, 42675-42684.

Gomez, T.A., Kolawa, N., Gee, M., Sweredoski, M.J., and Deshaies, R.J. (2011). Identification of a functional docking site in the Rpn1 LRR domain for the UBA-UBL domain protein Ddi1. BMC Biol *9*, 33-33.

Gosavi, R.A., Moon, A.F., Kunkel, T.A., Pedersen, L.C., and Bebenek, K. (2012). The catalytic cycle for ribonucleotide incorporation by human DNA Pol lambda. Nucleic acids research *40*, 7518-7527.

Graham, J.E., Marians, K.J., and Kowalczykowski, S.C. (2017). Independent and Stochastic Action of DNA Polymerases in the Replisome. Cell *169*, 1201-1213.e1217.

Guilliam, T.A., Jozwiakowski, S.K., Ehlinger, A., Barnes, R.P., Rudd, S.G., Bailey, L.J., Skehel, J.M., Eckert, K.A., Chazin, W.J., and Doherty, A.J. (2015). Human PrimPol is a highly error-prone polymerase regulated by single-stranded DNA binding proteins. Nucleic acids research *43*, 1056-1068.

Gunther, C., Kind, B., Reijns, M.A., Berndt, N., Martinez-Bueno, M., Wolf, C., Tungler, V., Chara, O., Lee, Y.A., Hubner, N.*, et al.* (2015). Defective removal of ribonucleotides from DNA promotes systemic autoimmunity. The Journal of clinical investigation *125*, 413-424.

Haahr, P., Hoffmann, S., Tollenaere, M.A., Ho, T., Toledo, L.I., Mann, M., Bekker-Jensen, S., Raschle, M., and Mailand, N. (2016). Activation of the ATR kinase by the RPA-binding protein ETAA1. Nature cell biology *18*, 1196-1207.

Han, J., Liu, T., Huen, M.S.Y., Hu, L., Chen, Z., and Huang, J. (2014). SIVA1 directs the E3 ubiquitin ligase RAD18 for PCNA monoubiquitination. The Journal of cell biology *205*, 811-827.

Hanada, K., Budzowska, M., Davies, S.L., van Drunen, E., Onizawa, H., Beverloo, H.B., Maas, A., Essers, J., Hickson, I.D., and Kanaar, R. (2007). The structure-specific endonuclease Mus81 contributes to replication restart by generating double-strand DNA breaks. Nature structural & molecular biology *14*, 1096-1104.

Hanzlikova, H., Kalasova, I., Demin, A.A., Pennicott, L.E., Cihlarova, Z., and Caldecott, K.W. (2018). The Importance of Poly(ADP-Ribose) Polymerase as a Sensor of Unligated Okazaki Fragments during DNA Replication. Molecular cell *71*, 319-331.e313.

Haracska, L., Prakash, L., and Prakash, S. (2002). Role of human DNA polymerase kappa as an extender in translesion synthesis. Proceedings of the National Academy of Sciences of the United States of America *99*, 16000-16005.

Harper, J.W., Elledge, S.J., Keyomarsi, K., Dynlacht, B., Tsai, L.H., Zhang, P., Dobrowolski, S., Bai, C., Connell-Crowley, L., Swindell, E.*, et al.* (1995). Inhibition of cyclin-dependent kinases by p21. Molecular biology of the cell *6*, 387-400.

Hart, T., Chandrashekhar, M., Aregger, M., Steinhart, Z., Brown, K.R., MacLeod, G., Mis, M., Zimmermann, M., Fradet-Turcotte, A., Sun, S.*, et al.* (2015). High-Resolution CRISPR Screens Reveal Fitness Genes and Genotype-Specific Cancer Liabilities. Cell *163*, 1515-1526.

Hashimoto, Y., Puddu, F., and Costanzo, V. (2011). RAD51- and MRE11-dependent reassembly of uncoupled CMG helicase complex at collapsed replication forks. Nature structural & molecular biology *19*, 17-24.

Heller, R.C., and Marians, K.J. (2006). Replisome assembly and the direct restart of stalled replication forks. Nature reviews Molecular cell biology *7*, 932-943.

Hendel, A., Krijger, P.H.L., Diamant, N., Goren, Z., Langerak, P., Kim, J., Reissner, T., Lee, K.-y., Geacintov, N.E., Carell, T.*, et al.* (2011). PCNA ubiquitination is important, but not essential for translesion DNA synthesis in mammalian cells. PLoS genetics *7*, e1002262-e1002262.

Hernandez-Perez, S., Cabrera, E., Amoedo, H., Rodriguez-Acebes, S., Koundrioukoff, S., Debatisse, M., Mendez, J., and Freire, R. (2016). USP37 deubiquitinates Cdt1 and contributes to regulate DNA replication. Molecular oncology *10*, 1196-1206.

Hidaka, M., Kobayashi, T., Takenaka, S., Takeya, H., and Horiuchi, T. (1989). Purification of a DNA replication terminus (ter) site-binding protein in Escherichia coli and identification of the structural gene. The Journal of biological chemistry *264*, 21031-21037.

Higgins, N.P., Kato, K., and Strauss, B. (1976). A model for replication repair in mammalian cells. Journal of molecular biology *101*, 417-425.

Higuchi, K., Katayama, T., Iwai, S., Hidaka, M., Horiuchi, T., and Maki, H. (2003). Fate of DNA replication fork encountering a single DNA lesion during oriC plasmid DNA replication in vitro. Genes to cells : devoted to molecular & cellular mechanisms *8*, 437-449.

Hiller, B., Achleitner, M., Glage, S., Naumann, R., Behrendt, R., and Roers, A. (2012). Mammalian RNase H2 removes ribonucleotides from DNA to maintain genome integrity. The Journal of experimental medicine *209*, 1419-1426.

Hiller, B., Hoppe, A., Haase, C., Hiller, C., Schubert, N., Muller, W., Reijns, M.A.M., Jackson, A.P., Kunkel, T.A., Wenzel, J.*, et al.* (2018). Ribonucleotide Excision Repair Is Essential to Prevent Squamous Cell Carcinoma of the Skin. Cancer research *78*, 5917-5926.

Hoege, C., Pfander, B., Moldovan, G.-L., Pyrowolakis, G., and Jentsch, S. (2002). RAD6-dependent DNA repair is linked to modification of PCNA by ubiquitin and SUMO. Nature *419*, 135-141.

Holzer, S., Rzechorzek, N.J., Short, I.R., Jenkyn-Bedford, M., Pellegrini, L., and Kilkenny, M.L. (2019). Structural basis for inhibition of human primase by arabinofuranosyl nucleoside analogues Fludarabine and Vidarabine. bioRxiv, 605279.

Hozák, P., Hassan, A.B., Jackson, D.A., and Cook, P.R. (1993). Visualization of replication factories attached to a nucleoskeleton. Cell *73*, 361-373.

Hromas, R., Kim, H.-S., Sidhu, G., Williamson, E., Jaiswal, A., Totterdale, T.A., Nole, J., Lee, S.-H., Nickoloff, J.A., and Kong, K.Y. (2017). The endonuclease EEPD1 mediates synthetic lethality in RAD52-depleted BRCA1 mutant breast cancer cells. Breast Cancer Research *19*, 122.

Hua, X.H., and Newport, J. (1998). Identification of a preinitiation step in DNA replication that is independent of origin recognition complex and cdc6, but dependent on cdk2. The Journal of cell biology *140*, 271-281.

Huang, J., Liu, S., Bellani, Marina A., Thazhathveetil, Arun K., Ling, C., de Winter, Johan P., Wang, Y., Wang, W., and Seidman, Michael M. (2013). The DNA Translocase FANCM/MHF Promotes Replication Traverse of DNA Interstrand Crosslinks. Molecular cell *52*, 434-446.

Huang, J., Zhang, J., Bellani, M.A., Pokharel, D., Gichimu, J., James, R.C., Gali, H., Ling, C., Yan, Z., Xu, D.*, et al.* (2019). Remodeling of Interstrand Crosslink Proximal

Replisomes Is Dependent on ATR, FANCM, and FANCD2. Cell reports *27*, 1794-1808.e1795.

Huang, T.T., Nijman, S.M.B., Mirchandani, K.D., Galardy, P.J., Cohn, M.A., Haas, W., Gygi, S.P., Ploegh, H.L., Bernards, R., and D'Andrea, A.D. (2006). Regulation of monoubiquitinated PCNA by DUB autocleavage. Nature cell biology *8*, 339-347.

Ikegami, S., Taguchi, T., Ohashi, M., Oguro, M., Nagano, H., and Mano, Y. (1978). Aphidicolin prevents mitotic cell division by interfering with the activity of DNA polymerase-α. Nature *275*, 458-460.

Ilves, I., Petojevic, T., Pesavento, J.J., and Botchan, M.R. (2010). Activation of the MCM2-7 helicase by association with Cdc45 and GINS proteins. Molecular cell *37*, 247-258.

Im, J.-S., Ki, S.-H., Farina, A., Jung, D.-S., Hurwitz, J., and Lee, J.-K. (2009). Assembly of the Cdc45-Mcm2–7-GINS complex in human cells requires the Ctf4/And-1, RecQL4, and Mcm10 proteins. Proceedings of the National Academy of Sciences *106*, 15628.

Inagawa, T., Yamada-Inagawa, T., Eydmann, T., Mian, I.S., Wang, T.S., and Dalgaard, J.Z. (2009). Schizosaccharomyces pombe Rtf2 mediates site-specific replication termination by inhibiting replication restart. Proceedings of the National Academy of Sciences of the United States of America *106*, 7927-7932.

Iraqui, I., Chekkal, Y., Jmari, N., Pietrobon, V., Fréon, K., Costes, A., and Lambert, S.A.E. (2012). Recovery of arrested replication forks by homologous recombination is error-prone. PLoS genetics *8*, e1002976-e1002976.

Ishimi, Y. (1997). A DNA helicase activity is associated with an MCM4, -6, and -7 protein complex. The Journal of biological chemistry *272*, 24508-24513.

Ivantsiv, Y., Kaplun, L., Tzirkin-Goldin, R., Shabek, N., and Raveh, D. (2006). Unique role for the UbL-UbA protein Ddi1 in turnover of SCFUfo1 complexes. Molecular and cellular biology *26*, 1579-1588.

Iyer, L.M., Koonin, E.V., Leipe, D.D., and Aravind, L. (2005). Origin and evolution of the archaeo-eukaryotic primase superfamily and related palm-domain proteins: structural insights and new members. Nucleic acids research *33*, 3875-3896.

Iyer, V.N., and Rupp, W.D. (1971). Usefulness of benzoylated naphthoylated DEAE-cellulose to distinguish and fractionate double-stranded DNA bearing different extents of single-stranded regions. Biochimica et biophysica acta *228*, 117-126.

Jalan, M., Oehler, J., Morrow, C.A., Osman, F., and Whitby, M.C. (2019). Factors affecting template switch recombination associated with restarted DNA replication. eLife *8*, e41697.

Jha, V., and Ling, H. (2018). 2.0 Å resolution crystal structure of human polκ reveals a new catalytic function of N-clasp in DNA replication. Scientific reports *8*, 15125.

Jiang, W., Wells, N.J., and Hunter, T. (1999). Multistep regulation of DNA replication by Cdk phosphorylation of HsCdc6. Proceedings of the National Academy of Sciences of the United States of America *96*, 6193-6198.

Jin, Y.H., Ayyagari, R., Resnick, M.A., Gordenin, D.A., and Burgers, P.M.J. (2003). Okazaki fragment maturation in yeast. II. Cooperation between the polymerase and 3'-5'-exonuclease activities of Pol delta in the creation of a ligatable nick. The Journal of biological chemistry *278*, 1626-1633.

Jin, Y.H., Obert, R., Burgers, P.M., Kunkel, T.A., Resnick, M.A., and Gordenin, D.A. (2001). The 3'-->5' exonuclease of DNA polymerase delta can substitute for the 5' flap endonuclease Rad27/Fen1 in processing Okazaki fragments and preventing genome instability. Proceedings of the National Academy of Sciences of the United States of America *98*, 5122-5127.

Job, A., Schmitt, L.M., von Wenserski, L., Lankat-Buttgereit, B., Gress, T.M., Buchholz, M., and Gallmeier, E. (2018). Inactivation of PRIM1 Function Sensitizes Cancer Cells to ATR and CHK1 Inhibitors. Neoplasia (New York, NY) *20*, 1135-1143.

Johnson, R.E., Washington, M.T., Haracska, L., Prakash, S., and Prakash, L. (2000). Eukaryotic polymerases iota and zeta act sequentially to bypass DNA lesions. Nature *406*, 1015-1019.

Jónsson, Z.O., Hindges, R., and Hübscher, U. (1998). Regulation of DNA replication and repair proteins through interaction with the front side of proliferating cell nuclear antigen. The EMBO journal *17*, 2412-2425.

Kang, Y., Vossler, R.A., Diaz-Martinez, L.A., Winter, N.S., Clarke, D.J., and Walters, K.J. (2006). UBL/UBA ubiquitin receptor proteins bind a common tetraubiquitin chain. Journal of molecular biology *356*, 1027-1035.

Kannouche, P.L., Wing, J., and Lehmann, A.R. (2004). Interaction of human DNA polymerase eta with monoubiquitinated PCNA: a possible mechanism for the polymerase switch in response to DNA damage. Molecular cell *14*, 491-500.

Kao, H.-I., Veeraraghavan, J., Polaczek, P., Campbell, J.L., and Bambara, R.A. (2004). On the roles of Saccharomyces cerevisiae Dna2p and Flap endonuclease 1 in Okazaki fragment processing. The Journal of biological chemistry *279*, 15014-15024.

Kao, H.I., and Bambara, R.A. (2003). The protein components and mechanism of eukaryotic Okazaki fragment maturation. Critical reviews in biochemistry and molecular biology *38*, 433-452.

Kaplun, L., Tzirkin, R., Bakhrat, A., Shabek, N., Ivantsiv, Y., and Raveh, D. (2005). The DNA damage-inducible UbL-UbA protein Ddi1 participates in Mec1-mediated degradation of Ho endonuclease. Molecular and cellular biology *25*, 5355-5362.

Kashiwaba, S.-i., Kanao, R., Masuda, Y., Kusumoto-Matsuo, R., Hanaoka, F., and Masutani, C. (2015). USP7 Is a Suppressor of PCNA Ubiquitination and Oxidative-Stress-Induced Mutagenesis in Human Cells. Cell reports *13*, 2072-2080.

Keen, B.A., Bailey, L.J., Jozwiakowski, S.K., and Doherty, A.J. (2014a). Human PrimPol mutation associated with high myopia has a DNA replication defect. Nucleic acids research *42*, 12102-12111.

Keen, B.A., Jozwiakowski, S.K., Bailey, L.J., Bianchi, J., and Doherty, A.J. (2014b). Molecular dissection of the domain architecture and catalytic activities of human PrimPol. Nucleic acids research *42*, 5830-5845.

Kelso, A.A., Lopezcolorado, F.W., Bhargava, R., and Stark, J.M. (2019). Distinct roles of RAD52 and POLQ in chromosomal break repair and replication stress response. PLoS genetics *15*, e1008319-e1008319.

Kile, Andrew C., Chavez, Diana A., Bacal, J., Eldirany, S., Korzhnev, Dmitry M., Bezsonova, I., Eichman, Brandt F., and Cimprich, Karlene A. (2015). HLTF's Ancient HIRAN Domain Binds 3′ DNA Ends to Drive Replication Fork Reversal. Molecular cell *58*, 1090-1100.

Kim, H., Dejsuphong, D., Adelmant, G., Ceccaldi, R., Yang, K., Marto, J.A., and D'Andrea, A.D. (2014). Transcriptional repressor ZBTB1 promotes chromatin remodeling and translesion DNA synthesis. Molecular cell *54*, 107-118.

Kim, N., Huang, S.N., Williams, J.S., Li, Y.C., Clark, A.B., Cho, J.E., Kunkel, T.A., Pommier, Y., and Jinks-Robertson, S. (2011). Mutagenic processing of ribonucleotides in DNA by yeast topoisomerase I. Science (New York, NY) *332*, 1561-1564.

Kind, B., Muster, B., Staroske, W., Herce, H.D., Sachse, R., Rapp, A., Schmidt, F., Koss, S., Cardoso, M.C., and Lee-Kirsch, M.A. (2014). Altered spatio-temporal dynamics of RNase H2 complex assembly at replication and repair sites in Aicardi-Goutieres syndrome. Human molecular genetics *23*, 5950-5960.

Kitamura, E., Blow, J.J., and Tanaka, T.U. (2006). Live-cell imaging reveals replication of individual replicons in eukaryotic replication factories. Cell *125*, 1297-1308.

Kobayashi, K., Guilliam, T.A., Tsuda, M., Yamamoto, J., Bailey, L.J., Iwai, S., Takeda, S., Doherty, A.J., and Hirota, K. (2016). Repriming by PrimPol is critical for DNA replication restart downstream of lesions and chain-terminating nucleosides. Cell cycle (Georgetown, Tex) *15*, 1997-2008.

Kondo, T., Kobayashi, M., Tanaka, J., Yokoyama, A., Suzuki, S., Kato, N., Onozawa, M., Chiba, K., Hashino, S., Imamura, M.*, et al.* (2004). Rapid degradation of Cdt1 upon UV-induced DNA damage is mediated by SCFSkp2 complex. The Journal of biological chemistry *279*, 27315-27319.

Kottemann, M.C., Conti, B.A., Lach, F.P., and Smogorzewska, A. (2018). Removal of RTF2 from Stalled Replisomes Promotes Maintenance of Genome Integrity. Molecular cell *69*, 24-35.e25.

Kreitz, S., Ritzi, M., Baack, M., and Knippers, R. (2001). The human origin recognition complex protein 1 dissociates from chromatin during S phase in HeLa cells. The Journal of biological chemistry *276*, 6337-6342.

Kuchta, R.D., Reid, B., and Chang, L.M. (1990). DNA primase. Processivity and the primase to polymerase alpha activity switch. The Journal of biological chemistry *265*, 16158-16165.

Kuchta, R.D., and Stengel, G. (2010). Mechanism and evolution of DNA primases. Biochimica et biophysica acta *1804*, 1180-1189.

Kumagai, A., Shevchenko, A., Shevchenko, A., and Dunphy, W.G. (2011). Direct regulation of Treslin by cyclin-dependent kinase is essential for the onset of DNA replication. The Journal of cell biology *193*, 995-1007.

Kurat, C.F., Yeeles, J.T.P., Patel, H., Early, A., and Diffley, J.F.X. (2017). Chromatin Controls DNA Replication Origin Selection, Lagging-Strand Synthesis, and Replication Fork Rates. Molecular Cell *65*, 117-130.

Lakso, M., Pichel, J.G., Gorman, J.R., Sauer, B., Okamoto, Y., Lee, E., Alt, F.W., and Westphal, H. (1996). Efficient in vivo manipulation of mouse genomic sequences at the zygote stage. Proc Natl Acad Sci U S A *93*, 5860-5865.

Lambert, S., Mizuno, K.i., Blaisonneau, J., Martineau, S., Chanet, R., Fréon, K., Murray, J.M., Carr, A.M., and Baldacci, G. (2010). Homologous recombination restarts blocked replication forks at the expense of genome rearrangements by template exchange. Molecular cell *39*, 346-359.

Lambert, S., Watson, A., Sheedy, D.M., Martin, B., and Carr, A.M. (2005). Gross chromosomal rearrangements and elevated recombination at an inducible site-specific replication fork barrier. Cell *121*, 689-702.

Land, M., Hauser, L., Jun, S.-R., Nookaew, I., Leuze, M.R., Ahn, T.-H., Karpinets, T., Lund, O., Kora, G., Wassenaar, T.*, et al.* (2015). Insights from 20 years of bacterial genome sequencing. Functional & integrative genomics *15*, 141-161.

Lebofsky, R., Takahashi, T., and Walter, J.C. (2009). DNA replication in nucleus-free Xenopus egg extracts. Methods in molecular biology (Clifton, NJ) *521*, 229-252.

Lebon, P., Badoual, J., Ponsot, G., Goutieres, F., Hemeury-Cukier, F., and Aicardi, J. (1988). Intrathecal synthesis of interferon-alpha in infants with progressive familial encephalopathy. Journal of the neurological sciences *84*, 201-208.

Lee, B.I., and Wilson, D.M., 3rd (1999). The RAD2 domain of human exonuclease 1 exhibits 5' to 3' exonuclease and flap structure-specific endonuclease activities. The Journal of biological chemistry *274*, 37763-37769.

Lee, H.-S., Seo, H.-R., Lee, S.-A., Choi, S., Kang, D., and Kwon, J. (2019). BAP1 promotes stalled fork restart and cell survival via INO80 in response to replication stress. Biochem J *476*, 3053-3066.

Lee, J., Chastain, P.D., Kusakabe, T., Griffith, J.D., and Richardson, C.C. (1998). Coordinated Leading and Lagging Strand DNA Synthesis on a Minicircular Template. Molecular cell *1*, 1001-1010.

Lee, J., Kumagai, A., and Dunphy, W.G. (2007a). The Rad9-Hus1-Rad1 checkpoint clamp regulates interaction of TopBP1 with ATR. The Journal of biological chemistry *282*, 28036-28044.

Lee, J.A., Carvalho, C.M.B., and Lupski, J.R. (2007b). A DNA Replication Mechanism for Generating Nonrecurrent Rearrangements Associated with Genomic Disorders. Cell *131*, 1235-1247.

Lee, Y.-S., Gregory, M.T., and Yang, W. (2014). Human Pol ζ purified with accessory subunits is active in translesion DNA synthesis and complements Pol η in cisplatin bypass. Proceedings of the National Academy of Sciences of the United States of America *111*, 2954-2959.

Leipe, D.D., Aravind, L., and Koonin, E.V. (1999). Did DNA replication evolve twice independently? Nucleic acids research *27*, 3389-3401.

Lemaçon, D., Jackson, J., Quinet, A., Brickner, J.R., Li, S., Yazinski, S., You, Z., Ira, G., Zou, L., Mosammaparast, N.*, et al.* (2017). MRE11 and EXO1 nucleases degrade reversed forks and elicit MUS81-dependent fork rescue in BRCA2-deficient cells. Nature communications *8*, 860.

Leonard, A.C., and Méchali, M. (2013). DNA replication origins. Cold Spring Harbor perspectives in biology *5*, a010116-a010116.

Leuzzi, G., Marabitti, V., Pichierri, P., and Franchitto, A. (2016). WRNIP1 protects stalled forks from degradation and promotes fork restart after replication stress. The EMBO journal *35*, 1437-1451.

Lewis, J.S., Spenkelink, L.M., Schauer, G.D., Hill, F.R., Georgescu, R.E., O'Donnell, M.E., and van Oijen, A.M. (2017). Single-molecule visualization of Saccharomyces cerevisiae leading-strand synthesis reveals dynamic interaction between MTC and the replisome. Proc Natl Acad Sci U S A.

Lewis, J.S., Spenkelink, L.M., Schauer, G.D., Yurieva, O., Mueller, S.H., Natarajan, V., Kaur, G., Maher, C., Kay, C., O'Donnell, M.E.*, et al.* (2019). Tunability of DNA Polymerase Stability during Eukaryotic DNA Replication. Molecular cell.

Li, C.-J., and DePamphilis, M.L. (2002). Mammalian Orc1 protein is selectively released from chromatin and ubiquitinated during the S-to-M transition in the cell division cycle. Molecular and cellular biology *22*, 105-116.

Li, C.J., Vassilev, A., and DePamphilis, M.L. (2004). Role for Cdk1 (Cdc2)/cyclin A in preventing the mammalian origin recognition complex's largest subunit (Orc1) from binding to chromatin during mitosis. Molecular and cellular biology *24*, 5875-5886.

Li, D., Zhao, R., Lilyestrom, W., Gai, D., Zhang, R., DeCaprio, J.A., Fanning, E., Jochimiak, A., Szakonyi, G., and Chen, X.S. (2003a). Structure of the replicative helicase of the oncoprotein SV40 large tumour antigen. Nature *423*, 512-518.

Li, X., Zhao, Q., Liao, R., Sun, P., and Wu, X. (2003b). The SCF(Skp2) ubiquitin ligase complex interacts with the human replication licensing factor Cdt1 and regulates Cdt1 degradation. The Journal of biological chemistry *278*, 30854-30858.

Liaw, H., Lee, D., and Myung, K. (2011). DNA-PK-Dependent RPA2 Hyperphosphorylation Facilitates DNA Repair and Suppresses Sister Chromatid Exchange. PloS one *6*, e21424.

Lima, W.F., Murray, H.M., Damle, S.S., Hart, C.E., Hung, G., De Hoyos, C.L., Liang, X.H., and Crooke, S.T. (2016). Viable RNaseH1 knockout mice show RNaseH1 is essential for R loop processing, mitochondrial and liver function. Nucleic acids research *44*, 5299-5312.

Lin, J.-R., Zeman, M.K., Chen, J.-Y., Yee, M.-C., and Cimprich, K.A. (2011). SHPRH and HLTF act in a damage-specific manner to coordinate different forms of postreplication repair and prevent mutagenesis. Molecular cell *42*, 237-249.

Lin, W., Xin, H., Zhang, Y., Wu, X., Yuan, F., and Wang, Z. (1999). The human REV1 gene codes for a DNA template-dependent dCMP transferase. Nucleic acids research *27*, 4468-4475.

Linskens, M.H., and Huberman, J.A. (1988). Organization of replication of ribosomal DNA in Saccharomyces cerevisiae. Molecular and cellular biology *8*, 4927-4935.

Little, R.D., Platt, T.H., and Schildkraut, C.L. (1993). Initiation and termination of DNA replication in human rRNA genes. Molecular and cellular biology *13*, 6600-6613.

Liu, B., Hu, J., Wang, J., and Kong, D. (2017). Direct Visualization of RNA-DNA Primer Removal from Okazaki Fragments Provides Support for Flap Cleavage and Exonucleolytic Pathways in Eukaryotic Cells. The Journal of biological chemistry *292*, 4777-4788.

Liu, E., Li, X., Yan, F., Zhao, Q., and Wu, X. (2004). Cyclin-dependent kinases phosphorylate human Cdt1 and induce its degradation. The Journal of biological chemistry *279*, 17283-17288.

Liu, S., Opiyo, S.O., Manthey, K., Glanzer, J.G., Ashley, A.K., Amerin, C., Troksa, K., Shrivastav, M., Nickoloff, J.A., and Oakley, G.G. (2012). Distinct roles for DNA-PK, ATM

and ATR in RPA phosphorylation and checkpoint activation in response to replication stress. Nucleic acids research *40*, 10780-10794.

Liu, Y., and Xiao, W. (1997). Bidirectional regulation of two DNA-damage-inducible genes, MAG1 and DDI1, from Saccharomyces cerevisiae. Mol Microbiol *23*, 777-789.

Lockhart, A., Pires, V.B., Bento, F., Kellner, V., Luke-Glaser, S., Yakoub, G., Ulrich, H.D., and Luke, B. (2019). RNase H1 and H2 Are Differentially Regulated to Process RNA-DNA Hybrids. Cell reports *29*, 2890-2900.e2895.

MacDougall, C.A., Byun, T.S., Van, C., Yee, M.C., and Cimprich, K.A. (2007). The structural determinants of checkpoint activation. Genes & development *21*, 898-903.

Machwe, A., Karale, R., Xu, X., Liu, Y., and Orren, D.K. (2011). The Werner and Bloom syndrome proteins help resolve replication blockage by converting (regressed) holliday junctions to functional replication forks. Biochemistry *50*, 6774-6788.

Mackenzie, K.J., Carroll, P., Lettice, L., Tarnauskaite, Z., Reddy, K., Dix, F., Revuelta, A., Abbondati, E., Rigby, R.E., Rabe, B.*, et al.* (2016). Ribonuclease H2 mutations induce a cGAS/STING-dependent innate immune response. The EMBO journal *35*, 831-844.

Mackenzie, K.J., Carroll, P., Martin, C.A., Murina, O., Fluteau, A., Simpson, D.J., Olova, N., Sutcliffe, H., Rainger, J.K., Leitch, A.*, et al.* (2017). cGAS surveillance of micronuclei links genome instability to innate immunity. Nature *548*, 461-465.

Maga, G., Villani, G., Tillement, V., Stucki, M., Locatelli, G.A., Frouin, I., Spadari, S., and Hübscher, U. (2001). Okazaki fragment processing: Modulation of the strand displacement activity of DNA polymerase δ by the concerted action of replication protein A, proliferating cell nuclear antigen, and flap endonuclease-1. Proceedings of the National Academy of Sciences *98*, 14298.

Mailand, N., and Diffley, J.F. (2005). CDKs promote DNA replication origin licensing in human cells by protecting Cdc6 from APC/C-dependent proteolysis. Cell *122*, 915-926.

Mailand, N., Falck, J., Lukas, C., Syljuasen, R.G., Welcker, M., Bartek, J., and Lukas, J. (2000). Rapid destruction of human Cdc25A in response to DNA damage. Science (New York, NY) *288*, 1425-1429.

Maiorano, D., Moreau, J., and Mechali, M. (2000). XCDT1 is required for the assembly of pre-replicative complexes in Xenopus laevis. Nature *404*, 622-625.

Makarova, A.V., Boldinova, E.O., Belousova, E.A., and Lavrik, O.I. (2018). In vitro lesion bypass by human PrimPol. DNA repair *70*, 18-24.

Maric, M., Maculins, T., De Piccoli, G., and Labib, K. (2014). Cdc48 and a ubiquitin ligase drive disassembly of the CMG helicase at the end of DNA replication. Science (New York, NY) *346*, 1253596.

Martinez-Jimenez, M.I., Garcia-Gomez, S., Bebenek, K., Sastre-Moreno, G., Calvo, P.A., Diaz-Talavera, A., Kunkel, T.A., and Blanco, L. (2015). Alternative solutions and new scenarios for translesion DNA synthesis by human PrimPol. DNA repair *29*, 127-138.

Masai, H., Matsumoto, S., You, Z., Yoshizawa-Sugata, N., and Oda, M. (2010). Eukaryotic chromosome DNA replication: where, when, and how? Annual review of biochemistry *79*, 89-130.

Masai, H., Sato, N., Takeda, T., and Arai, K. (1999). CDC7 kinase complex as a molecular switch for DNA replication. Frontiers in bioscience : a journal and virtual library *4*, D834-840.

Masuda, Y., Mitsuyuki, S., Kanao, R., Hishiki, A., Hashimoto, H., and Masutani, C. (2018). Regulation of HLTF-mediated PCNA polyubiquitination by RFC and PCNA monoubiquitination levels determines choice of damage tolerance pathway. Nucleic acids research *46*, 11340-11356.

Masuda, Y., Suzuki, M., Kawai, H., Hishiki, A., Hashimoto, H., Masutani, C., Hishida, T., Suzuki, F., and Kamiya, K. (2012). En bloc transfer of polyubiquitin chains to PCNA in vitro is mediated by two different human E2-E3 pairs. Nucleic acids research *40*, 10394-10407.

Masutani, C., Kusumoto, R., Iwai, S., and Hanaoka, F. (2000). Mechanisms of accurate translesion synthesis by human DNA polymerase eta. The EMBO journal *19*, 3100-3109.

Masutani, C., Kusumoto, R., Yamada, A., Dohmae, N., Yokoi, M., Yuasa, M., Araki, M., Iwai, S., Takio, K., and Hanaoka, F. (1999). The XPV (xeroderma pigmentosum variant) gene encodes human DNA polymerase eta. Nature *399*, 700-704.

Maya-Mendoza, A., Petermann, E., Gillespie, D.A., Caldecott, K.W., and Jackson, D.A. (2007). Chk1 regulates the density of active replication origins during the vertebrate S phase. The EMBO journal *26*, 2719-2731.

McCulloch, S.D., Kokoska, R.J., Masutani, C., Iwai, S., Hanaoka, F., and Kunkel, T.A. (2004). Preferential cis-syn thymine dimer bypass by DNA polymerase eta occurs with biased fidelity. Nature *428*, 97-100.

McCulloch, S.D., and Kunkel, T.A. (2008). The fidelity of DNA synthesis by eukaryotic replicative and translesion synthesis polymerases. Cell Research *18*, 148-161.

McInerney, P., and O'Donnell, M. (2004). Functional uncoupling of twin polymerases: mechanism of polymerase dissociation from a lagging-strand block. The Journal of biological chemistry *279*, 21543-21551.

Mendez, J., and Stillman, B. (2000). Chromatin association of human origin recognition complex, cdc6, and minichromosome maintenance proteins during the cell cycle: assembly of prereplication complexes in late mitosis. Molecular and cellular biology *20*, 8602-8612.

Mendez, J., Zou-Yang, X.H., Kim, S.Y., Hidaka, M., Tansey, W.P., and Stillman, B. (2002). Human origin recognition complex large subunit is degraded by ubiquitin-mediated proteolysis after initiation of DNA replication. Molecular cell *9*, 481-491.

Mijic, S., Zellweger, R., Chappidi, N., Berti, M., Jacobs, K., Mutreja, K., Ursich, S., Ray Chaudhuri, A., Nussenzweig, A., Janscak, P.*, et al.* (2017). Replication fork reversal triggers fork degradation in BRCA2-defective cells. Nature communications *8*, 859.

Minca, E.C., and Kowalski, D. (2010). Multiple Rad5 activities mediate sister chromatid recombination to bypass DNA damage at stalled replication forks. Molecular cell *38*, 649-661.

Mislak, A.C., and Anderson, K.S. (2016). Insights into the Molecular Mechanism of Polymerization and Nucleoside Reverse Transcriptase Inhibitor Incorporation by Human PrimPol. Antimicrobial agents and chemotherapy *60*, 561-569.

Miyabe, I., Kunkel, T.A., and Carr, A.M. (2011). The major roles of DNA polymerases epsilon and delta at the eukaryotic replication fork are evolutionarily conserved. PLoS genetics *7*, e1002407.

Miyabe, I., Mizuno, K.I., Keszthelyi, A., Daigaku, Y., Skouteri, M., Mohebi, S., Kunkel, T.A., Murray, J.M., and Carr, A.M. (2015). Polymerase δ replicates both strands after homologous recombination-dependent fork restart. Nature structural & molecular biology *22*, 932-938.

Mizuno, K.I., Lambert, S., Baldacci, G., Murray, J.M., and Carr, A.M. (2009). Nearby inverted repeats fuse to generate acentric and dicentric palindromic chromosomes by a replication template exchange mechanism. Genes & development *23*, 2876-2886.

Mohiuddin, M., Evans, T.J., Rahman, M.M., Keka, I.S., Tsuda, M., Sasanuma, H., and Takeda, S. (2018). SUMOylation of PCNA by PIAS1 and PIAS4 promotes template switch in the chicken and human B cell lines. Proceedings of the National Academy of Sciences *115*, 12793.

Moiseeva, T.N., and Bakkenist, C.J. (2018). Regulation of the initiation of DNA replication in human cells. DNA repair *72*, 99-106.

Moldovan, G.-L., Pfander, B., and Jentsch, S. (2007). PCNA, the Maestro of the Replication Fork. Cell *129*, 665-679.

Moreno, S.P., Bailey, R., Campion, N., Herron, S., and Gambus, A. (2014). Polyubiquitylation drives replisome disassembly at the termination of DNA replication. Science (New York, NY) *346*, 477-481.

Motegi, A., Liaw, H.-J., Lee, K.-Y., Roest, H.P., Maas, A., Wu, X., Moinova, H., Markowitz, S.D., Ding, H., Hoeijmakers, J.H.J.*, et al.* (2008). Polyubiquitination of proliferating cell nuclear antigen by HLTF and SHPRH prevents genomic instability from stalled replication forks. Proceedings of the National Academy of Sciences of the United States of America *105*, 12411-12416.

Mouron, S., Rodriguez-Acebes, S., Martinez-Jimenez, M.I., Garcia-Gomez, S., Chocron, S., Blanco, L., and Mendez, J. (2013). Repriming of DNA synthesis at stalled replication forks by human PrimPol. Nature structural & molecular biology *20*, 1383-1389.

Moyer, S.E., Lewis, P.W., and Botchan, M.R. (2006). Isolation of the Cdc45/Mcm2-7/GINS (CMG) complex, a candidate for the eukaryotic DNA replication fork helicase. Proceedings of the National Academy of Sciences of the United States of America *103*, 10236-10241.

Mukherjee, C., Tripathi, V., Manolika, E.M., Heijink, A.M., Ricci, G., Merzouk, S., de Boer, H.R., Demmers, J., van Vugt, M.A.T.M., and Ray Chaudhuri, A. (2019). RIF1 promotes replication fork protection and efficient restart to maintain genome stability. Nature communications *10*, 3287-3287.

Murante, R.S., Henricksen, L.A., and Bambara, R.A. (1998). Junction ribonuclease: an activity in Okazaki fragment processing. Proceedings of the National Academy of Sciences of the United States of America *95*, 2244-2249.

Natale, D.A., Li, C.J., Sun, W.H., and DePamphilis, M.L. (2000). Selective instability of Orc1 protein accounts for the absence of functional origin recognition complexes during the M-G(1) transition in mammals. The EMBO journal *19*, 2728-2738.

Nguyen, M.O., Jalan, M., Morrow, C.A., Osman, F., and Whitby, M.C. (2015). Recombination occurs within minutes of replication blockage by RTS1 producing restarted forks that are prone to collapse. eLife *4*, e04539.

Nick McElhinny, S.A., Gordenin, D.A., Stith, C.M., Burgers, P.M., and Kunkel, T.A. (2008). Division of labor at the eukaryotic replication fork. Molecular cell *30*, 137-144.

Nick McElhinny, S.A., and Ramsden, D.A. (2003). Polymerase Mu Is a DNA-Directed DNA/RNA Polymerase. Molecular and cellular biology *23*, 2309.

Nick McElhinny, S.A., Watts, B.E., Kumar, D., Watt, D.L., Lundstrom, E.B., Burgers, P.M., Johansson, E., Chabes, A., and Kunkel, T.A. (2010). Abundant ribonucleotide incorporation into DNA by yeast replicative polymerases. Proceedings of the National Academy of Sciences of the United States of America *107*, 4949-4954.

Nicolae, C.M., Aho, E.R., Vlahos, A.H.S., Choe, K.N., De, S., Karras, G.I., and Moldovan, G.-L. (2014). The ADP-ribosyltransferase PARP10/ARTD10 interacts with proliferating cell nuclear antigen (PCNA) and is required for DNA damage tolerance. The Journal of biological chemistry *289*, 13627-13637.

Nieminuszczy, J., Broderick, R., Bellani, M.A., Smethurst, E., Schwab, R.A., Cherdyntseva, V., Evmorfopoulou, T., Lin, Y.-L., Minczuk, M., Pasero, P.*, et al.* (2019). EXD2 Protects Stressed Replication Forks and Is Required for Cell Viability in the Absence of BRCA1/2. Molecular cell *75*, 605-619.e606.

Niimi, A., Hopkins, S.R., Downs, J.A., and Masutani, C. (2015). The BAH domain of BAF180 is required for PCNA ubiquitination. Mutat Res *779*, 16-23.

Nimonkar, A.V., Özsoy, A.Z., Genschel, J., Modrich, P., and Kowalczykowski, S.C. (2008). Human exonuclease 1 and BLM helicase interact to resect DNA and initiate DNA repair. Proceedings of the National Academy of Sciences *105*, 16906.

Nishimura, K., Fukagawa, T., Takisawa, H., Kakimoto, T., and Kanemaki, M. (2009). An auxin-based degron system for the rapid depletion of proteins in nonplant cells. Nat Methods *6*, 917-922.

Nishitani, H., Sugimoto, N., Roukos, V., Nakanishi, Y., Saijo, M., Obuse, C., Tsurimoto, T., Nakayama, K.I., Nakayama, K., Fujita, M.*, et al.* (2006). Two E3 ubiquitin ligases, SCF-Skp2 and DDB1-Cul4, target human Cdt1 for proteolysis. The EMBO journal *25*, 1126-1136.

Niu, H., Potenski, C.J., Epshtein, A., Sung, P., and Klein, H.L. (2016). Roles of DNA helicases and Exo1 in the avoidance of mutations induced by Top1-mediated cleavage at ribonucleotides in DNA. Cell cycle (Georgetown, Tex) *15*, 331-336.

Nowicka, U., Zhang, D., Walker, O., Krutauz, D., Castaneda, C.A., Chaturvedi, A., Chen, T.Y., Reis, N., Glickman, M.H., and Fushman, D. (2015). DNA-damage-inducible 1 protein (Ddi1) contains an uncharacteristic ubiquitin-like domain that binds ubiquitin. Structure (London, England : 1993) *23*, 542-557.

Nowotny, M., Cerritelli, S.M., Ghirlando, R., Gaidamakov, S.A., Crouch, R.J., and Yang, W. (2008). Specific recognition of RNA/DNA hybrid and enhancement of human RNase H1 activity by HBD. The EMBO journal *27*, 1172-1181.

Nowotny, M., Gaidamakov, S.A., Ghirlando, R., Cerritelli, S.M., Crouch, R.J., and Yang, W. (2007). Structure of Human RNase H1 Complexed with an RNA/DNA Hybrid: Insight into HIV Reverse Transcription. Molecular Cell *28*, 264-276.

O'Donnell, M., Langston, L., and Stillman, B. (2013). Principles and concepts of DNA replication in bacteria, archaea, and eukarya. Cold Spring Harbor perspectives in biology *5*.

Oda, H., Nakagawa, K., Abe, J., Awaya, T., Funabiki, M., Hijikata, A., Nishikomori, R., Funatsuka, M., Ohshima, Y., Sugawara, Y.*, et al.* (2014). Aicardi-Goutieres syndrome is caused by IFIH1 mutations. American journal of human genetics *95*, 121-125.

Ohle, C., Tesorero, R., Schermann, G., Dobrev, N., Sinning, I., and Fischer, T. (2016). Transient RNA-DNA Hybrids Are Required for Efficient Double-Strand Break Repair. Cell *167*, 1001-1013.e1007.

Ohta, S., Tatsumi, Y., Fujita, M., Tsurimoto, T., and Obuse, C. (2003). The ORC1 cycle in human cells: II. Dynamic changes in the human ORC complex during the cell cycle. The Journal of biological chemistry *278*, 41535-41540.

Ohtani, N., Haruki, M., Morikawa, M., Crouch, R.J., Itaya, M., and Kanaya, S. (1999). Identification of the Genes Encoding Mn2+-Dependent RNase HII and Mg2+-Dependent RNase HIII from Bacillus subtilis: Classification of RNases H into Three Families. Biochemistry *38*, 605-618.

Okazaki, R., Okazaki, T., Sakabe, K., Sugimoto, K., and Sugino, A. (1968). Mechanism of DNA chain growth. I. Possible discontinuity and unusual secondary structure of newly synthesized chains. Proceedings of the National Academy of Sciences of the United States of America *59*, 598-605.

Orans, J., McSweeney, E.A., Iyer, R.R., Hast, M.A., Hellinga, H.W., Modrich, P., and Beese, L.S. (2011). Structures of human exonuclease 1 DNA complexes suggest a unified mechanism for nuclease family. Cell *145*, 212-223.

Park, J.M., Yang, S.W., Yu, K.R., Ka, S.H., Lee, S.W., Seol, J.H., Jeon, Y.J., and Chung, C.H. (2014). Modification of PCNA by ISG15 plays a crucial role in termination of error-prone translesion DNA synthesis. Molecular cell *54*, 626-638.

Parker, W.B., and Cheng, Y.C. (1987). Inhibition of DNA primase by nucleoside triphosphates and their arabinofuranosyl analogs. Molecular pharmacology *31*, 146-151.

Parrilla-Castellar, E.R., and Karnitz, L.M. (2003). Cut5 is required for the binding of Atr and DNA polymerase alpha to genotoxin-damaged chromatin. The Journal of biological chemistry *278*, 45507-45511.

Perkins, G., and Diffley, J.F. (1998). Nucleotide-dependent prereplicative complex assembly by Cdc6p, a homolog of eukaryotic and prokaryotic clamp-loaders. Molecular cell *2*, 23-32.

Petermann, E., and Caldecott, K.W. (2006). Evidence that the ATR/Chk1 pathway maintains normal replication fork progression during unperturbed S phase. Cell cycle (Georgetown, Tex) *5*, 2203-2209.

Petermann, E., and Helleday, T. (2010). Pathways of mammalian replication fork restart. Nature reviews Molecular cell biology *11*, 683-687.

Petermann, E., Maya-Mendoza, A., Zachos, G., Gillespie, D.A., Jackson, D.A., and Caldecott, K.W. (2006). Chk1 requirement for high global rates of replication fork progression during normal vertebrate S phase. Molecular and cellular biology *26*, 3319-3326.

Petermann, E., Orta, M.L., Issaeva, N., Schultz, N., and Helleday, T. (2010a). Hydroxyurea-stalled replication forks become progressively inactivated and require two different RAD51-mediated pathways for restart and repair. Molecular cell *37*, 492-502.

Petermann, E., Woodcock, M., and Helleday, T. (2010b). Chk1 promotes replication fork progression by controlling replication initiation. Proceedings of the National Academy of Sciences *107*, 16090.

Petersen, B.O., Wagener, C., Marinoni, F., Kramer, E.R., Melixetian, M., Lazzerini Denchi, E., Gieffers, C., Matteucci, C., Peters, J.M., and Helin, K. (2000). Cell cycle- and cell growth-regulated proteolysis of mammalian CDC6 is dependent on APC-CDH1. Genes & development *14*, 2330-2343.

Piberger, A.L., Walker, A.K., Morris, J.R., Bryant, H.E., and Petermann, E. (2019). PrimPol-dependent single-stranded gap formation mediates homologous recombination at bulky DNA adducts. bioRxiv, 773242.

Pokatayev, V., Hasin, N., Chon, H., Cerritelli, S.M., Sakhuja, K., Ward, J.M., Morris, H.D., Yan, N., and Crouch, R.J. (2016). RNase H2 catalytic core Aicardi-Goutieres syndrome-related mutant invokes cGAS-STING innate immune-sensing pathway in mice. The Journal of experimental medicine *213*, 329-336.

Povlsen, L.K., Beli, P., Wagner, S.A., Poulsen, S.L., Sylvestersen, K.B., Poulsen, J.W., Nielsen, M.L., Bekker-Jensen, S., Mailand, N., and Choudhary, C. (2012). Systems-wide analysis of ubiquitylation dynamics reveals a key role for PAF15 ubiquitylation in DNA-damage bypass. Nature cell biology *14*, 1089-1098.

Prakash, L. (1981). Characterization of postreplication repair in Saccharomyces cerevisiae and effects of rad6, rad18, rev3 and rad52 mutations. Molecular and General Genetics MGG *184*, 471-478.

Prelich, G., Tan, C.-K., Kostura, M., Mathews, M.B., So, A.G., Downey, K.M., and Stillman, B. (1987). Functional identity of proliferating cell nuclear antigen and a DNA polymerase-δ auxiliary protein. Nature *326*, 517-520.

Prestel, A., Wichmann, N., Martins, J.M., Marabini, R., Kassem, N., Broendum, S.S., Otterlei, M., Nielsen, O., Willemoes, M., Ploug, M.*, et al.* (2019). The PCNA interaction motifs revisited: thinking outside the PIP-box. Cellular and molecular life sciences : CMLS *76*, 4923-4943.

Pryor, J.M., Conlin, M.P., Carvajal-Garcia, J., Luedeman, M.E., Luthman, A.J., Small, G.W., and Ramsden, D.A. (2018). Ribonucleotide incorporation enables repair of

chromosome breaks by nonhomologous end joining. Science (New York, NY) *361*, 1126-1129.

Pursell, Z.F., Isoz, I., Lundstrom, E.B., Johansson, E., and Kunkel, T.A. (2007). Yeast DNA polymerase epsilon participates in leading-strand DNA replication. Science (New York, NY) *317*, 127-130.

Pursell, Z.F., and Kunkel, T.A. (2008). DNA polymerase epsilon: a polymerase of unusual size (and complexity). Prog Nucleic Acid Res Mol Biol *82*, 101-145.

Qiu, J., Qian, Y., Chen, V., Guan, M.X., and Shen, B. (1999a). Human exonuclease 1 functionally complements its yeast homologues in DNA recombination, RNA primer removal, and mutation avoidance. The Journal of biological chemistry *274*, 17893-17900.

Qiu, J., Qian, Y., Frank, P., Wintersberger, U., and Shen, B. (1999b). Saccharomyces cerevisiae RNase H(35) functions in RNA primer removal during lagging-strand DNA synthesis, most efficiently in cooperation with Rad27 nuclease. Molecular and cellular biology *19*, 8361-8371.

Quinet, A., Tirman, S., Jackson, J., Šviković, S., Lemaçon, D., Carvajal-Maldonado, D., González-Acosta, D., Vessoni, A.T., Cybulla, E., Wood, M.*, et al.* (2019). PRIMPOL-Mediated Adaptive Response Suppresses Replication Fork Reversal in BRCA-Deficient Cells. Molecular cell.

Quinet, A., Vessoni, A.T., Rocha, C.R.R., Gottifredi, V., Biard, D., Sarasin, A., Menck, C.F.M., and Stary, A. (2014). Gap-filling and bypass at the replication fork are both active mechanisms for tolerance of low-dose ultraviolet-induced DNA damage in the human genome. DNA repair *14*, 27-38.

Raman, M., Havens, C.G., Walter, J.C., and Harper, J.W. (2011). A genome-wide screen identifies p97 as an essential regulator of DNA damage-dependent CDT1 destruction. Molecular cell *44*, 72-84.

Randell, J.C., Bowers, J.L., Rodriguez, H.K., and Bell, S.P. (2006). Sequential ATP hydrolysis by Cdc6 and ORC directs loading of the Mcm2-7 helicase. Molecular cell *21*, 29-39.

Rao, P.N., and Johnson, R.T. (1970). Mammalian Cell Fusion : Studies on the Regulation of DNA Synthesis and Mitosis. Nature *225*, 159-164.

Rechkoblit, O., Gupta, Y.K., Malik, R., Rajashankar, K.R., Johnson, R.E., Prakash, L., Prakash, S., and Aggarwal, A.K. (2016). Structure and mechanism of human PrimPol, a DNA polymerase with primase activity. Sci Adv *2*, e1601317-e1601317.

Rechkoblit, O., Zhang, Y., Guo, D., Wang, Z., Amin, S., Krzeminsky, J., Louneva, N., and Geacintov, N.E. (2002). trans-Lesion synthesis past bulky benzo[a]pyrene diol epoxide N2-dG and N6-dA lesions catalyzed by DNA bypass polymerases. The Journal of biological chemistry *277*, 30488-30494.

Reichard, P., and Ehrenberg, A. (1983). Ribonucleotide reductase--a radical enzyme. Science (New York, NY) *221*, 514-519.

Reijns, M.A., Rabe, B., Rigby, R.E., Mill, P., Astell, K.R., Lettice, L.A., Boyle, S., Leitch, A., Keighren, M., Kilanowski, F.*, et al.* (2012). Enzymatic removal of ribonucleotides from DNA is essential for mammalian genome integrity and development. Cell *149*, 1008-1022.

Remus, D., Beuron, F., Tolun, G., Griffith, J.D., Morris, E.P., and Diffley, J.F. (2009). Concerted loading of Mcm2-7 double hexamers around DNA during DNA replication origin licensing. Cell *139*, 719-730.

Rialland, M., Sola, F., and Santocanale, C. (2002). Essential role of human CDT1 in DNA replication and chromatin licensing. Journal of cell science *115*, 1435-1440.

Rice, G., Patrick, T., Parmar, R., Taylor, C.F., Aeby, A., Aicardi, J., Artuch, R., Montalto, S.A., Bacino, C.A., Barroso, B.*, et al.* (2007). Clinical and molecular phenotype of Aicardi-Goutieres syndrome. American journal of human genetics *81*, 713-725.

Rice, G.I., Bond, J., Asipu, A., Brunette, R.L., Manfield, I.W., Carr, I.M., Fuller, J.C., Jackson, R.M., Lamb, T., Briggs, T.A.*, et al.* (2009). Mutations involved in Aicardi-Goutieres syndrome implicate SAMHD1 as regulator of the innate immune response. Nature genetics *41*, 829-832.

Rice, G.I., Kasher, P.R., Forte, G.M., Mannion, N.M., Greenwood, S.M., Szynkiewicz, M., Dickerson, J.E., Bhaskar, S.S., Zampini, M., Briggs, T.A.*, et al.* (2012). Mutations in ADAR1 cause Aicardi-Goutieres syndrome associated with a type I interferon signature. Nature genetics *44*, 1243-1248.

Rodero, M.P., and Crow, Y.J. (2016). Type I interferon-mediated monogenic autoinflammation: The type I interferonopathies, a conceptual overview. The Journal of experimental medicine *213*, 2527-2538.

Rodriguez, C.I., Buchholz, F., Galloway, J., Sequerra, R., Kasper, J., Ayala, R., Stewart, A.F., and Dymecki, S.M. (2000). High-efficiency deleter mice show that FLPe is an alternative to Cre-loxP. Nat Genet *25*, 139-140.

Rowles, A., Tada, S., and Blow, J.J. (1999). Changes in association of the Xenopus origin recognition complex with chromatin on licensing of replication origins. Journal of cell science *112 (Pt 12)*, 2011-2018.

Rupp, W.D., and Howard-Flanders, P. (1968). Discontinuities in the DNA synthesized in an excision-defective strain of Escherichia coli following ultraviolet irradiation. Journal of molecular biology *31*, 291-304.

Saeki, Y. (2017). Ubiquitin recognition by the proteasome. Journal of biochemistry *161*, 113-124.

Saha, P., Chen, J., Thome, K.C., Lawlis, S.J., Hou, Z.H., Hendricks, M., Parvin, J.D., and Dutta, A. (1998). Human CDC6/Cdc18 associates with Orc1 and cyclin-cdk and is selectively eliminated from the nucleus at the onset of S phase. Molecular and cellular biology *18*, 2758-2767.

Sakabe, K., and Okazaki, R. (1966). A unique property of the replicating region of chromosomal DNA. Biochimica et biophysica acta *129*, 651-654.

Saldivar, J.C., Cortez, D., and Cimprich, K.A. (2017). The essential kinase ATR: ensuring faithful duplication of a challenging genome. Nature reviews Molecular cell biology *18*, 622-636.

Saldivar, J.C., Hamperl, S., Bocek, M.J., Chung, M., Bass, T.E., Cisneros-Soberanis, F., Samejima, K., Xie, L., Paulson, J.R., Earnshaw, W.C.*, et al.* (2018). An intrinsic S/G₂ checkpoint enforced by ATR. Science *361*, 806.

Sale, J.E. (2013). Translesion DNA synthesis and mutagenesis in eukaryotes. Cold Spring Harbor perspectives in biology *5*, a012708-a012708.

Sale, J.E., Lehmann, A.R., and Woodgate, R. (2012). Y-family DNA polymerases and their role in tolerance of cellular DNA damage. Nature Reviews Molecular Cell Biology *13*, 141.

Sasaki, T., Kanno, T., Liang, S.C., Chen, P.Y., Liao, W.W., Lin, W.D., Matzke, A.J., and Matzke, M. (2015). An Rtf2 Domain-Containing Protein Influences Pre-mRNA Splicing and Is Essential for Embryonic Development in Arabidopsis thaliana. Genetics *200*, 523-535.

Schiavone, D., Jozwiakowski, S.K., Romanello, M., Guilbaud, G., Guilliam, T.A., Bailey, L.J., Sale, J.E., and Doherty, A.J. (2016). PrimPol Is Required for Replicative Tolerance of G Quadruplexes in Vertebrate Cells. Molecular cell *61*, 161-169.

Schlacher, K., Christ, N., Siaud, N., Egashira, A., Wu, H., and Jasin, M. (2011). Double-strand break repair-independent role for BRCA2 in blocking stalled replication fork degradation by MRE11. Cell *145*, 529-542.

Schlacher, K., Wu, H., and Jasin, M. (2012). A distinct replication fork protection pathway connects Fanconi anemia tumor suppressors to RAD51-BRCA1/2. Cancer cell *22*, 106-116.

Schneider, A., Smith, R.W., Kautz, A.R., Weisshart, K., Grosse, F., and Nasheuer, H.P. (1998). Primase activity of human DNA polymerase alpha-primase. Divalent cations stabilize the enzyme activity of the p48 subunit. The Journal of biological chemistry *273*, 21608-21615.

Sekiguchi, J., and Shuman, S. (1997). Site-Specific Ribonuclease Activity of Eukaryotic DNA Topoisomerase I. Molecular cell *1*, 89-97.

Sheaff, R.J., and Kuchta, R.D. (1993). Mechanism of calf thymus DNA primase: slow initiation, rapid polymerization, and intelligent termination. Biochemistry *32*, 3027-3037.

Sheaff, R.J., Kuchta, R.D., and Ilsley, D. (1994). Calf Thymus DNA Polymerase .alpha.-Primase: "Communication" and Primer.cntdot.Template Movement between the Two Active Sites. Biochemistry *33*, 2247-2254.

Siddik, Z.H. (2003). Cisplatin: mode of cytotoxic action and molecular basis of resistance. Oncogene *22*, 7265-7279.

Sidorova, J.M., Kehrli, K., Mao, F., and Monnat, R., Jr. (2013). Distinct functions of human RECQ helicases WRN and BLM in replication fork recovery and progression after hydroxyurea-induced stalling. DNA repair *12*, 128-139.

Singh, A., and Xu, Y.-J. (2016). The Cell Killing Mechanisms of Hydroxyurea. Genes *7*, 99.

Singh, B., Bisht, K.K., Upadhyay, U., Kushwaha, A.C., Nanda, J.S., Srivastava, S., Saini, J.K., Klar, A.J.S., and Singh, J. (2019). Role of Cdc23/Mcm10 in generating the ribonucleotide imprint at the mat1 locus in fission yeast. Nucleic acids research *47*, 3422-3433.

Singh, J. (2019). RNA insertion in DNA as the imprint moiety: the fission yeast paradigm. Curr Genet *65*, 1301-1306.

Singh, J., and Klar, A.J. (1993). DNA polymerase-alpha is essential for mating-type switching in fission yeast. Nature *361*, 271-273.

Sirbu, B.M., McDonald, W.H., Dungrawala, H., Badu-Nkansah, A., Kavanaugh, G.M., Chen, Y., Tabb, D.L., and Cortez, D. (2013). Identification of proteins at active, stalled, and collapsed replication forks using isolation of proteins on nascent DNA (iPOND) coupled with mass spectrometry. The Journal of biological chemistry *288*, 31458-31467.

Siva, M., Svoboda, M., Veverka, V., Trempe, J.F., Hofmann, K., Kozisek, M., Hexnerova, R., Sedlak, F., Belza, J., Brynda, J.*, et al.* (2016). Human DNA-Damage-Inducible 2 Protein Is Structurally and Functionally Distinct from Its Yeast Ortholog. Scientific reports *6*, 30443.

Smith-Roe, S.L., Patel, S.S., Zhou, Y., Simpson, D.A., Rao, S., Ibrahim, J.G., Cordeiro-Stone, M., and Kaufmann, W.K. (2013). Separation of intra-S checkpoint protein contributions to DNA replication fork protection and genomic stability in normal human fibroblasts. Cell cycle (Georgetown, Tex) *12*, 332-345.

Sogo, J.M., Lopes, M., and Foiani, M. (2002). Fork reversal and ssDNA accumulation at stalled replication forks owing to checkpoint defects. Science (New York, NY) *297*, 599-602.

Sontheimer, D.-B.J. (2011). Functional characterization of proteins involved in cell cycle by structure-based computational methods (Technische Universitat Dresden).

Sorensen, C.S., Syljuasen, R.G., Falck, J., Schroeder, T., Ronnstrand, L., Khanna, K.K., Zhou, B.B., Bartek, J., and Lukas, J. (2003). Chk1 regulates the S phase checkpoint by coupling the physiological turnover and ionizing radiation-induced accelerated proteolysis of Cdc25A. Cancer cell *3*, 247-258.

Sotiriou, S.K., Kamileri, I., Lugli, N., Evangelou, K., Da-Ré, C., Huber, F., Padayachy, L., Tardy, S., Nicati, N.L., Barriot, S.*, et al.* (2016). Mammalian RAD52 Functions in Break-Induced Replication Repair of Collapsed DNA Replication Forks. Molecular cell *64*, 1127-1134.

Sparks, J.L., and Burgers, P.M. (2015). Error-free and mutagenic processing of topoisomerase 1-provoked damage at genomic ribonucleotides. The EMBO journal *34*, 1259-1269.

Sparks, J.L., Chistol, G., Gao, A.O., Räschle, M., Larsen, N.B., Mann, M., Duxin, J.P., and Walter, J.C. (2019). The CMG Helicase Bypasses DNA-Protein Cross-Links to Facilitate Their Repair. Cell *176*, 167-181.e121.

Sparks, J.L., Chon, H., Cerritelli, S.M., Kunkel, T.A., Johansson, E., Crouch, R.J., and Burgers, P.M. (2012). RNase H2-initiated ribonucleotide excision repair. Molecular cell *47*, 980-986.

Starokadomskyy, P., Gemelli, T., Rios, J.J., Xing, C., Wang, R.C., Li, H., Pokatayev, V., Dozmorov, I., Khan, S., Miyata, N.*, et al.* (2016). DNA polymerase-alpha regulates the activation of type I interferons through cytosolic RNA:DNA synthesis. Nature immunology *17*, 495-504.

Stein, H., and Hausen, P. (1969). Enzyme from calf thymus degrading the RNA moiety of DNA-RNA Hybrids: effect on DNA-dependent RNA polymerase. Science (New York, NY) *166*, 393-395.

Stelter, P., and Ulrich, H.D. (2003). Control of spontaneous and damage-induced mutagenesis by SUMO and ubiquitin conjugation. Nature *425*, 188-191.

Sturzenegger, A., Burdova, K., Kanagaraj, R., Levikova, M., Pinto, C., Cejka, P., and Janscak, P. (2014). DNA2 cooperates with the WRN and BLM RecQ helicases to mediate long-range DNA end resection in human cells. The Journal of biological chemistry *289*, 27314-27326.

Sugimoto, N., Tatsumi, Y., Tsurumi, T., Matsukage, A., Kiyono, T., Nishitani, H., and Fujita, M. (2004). Cdt1 phosphorylation by cyclin A-dependent kinases negatively regulates its function without affecting geminin binding. The Journal of biological chemistry *279*, 19691-19697.

Sun, J., Shi, Y., Georgescu, R.E., Yuan, Z., Chait, B.T., Li, H., and O'Donnell, M.E. (2015). The architecture of a eukaryotic replisome. Nature structural & molecular biology *22*, 976-982.

Suzuki, N., Ohashi, E., Kolbanovskiy, A., Geacintov, N.E., Grollman, A.P., Ohmori, H., and Shibutani, S. (2002). Translesion synthesis by human DNA polymerase kappa on a DNA template containing a single stereoisomer of dG-(+)- or dG-(-)-anti-N(2)-BPDE (7,8-dihydroxy-anti-9,10-epoxy-7,8,9,10-tetrahydrobenzo[a]pyrene). Biochemistry *41*, 6100-6106.

Svoboda, D.L., and Vos, J.M. (1995). Differential replication of a single, UV-induced lesion in the leading or lagging strand by a human cell extract: fork uncoupling or gap

formation. Proceedings of the National Academy of Sciences of the United States of America *92*, 11975-11979.

Svoboda, M., Konvalinka, J., Trempe, J.-F., and Grantz Saskova, K. (2019). The yeast proteases Ddi1 and Wss1 are both involved in the DNA replication stress response. DNA repair *80*, 45-51.

Tada, S., Li, A., Maiorano, D., Mechali, M., and Blow, J.J. (2001). Repression of origin assembly in metaphase depends on inhibition of RLF-B/Cdt1 by geminin. Nature cell biology *3*, 107-113.

Taglialatela, A., Alvarez, S., Leuzzi, G., Sannino, V., Ranjha, L., Huang, J.W., Madubata, C., Anand, R., Levy, B., Rabadan, R.*, et al.* (2017). Restoration of Replication Fork Stability in BRCA1- and BRCA2-Deficient Cells by Inactivation of SNF2-Family Fork Remodelers. Molecular cell *68*, 414-430.e418.

Takeda, D.Y., Shibata, Y., Parvin, J.D., and Dutta, A. (2005). Recruitment of ORC or CDC6 to DNA is sufficient to create an artificial origin of replication in mammalian cells. Genes & development *19*, 2827-2836.

Tan, C.K., Castillo, C., So, A.G., and Downey, K.M. (1986). An auxiliary protein for DNA polymerase-delta from fetal calf thymus. The Journal of biological chemistry *261*, 12310-12316.

Tanaka, S., and Araki, H. (2013). Helicase activation and establishment of replication forks at chromosomal origins of replication. Cold Spring Harbor perspectives in biology *5*, a010371.

Tatsumi, Y., Ohta, S., Kimura, H., Tsurimoto, T., and Obuse, C. (2003). The ORC1 cycle in human cells: I. cell cycle-regulated oscillation of human ORC1. The Journal of biological chemistry *278*, 41528-41534.

Taylor, M.R.G., and Yeeles, J.T.P. (2018). The Initial Response of a Eukaryotic Replisome to DNA Damage. Molecular cell *70*, 1067-1080.e1012.

Taylor, M.R.G., and Yeeles, J.T.P. (2019). Dynamics of Replication Fork Progression Following Helicase-Polymerase Uncoupling in Eukaryotes. Journal of molecular biology *431*, 2040-2049.

Teixeira-Silva, A., Ait Saada, A., Hardy, J., Iraqui, I., Nocente, M.C., Fréon, K., and Lambert, S.A.E. (2017). The end-joining factor Ku acts in the end-resection of double strand break-free arrested replication forks. Nature communications *8*, 1982-1982.

Terai, K., Abbas, T., Jazaeri, A.A., and Dutta, A. (2010). CRL4(Cdt2) E3 ubiquitin ligase monoubiquitinates PCNA to promote translesion DNA synthesis. Molecular cell *37*, 143-149.

Thangavel, S., Berti, M., Levikova, M., Pinto, C., Gomathinayagam, S., Vujanovic, M., Zellweger, R., Moore, H., Lee, E.H., Hendrickson, E.A.*, et al.* (2015). DNA2 drives processing and restart of reversed replication forks in human cells. The Journal of cell biology *208*, 545-562.

Tissier, A., McDonald, J.P., Frank, E.G., and Woodgate, R. (2000). poliota, a remarkably error-prone human DNA polymerase. Genes & development *14*, 1642-1650.

Tonzi, P., Yin, Y., Lee, C.W.T., Rothenberg, E., and Huang, T.T. (2018). Translesion polymerase kappa-dependent DNA synthesis underlies replication fork recovery. eLife *7*, e41426.

Torres-Ramos, C.A., Prakash, S., and Prakash, L. (2002). Requirement of RAD5 and MMS2 for postreplication repair of UV-damaged DNA in Saccharomyces cerevisiae. Molecular and cellular biology *22*, 2419-2426.

Tsuda, M., Ogawa, S., Ooka, M., Kobayashi, K., Hirota, K., Wakasugi, M., Matsunaga, T., Sakuma, T., Yamamoto, T., Chikuma, S.*, et al.* (2019). PDIP38/PolDIP2 controls the DNA damage tolerance pathways by increasing the relative usage of translesion DNA synthesis over template switching. PloS one *14*, e0213383.

Tsurimoto, T., Shinozaki, A., Yano, M., Seki, M., and Enomoto, T. (2005). Human Werner helicase interacting protein 1 (WRNIP1) functions as a novel modulator for DNA polymerase delta. Genes to cells : devoted to molecular & cellular mechanisms *10*, 13-22.

Turchi, J.J., Huang, L., Murante, R.S., Kim, Y., and Bambara, R.A. (1994). Enzymatic completion of mammalian lagging-strand DNA replication. Proceedings of the National Academy of Sciences of the United States of America *91*, 9803-9807.

U.S. Department of Energy Office of Science, O.o.B.a.E.R. (2016). Human Genome Project Information Archive 1990-2003.

Uehara, R., Cerritelli, S.M., Hasin, N., Sakhuja, K., London, M., Iranzo, J., Chon, H., Grinberg, A., and Crouch, R.J. (2018). Two RNase H2 Mutants with Differential rNMP Processing Activity Reveal a Threshold of Ribonucleotide Tolerance for Embryonic Development. Cell reports *25*, 1135-1145.e1135.

Unk, I., Hajdú, I., Fátyol, K., Hurwitz, J., Yoon, J.-H., Prakash, L., Prakash, S., and Haracska, L. (2008). Human HLTF functions as a ubiquitin ligase for proliferating cell nuclear antigen polyubiquitination. Proceedings of the National Academy of Sciences of the United States of America *105*, 3768-3773.

Unk, I., Hajdú, I., Fátyol, K., Szakál, B., Blastyák, A., Bermudez, V., Hurwitz, J., Prakash, L., Prakash, S., and Haracska, L. (2006). Human SHPRH is a ubiquitin ligase for Mms2–Ubc13-dependent polyubiquitylation of proliferating cell nuclear antigen. Proceedings of the National Academy of Sciences *103*, 18107.

Van, C., Yan, S., Michael, W.M., Waga, S., and Cimprich, K.A. (2010). Continued primer synthesis at stalled replication forks contributes to checkpoint activation. The Journal of cell biology *189*, 233-246.

Vanoli, F., Fumasoni, M., Szakal, B., Maloisel, L., and Branzei, D. (2010). Replication and Recombination Factors Contributing to Recombination-Dependent Bypass of DNA Lesions by Template Switch. PLoS genetics *6*, e1001205.

Vassilev, L.T., Tovar, C., Chen, S., Knezevic, D., Zhao, X., Sun, H., Heimbrook, D.C., and Chen, L. (2006). Selective small-molecule inhibitor reveals critical mitotic functions of human CDK1. Proceedings of the National Academy of Sciences of the United States of America *103*, 10660-10665.

Vassileva, I., Yanakieva, I., Peycheva, M., Gospodinov, A., and Anachkova, B. (2014). The mammalian INO80 chromatin remodeling complex is required for replication stress recovery. Nucleic acids research *42*, 9074-9086.

Venter, J.C., Adams, M.D., Myers, E.W., Li, P.W., Mural, R.J., Sutton, G.G., Smith, H.O., Yandell, M., Evans, C.A., Holt, R.A.*, et al.* (2001). The sequence of the human genome. Science (New York, NY) *291*, 1304-1351.

Voloshin, O., Bakhrat, A., Herrmann, S., and Raveh, D. (2012). Transfer of Ho endonuclease and Ufo1 to the proteasome by the UbL-UbA shuttle protein, Ddi1, analysed by complex formation in vitro. PloS one *7*, e39210.

Vujanovic, M., Krietsch, J., Raso, M.C., Terraneo, N., Zellweger, R., Schmid, J.A., Taglialatela, A., Huang, J.-W., Holland, C.L., Zwicky, K.*, et al.* (2017). Replication Fork Slowing and Reversal upon DNA Damage Require PCNA Polyubiquitination and ZRANB3 DNA Translocase Activity. Molecular cell *67*, 882-890.e885.

Walter, D., Hoffmann, S., Komseli, E.S., Rappsilber, J., Gorgoulis, V., and Sorensen, C.S. (2016). SCF(Cyclin F)-dependent degradation of CDC6 suppresses DNA re-replication. Nature communications *7*, 10530.

Wan, L., Lou, J., Xia, Y., Su, B., Liu, T., Cui, J., Sun, Y., Lou, H., and Huang, J. (2013). hPrimpol1/CCDC111 is a human DNA primase-polymerase required for the maintenance of genome integrity. EMBO reports *14*, 1104-1112.

Wang, A.T., Kim, T., Wagner, J.E., Conti, B.A., Lach, F.P., Huang, A.L., Molina, H., Sanborn, E.M., Zierhut, H., Cornes, B.K.*, et al.* (2015a). A Dominant Mutation in Human RAD51 Reveals Its Function in DNA Interstrand Crosslink Repair Independent of Homologous Recombination. Molecular cell *59*, 478-490.

Wang, C., Wang, G., Feng, X., Shepherd, P., Zhang, J., Tang, M., Chen, Z., Srivastava, M., McLaughlin, M.E., Navone, N.M.*, et al.* (2018). Genome-wide CRISPR screens reveal synthetic lethality of RNASEH2 deficiency and ATR inhibition. Oncogene.

Wang, T., Birsoy, K., Hughes, N.W., Krupczak, K.M., Post, Y., Wei, J.J., Lander, E.S., and Sabatini, D.M. (2015b). Identification and characterization of essential genes in the human genome. Science (New York, NY) *350*, 1096-1101.

Washington, M.T., Johnson, R.E., Prakash, L., and Prakash, S. (2002). Human DINB1-encoded DNA polymerase κ is a promiscuous extender of mispaired primer termini. Proceedings of the National Academy of Sciences *99*, 1910.

Wasserman, M.R., Schauer, G.D., O'Donnell, M.E., and Liu, S. (2019). Replication Fork Activation Is Enabled by a Single-Stranded DNA Gate in CMG Helicase. Cell *178*, 600-611.e616.

Watson, J.D., and Crick, F.H. (1953). Molecular structure of nucleic acids; a structure for deoxyribose nucleic acid. Nature *171*, 737-738.

Watt, D.L., Johansson, E., Burgers, P.M., and Kunkel, T.A. (2011). Replication of ribonucleotide-containing DNA templates by yeast replicative polymerases. DNA repair *10*, 897-902.

Wessel, S.R., Mohni, K.N., Luzwick, J.W., Dungrawala, H., and Cortez, D. (2019). Functional Analysis of the Replication Fork Proteome Identifies BET Proteins as PCNA Regulators. Cell reports *28*, 3497-3509.e3494.

Williams, J.S., Lujan, S.A., and Kunkel, T.A. (2016). Processing ribonucleotides incorporated during eukaryotic DNA replication. Nature reviews Molecular cell biology *17*, 350-363.

Williams, J.S., Smith, D.J., Marjavaara, L., Lujan, S.A., Chabes, A., and Kunkel, T.A. (2013). Topoisomerase 1-mediated removal of ribonucleotides from nascent leading-strand DNA. Molecular cell *49*, 1010-1015.

Wobbe, C.R., Weissbach, L., Borowiec, J.A., Dean, F.B., Murakami, Y., Bullock, P., and Hurwitz, J. (1987). Replication of simian virus 40 origin-containing DNA in vitro with purified proteins. Proceedings of the National Academy of Sciences *84*, 1834.

Wohlschlegel, J.A., Dwyer, B.T., Dhar, S.K., Cvetic, C., Walter, J.C., and Dutta, A. (2000). Inhibition of eukaryotic DNA replication by geminin binding to Cdt1. Science (New York, NY) *290*, 2309-2312.

Wold, M.S., and Kelly, T. (1988). Purification and characterization of replication protein A, a cellular protein required for in vitro replication of simian virus 40 DNA. Proceedings of the National Academy of Sciences of the United States of America *85*, 2523-2527.

Wu, M., Lu, W., Santos, R.E., Frattini, M.G., and Kelly, T.J. (2014). Geminin inhibits a late step in the formation of human pre-replicative complexes. The Journal of biological chemistry *289*, 30810-30821.

Yamada-Inagawa, T., Klar, A.J.S., and Dalgaard, J.Z. (2007). Schizosaccharomyces pombe switches mating type by the synthesis-dependent strand-annealing mechanism. Genetics *177*, 255-265.

Yan, S., and Michael, W.M. (2009). TopBP1 and DNA polymerase alpha-mediated recruitment of the 9-1-1 complex to stalled replication forks: implications for a replication restart-based mechanism for ATR checkpoint activation. Cell cycle (Georgetown, Tex) *8*, 2877-2884.

Yanagi, K., Mizuno, T., You, Z., and Hanaoka, F. (2002). Mouse geminin inhibits not only Cdt1-MCM6 interactions but also a novel intrinsic Cdt1 DNA binding activity. The Journal of biological chemistry *277*, 40871-40880.

Yanagihara, H., Kobayashi, J., Tateishi, S., Kato, A., Matsuura, S., Tauchi, H., Yamada, K., Takezawa, J., Sugasawa, K., Masutani, C.*, et al.* (2011). NBS1 recruits RAD18 via a RAD6-like domain and regulates Pol η-dependent translesion DNA synthesis. Molecular cell *43*, 788-797.

Yao, N.Y., Schroeder, J.W., Yurieva, O., Simmons, L.A., and O'Donnell, M.E. (2013). Cost of rNTP/dNTP pool imbalance at the replication fork. Proceedings of the National Academy of Sciences of the United States of America *110*, 12942-12947.

Yeeles, J.T., Janska, A., Early, A., and Diffley, J.F. (2017). How the Eukaryotic Replisome Achieves Rapid and Efficient DNA Replication. Mol Cell *65*, 105-116.

Yeeles, J.T.P., and Marians, K.J. (2011). The Escherichia coli replisome is inherently DNA damage tolerant. Science (New York, NY) *334*, 235-238.

Yeeles, J.T.P., and Marians, K.J. (2013). Dynamics of leading-strand lesion skipping by the replisome. Molecular cell *52*, 855-865.

Yeeles, J.T.P., Poli, J., Marians, K.J., and Pasero, P. (2013). Rescuing stalled or damaged replication forks. Cold Spring Harbor perspectives in biology *5*, a012815-a012815.

Yoshida, S., Suzuki, R., Masaki, S., and Koiwai, O. (1985). Arabinosylnucleoside 5'-triphosphate inhibits DNA primase of calf thymus. Journal of biochemistry *98*, 427-433.

You, Z., Komamura, Y., and Ishimi, Y. (1999). Biochemical analysis of the intrinsic Mcm4-Mcm6-mcm7 DNA helicase activity. Molecular and cellular biology *19*, 8003-8015.

Yuan, J., Ghosal, G., and Chen, J. (2012). The HARP-like domain-containing protein AH2/ZRANB3 binds to PCNA and participates in cellular response to replication stress. Molecular cell *47*, 410-421.

Yuan, Z., Bai, L., Sun, J., Georgescu, R., Liu, J., O'Donnell, M.E., and Li, H. (2016). Structure of the eukaryotic replicative CMG helicase suggests a pumpjack motion for translocation. Nature structural & molecular biology *23*, 217-224.

Yusufzai, T., and Kadonaga, J.T. (2008). HARP Is an ATP-Driven Annealing Helicase. Science (New York, NY) *322*, 748.

Yusufzai, T., and Kadonaga, J.T. (2010). Annealing helicase 2 (AH2), a DNA-rewinding motor with an HNH motif. Proceedings of the National Academy of Sciences *107*, 20970.

Zafar, M.K., Ketkar, A., Lodeiro, M.F., Cameron, C.E., and Eoff, R.L. (2014). Kinetic analysis of human PrimPol DNA polymerase activity reveals a generally error-prone

enzyme capable of accurately bypassing 7,8-dihydro-8-oxo-2'-deoxyguanosine. Biochemistry *53*, 6584-6594.

Zaher, M.S., Rashid, F., Song, B., Joudeh, L.I., Sobhy, M.A., Tehseen, M., Hingorani, M.M., and Hamdan, S.M. (2018). Missed cleavage opportunities by FEN1 lead to Okazaki fragment maturation via the long-flap pathway. Nucleic acids research *46*, 2956-2974.

Zech, J., Godfrey, E.L., Masai, H., Hartsuiker, E., and Dalgaard, J.Z. (2015). The DNA-Binding Domain of S. pombe Mrc1 (Claspin) Acts to Enhance Stalling at Replication Barriers. PloS one *10*, e0132595.

Zellweger, R., Dalcher, D., Mutreja, K., Berti, M., Schmid, J.A., Herrador, R., Vindigni, A., and Lopes, M. (2015). Rad51-mediated replication fork reversal is a global response to genotoxic treatments in human cells. The Journal of cell biology *208*, 563.

Zeman, M.K., and Cimprich, K.A. (2014). Causes and consequences of replication stress. Nature cell biology *16*, 2-9.

Zhang, S., Chea, J., Meng, X., Zhou, Y., Lee, E.Y.C., and Lee, M.Y.W.T. (2008). PCNA is ubiquitinated by RNF8. Cell cycle (Georgetown, Tex) *7*, 3399-3404.

Zhang, Y., Yuan, F., Wu, X., Taylor, J.S., and Wang, Z. (2001). Response of human DNA polymerase iota to DNA lesions. Nucleic acids research *29*, 928-935.

Zhang, Y., Yuan, F., Wu, X., Wang, M., Rechkoblit, O., Taylor, J.S., Geacintov, N.E., and Wang, Z. (2000a). Error-free and error-prone lesion bypass by human DNA polymerase kappa in vitro. Nucleic acids research *28*, 4138-4146.

Zhang, Y., Yuan, F., Wu, X., and Wang, Z. (2000b). Preferential incorporation of G opposite template T by the low-fidelity human DNA polymerase iota. Molecular and cellular biology *20*, 7099-7108.

Zhao, F., Wu, J., Xue, A., Su, Y., Wang, X., Lu, X., Zhou, Z., Qu, J., and Zhou, X. (2013). Exome sequencing reveals CCDC111 mutation associated with high myopia. Hum Genet *132*, 913-921.

Zhao, H., and Piwnica-Worms, H. (2001). ATR-mediated checkpoint pathways regulate phosphorylation and activation of human Chk1. Molecular and cellular biology *21*, 4129-4139.

Zhao, Y., Biertümpfel, C., Gregory, M.T., Hua, Y.-J., Hanaoka, F., and Yang, W. (2012). Structural basis of human DNA polymerase η-mediated chemoresistance to cisplatin. Proceedings of the National Academy of Sciences of the United States of America *109*, 7269-7274.

Zhu, J.Y., Abate, M., Rice, P.W., and Cole, C.N. (1991). The ability of simian virus 40 large T antigen to immortalize primary mouse embryo fibroblasts cosegregates with its ability to bind to p53. Journal of Virology *65*, 6872.

Zimmermann, M., Murina, O., Reijns, M.A.M., Agathanggelou, A., Challis, R., Tarnauskaite, Z., Muir, M., Fluteau, A., Aregger, M., McEwan, A.*, et al.* (2018). CRISPR screens identify genomic ribonucleotides as a source of PARP-trapping lesions. Nature *559*, 285-289.

Zou, L., and Elledge, S.J. (2003). Sensing DNA damage through ATRIP recognition of RPA-ssDNA complexes. Science (New York, NY) *300*, 1542-1548.

Zou, Y., Liu, Y., Wu, X., and Shell, S.M. (2006). Functions of human replication protein A (RPA): from DNA replication to DNA damage and stress responses. Journal of cellular physiology *208*, 267-273.